Journal of Cardiovascular Magnetic Resonance (2007) **9,** 175–326

ISSN: 1097-6647 print / 1532-429X online
DOI: 10.1080/10976640601152723

informa
healthcare

Friday Poster Session

Abstract Session IX: Friday, February 2, 2007

307. MAGNETIZATION TRANSFER IN CARDIAC TRUEFISP IMAGING

Oliver M. Weber, PhD, Klaus Scheffler, PhD, Oliver Bieri, PhD. ***University of Basel, Switzerland, Basel, Switzerland.***

Introduction: Recently, we showed that the rapid succession of high flip angle RF pulses in conventional balanced steady state free precession (bSSFP) sequences causes an on-resonance magnetization transfer (MT) effect, resulting in signal attenuation in tissue with bound macromolecules (1). The degree of the MT effect depends on the deposited power of the RF pulse train. Variation of the RF power thus results in different MT weighting and can be used to quantify the MT effect. We applied this principle to calculate MT ratios (MTR) in myocardial tissue.

Materials and Methods: A cardiac bSSFP sequence with adjustable TR was implemented on a 1.5 T MR imager (Avanto; Siemens Medical Solutions) to assess MT variation in myocardial tissue. Short axis views of the left ventricle (LV) were acquired in a normal volunteer. A single phase was acquired using a

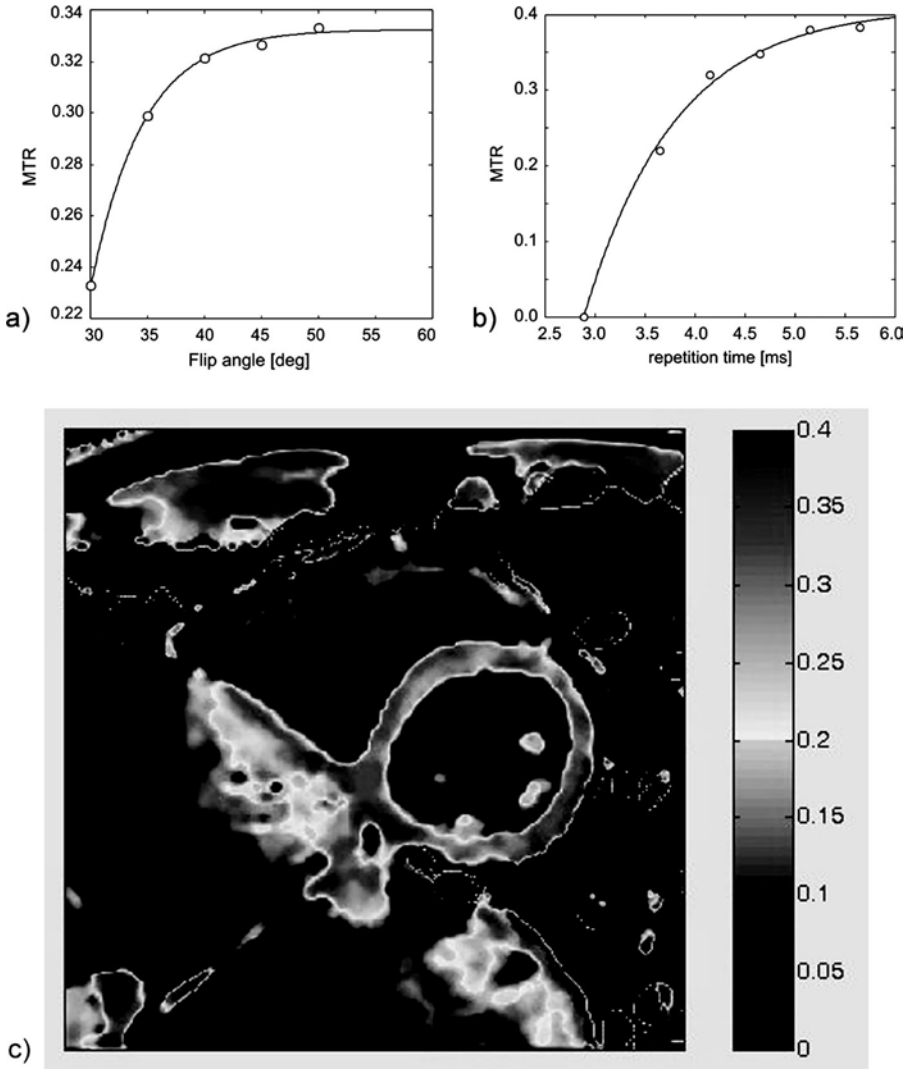

FIG. 1. MTR in dependence of a) flip angle ($TR_{strongMT} = 2.9$ ms; $TR_{weakMT} = 4.4$ ms) and b) TR_{weakMT} (flip angle = 45°, $TR_{strongMT} = 2.9$ ms). Circles: measured points; line: exponential fit. c) MTR map of a LV short axis view.

segmented bSSFP sequence during a breathhold (spatial resolution, $1.8 \times 1.8 \times 8.0\ mm^3$; 24 segments per heart cycle). Steady state was maintained throughout the cardiac cycle, whereas data acquisition was restricted to diastole to avoid motion artifacts. In a first experiment, flip angle was varied from 30° to 50°. To allow for subsequent MTR determination, 2 images with different repetition times (TR) were acquired: TR = 2.9 ms for the high-RF power deposition image (strong MT effect), and TR = 4.4 ms for the low-RF power deposition image (weak MT effect). In a second experiment, the flip angle was fixed at 45°, but TR of the image with weak MT was varied from 3.6 ms to 5.7 ms. Signal intensity (SI) of the myocardial muscle was determined on all images in regions of interest (ROI's) drawn manually and including the entire ring-shaped LV. MTR was calculated according to $MTR = (SI_{weakMT} - SI_{strongMT}) / SI_{weakMT}$. In a third experiment, 2 cine data sets were acquired with a retrospectively triggered version of the same sequence (40 reconstructed phases). The flip angle was set to 45°, and $TR_{strongMT} = 2.9$ ms, $TR_{weakMT} = 4.4$ ms. For each heart phase, an MTR map was generated by performing the above-mentioned calculation on a pixel-by-pixel base.

Results and Discussion: Variation of the flip angle while keeping $TR_{strongMT}$ and TR_{weakMT} constant showed clear increase of MTR with higher flip angles (Fig. 1a). Changes in MTR were found to be smaller towards higher flip angles and seemed to approach an asymptomatic maximum value as shown by the exponential fit of the data points. Increasing TR_{weakMT}, while keeping the flip angle constant, resulted in higher MTR values as well, also with reduced changes towards longer TR_{weakMT} (Fig. 1b). The cine sequence finally allowed simultaneous visualization of cardiac function and MTR maps with good homogeneity in this healthy volunteer (Fig. 1c).

Overall, higher flip angles and larger differences in TR resulted in an increased sensitivity to MT differences. However, limits in power deposition (SAR) and the occurrence of off-resonance banding artefacts in practice limited these parameters to the range used in this study, which provide a good compromise between magnitued of MR effect and avoidance of artifacts. Furthermore, optimal shimming was found to be key for the reproducible determination of MTR values.

Conclusion: A novel technique to visualize and quantify magnetization transfer in the myocardium is reported. Potential applications include detection of infarcts and inflammation of the myocardial tissue.

REFERENCE

1. Bierio, Scheffler K. On the Origin of Apparent Low Tissue Signals in Balanced SSFP. MRM (in press).

308. ADIABATIC T_2 PREPARED 3T MAGNETIC RESONANCE ANGIOGRAPHY FOR THE DETECTION OF ARTERIOGENESIS IN A RABBIT MODEL OF HINDLIMB ISCHEMIA

Grigorios Korosoglou, MD, Wesley D. Gilson, PhD, Mike Schar, PhD, Ali Ustun, MS, Lawrence V. Hofmann, MD, Dara L. Kraitchman, VMD, PhD, Matthias Stuber, PhD. ***Johns Hopkins University Medical School, Baltimore, Maryland, USA.***

Introduction: Therapeutic angiogenesis is a promising treatment used to stimulate the growth of new or existing arteries in patients with peripheral arterial occlusive disease (PAOD). In particular, a wide variety of arteriogenic therapies, based on protein, gene, and cellular products, are in preclinical(1) or clinical (2) testing. X-Ray angiography is the current clinical gold-standard for the detection of these newly formed arteries(3). However, this technique is invasive so that magnetic resonance angiography (MRA) may provide a valuable alternative for the serial evaluation of arteriogenesis.

Purpose: To investigate the feasibility of 2 high-field (3T) MRA techniques, time of flight (TOF) and adiabatic T_2 preparation (T_2 prep) to evaluate arteriogenesis in a rabbit model of hindlimb ischemia.

Methods: Eleven New Zealand White rabbits underwent endovascular occlusion of their left superficial femoral artery (SFA). Two weeks after occlusion MRA using TOF and T_2 prep at 3T and X-Ray angiograms were performed. Vessel sharpness was evaluated visually and quantitatively utilizing the Deriche algorithm[4]. Fig. 2a shows an example of a MIP image of a normal SFA imaged by T_2 prep and the multiplanar reformat reconstructed vessels (Fig. 2b) using the soap bubble tool (4). Vessel sharpness was measured in multiple equidistance steps of 0.2 mm (Fig. 2c) and was plotted versus the length of this arterial segment (Fig. 2d) using automatic vessel tracking. This was assessed in 7 normal arterial segments in the nonischemic limb and in the saphenous and popliteal branches distal to the occluded SFA in the ischemic limb. Transverse diameters were obtained automatically from the nonoccluded limb on TOF and T_2 prep images and were compared to those obtained in identical anatomical points on X-Ray angiographies.

Results: Vessel sharpness in TOF and T_2 prep MRA was similar in arteries in the nonischemic limb. However, smaller secondary branches originating from normal arterial segments (arrowheads) were to a significantly greater extend detectable by T_2 prep compared with TOF (1.3 ± 0.5 versus 0.6 ± 0.3 per segment, $p < 0.001$), (Fig. 2). Furthermore, T_2 prep was superior to TOF for the delineation of arterial segments with diminished blood flow including collateral vessels and branches distal to vessel occlusion (Fig. 3, arrows), (44% versus 31% for the left popliteal and 44% versus 32% for the left saphenous arteries, $p < 0.001$ for both). T_2 prep was superior for the visualization of small collateral vessels in the ischemic limb, allowing the detection of 91% compared to only 45% of collateral vessels that could be depicted on TOF angiograms ($p < 0.05$), (Fig. 3, circle). Transverse diameters of normal vessels by TOF and T_2 prep both closely correlated with the diameters assessed by X-Ray angiography ($r = 0.86$ versus $r = 0.83$, $p < 0.001$ for both),

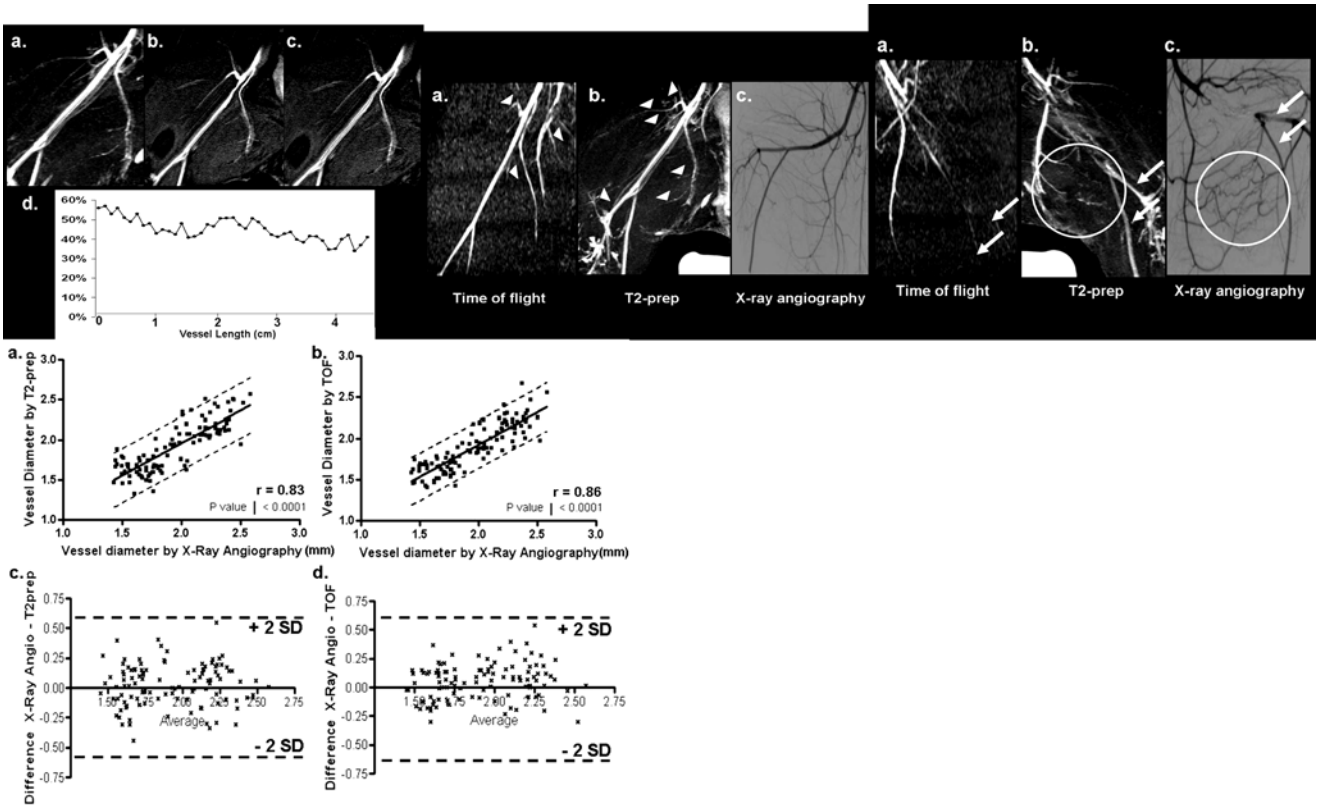

FIGS. 1–4.

(Fig. 4a-b). Both MRA methods showed good agreement with X-Ray angiography as demonstrated in the Bland-Altman plots (Fig. 4c-d).

Conclusions: Adiabatic T_2 prep at 3T is a novel technique for high spatial resolution MRA of small arteries. Since, contrast formation by this technique is blood-flow independent, T_2 prep may offer high anatomical vessel definition in segments with diminished blood flow. Thus, this technique may represent a valuable tool for the serial noninvasive evaluation of efficacy of gene, protein, and cellular therapies for PAOD.

REFERENCES

1. Kraitchman DL, et al. Circulation 2005;112:1451–61.
2. Tateishi-Yuyama E, et al. Lancet 2002;360:427–35.
3. Ouriel K. Lancet 2001;358:1257–64.
4. Etienne A, et al. MRM 2002;48:658–66.

309. FRACTIONAL SHORTENING, EJECTION FRACTION, AND MORTALITY: A QUANTITATIVE ANALYSIS

Erik B. Schelbert, MD, MS, Jie J. Cao, MD, MPH, Andrew E. Arai, MD. ***National Institutes of Health, Bethesda, MD, USA.***

Introduction: Large cohort studies have used fractional shortening (FS) as a surrogate for left ventricular systolic function, but ejection fraction (EF), a volumetric assessment, is accepted as the gold standard. Whether fractional shortening, a one-dimensional measure, captures the prognostic value of EF is unclear.

Purpose: Thus, we studied the prognostic value of FS and EF in cohort of 1,185 patients referred for cardiac MRI. We also studied of the relation between FS and ES.

Methods: At a community hospital from September 2001 to December 2004, cardiac function was imaged in 1,118 patients using 1.5 T CMRI scanners with SSFP cine pulse sequences. FS was calculated as the 1 minus the ratio of end-systolic to end-diastolic endocardial diameter measured from the basal anteroseptum to the posterolateral wall. EF was measured on a volumetric stack of manually-traced short axis images. The National Death Index identified all cause mortality. Survival analysis used Cox regression models to quantify the predictive value of EF and FS, alone or in combination. Discrimination of univariable Cox models was compared using R^2 derived from the maximum likelihood. Linear regression models quantified the variation in EF explained by FS (R^2). The sensitivity/specificity of FS for detecting systolic dysfunction was assessed by dichotomizing EF and FS (i.e., EF $< 55\%$; FS $< 25\%$).

Results: Most patients were male (68%); the mean age was 57 years (interquartile range 48–67). There were 45 deaths (4%) over a median follow-up of 1.4 years (interquartile range 0.6–2.4). Although in univariable Cox regression models lower EF and FS were each significantly associated with mortality (Chi

square = 33.3 and 15.0, respectively; p value < 0.001 for both), FS had only 52% of the discrimination of EF for predicting mortality. Accordingly, when both EF and FS were combined in a Cox regression model, lower EF remained strongly associated with mortality (Chi square = 16.9, p value =<0.001) whereas FS provided no significant additional prognostic information (Chi square = 0.3; p value = 0.59). Dichotomizing the variables or adjustment for age, gender, and/or end diastolic dimension yielded similar results. In addition, FS accounted for less than two thirds of the variation in EF in linear regression models ($R^2 = 0.58$) regardless of whether models were adjusted for end diastolic dimension. Moreover, when the variables were dichotomized, FS < 25% had a 64% sensitivity and 94% specificity for detecting EF < 55%.

Conclusions: FS is an imprecise and insensitive measure of systolic function and provides no additional discrimination over EF for predicting mortality. Cohort studies relying on FS will be insensitive to clinically relevant differences in systolic function. FS is a poor surrogate for systolic function.

310. CARDIAC MRI FOR DETECTION OF ACUTE CORONARY SYNDROME IN THE EMERGENCY DEPARTMENT

Christoph Tillmanns, Anja Zagrosek, Philipp Boyé, Hassan Abdel-Aty, Rainer Dietz, Jeanette Schulz-Menger. ***Franz-Volhard-Clinic, Charité-Campus-Buch. University Berlin, Helios-Klinikum, Berlin, Germany.***

Introduction : The management of patients with acute chest pain in the emergency department (ER) remains a challenge with current diagnostic strategies. Cardiac magnetic resonance (CMR)—using functional and contrast enhanced techniques—has been shown to accurately detect myocardial damage but failed to differentiate between acute and chronic myocardial injury. Adding T2-weighted techniques, CMR might identify acute coronary syndrome (ACS) by detecting myocardial edema. This approach might improve the diagnostic performance of CMR in an emergency setting and therefore speed up the diagnostic process in patients with suspected ACS.

Purpose: The aim of this preliminary study was to assess the impact of urgent CMR (including T2-weighted techniques) on time-to-decision in the management of patients with acute chest pain presenting in the ER.

Methods: We prospectively enrolled 11 patients (8 male, mean age ± SD 57 ± 14 years) with acute chest pain lasting ≥ 30 min, who had a first ECG and laboratory test done that did not exhibit pathbreaking pathological findings. Patients with ST elevation myocardial infarction, positive troponin on presentation or other pathology matching the criteria for immediate coronary intervention (ESC Guidelines 2002) were excluded from this study. CMR (1.5 T, Sonata, Siemens) was performed as early as possible (150 ± 54 min) after the first laboratory test and included biplane cine SSFP sequences, TIRM sequences for visualization of edema, and contrast enhanced IR-GRE sequences for delayed enhancement imaging. Patients were continously monitored by a cardiologist during transport and CMR.

CMR data was interpreted online during the examination by an experienced observer, and by a second observer blinded to the patients' data at the end of the study. The detection of wall motion abnormalities matching an area of signal hyperintensity <2 SD of normal myocardium on T2-weighted images was interpreted as suggestive for ACS. The moment in which CMR allowed for a therapeutic decision according to the first observer was noted. The therapeutic decision in the ER was independent of the CMR results, with only wall motion abnormalities being revealed to the emergency doctor.

Primary endpoint was the time-to-decision by CMR, as defined by the moment in which the examination yielded a result allowing for a therapeutic decision. Serial measurements of Troponin T served as the goldstandard for this study. Five patients (45%) underwent coronary angiography after CMR.

Results: No clinical difficulties occurred during transport or during CMR. The mean absence time from the ER was 46 ± 15 min. The mean duration of CMR was 34 ± 11 min, while a therapeutic decision was reached after a mean examination time of 23 ± 12 min. Overall, the time-to-decision with support of MRI was 179 ± 60 min, wheras the standard work-up following the current recommendations took 344 ± 81 min (p < 0.001).

According to CMR, ACS was excluded in 10 patients. One patient was diagnosed with ACS. All patients had negative biochemical markers in at least 2 serial measurements and an ACS was therefore excluded. Nevertheless, 5 patients (45%) underwent coronary angiography afterwards, confirming the exclusion of ACS.

In this emergency setting, cardiac MRI featured a specificity of 90% and a negative predictive value of 100%.

Conclusion: Although the number of patients in this preliminary study is rather small and no true-positive patients could be included, the results suggest that an urgent CMR scan in an emergency setting is able to speed up the diagnostic process considerably. The CMR protocol in this study was short and simple, saved almost 3 hrs (165 min) as compared to the clinical standard approach and added diagnostical value over clinical parameters. Larger studies with inclusion of ACS-positive patients are required to confirm the benefit of CMR in an emergency setting.

311. REAL-TIME DELAYED ENHANCEMENT VIABILITY IMAGING

Jay S. Detsky,[1] John J. Graham, MBChB MRCP,[1] Ram Vijayaraghavan, MD,[1] Jeff A. Stainsby, MSc, [2]Alexander J. Dick, MD,[1] Graham A. Wright, PhD.[1] ***[1]Sunnybrook Health Sciences Centre, Toronto, Ontario, Canada, [2]GE Healthcare Canada, Mississauga, Ontario, Canada.***

Introduction: Conventional delayed enhancement magnetic resonance imaging (DE-MRI) uses an inversion-recovery gradient echo (IR-GRE) sequence. IR-GRE requires cardiac gating and repeated breath-holds, which can be difficult to achieve in all cardiac patients. A real-time delayed hyperenhancement (RTDHE) method has recently been developed (1) that uses real-time steady-state free precession (SSFP) imaging with intermittent inversion pulses. RTDHE does not require cardiac gating or breath-holds. We tested the hypothesis that RTDHE can be used to detect and quantify myocardial infarct (MI) in a patient population.

Methods: Twenty-three patients (age = 66 ± 12 yrs) with suspected MI underwent DE-MRI with IR-GRE and RTDHE. Infarcts at various stages of healing were examined, with a median infarct age of ten months but with a range of one week to 18 years. The IR-GRE parameters were a $1.25 \times 1.67 \times 8\,mm^3$ spatial resolution over a 32×32 cm field of view, TR/TE/$\theta = 7.7$ ms/3.7 ms/20^0, 24 views per segment (185 ms in mid diastole), 2 averages, and a TI optimized to null healthy myocardium (range = 175–250 ms). Each imaging slice was acquired with a 12–18 second breath-hold. Using RTDHE, 4 images are acquired after an inversion pulse and variable delay time; the first image is the infarct-enhanced image, and the 3 subsequent images are used to visualize the motion of the heart and to allow the magnetization to recover to its steady state. Images were continuously displayed on a custom built real-time interface. The RTDHE parameters were a $2 \times 2 \times 8\,mm^3$ spatial resolution covering a 32×32 cm field of view, TR/TE/$\theta = 2.7$ ms/1.3 ms/30^0 with view-shared images reconstructed at 4.7 frames per second. The delay time was varied by a slider bar on the real-time interface to create an effective TI to null healthy myocardium (range of TI = 200–250 ms). All imaging was performed on a GE 1.5-T scanner, using the GE 8-channel cardiac array for signal reception. Short-axis LV imaging slices were acquired and divided into 6segments as per the AHA recommendation. The presence or absence of MI was determined for each segment, and total infarct surface area was measured for each patient.

Results: Representative images using IR-GRE and RTDHE are shown in Fig. 1. RTDHE images have a black blood appearance, and therefore subendocardial infarcts are more readily apparent with RTDHE than IR-GRE (Fig. 1). Using IR-GRE as the gold standard, RTDHE had a sensitivity of 94% (287/307 segments), with no single lesion being missed. RTDHE had a specificity of 96% (664/689 segments), although most of the 'false positives' were in actuality small subendocardial infarcts obscured by the bright blood pool in the IR-GRE images. Excellent agreement was shown between the two methods in the quantitative measure of infarct surface area (slope = 1.01 ± 0.04, R = 0.97). The average time to acquire a set of DE images with IR-GRE (12 ± 2 minutes) was significantly longer than with RTDHE (6 ± 1 minute, $p < 0.001$).

Conclusions: RTDHE has the advantage of not requiring breath-holding or cardiac gating for the assessment of myocardial infarction. We have demonstrated that RTDHE can predict the presence, location and size of infarction when compared to standard gated and breath-held IR-GRE. RTDHE has also been shown to be superior to IR-GRE in detecting small subendocardial infarcts.

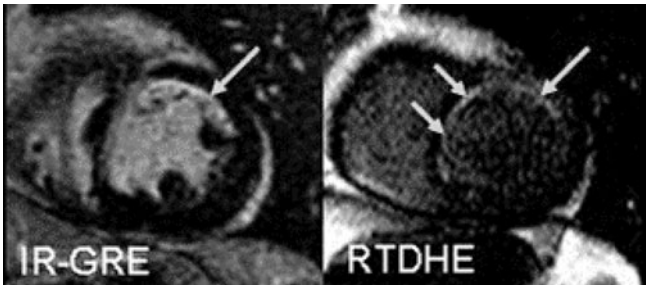

FIG. 1. DE-MRI images using IR-GRE and RTDHE in a 61-year-old male patient. Note the greater extent of infarct that can be visualized by RTDHE (arrows) because of the low signal from blood.

REFERENCE

1. Guttman MA. Magn Res Med 2004; 52: 354–361.

312. TOWARD OPTIMAL MEASURE OF 3-D MYOCARDIUM DISPLACEMENTS FROM A SINGLE SLICE USING ZHARP: IN-VIVO VALIDATION AND COMPARISON WITH CSPAMM

Khaled Z. Abd-Elmoniem, MSc, Nael Osman, PhD, Matthias Stuber, PhD, Jerrry Prince. ***Johns Hopkins University, Baltimore, Maryland, USA.***

Introduction: Quantitative functional cardiac imaging can be used to characterize healthy and diseased myocardial tissues. Imaging should take into account the 3D motion of the heart, but acquisition must be fast for diagnostic and practical considerations. zHARP(1) is a fast technique for encoding and acquisition of 3D myocardium displacements from a single slice. The technique is based on slice-following CSPAMM (2) tagging, adding a z-gradient to encode the through-plane displacement of the tagged CINE images.

Purpose: The area of the z-encoding gradient is a critical aspect in zHARP. Small-area gradients produce low SNR through-plane displacement estimates while large-area gradients cause intravoxel dephasing which also reduces the SNR of the acquired signal. The purpose of this work is to establish the mathematical framework for the intravoxel dephasing effect on zHARP 3D displacement measures. Through-plane displacements in short axis slices obtained using zHARP are validated against the in-plane displacements obtained using slice-following CSPAMM in the orthogonal 4CH and 2CH slices using in-vivo normal subjects. The optimal z-gradient strength is then determined by experimental comparison of the in-plane and through-plane displacement maps computed in orthogonal slices.

Methods: Theory: zHARP is a recently developed tagging CMRI methodology that images and automatically tracks the 3D myocardial displacement of all points in an image plane(1). The z-encoding gradient can be described by its z-encoding frequency κ_z. As shown in Eq.1, the gradient thus encodes through-plane displacement in the phase of the complex data but also causes intravoxel dephasing in the slice-select direction. This reduces the magnitude of the tagged image by multiplication with sinc function that is dependent on both slice thickness and the z-encode gradient strength.

Implementation: A normal adult was imaged in a 3T CMRI system (Achieve, Philips) using a cardiac phased-array coil and zHARP pulse sequence with 6 different z-gradient encoding frequencies ($0, \pi/25, 2\pi/25, 3\pi/25, 4\pi/25, 5\pi/25$ rad/mm). Basal, equatorial, and apical SA slices were acquired. Four LA slices were acquired using SF-CSPAMM. All data had FOV = 300 mm, 12 spirals, TR = 20 ms, flip angle = 20, and 8 mm slice thickness. The lines of intersection between the LA and the SA planes were tracked. The through-plane displacement in the SA slices were compared against the equivalent in-plane displacement in the LA slices. The mean correlation coefficient was calculated in each dataset. In addition, SA in-plane tracking was done for 2000 points per slice evenly distributed throughout the myocardium.

Results: Fig. 1a shows the SA in-plane/in-plane correlation coefficient (r1) as a function of κ_z. Even with κ_z as high as $2\pi/25$, r1 is still above 0.95. In addition, the SA through-plane/LA in-plane correlation coefficient (r2) shows a peak value above 0.87 for κ_z around $2\pi/25$. An example equatorial SA slice is shown in Fig. 1b and its through-plane displacement at the end-systole is shown in Fig. 1c with $\kappa_z = 2\pi/25$. Notice the in-plane radial thickening and the smooth downward shortening.

Conclusion: zHARP can acquire 3D displacement in a single slice. An experimental optimization was developed to select the best z-encoding gradient that will maintain high SNR in both in-plane and through-plane displacement maps with minimal

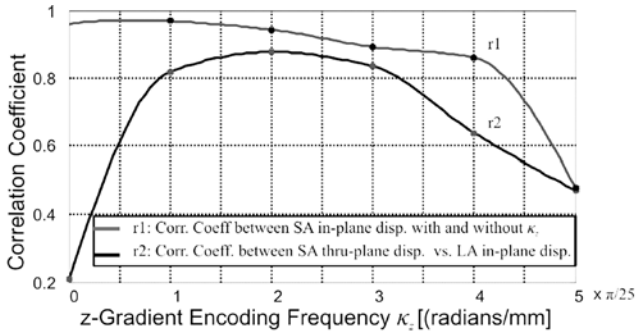

(a)

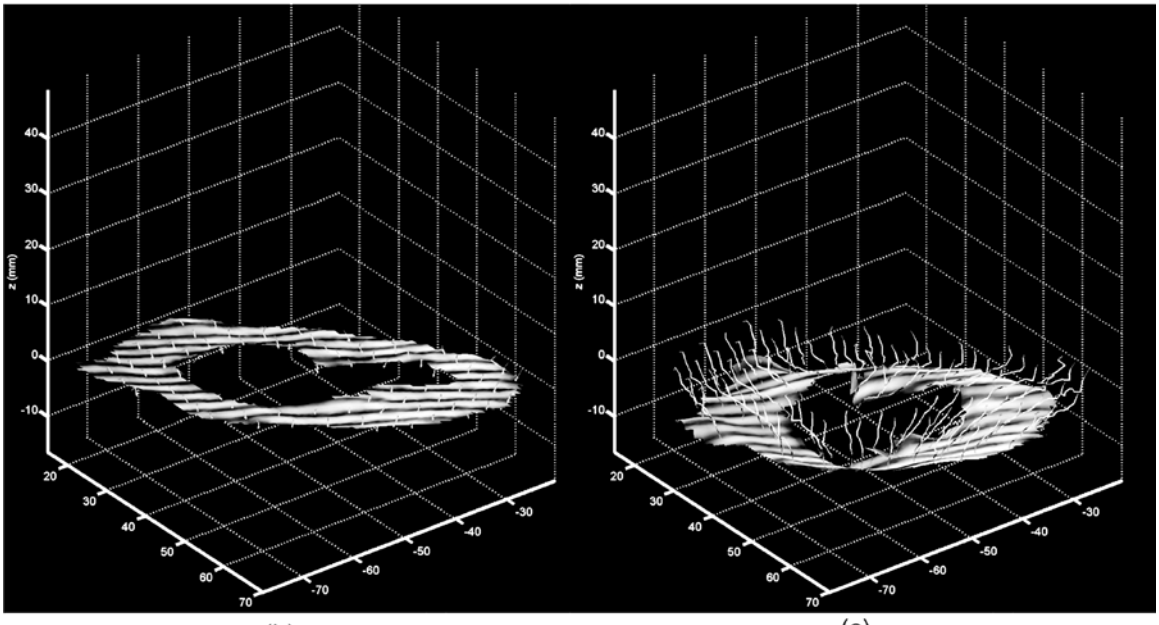

(b) (c)

FIG. 1. (a) Correlation between in-plane/in-plane displacement and in-plane/through-plane displacements with different κ_2 values. (b) An example equatorial SA slice at end-diastole. (c) The slice at end-systole with both in-plane and through-plane zHARP tracking.

intravoxel dephasing effect. With such optimal selection, zHARP method can be used to acquire 3D displacements comparable to conventional tagging with minimal mis-registration and without the need for the time-consuming, 3D tagging acquisitions.

REFERENCES

1. Abd-Elmoniem, et al. ZHARP: Three-Dimensional Motion Tracking From a Single Image Plane. IPMI 2005
2. Fischer, et al. True myocardial motion tracking.MRM 1994
3. Haacke, et al. Magnetic Resonance Imaging: Physical Principles and Sequence Design. New York, Wiley-Liss, 1999.

313. ABSOLUTE MYOCARDIAL BLOOD FLOW MEASURES BY FIRST-PASS CMR PERFUSION IMAGING: COMPARISON WITH O-15 POSITRON EMISSION TOMOGRAPHY

Timothy F. Christian, MD,[1] Su Min Chang, MD,[2] Terrance Oakes, PhD.[2] [1] *University of Vermont, Burlington, Vermont, USA,* [2] *University of Wisconsin, Madison, Wisconsin, USA.*

Introduction: Absolute myocardial blood flow (MBF) measurement by positron emission tomography (PET) using O-15 labeled water has been considered the gold standard due to the favorable diffusion kinetics of water. These measures are made using deconvolution techniques but are problematic due to the poor definition of the blood pool that serves as the arterial input function and spillover into the myocardial regions of interest (ROI). Absolute MBF can also be measured by MR 1st-pass perfusion. The arterial input function and myocardial ROIs are sharply defined without contamination, but the kinetics of gadolinium are less favorable.

Purpose: To compare measures of absolute MBF generated by O-15 water and 1st-pass MRI to microsphere values in an animal model of coronary ischemia.

Methods: Model: This is a pig model of transient ischemia (15 minutes). The chest was surgically opened and a plastic hydraulic occluder was placed around the mid-LAD artery to produce reversible ischemia in a pig, after which the chest was closed. During ischemia, flourescent microspheres were injected into the left atrium with reference sampling from the descending aorta for absolute MBF. Microsphere injection was followed immediately by imaging during ischemia (MR or PET).

MR Imaging: Pigs were imaged in a 1.5 T GE scanner (n = 7) using a gradient echo saturation reovery sequence with an echotrain readout. Gd-DTPA was injected at 0.025 mmole/Kg at 5 cc/sec. Images were analyzed using Cine Tool software (GEMS). Fermi function deconvolution was performed in the ischemic and control ROI from short-axis slices with the AIF generated from the LV cavity.

PET imaging: Pigs were imaged in a GE Advance scanner with 1.5 mCi/Kg of O-15 water (n = 5). Acquisitions were dynamic over 5 minutes. Images were quantified using deconvolution methods (pmod software) in an ischemic and control ROI with the AIF from the LV cavity using a double spillover single compartment model.

Results: MBF ranged from 0.003 to 1.47 mL/min/g. Mean ischemic MBF = 0.37 ± 0.26 mL/min/g and control MBF = 0.72 ± 0.28mL/min/g by microsphere analysis with more than 1/3 ischemic ROIs < 0.20 mL/min/g. The correlation of microsphere MBF with 1) PET MBF values was 0.76, $p < 0.0001$, SEE = 0.14 mL/min/g) and 2) MRI MBF was 0.83, $p < 0.0001$, SEE 0.20 mL/min/g (Fig.).

Conclusions: Quantitation of 1st-pass MR imaging using a Fermi function deconvolution technique correlates well with true absolute MBF and is equivalent to O-15 PET measures. The lower correlations for both techniques with absolute MBF are likely due to the truncated range of MBF, as only ischemic and not hyperemic values were generated.

314. MRI OF AORTIC WALL ELASTICITY, AORTIC VALVE COMPETENCE AND LV FUNCTION IN PATIENTS WITH A NON-STENOTIC BICUSPID AORTIC VALVE

Heynric B. Grotenhuis, MD, Jaap Ottenkamp, MD, Jos J. M. Westenberg, PhD, Jeroen J. Bax, MD, Lucia J. M. Kroft, MD, Albert de Roos, MD. *Leiden University Medical Center, Leiden, The Netherlands.*

Introduction: Intrinsic pathology of the aortic wall is a possible explanation for aortic dilatation in patients with a bicuspid aortic

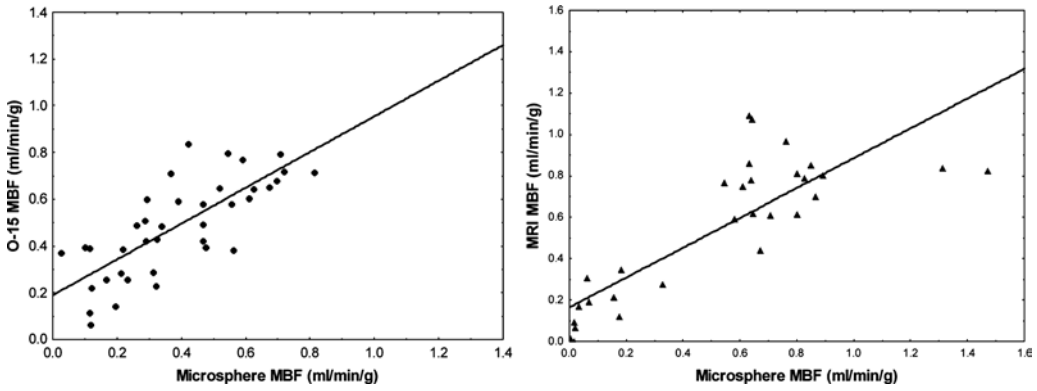

valve (BAV), even in the absence of a stenotic aortic valve. The relationship between aortic dimensions, aortic wall elasticity, aortic valve competence and left ventricular (LV) function in patients with BAVs has not previously been studied.

Purpose: To evaluate aortic dimensions, aortic wall elasticity, aortic valve competence and LV function in patients with a nonstenotic BAV using magnetic resonance imaging (MRI).

Methods: MRI was performed in 20 patients with nonstenotic BAVs (13 male; mean ± SD age (yrs.): 27 ± 11) and 20 matched healthy subjects. Aortic root diameters at 4 predefined levels, aortic valve competence and systolic LV function were measured using standard MRI sequences. Pulse wave velocity (PWV) in the aortic arch and descending aorta, and aortic root distensibility were used as markers of aortic wall elasticity.

Results: Patients with BAVs showed aortic root dilatation as compared to controls (mean difference 3.6–4.2 mm, with $p \leq 0.04$ at all 4 levels). Increased PWV in the aortic arch and descending aorta was observed in patients (5.6 m/s ± 1.3 vs. 4.5 m/s ± 1.1, $p = 0.01$; and 5.2 m/s ± 1.8 vs. 4.3 m/s ± 0.9, $p = 0.03$, respectively), as well as reduced aortic root distensibility ($3.1 * 10^{-3}$ $mmHg^{-1}$ ± 1.2 vs. $5.6 * 10^{-3}$ $mmHg^{-1}$ ± 3.2, $p < 0.01$). Minor degrees of aortic regurgitation (AR) ranging between 5 and 16% were present in 11 patients (AR fraction 6% ± 8 vs. 1% ± 1, $p < 0.01$). LV ejection fraction was normal (55% ± 8 vs. 56% ± 6, $p = 0.61$), whereas LV mass was significantly increased in patients (54 g/m^2 ± 12 vs. 46 g/m^2 ± 12, $p = 0.04$). Aortic root dilatation (r ranging 0.43–0.59, $p \leq 0.01$ for all) and reduced root distensibility ($r = 0.38$, $P = 0.01$) correlated with AR fraction. Increased PWV in the aortic arch and reduced root distensibility correlated with increased LV mass ($r = 0.38$, $p = 0.01$; $r = 0.35$, $P = 0.02$; respectively).

Conclusions: Aortic root dilatation and minor degrees of AR are shown by MRI in patients with nonstenotic BAVs. In addition, MRI reveals reduced aortic wall elasticity that correlates with the severity of AR and LV mass. MRI may be useful for monitoring of aortic dimensions and aortic elasticity, in conjunction with aortic valve competence and LV function in patients with BAVs.

315. RIGHT VENTRICULAR FUNCTION AND PULMONARY FLOW DYNAMICS LATE AFTER THE ROSS OPERATION, ASSESSED WITH MRI

Heynric B. Grotenhuis, MD, Albert de Roos, MD, Jaap Ottenkamp, MD, Hubert W. Vliegen, MD, Jos J. M. Westenberg, PhD, Lucia J. M. Kroft, MD. ***Leiden University Medical Center, Leiden, The Netherlands.***

Introduction: Pulmonary homograft stenosis has been reported after the Ross procedure, but little is known about the effect of homograft stenosis on right ventricular (RV) function. Insight in this relationship may have prognostic value as RV function is important in patient survival and exercise tolerance and may contribute to clinical decision making to replace a dysfunctioning homograft in the pulmonary position.

Purpose: To assess pulmonary flow dynamics and RV function in patients late after the Ross operation using magnetic resonance imaging (MRI).

Methods: Seventeen patients (8.3 ± 3.2 years after surgery) and 17 matched healthy subjects were prospectively studied with MRI, to assess pulmonary valve (PV) flow, RV systolic and diastolic function, and RV mass.

Results: Pulmonary valve stenosis (peak-flow velocity >1.5 m/s across the PV) was found in 12 of 17 patients but not in healthy subjects. Increased RV mass was present in Ross patients: 17.0 g/m^2 ± 4.8 versus 10.9 g/m^2 ± 5.6 in healthy subjects, $p < 0.01$. In addition, impaired diastolic RV function was found late after the Ross procedure: mean tricuspid valve E/A peak-flow velocity ratio was 1.56 ± 0.75 versus 2.05 ± 0.58 in healthy subjects ($p = 0.03$). After Ross, PV peak-flow velocity correlated with RV mass ($r = 0.40$, $p = 0.02$) and tricuspid valve E/A peak-flow velocity ratio ($r = 0.39$, $p = 0.02$). RV systolic function was normal in Ross patients as RV ejection fraction was 52% ± 8 versus 51% ± 5 in healthy subjects, $p = 0.74$.

Conclusions: Pulmonary valve stenosis as indicated by increased peak-flow velocity across the PV was frequently observed late after the Ross operation. Hemodynamic consequences were RV hypertrophy and RV diastolic dysfunction, whereas systolic RV function was still well preserved. MRI proved to be an excellent imaging tool to assess pulmonary flow dynamics and RV function in patients late after the Ross operation. Additionally, replacement of a dysfunctioning homograft in the pulmonary position should be addressed after assessment of homograft and RV function.

316. MINIMUM SIGNAL-TO-NOISE RATIO DETERMINATION FOR MYOCARDIAL PERFUSION IMAGING

David M. Higgins, PhD,[1] Aleksandra Radjenovic, PhD,[2] John P. Greenwood, PhD,[2] John P. Ridgway, PhD.[1] ***[1] Leeds Teaching Hospitals NHS Trust, Leeds, United Kingdom, [2] University of Leeds, Leeds, United Kingdom.***

Synopsis: Myocardial perfusion may be characterised semi-quantitatively by the maximum upslope of a time-intensity curve representing the arrival of contrast agent in a region of interest. Imprecision in upslope data values will reduce the utility of the associated myocardial perfusion reserve index (upslope MPRI), from which hypoperfusion can be indicated (1). In this work, variation of precision in upslope data values is simulated, and a limit on the variation of precontrast baseline data values is made. By choosing an acceptable upslope MPRI error magnitude, the signal-to-noise ratio (SNR) of a ROI mean value (not image SNR) from a series of images without contrast agent may be calculated. It is envisaged that minimum native myocardial

image SNR levels may then be determined and used in this imaging context in future pulse sequence design and optimization.

Methods: Noise was introduced to clean simulated upslope data sets (Y^{clean}). Noise was added to Y^{clean} according to:

$$Y^{noisy} = Y^{clean} + \left(\left(Y_0^{clean}/SNR_i\right) \cdot rand\right) \quad [1]$$

where *rand* is a random number and Y_0^{clean} represents the first upslope data point. The coefficient of variation (CoV) of upslope gradients was determined from repeated cycles of the noise addition and fitting process for each data set.

Perfusion may be defined as abnormal if the absolute local MPRI is ≥ 0.3 below the maximum upslope MPRI in the same imaging slice (1). By defining an acceptable error in this MPRI difference threshold value (e.g., arbitrarily, 10%), the uncertainty in the maximum MPRI and local MPRI may be defined. Thus, the corresponding maximum acceptable standard deviation of the MPRI difference is 0.03, and the uncertainty in each MPRI estimate must be less than 0.0212. Since local MPRI values are likely to be greater than 0.95 (1), the maximum CoV limit of each upslope value (stress and rest) may then be calculated to be 1.6%. Hence, a maximum CoV limit in upslope values of 1.6% will restrict the error in the MPRI difference threshold value to 10%. Working backwards from the maximum upslope CoV limit, required ROI-mean-value SNR values may be deduced.

The ROI-mean-value SNR limit was assessed in a recent myocardial perfusion pulse sequence which yielded a high diagnostic accuracy in the detection of coronary artery disease by purely visual assessment (2). Data sets from ten patients presenting sequentially were assessed, using ten images from the dynamic series immediately before injections of contrast agent.

Results and Discussion: The SNR of a ROI mean value obtained from a series of baseline images (without contrast agent) must be 46 or greater if 3 upslope data values are used, 30 or greater if 4 upslope data values are used, and 22 or greater if 5 upslope data values are used. The CoV of ROI-mean-values of subendocardial and subepicardial segments is well over the threshold of 1.6%. Taking an average of the ROI-mean-value SNR values yielded 7.2% (basal), 4.8% (mid), 4.7% (apical) prior to the first contrast injection, and 5.4% (basal), 3.9% (mid), 3.6% (apical) prior to the second contrast injection. These data indicate that noise variation in the mean values of ROIs drawn in these segments using this particular pulse sequence will result in significant error propagation into an upslope MPRI estimate (with respect to the chosen acceptable error value). This method may be similarly applied to other pulse sequences. It accommodates choice of myocardial segmentation model, pulse sequence parameters and cardiac analysis software.

REFERENCES

1. Thiele H, et al. Int J Cardiovas Imag 2004;20:371–84.
2. Plein S, et al. Radiology 2005;235:423–30.

317. THE BIPLANE AREA-LENGTH METHOD OVERESTIMATES LEFT ATRIAL VOLUMES IN CARDIOMYOPATHY

Lucy E. Hudsmith, MA, MRCP, Yaso Emmanuel, MRCP, Jane M. Francis, Steffen E. Petersen, Dphil, MD, Kieran Clarck, PhD, Hugh Watkins , PhD, MD, FRCP, Stefan Neubauer, MD, FRCP. ***Oxford University , Oxford, United Kingdom.***

Introduction: Increasing atrial size is correlated to the risk of developing atrial fibrillation, and the development of atrial fibrillation is responsible for symptoms and heart failure in a number of cardiomyopathy patients. We aimed to investigate the use of the biplane area-length method of left atrial assessment in comparison to the short-axis method in cardiomyopathy patients without atrial arrhythmias or significant regurgitation compared with age and sex-matched healthy volunteers.

Method: Twenty-four patients with cardiomyopathy (mean age 43 ± 15 years, 18 male, 14 with hypertrophic cardiomyopathy, 5 with dilated cardiomyopathy and 5 with left ventricular noncompaction, mean blood pressure 120 ± 15/74 ± 13 mmHg) with no history of atrial arrhythmias or significant mitral regurgitation were recruited. Eleven age-matched healthy volunteers (mean age 35 ± 8 years, 8 male, mean blood pressure 118 ± 9/70 ± 9 mmHg) with no history of cardiac disease, hypertension, cardiac risk factors and normal left ventricular volumes and function on CMR were also recruited.

All CMR examinations were performed using a 1.5 T (Sonata, Siemens) MR with retrospective ECG-gating. After piloting, steady-state free precession (SSFP) cine images (TE/TR 1.5/3.0 ms, flip angle 60°, slice thickness 7 mm, 3 mm inter-slice gap, in-plane resolution 1.5 × 1.5 mm^2, temporal resolution 43.7 ms, breathold duration of 14–17 heartbeats per breathold) were acquired in the horizontal and vertical long axis views during breath holding in end-expiration. Atrial slices were then planned parallel to the atrioventricular groove, with the left atrium covered by 4 to 8 slices of 7 mm with an interslice gap of 3 mm.

The left atrial volumes, ejection fraction and stroke volume were measured using both the biplane area-length method in the horizontal and vertical long axes (Fig. 1) and also using the short-axis method. Manual tracing of the left atrial endocardial borders at ventricular end-diastole and end-systole was performed.

Results: Dilated cardiomyopathy patients had reduced left ventricular ejection fraction (53 ± 3%), increased left ventricular end-diastolic and end-systolic volumes (183 ± 32 mL and 87 ± 16 mL, respectively) and hypertrophic cardiomyopathy patients demonstrated hyperdynamic left ventricular ejection fractions (75 ± 8%) and reduced left ventricular volumes (LVEDV 116 ± 28 mLs and LVESV 30 ± 14 mLs). Cardiomyopathy patients had a significantly larger LV mass index, 90 ± 27 g/m^2 vs. 60 ± 10 g/m^2, $p = 0.001$. The left atrial volumes for patients and volunteers measured using the short-axis method were not significantly different (eg, mean maximal left atrial volume patients 88 ± 25 mL vs. cardiomyopathy patients 89 ± 29 mL, $p > 0.05$,

TABLE
Left atrial volumes in cardiomyopathy patients and healthy volunteers

Mean ± SD	Short-axis Maximal volume (mL)	Biplane area-length Maximal volume (mL)	Short-axis Minimal volume (mL)	Biplane area-length Minimal volume (mL)
Cardiomyopathy patients	89 ± 29	118 ± 33	51 ± 20	64 ± 23
Healthy Volunteers	88 ± 25	91 ± 22	40 ± 11	43 ± 11

Table). When comparing the two methods of left atrial analysis, there was no difference in the left atrial parameters measured by either method for the healthy volunteers, $p > 0.05$ for all. However, in the cardiomyopathy patients, the biplane area-length method overestimated the maximal left atrial volume by a mean value of 29 mL (short-axis 89 ± 29 mL vs. biplane area-length 118 ± 33 mL, $p < 0.001$), the minimal left atrial volume by a mean value of 13 mL (51 ± 20 mL vs. 64 ± 23 mL, $p < 0.001$) with a trend to overestimate the left atrial ejection fraction in comparison to the short-axis method, $p = 0.05$.

Conclusion: There was no difference in the short-axis left atrial volumes between cardiomyopathy patients and healthy volunteers. In healthy volunteers, the short-axis and biplane area-length method resulted in similar left atrial volumes. However, the biplane area-length method overestimates the left atrial volumes and function in cardiomyopathy patients without a history of atrial fibrillation. These overestimations may reflect a combination of pathophysiological remodelling changes of diastolic dysfunction, larger left atrial appendages and pulmonary veins (difficult to separate from LA volumes) in cardiomyopathy patients and valvular regurgitation. We would recommend the use of the short-axis method of left atrial assessment in all patients, albeit with a slightly longer acquisition and analysis time to optimise accuracy of parameters.

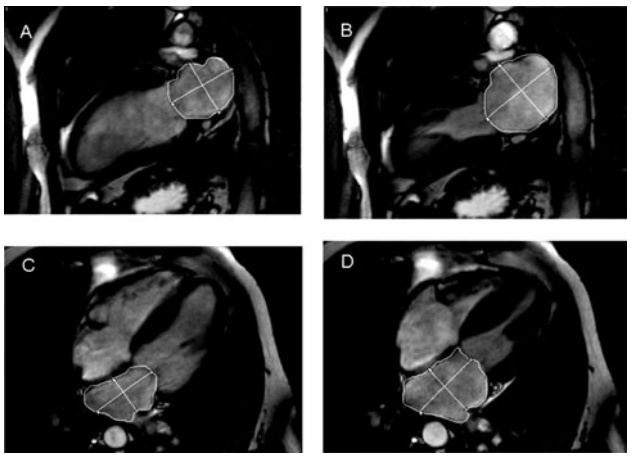

FIG. 1.

318. DETAILED ANALYSIS OF MYOCARDIAL MOTION IN HEALTHY VOLUNTEERS USING HIGH TEMPORAL RESOLUTION MR TISSUE PHASE MAPPING

Bernd A. Jung,[1] Jürgen Hennig,[1] Daniela Föll.[2] [1]*University Hospital, Department of Radiology, Freiburg, Germany,* [2]*University Hospital, Department of Cardiology, Freiburg, Germany.*

Introduction: Magnetic resonance high temporal resolution Tissue Phase Mapping (TPM) allows for a quantitative myocardial motion analysis without limitations to certain ventricular regions such as in Tissue Doppler Imaging (1). TPM measurements with 3D velocity encoding were performed in healthy volunteers in 2 different age groups. Global and regional motion patterns were analyzed in order to determine whether different age groups demonstrate changes in myocardial velocities.

Methods: Measurements were performed on a 1.5 T Siemens Sonata. TPM images were acquired with a black blood prepared gradient echo sequence (TR = 6.9 ms; temporal resolution 13.8 ms; spatial resolution 1.3 × 2.6 mm; *venc* = 15 cm/s in-plane, 25 cm/s through-plane) with prospective ECG-gating, an advanced navigator gating (2), view sharing, and first-order flow compensation. Three slices (8 mm thickness) in short axis view (basal, midventricular, apical) were acquired in 16 healthy volunteers that were subdivided in 2 different age groups (age 40 y:N = 6, mean 55 y). The mean scan time was about 5 minutes per slice.

Data postprocessing include contour segmentation, correction for translational motion components and a transformation of the measured in-plane velocities to radial and circumferential velocities as well as global velocity time courses. To avoid temporal jitter, the temporal axis was normalized. Diastolic peak velocities and time to peak were determined. To analyze local differences in left ventricular performance, a ROI analysis was performed according to the 17 segment model. Mean velocities were calculated to generate regional velocity time courses in 6 basal, 6 midventricular and 4 apical regions.

Results: Fig. 1 shows time courses of global longitudinal velocities averaged over the younger volunteer group (pink, with standard deviations) and averaged over the older volunteer group (blue). A significant difference (t-test; $p < 0.05$) in all slice locations in diastolic peak velocities as well as in time to diastolic peak was revealed between the two different age groups of volunteers. Fig. 2 shows the evolution of regional radial velocities averaged over the younger volunteer group in the 6 basal and 6 midventricular ROIs. Systolic velocity time courses are similar in all segments (except for the amplitudes), whereas motion patterns during diastole exhibit considerably different local ventricular expansion in segments within a single slice and between different slices. Notably, the septum demonstrates highly complex motion patterns, especially in the basal slice where much

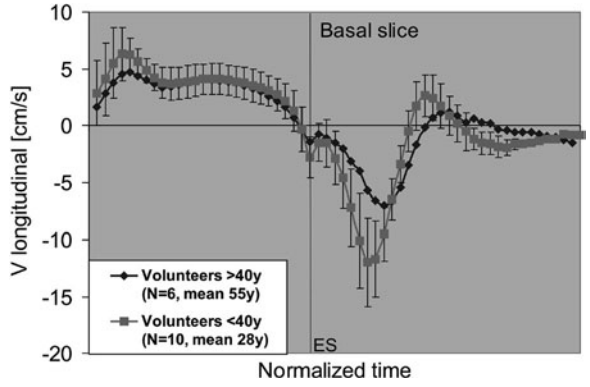

FIG. 1.

lower peak velocities occur, indicating distinct differences in regional expansion behavior. The early diastolic bi-phasic pattern (arrow 1) can be observed in all ROIs but with different amplitudes. An overshoot after the rapid relaxation during diastole similar to the longitudinal velocities can be observed in anterior and inferolateral regions of the midventricular slice (arrow 2). ES=end-systole.

Discussion: TPM is a comprehensive modality for the assessment of regional wall motion with a temporal resolution comparable to Tissue Doppler Imaging (TDI), revealing LV dynamics that are only known from TDI measurements such as the small biphasic wave during early diastole. The age related changes in the diastolic expansion behavior indicate the importance of age matched studies and show the potential to provide valuable information in the evaluation of global and regional function in cardiac pathologies, e.g., in patients with diastolic dysfunction (3, 4). A clinically valid reference standard requires a larger data base from at least 3different age groups to permit a correlation of global and local motion patterns between age-matched volunteers and patients with potentially disturbed myocardial motion.

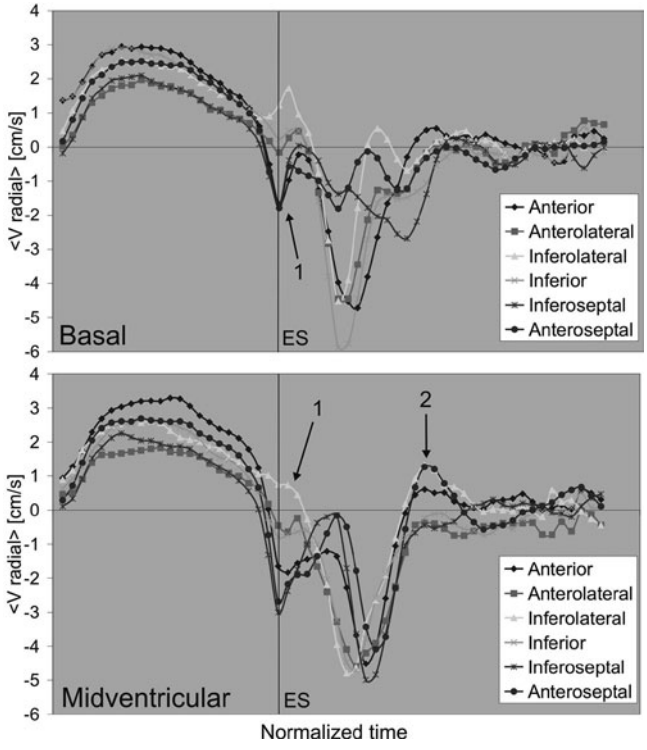

FIG. 2.

REFERENCES

1. Jung, et al. J Magn Res Imaging 2007; in press.
2. Jung, et al. Magn Res Med 2005;55:937–42.
3. Garcia-Fernandez, et al. Eur Heart J 1999;20:496–505.
4. Nagueh, et al. Circulation 2001;104:128–30.

319. CORONARY ARTERY EVALUATION IN CREST SYNDROME AND IN SYSTEMIC SCLEROSIS USING MAGNETIC RESONANCE ANGIOGRAPHY

Sophie Mavrogeni,[1] Theodora Karagiorga,[2] Menelaos Manousakis,[2] Marouso Douskou,[3] Sotirios Plastiras,[2] George Tzelepis,[2] Panagiotis Vlachogiannopoulos,[2] Dennis V. Cokkinos,[1] Haralambos Moutsopoulos.[2] [1]*Onassis Cardiac Surgery Center, Athens, Greece,* [2]*Department Pathophysiology, Athens University, Athens, Greece,* [3]*Bioiatriki MRI Unit, Athens, Greece.*

Introduction: Systemic sclerosis manifests with 2 major entities: limited (calcinosis, Raynauds's phenomenon, esophageal dysfunction, sclerodactyly and telangiectasia known as CREST syndrome) and diffuse (SSc). The aim of this study was to evaluate the morphology of the coronary vessels in these two subsets using coronary magnetic resonance angiography (CMRA).

Patients and Methods: Five patients with CREST syndrome and 5 patients with SSc, without cardiac symptoms and with normal routine cardiac examination, were studied by CMRA, and their results were compared with 5 controls. The maximal diameter of the proximal 1/3 of each coronary vessel was recorded. CMRA was performed using a 1.5 T system with ECG-gating, data acquisition during mid-diastole and patient free-breathing technique.

Results: CREST syndrome patients had dilated coronaries compared to controls ($p < 0.001$ for both LAD and RCA). SSc patients were not significantly different from controls. CREST patients had dilated coronaries compared to SSc ($p < 0.03$ for LAD and $p < 0.005$ for RCA). Criteria for coronary artery ectasia (dilatation of an arterial segment to a diameter at least 1.5 that the adjacent normal artery) were fulfilled by 4/5 CREST syndrome patients. All LCx measurements were within normal (Table 1).

Conclusion: Coronary ectasia appears a common finding in CREST syndrome, but not in SSc. MRA assessment can be useful in the noninvasive coronary evaluation of these patients.

TABLE 1
Coronary vessel diameters in patients and controls

Cor. vessel	CREST	SSc	CONTROLS
LAD (mm)	5.03 ± 1.73	3.02 ± 0.40	3.05 ± 0.15
RCA (mm)	5.02 ± 1.24	2.86 ± 0.29	3.17 ± 0.20
LCx (mm)	2.94 ± 0.67	2.40 ± 0.41	3.08 ± 0.19

320. COMPREHENSIVE VALVULAR EVALUATION SYSTEM

Juan M. Santos, PhD,[1] Adam B. Kerr, PhD,[1] Bob S. Hu, MD,[2] John M. Pauly, PhD.[1] [1] *Stanford University, Stanford, California, USA,* [2] *Palo Alto Medical Foundation, Palo Alto, California, USA.*

Introduction: Valvular heart disease affects approximately 10% of patients with heart disease in the United. Over the past 20 years, noninvasive valvular diagnosis has undergone a revolution due to advances in cardiac ultrasound. However, ultrasound has inherent limitations with respect to tissue characterization, spatial resolution, and the need for acoustic windows. Particularly challenging are the quantitation of valvular stenosis, quantitation of valvular regurgitation, and the accurate evaluation of valvular morphology.

The examination of valvular heart disease includes the assessment of valvular morphology, cardiac output, intracardiac pressures, ventricular volume and volume regurgitations. Magnetic resonance imaging (MRI) is potentially the most appropriate technique for addressing all of these areas in a single examination. We have designed an MRI subsystem that seamlessly integrates most of the capabilities needed for a comprehensive valve evaluation.

*Methods:*We have previously developed a real-time interactive system (1) that allows for rapid switching (in one TR) and interleaving completely different pulse sequences. Under this platform, we implemented a high frame rate continuous real-time acquisition (9–12 fps) using SSFP and GRE contrast for evaluation of aperiodic valve motion. Valvular morphology is imaged using a double inversion cardiac gated black blood technique with 16 spiral interleaves. As localization is critical, the real-time acquisition is used to precisely prescribe the view of interest and within one TR the system can start acquiring the high-resolution images. To evaluate valvular regurgitation, we have implemented a color flow sequence (2). This is a real-time phase contrast sequence that can acquire a full frame at a rate of 6 fps. The images are then reconstructed at 20 fps.

Intracardiac flow velocities are evaluated using a real-time velocity spectra or MR Doppler sequence (3) where the MR signal is restricted to a 2D cylinder. The cylinder is then resolved in both velocity and along its length using an oscillating readout gradient. A measurement can be obtained every 25 ms, and different range of velocities can be resolved depending on the readout trajectory.

One of the aims in the design of this system is to be comparable with cardiac ultrasound. A typical procedure is to first locate the anatomy with the real-time sequence. Then, color flow is activated to precisely scout for the areas were flow is to be

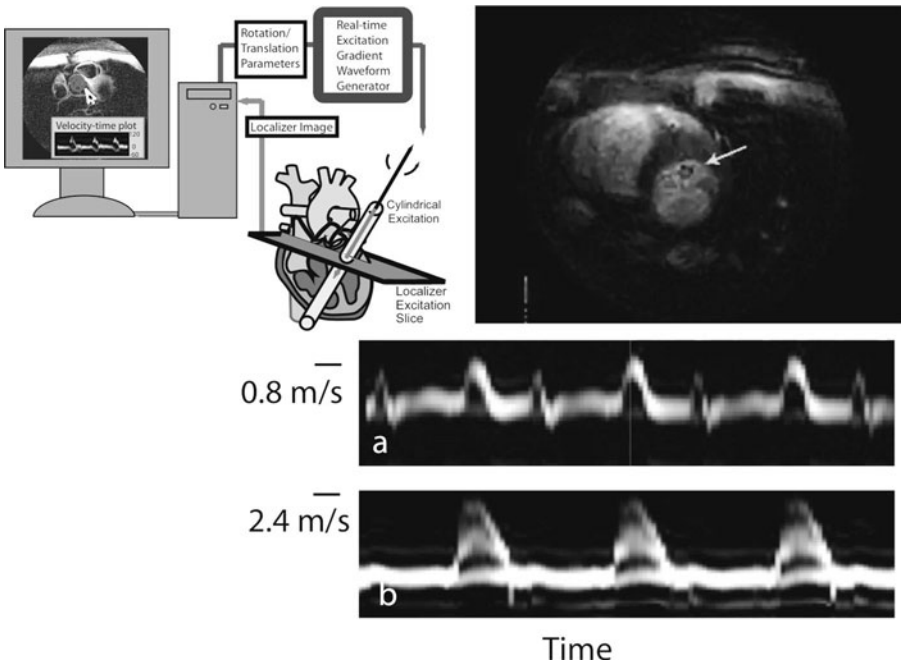

FIG. 1. A real-time user interface allows for rapid and precise prescription of the CMR Doppler excitation based on a localizer or real-time color-flow sequence. The real-time color-flow image shows regurgitation through the aortic valve. The real-time CMR Doppler waveforms show flow through the mitral and aortic valve on a patient with moderate stenosis.

measured. Finally, MR Doppler can be activated over the color flow images, which can then be stopped for better velocity spectra temporal resolution. The top-left of Fig. 1 shows a diagram of how the system operates.

*Results and Discussion:*Three patients and 4 volunteers were evaluated with this system. For all the cases, anatomical information was obtained in real-time. Then color flow and MR Doppler were used to obtain flow information. Fig. 1 shows a color flow image in the aortic valve plane with through-plane flow encoding. The arrow shows the regurgitation through the valve. Using the MR Doppler technique, Fig. 1 shows the waveforms from the mitral (top) and aortic valve (bottom) of a patient with moderate stenosis.

These preliminary studies have shown that this system is capable of rapidly and accurately identifying clinically significant valve regurgitation and stenosis.

REFERENCES

1. Santos J, et al. IEEE EMBS Conf, 1048, 2004.
2. Nayak KS, et al. MRM 2000;43:251–58.
3. DiCarlo JC, et al. MRM 2005:54:645–55.

321. SAFETY OF MAGNETIC RESONANCE IMAGING IN CHILDREN WITH PACEMAKERS

Licheng Lee, William A. Scott, Ilana J. Zeltser, Elizabeth A. Brantley, Reenu S. Eapen. ***University of Texas-Southwestern Medical Center, Dallas, Texas, USA.***

Background: Magnetic resonance imaging (MRI) is an important tool for diagnosis and management in pediatrics. Cardiac pacemakers and defibrillators (ICDs) have traditionally been considered a contraindication to MRI given the potential risks of device dysfunction, cardiac injury, or arrhythmias. The objective of this study was to assess dislodgement or damage to pacemaker leads and generators secondary to MRI and to evaluate the incidence of arrhythmias secondary to programmable changes associated with exposure to a magnetic field.

Methods: We performed a retrospective chart review of all patients with cardiac pacemakers and ICDs who required a noncardiac MRI for diagnosis and management of extracardiac disease from 1999 to 2006. All patients undergoing MRI had their devices interrogated immediately before and after the MRI. In addition, they were monitored by a pacemaker specialist for any adverse events during the scan. Sensing and stimulation thresholds, current, pulse amplitude, sensitivity, pulse width, lead impedance, and battery voltage were recorded.

Results: Eighteen head MRI studies were performed on patients with devices: 7 DDD, 10 VVI, and 1 AAI. One ICD patient had the defibrillator function deactivated during the MRI. There were no significant differences between atrial and ventricular pacemaker parameters following MRI (Yates, p value $= 0.37$). Changes in lead impedance, sensing parameters, and threshold testing were not significant and did not require reprogramming of devices after the MRI. Premature ventricular contractions were noted during 1 of 18 studies (5%). Asynchronous pacing was noted during exposure to the magnetic field in 5 of 18 studies (28%) without any inducible arrhythmias.

Conclusions: Noncardiac MRI studies can be performed in pediatric patients with pacemakers and ICDs without adverse events. The integrity of the device system remains intact. However, asynchronous pacing triggered by the magnetic field mandates that these studies be performed under close supervision.

322. IMPACT OF THE EXTENT OF DELAYED ENHANCEMENT ON SEGMENTAL AND GLOBAL SYSTOLIC FUNCTION IN PATIENTS WITH ACUTE MYOCARDITIS AND ACUTE MYOCARDIAL INFARCTION

Oliver Bruder,[1] Peter Hunold,[2] Markus Jochims,[1] Christoph Jensen,[1], Georg Sabin,[1] Joerg Barkhausen.[2] ***[1]Department of Cardiology, Elisabeth Hospital, Essen, Germany, [2]Department of Diagnostic and Interventional Radiology and Neuroradiology University Hospital, Essen, Germany.***

Background: Acute myocardial infarction and acute myocarditis are associated with impaired contractile function. Although, the area of myocardial dysfunction is typically larger than the area of myocardial infarction, several studies have demonstrated that the extent of MI defined by delayed enhancement is inversely proportional to the regional myocardial dysfunction. However, in patients with acute myocarditis, the relationship of myocardial damage defined by delayed enhancement and function is less clear.

Objectives: Our study aimed to investigate the impact of the transmural extent of delayed enhancement (DE) on regional and global left ventricular function in patients with acute myocarditis and acute myocardial infarction.

Methods: The study was performed in accordance with the regulations of the local institutional review board, and only patients without contraindication to MRI were included. In an 18 month period, 22 consecutive patients (8 females, 14 males, mean age 36.9 $\pm$ 15.9 y) with acute myocarditis defined by clinical criteria and delayed enhancement on CMR as well as 43 patients (7 females, 35 males, mean age 59.3 $\pm$ 11.7 y) with first acute myocardial infarction were enrolled. All infarct patients underwent successful primary percutaneous coronary intervention (PCI) with restoration of TIMI grade 3 flow. All examinations were performed on a 1.5 T scanner (Magnetom Sonata, Siemens Medical Solutions, Erlangen, Germany). The imaging protocol included SSFP Cine sequences (TR 3ms, TE 1.5ms, FA 60°) in contiguous short-axis views covering the entire left ventricle from the atrioventricular ring to the apex using a segmented steady-state free precession (SSFP) sequence and

delayed enhancement imaging in corresponding slices following injection of 0.2 mmol/kg of gadodiamide (GE Healthcare Buchler, Munich, Germany) using a segmented 2D inversion recovery fast low angle shot (IR-FLASH) sequence (TR 8 ms, TE 4 ms, FA 25°, 1.4 × 1.8 mm in-plane resolution). All images were analyzed by two blinded observers (radiologist/cardiologist) in consensus using the AHA/ACC recommended 17 segment model. Regional wall motion (WM) for all segments was assessed on a five point scale (0 = normal, 1 = mild hypokinesis, 2 = moderate to severe hypokinesis, 3 = akinesis, 4 = dyskinesis). The transmural extent of DE was analyzed qualitatively as follows: 0%, 1–25%, 26–50%, 51–75%, 76–100% of total wall thickness. Total DE volumes were calculates based on manual planimetry.

Results: Three hundred seventy-four myocardial segments (22 patients × 17 segments) in the myocarditis group and 761 segments (43 patients × 17 segments) in the infarct group were analyzed. In the myocarditis group, 35% of patients with DE showed normal WM, whereas only 12% of patients with DE caused by acute myocardial infarction demonstrated normal WM ($p < 0.05$). In patients with acute MI, there was a close correlation between DE scores and WM scores $r = 0.72$ as well as between the total volume of DE and the ejection fraction $r = 0.67$ in contrast to a weak correlation only ($r = 0.43$, respectively $r = 0.52$) in patients with acute myocarditis.

Conclusions: In contrast to the linear relationship of DE and dysfunction in acute myocardial infarction, the impact of delayed enhancement on regional wall motion abnormalities is less obvious in patients suffering from acute myocarditis. Possible explanation for this effect include the more patchy pattern of necrosis in myocarditis compared to the uniform "wavefront" of necrosis in myocardial infarction and a disproportional role of the subendocardial myocardium, which is always involved in acute MI but frequently spared out in myocarditis, for overall regional wall thickening.

323. NON-MODEL BASED CORRECTION OF RESPIRATORY MOTION USING BEAT-TO-BEAT 3D SPIRAL FAT-SELECTIVE IMAGING

Jennifer Keegan, PhD,[1] Peter Gatehouse, PhD,[1] Guang-Zhong Yang, PhD,[2] David Firmin, PhD.[1] [1]***Royal Brompton Hospital, London, United Kingdom,*** [2]***Imperial College, London, United Kingdom.***

Introduction: The most recent approach to dealing with respiratory motion has been to develop subject-specific motion models which have enabled the use of extended navigator acceptance windows (1, 2). This approach relies on the acquisition of a calibrating prescan to determine the model which may become inaccurate if the respiratory pattern changes during the subsequent scans. An alternative approach would be to acquire a low resolution 3D dataset in each cardiac cycle, immediately prior to the acquisition of each data segment contributing to the high resolution image, and use beat-to-beat correlation of these low-resolution datasets to determine the beat-to-beat respiratory motion which could be corrected for in postprocessing (3).

Purpose: To determine the feasibility of nonmodel based beat-to-beat correction of respiratory motion for coronary vessel wall imaging.

Methods: This work was carried out on a Siemens Sonata 1.5Tesla scanner. *Data acquisition*: A high resolution (true res: 0.8 × 0.8 × 3 mm; reconstructed: 16 × 1.5 mm slices, 0.4 × 0.4 mm) 3D spiral black-blood scan of the right coronary artery was acquired over 160 cardiac cycles without respiratory gating in 6 healthy volunteers. One spiral interleaf was acquired per cardiac cycle (acquisition window 20 ms), prior to each of which, a complete low resolution fat-selective 3D spiral dataset (true res: 6 × 6 × 3 mm; reconstructed 16 × 1.5 mm slices, 3 × 3 mm) was acquired (acquisition window 160 ms). Each low resolution dataset was used as a marker of the heart position for the high resolution interleaf that followed immediately after. A following diaphragmatic navigator was also implemented, purely for monitoring purposes. *Data processing:* The respiratory motion (3D translation) on each cardiac cycle was determined by cross-correlating a region of interest in the fat around the artery in the low resolution datasets with that on a reference end expiratory dataset. The measured translations were then used to correct the raw data of the high resolution spiral interleaf acquired immediately after. The images obtained were compared with those using a fixed superior-inferior tracking factor of 0.6 (as used conventionally) and with those obtained using a retrospective 3D translation model. For this model, the x, y and z linear tracking factors were determined as the slopes of the plots of the x, y and z translations measured in the low resolution datasets against the diaphragm displacements, as measured by the following navigator.

Results: Example results are shown in Fig. 1, the data here being acquired over a 25 mm range of diaphragm motion (100%

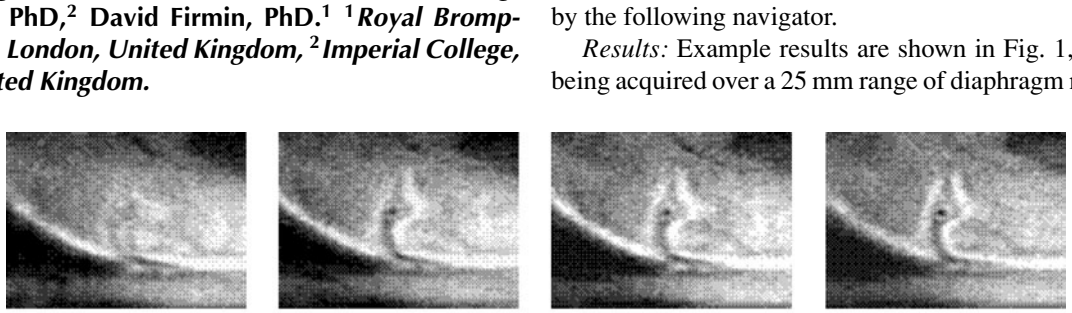

FIG. 1. Example images acquired over 25 mm of diaphragm motion (100% efficiency) with various methods of respiratory correction.

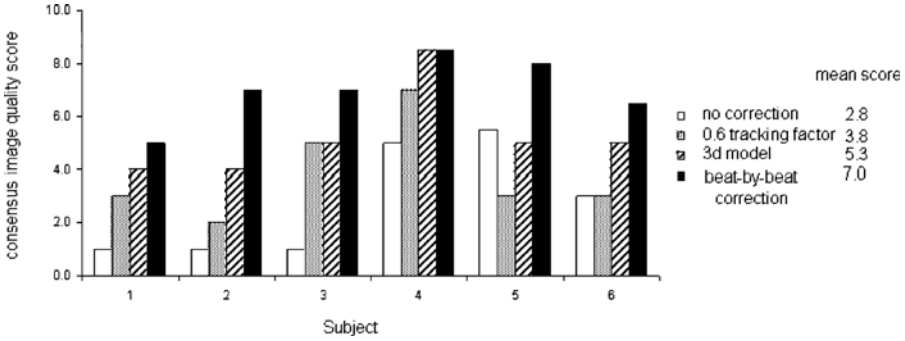

FIG. 2. Mean image quality scores (as assessed by 2 independent observers) in each of 6 subjects. Images were acquired over the full range of respiratory motion.

respiratory efficiency). Beat-to-beat correction provided consistently good results, the image quality being better than that obtained with a fixed superior-inferior tracking factor of 0.6 (as is used conventionally) and better than (N = 5) or equal to (N = 1) that achieved using a subject-specific retrospective 3D translation motion model, as shown in Fig. 2.

Conclusion: Determination of the translational components of respiratory motion by tracking fat-excitation 3D images from beat to beat appears to be feasible. This has allowed high quality images of the right coronary artery vessel wall to be generated during free-breathing with 100% respiratory efficiency, without the need to determine a respiratory motion model. In this small group of healthy volunteers, the image quality obtained was better than that using a retrospective 3D translation motion model. Future work will focus on improving the image correlation process, allowing more complex motion (such as affine transformations) to be accounted for, and performing a full comparative study against navigator-based techniques.

REFERENCES

1. Manke, et al. Magn Reson Med 2003.
2. Nehrke, et al. Magn Reson Med 2005.
3. Korin et al. Radiology 1990.

324. EFFICIENT T_1 MAPPING OF THE HEART USING AN INTERLEAVED LOOK-LOCKER ACQUISITION WITH SATURATION RECOVERY

Glenn S. Slavin, PhD, Sandeep N. Gupta, PhD. ***Applied Science Lab, GE Healthcare, Bethesda, Maryland, USA.***

Introduction: Myocardial delayed enhancement (MDE) using inversion-recovery (IR) segmented gradient-echo (GRE) imaging is currently used for differentiating infarcted and normal myocardium. Infarct sizing is difficult because the size of the hyperenhanced infarcted region is dependent on the inversion time (TI) and the delay after contrast injection. An alternative to MDE, which may eliminate the need for contrast agents, is T_1 mapping. T_1 mapping is typically performed with IR, which requires 4–5 times the T_1 for magnetization to recover to equilibrium before the next excitation. Because T_1 of normal myocardium is approximately 900 ms at 1.5 T, this makes high-resolution breath-hold imaging challenging. A recent study (1)has demonstrated a modified Look-Locker (LL) (2) method that allows T_1 mapping in a single breath-hold. However, because the method included 8 dummy heartbeats for magnetization recovery during the 17 heartbeat scan, efficiency was significantly compromised. The purpose of the present work was to evaluate a more efficient modified-LL acquisition using saturation recovery (SR) for T_1-based mapping of the heart.

Methods: Two patients with myocardial infarctions were imaged on a 1.5 T GE Signa CV/i scanner. The pulse sequence shown in Fig. 1 is based on the MOLLI technique (1) and employs 3 LL imaging blocks, consisting of 2, 2, and 4 heartbeats, each. However, unlike traditional LL sequences, SR is used rather than IR. This offers several benefits: it obviates

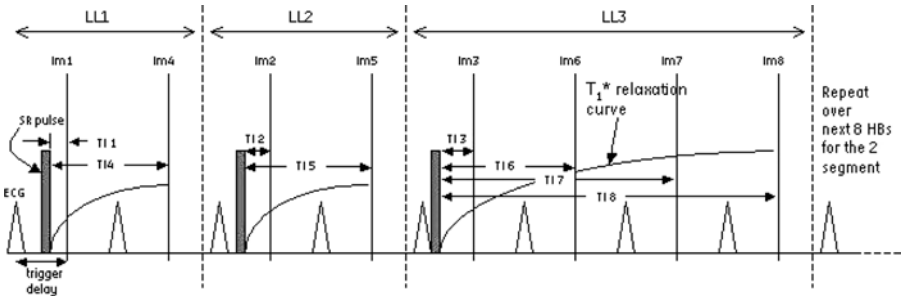

FIG. 1.

dummy heartbeats used for magnetization recovery, while still allowing T_1 measurement; fewer data points should be required to sample the saturation-recovery curve; and it eliminates the need to identify the signal polarity during image analysis.

A two-segment balanced SSFP sequence was used for readout. After the first ECG trigger, a nonselective saturation pulse is played out, and one half of k-space is acquired after a TI of 100 ms. After the second ECG trigger, no saturation pulse is played out, and data is acquired at the same trigger delay time, providing a TI = 100 + RR ms, where RR is the duration of the cardiac cycle. On the third and fourth heartbeats, data is acquired at TIs of 200 and 200 + RR ms, respectively. On the fifth through eighth heartbeats, data is acquired at TIs of 300, 300 + RR, 300 + 2RR, and 300 + 3RR ms, respectively. Eight additional heartbeats are used to acquire the second half of k-space. Imaging was performed with the following parameters: TE/TR 1.5/3.6 ms, 45° excitation, 256 × 160 matrix, $^1/_2$NEX, 36 × 27 cm FOV, 38 VPS, 8 mm slice, 350 ms trigger delay, 137 ms acquisition window, 8 pulse linear-flip-angle steady-state preparation. Total scan time was 16 heartbeats. Apparent T_1 (T_1*) was calculated using nonlinear least-squares curve fitting to the equation A-B exp($-t/T_1$*).

Discussion: Figure 2 shows an MDE image (left) and the corresponding overlaid pixel-wise map of left-ventricular myocardial T_1* (right). This semi-quantitative map provides clear differentiation between ROIs in normal (T_1* = 407) and infarcted (T_1* = 233) myocardium and agrees well with the MDE image. However, it is necessary to obtain the true T_1 from T_1* by removing the effects of the SSFP imaging process, as has been done for GRE imaging (3). Messroghli (1) used this GRE-based method of T_1 calculation for their SSFP-based acquisition; however, it is unclear if this was an appropriate approach. The solution for T_1 in (3)assumes a flip angle < 10° and is based specifically on the equations for spoiled GRE imaging, which differ substantially from those for balanced SSFP.

This work has presented an efficient saturation-recovery-based, modified-LL method for myocardial T_1 mapping.

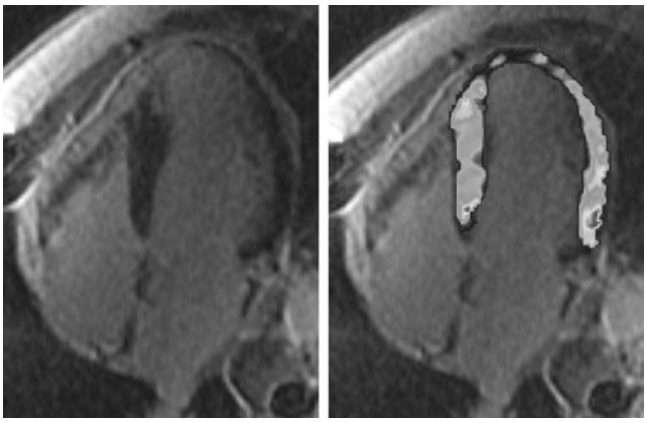

FIG. 2.

REFERENCES

1. Messroghli DR. MRM 2004;52:141.
2. Look DC. Rev Sci Instrum 1970:41:250.
3. Deichmann R. JMR 1992;96:608.

325. ALTERED PAPILLARY MUSCLE MORPHOLOGY RESULTS IN INCREASED LEFT VENTRICULAR OUTFLOW TRACT OBSTRUCTION IN HYPERTROPHIC CARDIOMYOPATHY

Deboarh Kwon, MD, Randy M. Setser, PhD, Maran Thamilarasan, MD, Paul Schoenhagen, MD, Zoran Popovic, MD PhD, Nicholas Smedira, MD, Mario MD J. Garcia, MD, Harry Lever, MD, Milind Y. Desai, MD. ***Cleveland Clinic Foundation, Cleveland, Ohio, USA.***

Introduction: Morphologic alterations (including apical insertion) of papillary muscles (PM) in patients with hypertrophic cardiomyopathy (HCM) can potentially contribute to left ventricle outflow tract (LVOT) obstruction. While doppler echocardiography can accurately assess the physiologic aspects of LVOT obstruction, magnetic resonance imaging (MRI) can better characterize morphologic aspects of HCM (including PM anatomy) because of its ability to image in multiple planes.

Purpose: The purpose of this study was to assess the prevalence of morphologic alterations of PM in HCM patients and assess if such PM alterations result in significant left ventricle outflow tract (LVOT) obstruction.

Methods: Fifty-six consecutive patients (mean age 42 [interquartile range 27, 51] years, 70% males) and with echo-confirmed HCM and 30 consecutive controls (no documented HCM, mean age (42 interquartile range 30, 53 years, 80% males) underwent MRI on 1.5T scanner (Siemens, Erlangen, Germany). For assessment of papillary muscle morphology, cine images, using a balanced steady state free precession (TrueFISP) technique with retrospective ECG-triggering [TE = 1.6 ms, TR = 65 ms, flip angle = 70°, slice thickness = 6 mm (long axis images) or 8–10 mm (short axis images), matrix = 256 × 256], were acquired at the following anatomic locations: 3 short axis slices (base, mid ventricle and apex), along with standard 2, 3 & 4 chamber long axis views. Maximal septal thickness was recorded at end-diastole on short axis images. Minimum distance between septum and anterolateral PM was determined in 4 chamber view at end-diastole. Presence of bifid papillary muscle (involving none, one or double papillary muscle) was recorded (Fig. 1). Apical insertion was defined when the PM were displaced distally in 2 or 4 chamber views and visible on the distal-most apical short axis image (Fig. 2). Resting LVOT gradients were recorded by Doppler echocardiography. Resting heart rate (HR) and medication use was also recorded.

Results: Double bifid PM (70%) vs. 17%) and apical PM insertion (77%) vs. 17%) were significantly more prevalent in HCM patients vs. controls ($p < 0.0001$). Mean distance from anterolateral PM to septum (cm) was lower (0.6 [0.38, 0.69] vs.

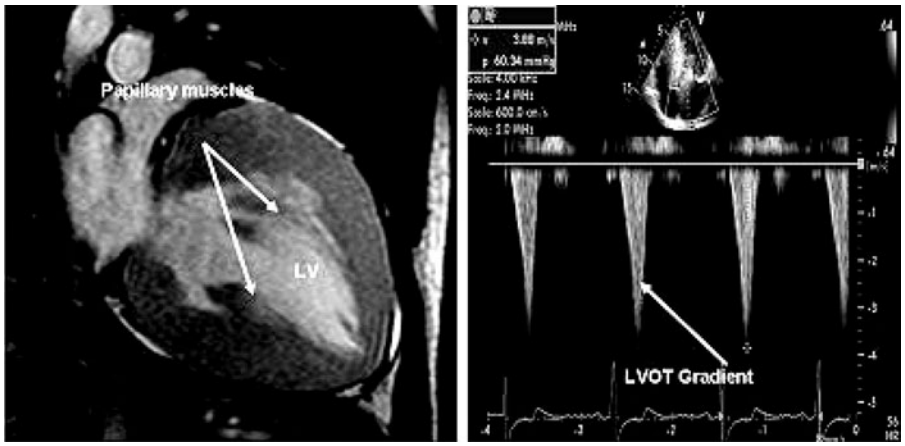

FIG. 1. Bilateral bifid papillary muscles (PM) noted on MRI (left) with corresponding left ventricular outflow tract (LVOT) resting pressure gradient on doppler echocardiography (right).

1.1 [0.9, 1.4]), and septal thickness (cm) was greater (2.3 [1.9, 2.6] vs. 1.2[1, 1.3]) in HCM vs. controls (both $p < 0.001$). HCM patients with apically displaced PM ($p < 0.01$) and double bifid PM ($p = 0.02$) had higher resting LVOT gradient compared to those without (45 [6, 81] vs. 12 [0, 12] mm Hg and 42 [6, 64] vs. 11 [0, 17] mm Hg respectively (Figs. 1 and 2). In HCM patients, both apical displacement & double bifid PM were significantly associated with resting LVOT gradient (both $p < 0.05$) independent of septal thickness. In HCM patients with significant ($\geq$30 mm Hg) resting gradient, using stepwise logistic regression, the odds ratio of having apically displaced PM & double bifid PM were 7.1 and 10.4, respectively ($p < 0.005$); independent of septal thickness, beta-blockers and/or calcium blockers use and HR.

Conclusions: A significant proportion of HCM patients have a high prevalence of altered papillary muscle morphology, i.e., apical displacement or double bifid PM, compared to controls. These alterations are associated with significant resting LVOT gradient, independent of septal thickness and resting HR, likely due to increased slack of anterior mitral leaflet, resulting in exaggerated dynamic systolic LVOT obstruction. Further studies are required to determine if altered PM morphology is independently associated with adverse outcomes and whether an altered surgical technique (which corrects abnormal PM morphology) add incremental value to septal myectomy alone.

326. PERSISTENT MICROVASCULAR OBSTRUCTION AND LEFT VENTRICULAR REMODELING IN REPERFUSED ACUTE MYOCARDIAL INFARCTION: AN EXPERIMENTAL SHORT-TIME COURSE STUDY USING MAGNETIC RESONANCE IMAGING

Yuesong Yang, MD, PhD,[1] John J. Graham, MBChB,[2] Warren D. Foltz, PhD,[3] Alexander J. Dick, MD,[2] Graham A. Wright, PhD.[1] [1]***Imaging Research, Sunnybrook Health Sciences Centre, University of Toronto, Toronto, Onatrio, Canada,*** [2]***Division of Cardiology, Sunnybrook Health Sciences Centre, University of Toronto, Toronto, Ontario, Canada,*** [3]***Division of Cardiology, St. Michael's Hospital, Toronto, Ontario, Canada.***

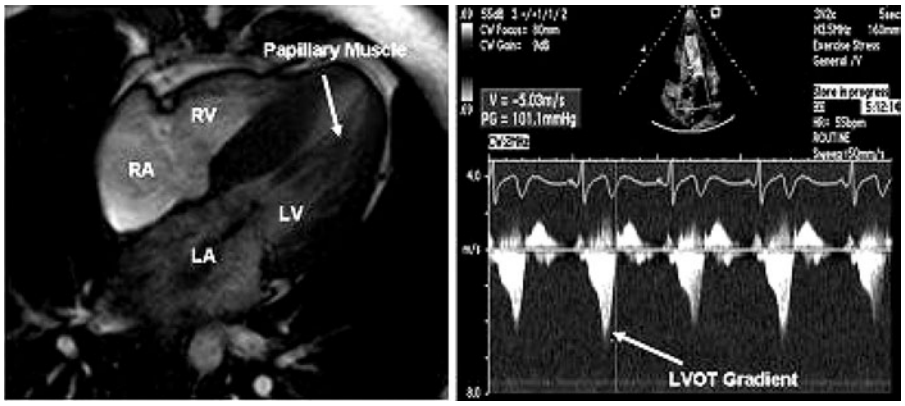

FIG. 2. Apically displaced papillary muscle demonstrated on 4-chamber view on MRI (left) with corresponding left ventricular outflow tract (LVOT) resting pressure gradient on doppler echocardiography (right).

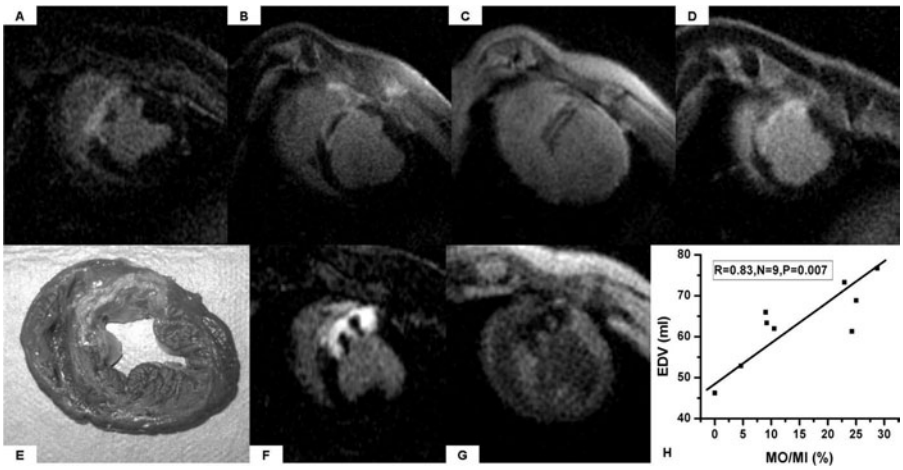

FIG. 1. A–E from the same subject: A. DE-MRI at day 0: MO predominantly in subendocardial region; B-C (DE-MRI and T1 difference images at day 2): MO as a core within the MI region and with an increased volume, D: DE-MRI at day 7: MO vanished; E:TTC stain. F-G (DE-MRI and T1 difference images) from another subject multiple foci of MO. H. Correlation between the relative extent of persistent MO in the infarcted myocardium (% MO/MI) and EDV: the correlatin coefficient was 0.83, n = 9, P = 0.007.

Purpose: This MRI study investigates the varied appearance of persistent microvascular obstruction (PMO) and left ventricular (LV) remodeling in a porcine model of reperfused acute myocardial infarction (AMI) in a short-time course using magnetic resonance imaging (MRI).

Materials and Methods: In 10 Yorkshire pigs (22–28 kg) a reperfused AMI was produced through a 90 minute percutaneous balloon occlusion of the distal left anterior descending coronary artery, followed by reperfusion. After the intervention all pigs underwent an MRI examination on a GE 1.5 T Signa Excite system including a SSFP functional study, first pass myocardial perfusion (FPMP), T1 measurement and delayed hyperenhancement MRI (DE-MRI). A repeated MRI examination was performed in 4 pigs at day 2 and in all of 10 pigs at days 7–9. Upon the completion of MRI examination all pigs were sacrificed for TTC staining and/or histology.

The T1 measurement uses a modified Look-Locker sequence that samples approach to steady state with and without a preceding inversion at the same cardiac phase. In difference images longer T1 values yield bright signal at later points (effectively longer TI). FPMP was obtained immediately after a Gd-DTPA bolus injection (0.2 mmol/kg) followed by a continuous intravenous drip of Gd-DTPA. DE-MRI was performed 30 minutes post-injection and T1 measurement was applied 45 minutes post-injection. The SSFP covered the whole LV. SSFP, FPMP and DE-MRI analyses were conducted using Mass Plus software (Medis). T1 mapping was conducted using Xcinema (Stanford) or Functool 2 (GE Healthcare).

Results: PMO was defined as the persistent hypoenhanced area in the infarcted myocardium in FPMP and DE-CMRI. PMO was identified as bright regions in later T1 difference images. PMO was observed in 9 of 10 pigs. In 1 of these pigs, PMO was identified only at day 2. The other 8 pigs demonstrated a PMO at day 0. Various MR appearances of PMO were noticed on DE-CMRI and T1 difference images ranging from predominance in subendocardial region or a core within the infarcted tissue to multiple distributions (Fig. 1A-G).

The volume of PMO (corresponding to the hypoenhanced region) was measured on DE-MRI images; the volume of infarcted myocardium (MI) was the addition of PMO and delayed hyperenhanced area. There was a trend toward a greater volume of PMO and MI at day 2 in comparison to data from day 0 although the statistical significance was not reached (PMO volume at day 2 vs. day 0: 2.5 ± 1.92 vs. 1.9 ± 1.8 mL; MI volume at day 2 vs. day 0: 10.5 ± 3.3 vs. 9.9 ± 3.5 mL; n = 4). At day 7–9 no PMO could be identified on late DE-MRI and T1 difference images (around 45 minutes postcontrast). However, an increased end-diastolic LV volume (EDV) without changes in end-systolic LV volume (ESV) and LV mass at end-diastolic phase (LVM) was observed in comparison to data from day 0 (EDV: 63.4 ± 9.5 vs. 55.2 ± 9.2 mL, n = 9, p = 0.003; ESV: 42.4 ± 9.9 vs. 41.1 ± 8.4 mL, n = 9, p = 0.62; LVM: 47.7 ± 4.7 vs. 46.7 ± 4.7 g, n = 9, p = 0.37). There was a close correlation between the relative extent of PMO in the infarcted myocardium (% MO/MI) and EDV (Fig. 1H): r = 0.83, n = 9, p = 0.007. All pigs had a reperfused AMI demonstrated by TTC staining and/or histology.

Conclusions: A varied MR appearance of persistent microvasular obstruction was observed on T1 difference and DE-MRI images during a short-time course study of reperfused AMI. The optimal timing to demonstrate the persistent microvasular obstruction might be around two days after reperfused AMI. Negative LV remodeling was closely related to the relative extent of persistent microvasular obstruction within the infarcted myocardium.

REFERENCES

1. Gerber BL, et al. Circulation 2000;101:2734.
2. Hombach V, et al. EHJ 2005;26:549.
3. Yang Y, et al. JCMR 2006;8:118.

327. CMR OF MITRAL ISTHMUS IN ATRIAL FIBRILLATION: IMPLICATIONS FOR ELECTROPHYSIOLOGICAL ABLATION

Justin Lee,[1] Saul Myerson,[1] Jane Francis,[1] Yaver Bashir,[2] Tim Betts,[2] Stefan Neubauer.[1] [1]***University of Oxford, Oxford, United Kingdom,*** [2]***John Radcliffe Hospital, Oxford, United Kingdom.***

Introduction: Atrial fibrillation (AF) prevalence is rising worldwide. Recent changes to joint ACC/AHA/ESC guidelines for AF management incorporate an increasing role for left atrial (LA) ablation (pulmonary vein isolation). Up to 10% of patients undergoing atrial fibrillation ablation develop LA flutter as a consequence. One strategy to prevent or treat this complication is linear ablation at the 'isthmus' between either left (LIPV) or right inferior pulmonary vein (RIPV) and the mitral annulus (MA) to interrupt the flutter circuit. Variations in PV anatomy are common and might also influence the length of the mitral isthmus and the success of linear ablation techniques.

Purpose: To examine the relationship of the inferior PVs to the MA in order to determine the optimum site for mitral isthmus catheter ablation.

Methods: Forty-eightconsecutive patients (mean age 53 $\pm$ 10 years) with AF and structurally normal heart on echocardiography were studied using 3D gadolinium contrast enhanced CMR angiography prior to ablation procedure. TR/TE = 2.8/1.1 ms, resolution = 1.6 $\times$ 1.0 $\times$ 1.0 mm. Siemens Syngo software was used for multi-planar reconstruction to assess pulmonary venous anatomy and measure the shortest distance along the endocardial surface of the left atrium between the MA and the ostium of the inferior PVs.

Results: Figure 1 shows LIPV-MA endocardial distance (3.8 $\pm$ 0.8 cm) is shorter than RIPV-MA (5.0 $\pm$ 1.0 cm). The commonest pattern of veins was 2 left and 2 right sided veins (52%) though left sided common trunk (23%), and right sided accessory vein (23%) were common variants. Compared to the remaining patients, neither variant had significantly different LIPV-MA or RIPV-MA distance.

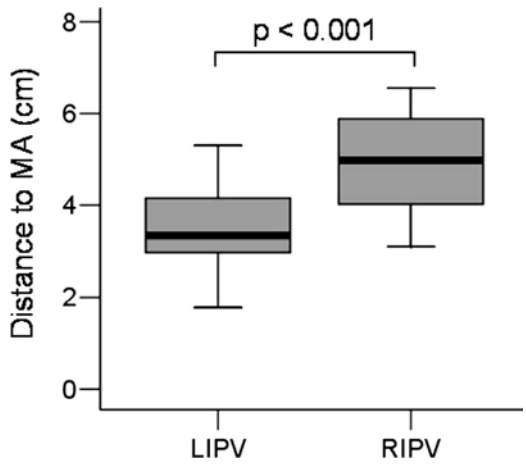

FIG. 1.

Conclusions: The LIPV-MA isthmus is shorter than the RIPV-MA isthmus irrespective of PV pattern and may be the most appropriate site for linear ablation to prevent and treat post-AF ablation LA flutter.

328. VISUAL VERSUS PLANIMETRIC INFARCT SIZE ESTIMATIONS WITH DELAYED ENHANCED CMR: CORRELATIONS WITH BIOMARKERS OF MYOCARDIAL NECROSIS

Nathan Mewton, Sr, MD,[1] Eric Bonnefoy, Sr, MD,[1] Didier Revel, Sr, MD, PhD,[2] Gilbert Kirkorian, Sr, MD, PhD,[1] Pierre Croisille, Sr, MD.[2] [1]***Hopital Cardiologique Louis Pradel, Intensive Care Department, Lyon, France,*** [2]***Hopital Cardiologique Louis Pradel , Radiology Department, Lyon, France.***

Introduction: Delayed enhanced cardiovascular magnetic resonance (DE-CMR) allows the assessment of the extent of myocardial tissue injury after infarction. Different methods are used to define the extent of infarcted myocardium, but there is little knowledge on the performance of the visual segmental scoring method compared to the planimetric evaluation of hyperenhancement for the assessment of infarct extent.

Purpose: In the current study, we assessed the correlation between visual segmental scoring and planimetric evaluation of hyperenhancement in patients with small acute myocardial infarctions (non ST-elevated myocardial infarction or NSTEMI). We also compared acute infarct mass obtained by the two methods with peak troponin I, peak creatine kinase (CK) and the area under curve (AUC) of troponin I and CK releases

Methods: Patients (n = 25) with first acute non ST-elevated myocardial infarction underwent gadolinium DE-CMR 72 hours after infarction. The transmural extent of hyperenhanced myocardium was evaluated by manual planimetry and by visual segmental scoring. By summing all the segmental scores using a 17 segment model, a global index of the size of the infarcted myocardium is easily obtained. The global score was defined as the sum of the scores on each segment and expressed as a percentage of the maximum possible score. This index was compared with the planimetric evaluation, expressed as a percentage of the left ventricle (LV) myocardial volume.

Results: The mean relative infarct size determined by planimetry in our study population was of 8.1 $\pm$ 6.2% of LV.

There was a good correlation between the two methods ($r = 0.9$; $y = 0.83 \times + 1.05$; $p < 0.001$). The Bland-Altman plot showed a high concordance between the 2 methods (mean value of the differences = 0.1; 95% CI [-1.02 to 1.22]) (Fig. 1). There was significant correlation between relative infarct size (LV%) obtained by planimetry and the AUC of troponin-I release ($r = 0.761$, $p < 0.001$) and the AUC of CK release ($r = 0.791$, $p < 0.001$) There was also a good correlation with maximal

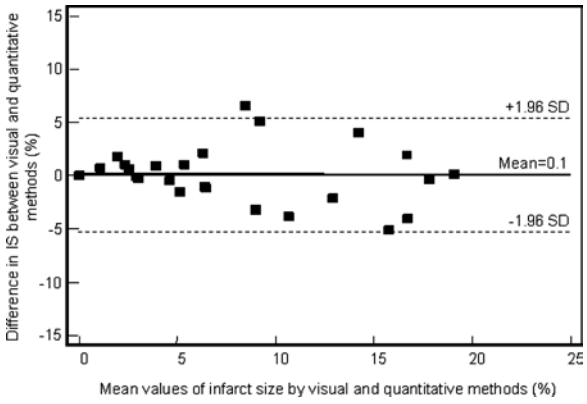

FIG. 1. Bland-Altman plots for comparison of the visual and planimetric methods for infarct size (IS) determination with cardiovascular magnetic resonance (CMR) late enhancement. The agreement between the two methods is very close 72 hours after infarction.

troponin-I level in-hospital and maximal CK in-hospital level ($p \leq 0.001$) (Fig. 2).

Global infarct score obtained by visual segmental estimation of infarct size also correlated with the AUC of troponin-I release ($r = 0.646$; $p < 0.001$) and the AUC of CK release ($r = 0.697$; $p < 0.001$). Correlations were also significant with maximal troponin-I level in-hospital ($r = 0.497$; $p = 0.01$) and maximal CK inhospital level ($r = 0.662$; $p < 0.001$).

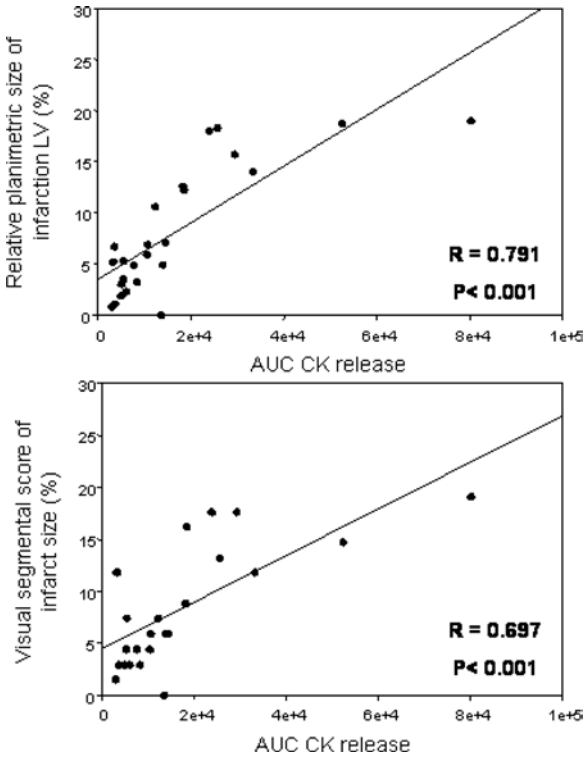

FIG. 2. Correlation between relative size of myocardial infarction (LV%) measured with CMR late enhancement by planimetry or visual scoring, and the area under curve (AUC, arbitrary units) of creatine kinase (CK) release over 48 hours.

Conclusions: A visual approach based on a 17 segment model can be used to evaluate the global myocardial extent of the hyperenhancement accurately and with similar results to planimetry. Irrespectively of the visual or planimetric methods, acute DE-CMR correlates well with the biomarkers of myocardial necrosis even in small size myocardial infarctions.

329. SPIRAL IMAGING SEQUENCE IS SUPERIOR TO GRADIENT ECHO FOR IMAGING CARDIAC FUNCTION AND TRACKING STEM CELLS IN A SMALL ANIMAL MODEL USING A CLINICAL MR SCANNER

John Terrovitis, MD, Connie Y. Chang, Michelle Leppo, Khaled Abd-Elmoniem, Robert G. Weiss, Gary Gerstenblith, Eduardo Marbán, M. Roselle Abraham, Matthias Stuber. ***Johns Hopkins University, Baltimore, Maryland, USA.***

Introduction: Small animal imaging studies for tracking stem cells and evaluating treatment response after transplantation play an increasingly important role in translating basic science results into clinical medicine. Often, imaging is performed in dedicated small bore, high field magnets. Despite the acknowledged importance of these studies, there are major problems with these systems: a) the results are not readily translatable to commercial human systems, b) many of the most advanced developments in hard and software are not readily available, c) sophisticated third party systems for ECG and respiratory gating are needed, and d) the availability of small bore high-field systems is often limited to large research centers.

Purpose: To implement and optimize functional CMR imaging after intra-myocardial stem cell injection in a rodent (rat) model on a commercial 3T clinical scanner and to compare functional images as well as signal-to-noise (SNR) and contrast-to-noise (CNR) ratios obtained by two different imaging sequences.

Methods: Ninteen imaging studies were performed on 12 male Wistar Kyoto rats (1–3 months old, 220–340 g) on a Philips Achieva 3T scanner . Seven hundred fifty-thousand to 1 million Feridex (Berlex, USA) labeled Cardiac Derived Stem Cells (CDCs) were injected intramyocardially via direct visualization. Animals were imaged at 2 and 21 days postinjection. They were anesthetized by isoflurane inhalation (4% for induction, 2% maintenance) and placed prone, head first in the magnet. Small-diameter (8 cm) 4element phased array coil was used for signal reception. ECG triggering was performed using the standard 4lead vector ECG unit. Cardiac function was assessed using two sequences: a) a segmented k-space gradient echo (GRE) imaging sequence, slice thickness 2 mm, flip angle 20°, FOV 90 mm, matrix 400 × 400, 26 cine frames, TR: 7.5 ms, TE: 2.8 ms, and b) a spiral imaging sequence with 380 spiral interleaves, slice thickness 2 mm, flip angle 20°, FOV 90 mm, matrix 400 × 400, 16 cine frames, TR: 12 ms, TE: 1.49 ms. Images were analyzed with Image J software. Calculations of SNR and CNR were based on signal intensity measured in the remote myocardium,

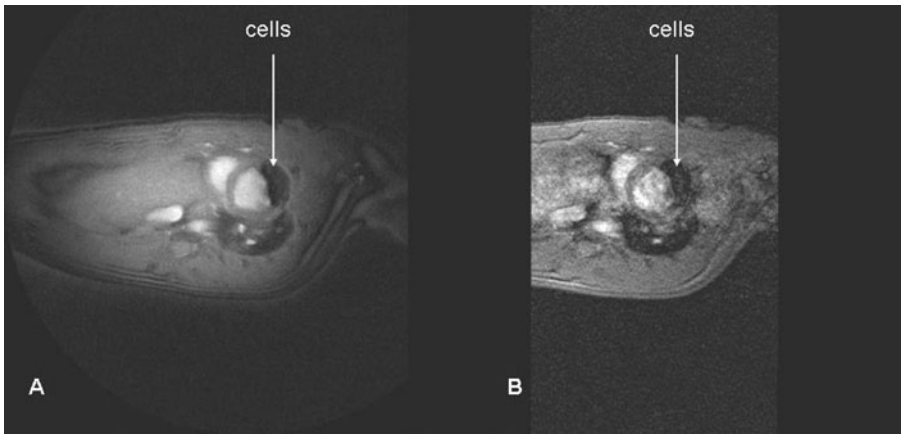

FIG. 1. Images of the same short axis slice acquired by the sprial (A) and GRE (B) sequences Slice thickness, in plane resolution and number of averages were the same for both images

the area of the labeled stem cells, and left ventricular (LV) cavity, while noise (standard deviation) was measured in regions of interest in the lungs. Values are expressed as mean ± standard deviation.

Results: Both sequences provided adequate functional cine images of the rat heart. Acquisition times were similar (90–110 s/slice). The SNR of the myocardium was consistently higher in the spiral images (13.0 ± 3.6 vs 8.6 ± 2.5, $p < 0.001$). CNR (signal in the blood pool—signal in the myocardium/noise) was higher in the GRE images (9.9 ± 2.5 vs 8.0 ± 4.2, $p = 0.028$). GRE images, however, were more susceptible to blood flow artifacts, which made delineation of the endocardial and epicardial borders more difficult despite the higher CNR, a fact of major importance in small animal studies, where high heart rates exaggerate this type of artifact.

Iron labeled cells were successfully visualized as dark spots by both sequences; however, the CNR (signal in remote myocardium—signal in cell containing areas/noise) was always higher in images obtained by the spiral sequence (8.9 ± 2.9 vs 6.6 ± 3.1, $p < 0.001$).

Conclusions: Small animal imaging in a clinical scanner is both a feasible and efficient method for visualizing labeled cells and acquiring high quality functional cardiac images after stem cell injection, without the need for any special additional software or hardware. Spiral acquisition significantly improves image quality and is the method of choice for these studies.

330. DELAYED ENHANCEMENT CARDIAC MR IMAGING FOR THE ASSESSMENT OF MYOCARDIAL INVOLVEMENT IN PATIENTS WITH DESMIN MYOPATHIES

Katharina Strach, MD,[1] Carsten Meyer, MD,[1] Rolf Schroeder, MD,[2] Daniel Thomas, MD,[1] Hans H. Schild, MD,[1] Torsten Sommer, MD.[1] [1] *Radiology, University Hospital Bonn, Germany,* [2] *Neurology, University Hospital Bonn, Germany.*

Introduction: Mutations of the human desmin gene cause a familial or sporadic form of skeletal and/or cardiac myopathy, which is characterized by a loss of desmin function and intracellular accumulation of insoluble protein aggregates eventually leading to cell death and replacement fibrosis. Desmin myopathies usually manifest in the second to the fourth decade of life with lower limb muscle weakness slowly spreading to involve truncal, neck-flexor, facial, bulbar and respiratory muscles. Cardiac involvement is the second classical clinical hallmark of desmin myopathies and may either precede, coincide with or succeed skeletal muscle weakness. Patient prognosis is usually determined by cardiac involvement leading to cardiac arrhythmias, heart failure and sudden cardiac death, thus early diagnosis is crucial.

Purpose: Delayed enhancement cardiac MR imaging (CMR) allows to differentiate normal myocardium from a variety of myocardial diseases associated with necrosis or fibrosis. The purpose of this study was to evaluate whether delayed enhancement CMR may be useful to detect early myocardial involvement in patients with desmin myopathy independent of cardiac function.

Methods: The study group consisted of 10 patients without cardiac symptoms and genetically confirmed desmin myopathy. Sequential short axis (SA) left ventricular (LV) cine loops

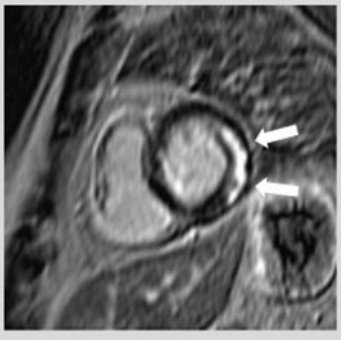

Intramyocardial hyperenhancing lesion (white arrows) in the lateral LV wall of a 41 year old, asymptomatic patient with genetically confirmed desmin myopathy indicating myocardial involvement. No associated focal wall motion abnormalities were detected. ECG revealed no pathological findings and serum Troponin levels were within normal limitis.

(SSFP: 8 mm slice thickness, no gap; Intera 1.5T, Philips Medical Systems) were performed from the atrioventricular ring to the apex. An additional long axis view was acquired for the assessment of the LV apex. Right ventricular (RV) and LV end-diastolic (ED) volumes were measured, LV mass and RV and LV ejection fraction (EF) was calculated. Furthermore, images were evaluated for the presence of focal wall motion abnormalities and hypertrophy. In the setting of focal LV pathology, ED and end-systolic (ES) wall thickness measurements were taken in the respective region and segmental wall thickening ([ES wall thickness–ED wall thickness]/ED wall thickness) was calculated. If segmental wall thickening was $\leq 45\%$ myocardial segments were considered dysfunctional.

Eight minutes after administration of 0.2 mmol/kg of Gd-DTPA a k-space segmented 3D Inversion Recovery gradient echo sequence (in-plane resolution 1.3×1.3 mm^2, slice thickness 5 mm) with complete coverage of the LV myocardium in SA slices and an additional long axis view for the assessment of the LV apex was performed. Images were assessed by two observers for the presence of hyperenhancing LV lesions indicative of myocardial tissue changes. Areas of hyperenhancement were manually planimetered on each SA slice. The mass of affected tissue based on the volume of hyperenhanced myocardium was calculated assuming a myocardial specific gravity of 1.05 g/cm^3 and expressed in absolute (g) numbers as well as in relative values in relationship to the total mass of LV myocardium (LV%).

Results: Mean RV and LV end-diastolic volumes (131.9 ± 19.8 mL and 141.5 ± 18.9 mL) and LV mass (132.6 ± 34.7 g) were within normal limits in all patients (n = 10/10). Global RV and LV function was normal in all patients (EF: $60.1 \pm 3.3\%$ and $64.6 \pm 3.9\%$). Regional wall motion abnormalities were not observed (n = 0/10). In 2 patients (n = 2/10, 20%) focal LV hypertrophy without associated wall motion abnormalities was detected. Delayed enhancement imaging revealed intramyocardial hyperenhancing lesions in the LV myocardium in 3 patients (n = 3/10, 30%). The mass of hyperenhancing tissue varied between 1.9 g and 21.7 g (2%- 13% of LV mass).

Conclusions: Preliminary data suggests, that delayed enhancement CMR is useful for the early detection of myocardial tissue changes indicating cardiac involvement in patients with desmin myopathies and normal cardiac function. Thus, delayed enhancement CMR may serve as a screening tool to identify patients at risk which need close cardiological follow-up and might profit from implantation of cardioverter/defibrillator devices.

331. SURGICAL PULMONARY VALVE REPLACEMENT AND RIGHT VENTRICULAR OUTFLOW TRACT REMODELLING: EFFECT ON EXERCISE CAPACITY AND BIVENTRICULAR FUNCTION

Alessandra Frigiola,[1] Louise Coats,[1] Sachin Khambadkone,[1] Graham Derrik,[1] Shay Cullen,[1] Olivier Ghez,[1] Carin Van Doorn,[1] Philipp Bonhoeffer,[1] Victor Tsang,[1] Andrew M. Taylor.[1] ***[1]Great Ormond Street Hospital for Children, London, United Kingdom, [2]The Heart Hospital, London, United Kingdom.***

Introduction: The adverse effects of chronic pulmonary regurgitation are well recognised. However, there are conflicting reports regarding the potential for improvement following pulmonary valve replacement (PVR). In our institution, acceptance for surgery requires severe pulmonary incompetence (>35%), evidence of significant right ventricular (RV) dilatation (RV: left ventricular (LV) end-diastolic volume (EDV) ratio >1.5:1) and either symptoms or objective evidence of exercise impairment.

Purpose: This study reports the clinical and physiological consequences of this approach.

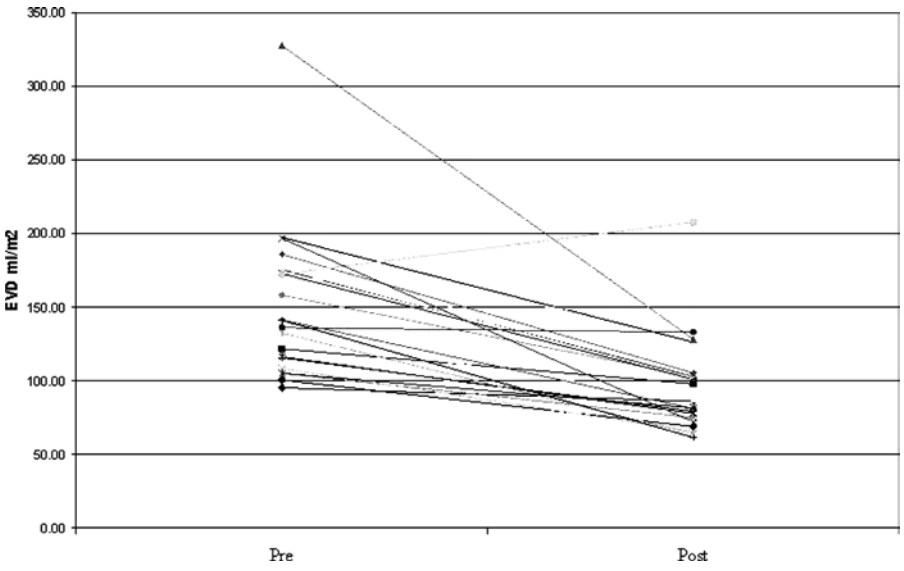

FIG. 1. RV EDV before and after pulmonary valve replacement.

Methods: We studied 25 consecutive patients (52% male, median age 21 years (9.9–65), 84% tetralogy of Fallot) who underwent surgery with placement of a homograft and excision of the right ventricular outflow tract (RVOT) aneurysm. Clinical examination, tissue Doppler echocardiography, magnetic resonance (MR) imaging and cardiopulmonary exercise testing (CPEX) were performed before and 1 year after surgery.

Results: After surgery, there was a significant reduction in RV EDV (151 ± 49 to 97 ± 32 mL/m^2, $p < 0.0001$, Fig. 1) and RV end-systolic volume (80 ± 43 to 46 ± 23 mL/m^2, $p < 0.0001$), and an improvement in RV effective stroke volume (63 ± 20 to 72 ± 16 mL/m^2, $p = 0.004$) and ejection fraction (50 ± 11 to 55 ± 8%, $p = 0.006$). There was a trend to an increase in LV EDV (68 ± 12 to 72 ± 14 mL/m^2, $p = 0.09$) and increases in LV stroke volume (61 ± 18 to 73 ± 16 mL/m^2, $p < 0.0001$) and LV ejection fraction (60 ± 10 to 65 ± 6%, $p = 0.016$). The RV:LV EDV ratio improved significantly (2.2 ± 0.5 to 1.4 ± 0.5, $p < 0.0001$). On tissue Doppler imaging, systolic velocity at the tricuspid annulus fell (6.7 ± 1.5 to 5.4 ± 1.4 cm/s, $p = 0.001$), but did not change in the LV. Isovolumic acceleration did not change in either ventricle. In both ventricles, there was a significant reduction in early diastolic velocity (RV: 7.9 ± 2.2 to 4.8 ± 2.1 cm/s, $p < 0.0001$; LV: 11.1 ± 2.8 to 9.6 ± 2.2cm/s, $p = 0.009$). There was no significant change in CPEX,despite patient reported improvement in symptoms.

Conclusions: Following PVR, cardiac performance improved according to MR assessment. The marked reduction in RV ESV probably reflects the removal of an RVOT aneurysm that fills paradoxically during systole prior to surgery. Tissue Doppler parameters were reduced in the RV, which is likely to be load related but may also reflect the deleterious effect of cardiopulmonary by-pass. The overall improvement in function did not translate to an objective clinical improvement in this population.

332. DETERMINATION OF NORMAL GREAT VESSEL MEASUREMENTS BY CARDIAC MAGNETIC RESONANCE IMAGING

Aaron Weaver, MD, Hector E. Busto, Gerri K. Jelaco, Julie A. Cha, Kurt R. Jensen, MS, Duane D. Blatter, MD, Jeffrey L. Anderson, MD. ***LDS Hospital, Salt Lake City, Utah, USA.***

Introduction: The great vessels are essential to full cardiovascular evaluation. Cardiac magnetic resonance imaging (CMR) could provide superior quantitative assessment, but a normal range of measurements has not been established.

Purpose: The purpose of the abstract is to establish a normal range of values to be used with CMR of the great vessels.

Methods: Thirty normal adult volunteers (15 M, 15 F), mean age 47, were studied. CMR included thoracic axial and sagittal scout views and short- and 2, 3, and 4 chamber long-axis SSFP cines on a GE 1.5 Tesla magnet (EXCITE platform, version 11.0). Images were analyzed independently by 3 physicians. Great vessel measurements included diameters of the aorta at the level of the sinuses of Valsalva (3 chamber view); the main pulmonary artery, the ascending aorta, and superior vena cava (SVC) on the same axial slice; and the inferior vena cava (IVC) near the right atrium in sagittal and axial planes. When cross-sections deviated from circular, major and minor diameters were averaged. Individual measurements >20% discrepant from the mean were excluded (3.4%). Means and variances were computed. Results were indexed to body surface area (BSA), and the 5th and 95th percentile range was taken as normal.

TABLE 1

Measurement (mm)	Mean	SD	5th Percentile*	95th Percentile*
Aorta—Sinus of Valsalva	32.7	3.6	27	40
AOSOV index	17.6	1.8	15	21
Aorta—Ascending	31.6	3.6	26	39
AOASC index	17.0	1.9	14	21
Pulmonary Artery	30.4	4.5	24	39
PA index	16.2	2.0	14	20
SVC	19.7	2.9	15	25
SVC index	10.6	1.4	9	13
IVC—Axial	22.7	3.3	17	29
IVC-Ax index	12.2	1.9	9	15
IVC—Sagittal	20.6	3.6	14	27
IVC-Sag index	11.0	1.6	8	13

Results: BSA averaged 2.0 sq m in men and 1.7 in women. Results are shown in Table 1. Indexing to BSA eliminated most of sex-related differences.

Conclusion: CMR provides excellent qualitative assessment of the great vessels. Using CMR, we have determined a normal range of great vessel measurements, which can assist in the non-invasive distinction of cardiovascular health and disease.

333. ASSESSMENT OF MYOCARDIAL OXYGEN DEFICITS DUE TO CORONARY STENOSIS WITH BALANCED SSFP IMAGING AT 3.0T IN A CANINE MODEL

Rohan Dharmakumar, PhD, Jain Mangalathu Arumana, BE, Richard Tang, MD, Kathleen Harris, BS, Debiao Li, PhD. ***Northwestern University, Chicago, Illinois, USA.***

Introduction: Myocardial oxygen deficits (MODs) secondary to coronary stenosis may be detected with blood-oxygen-level-dependent (BOLD) MRI at 1.5T. In a number of organ systems, excluding the heart, BOLD contrast has been shown to be directly dependent on field strength. These findings have instilled a longstanding interest in assessing MODs at 3.0T.

Purpose: This work investigates whether SSFP-based BOLD imaging can be used to obtain artifact-reduced, oxygen-weighted images for detecting MODs secondary to coronary

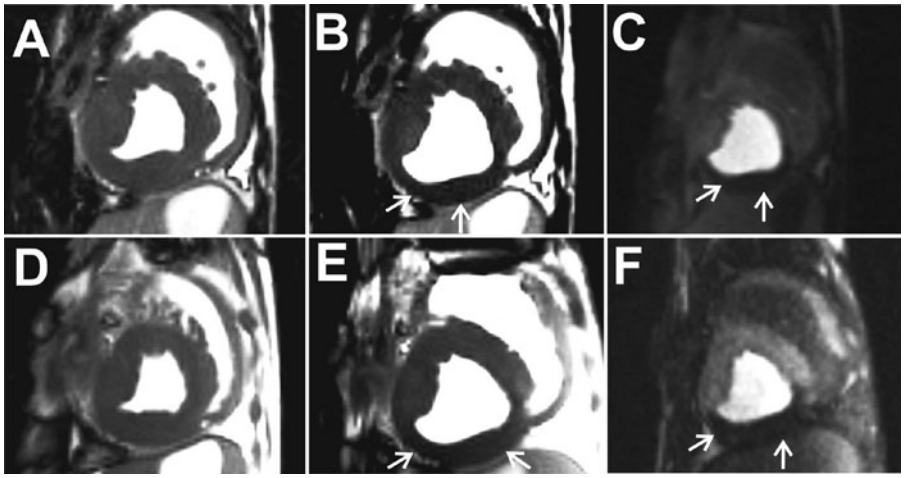

FIG. 1. Shows a set of short axis images acquired at 1.5T (top row) and 3.0T (bottom row). Images A and D are SSFP images at systole under adenosine infusion (with no occlusion), images B and E are also SSFP images at systole under LCX stenosis of similar extent, and images C and F are the corresponding first pass images acquired under the same stenosis level as in B and E. Note the perfusion deficit region in th LCX territory (arrows) assessed with first place perfusion and its close correspondence to BOLD images in the LCX territories. Also note the overall improvement in image quality at 3.0T compared to 1.5T, allowing for a more accurate detection of oxygen deficit (B and E) in the LCX territory.

stenosis in a canine model at 3.0T and whether the BOLD contrast at 3.0T is greater than at 1.5T.

Methods: Four Mongrel dogs underwent thoracotomies and three catheters were routed for injections into the aorta and LA and RA. In all animals, a portion of the LCX was isolated and an occluder was secured around the LCX. To estimate the extent of LCX stenosis during the MR studies, a Doppler flow probe was secured distal to the LCX occluder. Each study consisted of 3 sets of cardiac-gated and breath-held scans (13–19 s) employing b-SSFP sequence on a Siemens 1.5T (Sonata) and 3.0T (Tim Trio) scanners: (A) baseline adenosine scan with constant adenosine infusion into the RA catheter; (B) at least 2 levels of LCX stenosis with adenosine; and (C) a first-pass perfusion at the severe the stenosis. True flow deficits due to LCX stenoses were measured with microsphere flow analysis. In total, 17 stress-stenosis studies (8 at 1.5 T and 9 at 3.0 T) were performed. Based on the scout images, slice positions were matched between 1.5 T and 3.0 T studies and microsphere analysis. Manual shimming, center frequency scouts, and when the magnetic inhomogeneities were severe, maximum intensity projections constructed from phase-cycled and non phase-cycled acquisitions were used to improve image quality at 3.0 T. The scan parameters were: voxel size $= 1.8 \times 1.4 \times 5.0$ mm^3, 10-12 phases/heart beat, $T_E/T_R =$ 2.6/5.2 ms, flip angle $= 60^\circ$, bandwidth (1.5T/3.0T) = 241/345 Hz/pixel, and averages = 2. From the MR and fluorescence (microsphere) signals measured at the LCX and LAD territories, BOLD contrast and fluorescence contrast (microsphere-based flow changes) were computed relative to the adenosine baseline state as $(S_{aden} - S_{sten})/S_{aden}$, where S_{aden} and S_{sten} are the signal magnitudes from the LCX territory normalized by the signal magnitudes from the LAD territory at adenosine baseline and occlusion states, respectively. MR signals were measured at systole.

Results: Fig. 1 shows typical short axis SSFP-based cardiac BOLD images obtained at adenosine baseline (A/D) and stress-stenosis (B/E) conditions and a first pass perfusion image (C/F) obtained during the severe stress-stenosis at 1.5 T and 3.0 T, respectively. Regional BOLD contrast was observed at the LCX territory at both field strengths and correlated well with the perfusion deficits observed from the first pass images. The BOLD contrast was significantly greater at 3.0 T than at 1.5 T (Fig. 2), approximately by a factor of 2 (t-test, $p < 0.01$). Results also showed that the microsphere-based flow and BOLD-based contrast changes were strongly correlated at both field strengths($r = 0.7$, $p < 0.01$).

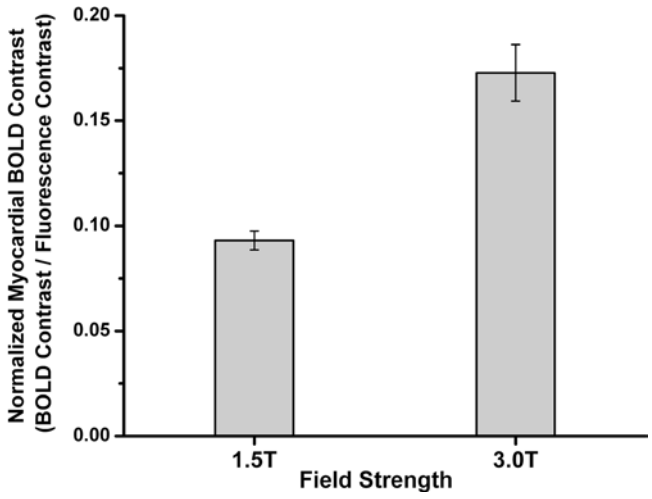

FIG. 2. Bar plot shows the mean myocardial BOLD contrast changes (normalized by true flow changes) observedat 1.5T and 3.0T in the LCX territory (relative to the LAD territory) due to preferential stenosis of the LCX in dogs. Note the improvement of contrast at 3.0T compared to 1.5T and 3.0T.

Conclusions: This work demonstrated that SSFP imaging can be useful for acquiring high quality, artifact-reduced images that show MODs due to acute coronary stenosis at 3.0 T. Consistent with previous theoretical predictions and work in other organ systems, results show that significantly greater myocardial BOLD contrast can be achieved at 3.0 T compared to 1.5 T.

334. QUANTIFICATION OF SEVERITY AND EXTENT OF LEFT VENTRICULAR NONCOMPACTION AND TRABECULAR DELAYED HYPERENHANCEMENT WITH CARDIAC MAGNETIC RESONANCE IMAGING: CORRELATION WITH CLINICAL SEVERITY

Jonathan D. Dodd, Godtfred Holmvang, Udo Hoffmann, Maros Ferencik, Thomas J. Brady, Suhny Abbara, Ricardo C. Cury. ***Massachusetts General Hospital, Boston, Massachusetts, USA.***

Introduction: Delayed hyperenhancement MRI can detect interstitial fibrosis. Pathological studies have shown trabecular fibrosis in patients with Left Ventricular NonCompaction(LVNC).

Purpose: We investigated whether magnetic resonance imaging (MRI) can quantify the severity/extent of LVNC and detect trabecular delayed hyperenhancement (DE), and whether these demonstrate a relationship with clinical disease severity.

Methods: In a case-control blinded study, 9 patients with LVNC and 10 controls had cardiac MRI studies evaluated for severity/extent of LVNC and trabecular DE on a myocardial segmental basis (17 segment model). Findings were correlated with parameters of clinical disease severity.

Results: Fifty-seven segments (39%) demonstrated LVNC, 22 segments (15%) demonstrated trabecular DE. Significant differences between clinical severity groups were noted in: severity/extent of LVNC at the mid ($p < 0.05$ and $p < 0.005$ respectively) and apical levels ($p < 0.003$ and $p < 0.001$ respectively); severity of trabecular DE at the mid ($p < 0.04$) and apical levels ($p < 0.02$);and extent of trabecular DE at the apical level ($p < 0.006$). Extent of LVNC and severity/extent of trabecular DE correlated significantly with EF% ($r = -0.47$, $-0.53/-0.53$, respectively, $p < 0.05$). Severity of trabecular DE was an independent predictor of EF ($R^2 = 0.73$, $p < 0.0001$). Significant differences in severity of trabecular DE were detected between patients with mild clinical severity and those with moderate and severe clinical severity ($p < 0.0001$).

Conclusions: Cardiac MRI demonstrates trabecular DE in LVNC. Evidence of trabecular DE may increase the ability of CMRI to predict clinical disease severity in LVNC.

335. LIMITED DIAGNOSTIC VALUE OF T2 WEIGHTED MR IMAGING IN DETECTING ACUTE MYOCARDIAL INFARCTION WITH MICROVASCULAR OBSTRUCTION

Yoko Mikami,[1] Hajime Sakuma,[1] Motonori Nagata,[1] Nanaka Ishida,[1] Masaki Ishida,[1] Tairo Kurita,[2] Takashi Tanigawa,[2] Katsuya Onishi,[3] Issei Komuro,[4] Masaaki Ito.[2] ***[1]Department of Radiology, Mie University School of Medicine, Tsu ity, Mie prefecture, Japan, [2]Department of Cardiology, Mie University Graduate School of Medicine, Tsu City, Mie prefecture, Japan, [3]Department of Molecular and Laboratory Medicine,Mie University Graduate School of Medicine, Tsu City, Mie prefecture, Japan, [4]Department of Cardiovascular Science and Medicine, Chiba University Graduate School of Medicine, Chiba, Japan.***

Background: Previous studies demonstrated that high signal intensity on T2-weighted MRI indicate infarct-associated myocardial edema in patients with acute myocardial infarction (MI), and an imaging approach combining late gadolinium enhancement (LGE) MRI and T2-weighted MRI accurately differentiates acute from chronic MI. However, similar to hemorrhagic infarction of the brain, area with acute and subacute hemorrhage in infracted myocardium may exhibit iso- or hypo-intensity on T2 weighted MRI, which can be a potential pitfall in interpreting CMR images in AMI patients.

Objectives: The purpose of this study was to determine the relation between the signal intensity in infarction zone or periinfarction zone on T2 weighted MR images and the presence of microvascular obstruction (MO) in patients with acute MI.

Methods: T2 weighted MRI and LGE MRI were obtained in 28 patients with AMI 5.0 ± 2.7 days after onset of MI. MR images were analyzed based on a 16 segment model (6 basal, 6 midventicular, 4 apical). We determined the presence and transmural extent of LGE (Grade I: $< 25\%$ of wall thickness, Grade II: 25–50%, Grade III: 50–75%, Grade IV: $>75\%$), and the presence and transmural extent of MO. The signal intensity (SI) was measured in the infarction zone, periinfarction zone and remote zone, and the results on T2 weighted MR images were presented as the relative SI compared to SI of remote zone.

Results: Of the 448 segments, 51 segments exhibited transmural MO, 4 subendocardial MO, 55 LGE without MO (Grade I: 9 segments, Grade II: 23 segments, Grade III: 11 segments, Grade IV: 12 segments), and 28 periinfarction edema without LGE. All LGE segments without MO demonstrated transmural high intensity on T2 weighted MR images regardless of transmural extent of LGE. The SI in the LGE zones without MO (relative SI 1.88 ± 0.51, $p < 0.001$) and the SI in periinfarction zones (relative SI 1.63 ± 0.20, $p < 0.001$) were significantly higher than that in normal myocardium (Fig. 1). However, the SI in the MO zone was mostly isointense to normal myocardium (relative SI 1.09 ± 0.19), being significantly lower than the SI in infarction zones without MO ($p < 0.001$) and the SI in periinfarction zones ($p < 0.01$)

Conclusion: Acute MI with hemorrhage does not exhibit high signal intensity on T2 weighted MRI. Careful observation is required when interpreting late gadolinium enhanced MRI and T2-weighted CMRI in AMI patients with MO.

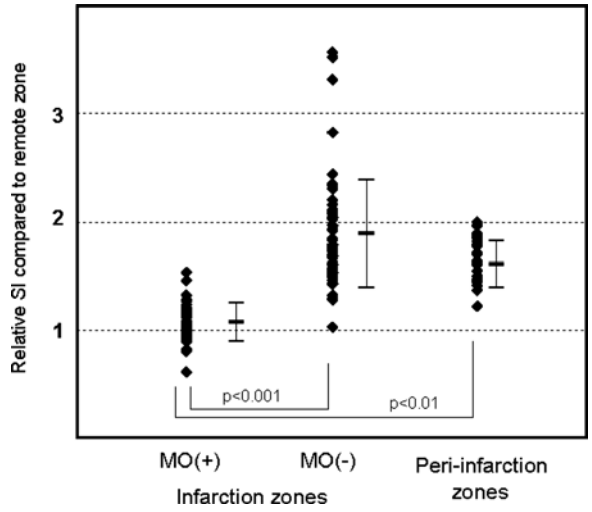

FIG. 1. Relative signal intensity in infarction zones and periinfarction zones compared to normal myocardium on T2 weighted MRI.

336. CINE 3D CMR IMAGING WITH $k - t$ SENSE

Sven Plein, MD, PhD,[1] Marc Kouwenhoven,[2] Peter Boesiger, PhD,[3] Sebastian Kozerke, PhD.[3] [1] *University of Leeds, Leeds, United Kingdom,* [2] *Philips Medical Systems, Best, The Netherlands,* [3] *University and ETH Zurich, Zurich, Switzerland*

Introduction: The faster data acquisition that can be provided by $k - t$ SENSE (1) allows for cine imaging with whole heart coverage in 3D data sets. A previous report has suggested that measurements of left ventricular volumes were significantly different using $k-t$ accelerated 3D cine acquisition compared with conventional cine imaging (2).

Purpose: In this study, we tested the hypothesis that CMR measurements of LV volumes and mass are similar in 3D $k - t$ accelerated cine imaging compared with nonaccelerated 2D multi-slice cine imaging. We also studied the effect of different $k-t$ acceleration factors on image quality and LV volumes and assessed the impact of contrast agent administration on $k - t$ accelerated 3D data sets.

Methods: Fifteen subjects were studied: 10 healthy volunteers and 5 patients. In all subjects cine imaging with a $k-t$ factor of 5 was carried out before and after the intravenous administration of 0.1 mmol Gd-DTPA. In 3 volunteers 3D $k - t$ cine imaging was also performed with $k - t$ acceleration factors of 5, 7 and 10. As a reference, a "conventional" 2D balanced SSFP pulse sequence was acquired in an identical slice orientation.

For $k-t$ data sets, a balanced SSFP pulse sequence was used (TR 3.3 ms, TE 1.7 ms, flip angle 50 deg., 20 cardiac phases, spatial resolution $2 \times 2 \times 10$ mm^3, 10–12 nonovercontiguous slices). In $k - t$ SENSE, undersampled and training data were acquired in separate breathholds. For the conventional 2D reference data, a balanced SSFP pulse sequence was used (TR 3.1 ms, TE 1.5 ms, flip angle 60 deg., 20 cardiac phases, spatial resolution $2 \times 2 \times 10$ mm^3, 10–12 slices). Image artefacts and temporal blurring were reported on a scale from 1 to 4. LV volumes and mass were calculated with planimetry and using the Simpson's method. Results were compared with t-tests and Bland-Altman analysis.

TABLE 1

	k-t cine pre contrast	k-t cine post contrast	Reference non k-t cine
Image quality (1–5)	3.5	4.2	4.6
Artefact score (0–3)	1.4	0.8	0.2
EDV	133.0*	139.2*	143.5
ESV	63.0*	66.5	67.2
EF	53.6	53.4	54.7
LVMass	97.1	97.7	99.5

*Denotes $p < 0.05$ versus reference.

Results: Breathhold duration was 18 s for a $k - t$ factor of 5, 12 s for a $k - t$ factor of 7 and 10 s for a $k - t$ factor of 10. The additonal separate breathhold for acquisition of training data lasted 4 s.

Up to a $k - t$ factor of 7, no significant temporal blurring was seen and image artifacts were minimal. For higher acceleration factors, image degradation through temporal blurring was clearly evident. In the 3 data sets acquired with $k - t$ factors of 5, 7, and 10, LV volume measurements were similar for all$k - t$ factors used.

Image quality improved and artifacts were graded lower in all subjects on the postcontrast compared with pre-contrast 3D $k - t$ images (Table 1). Table 1 also lists LV volumes and mass for 3D $k - t$ imaging with a $k - t$factor of 5 before and after contrast administration and for the 2D reference data sets. Small differences were seen for all measurements, which were reduced and nonsignificant after contrast administration.

Conclusions: $k - t$ SENSE acceleration for cine imaging is feasible and allows 3D coverage of the whole heart in a convenient breathhold. Acceleration factors of 5 and 7 were found to produce only minimal image degredation and at an acceleration factor of 5, 3D $k - t$ imaging after contrast application has no significant effect on LV volumetric assessment. Beyond $k-t$ acceleration factors of 7, images are affected by temporal blurring, but LV volume measurements appear not to be affected.

REFERENCES

1. Tsao J, et al. Magn Reson Med 2003;50:1031–42.
2. Katoh M, et al. Proc Intl Soc Mag Reson Med 2006:1634.

337. RAPID FLOW IMAGING WITH PC HYPR PROCESSING

Oliver Wieben, Kevin Johnson, BS, Julia Velikina, PhD, Frank Korosec, PhD, Charles Mistretta, PhD. *University of Wisconsin-Madison, Madison, Wisconsin, USA.*

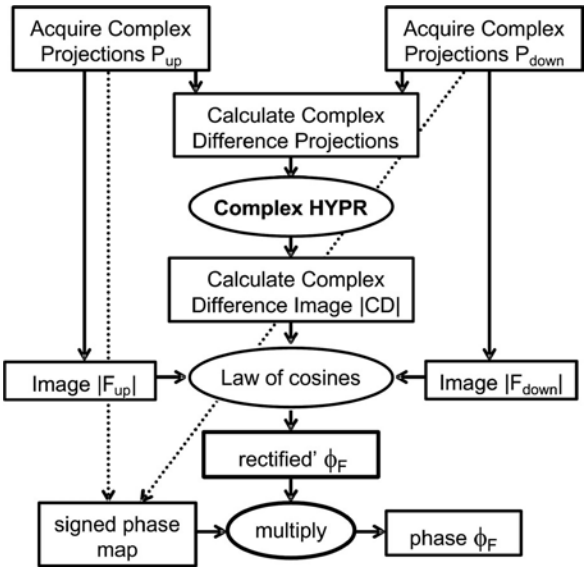

FIG. 1. Block diagram for phase contrast HYPR processing.

Introduction: Two dimensional and 3D angularly undersampled radial trajectories can significantly reduce scan time in phase contrast MRI with very few streak artifacts due to the inherent background subtraction (1, 2). HYPR (HighlY constrained backPRojection) (3) was introduced as a novel acquisition and reconstruction method to achieve improved temporal resolution in contrast enhanced MR Angiography (CE-MRA) by exploring sparsity and/or spatio-temporal correlations in the data.

Purpose: To modify and evaluate the HYPR algorithm for MR phase contrast measurements.

Methods: HYPR processing uses an angularly undersampled radial trajectory in combination with a constrained reconstruction to achieve high spatial and temporal resolution for the imaging of dynamic processes. While individual time points in a time resolved series or individual cardiac phases within the cardiac cycle are represented by very few projections only, their proper reconstruction via backprojection is supported by the use of time averaged 'composite' images. These images constrain an unfiltered backprojection process by weighting the signal distribution to voxels that contain signal in the composite images. The use of the high-quality composite images to constrain the reconstruction allows for significant reduction of artifact level as well as increase in the SNR of individual time frames.

The ultimate temporal resolution achievable with HYPR processing depends on the sparsity and the variation of the spatio-temporal correlation across the imaging scene. PC MR data sets are well suited for HYPR processing because of their sparsity achieved by background subtraction. However, proper HYPR reconstruction of phase sensitive data is more challenging than the analysis of magnitude data, because there is no positivity constraint and data along projection paths in the composite image and the individual time frames can cancel each other. The original algorithm (3) was modified to address these issues and is shown in Fig. 1. The data sets for both encoding patterns of the bipolar gradients are used to calculate complex difference projections for HYPR processing with the magnitude of the complex difference data as the constraint. The desired phase can be calculated from the law of cosines and a signed phase map.

PC HYPR processing was simulated with a numerical phantom for through-plane flow consisting of circles of various radii with various sinusoidal and linear flow patterns and noise was added to the data (Fig. 2). A PC VIPR acquisition and reconstruction was implemented for the examination of volunteers, which necessitates a 3D forward and inverse Radon transform or regridding alternatives. At this point, the 3D radial

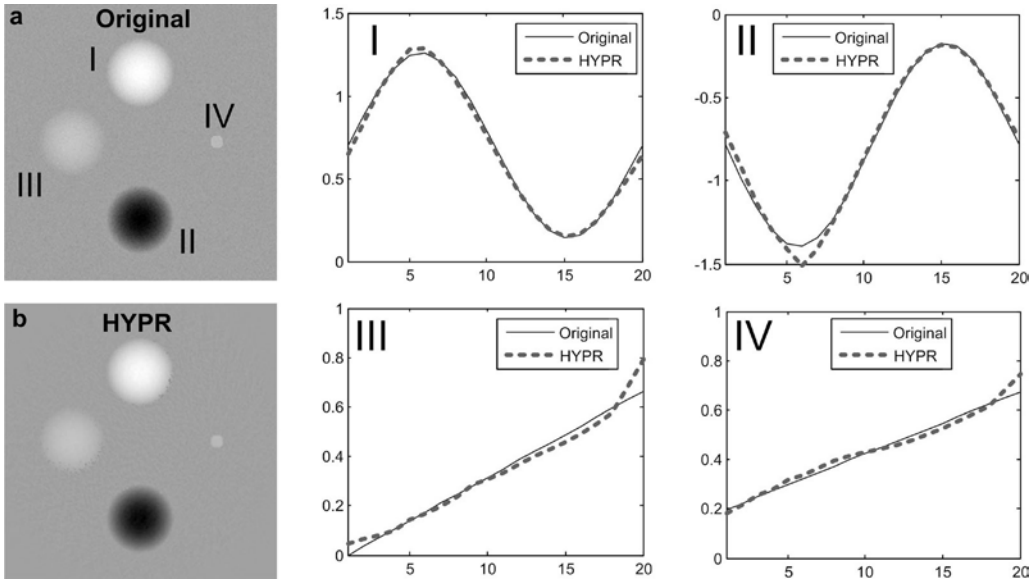

FIG. 2. Numerical phantom with four circular objects representing vessels with through-plane flow (I-IV) at time frame 8 (a) and the corresponding HYPR frame (b) and their waveforms from an ROI analysis in the four regions.

HYPR reconstruction produces complex difference ('speed') images only, which are processed similar to the CE-MRA images.

Results: The numerical simulations showed good waveform fidelity in the flow data for undersampling factors of 10 in the 2D case. For 3D processing of complex difference PC VIPR data, total undersampling factors of 930 were achieved with good image quality.

Conclusions: Our preliminary results showed that complex difference images with high undersampling factors could be achieved with HYPR processing. A modified algorithm also allowed for phase sensitive reconstruction of projection data. The simulation results suggest that PC MRI datasets can be acquired with HYPR processing to obtain faster sampling rates within the cardiac cycle or reductions in scan time. We are currently implementing the 2D and 3D phase sensitive processing for in vivo studies and will validate the waveform fidelity in phantoms and in-vivo to determine suitable protocols for various vascular regions.

REFERENCES

1. A. Barger, et al. MRM 2000;43:503–9.
2. Gu T.L., et al. AJNR 2005;26:743-9.
3. CA Mistretta et al. MRM 2006;55:30–40.

338. AUTOMATIC VOLUME THICKNESS DETECTION IN NONSELECTIVE MRA

Andres Carrillo,[1] Ajit Shankaranarayanan, PhD,[2] Jeffrey A. Stainsby,[3] Robert R. Edelman, MD.[4] [1]***GE Healthcare, Evanston, Illinois, USA,*** [2]***GE Healthcare, Baltimore, Maryland, USA,*** [3]***GE Healthcare, Toronto, Ontario, Canada,*** [4]***Evanston Hospital, Evanston, Illinoise, USA.***

Introduction: Recently EZ-STEP, a new angiographic method using nonselective RF excitation, was proposed for the scoutless acquisition of MRA (1, 2). The main benefit of the method is the workflow efficiency gained by the elimination of the need to acquire scout images and to carefully position the imaging volume. However, if the full anatomy is not covered, tissue from outside the slice field of view will wrap into the imaging volume potentially obscuring important anatomical information. To avoid this problem the slice coverage has to be carefully determined, diminishing the benefits of the technique, or it has to be made significantly wider than the anatomy, introducing unnecessary imaging time. We propose the use of an embedded edge-detection method, which will automatically determine the edges of the imaging volume and modify the sequence to acquire only the relevant field of view.

Methods: A modified version of the EZ-STEP sequence (1) was implemented on a GE 3.0T Signa Twinspeed system (GE Healthcare Technologies, Waukesha, Wisconsin, USA). A single k-space line is acquired along the slice direction just prior to the imaging section of the sequence. A hard RF pulse used is used for excitation, and no gradients are played along the phase and slice encode directions. After combining data from all channels, a 1D FFT is performed followed by an edge detection algorithm (3) that calculates the edges of the volume. The sequence recalculates the slice gradient table and the excitation frequency based on this information while maintaining the prescribed slice resolution.

Following informed consent, healthy volunteers were placed in the scanner. A 3D dataset was prescribed coronally with the slice FOV matching the coil coverage in the A/P direction. An initial acquisition without contrast covering the full prescribed volume was followed by an acquisition with contrast administration and automatic volume thickness adjustment. The coverage using the automatic thickness adjustment was validated by comparing axial reformats with and without the algorithm along different sections of the anatomy.

Results: Figure 1 shows 3 axial reformats of a pelvic MRA acquired with and without the use of the automatic volume thickness prescription. Only the full anatomy is covered by the acquisition using the automatic thickness detection, with no data coming from outside the body. Fig. 2 shows the maximum intensity projection of the MRA acquired using the volume thickness adjustment algorithm.

Discussion and Conclusion: The use of an automatic volume thickness adjustment algorithm further simplifies the acquisition of an angiographic examination. This method ensures proper coverage, thus eliminating failed examinations due to the appearance of wrap in the slice direction. It also maximizes the scan efficiency by utilizing the minimum amount of time necessary to cover the target anatomy, therefore reducing artifacts due to longer breathholds and to motion during the acquisition. This technique is especially well suited for multi-station

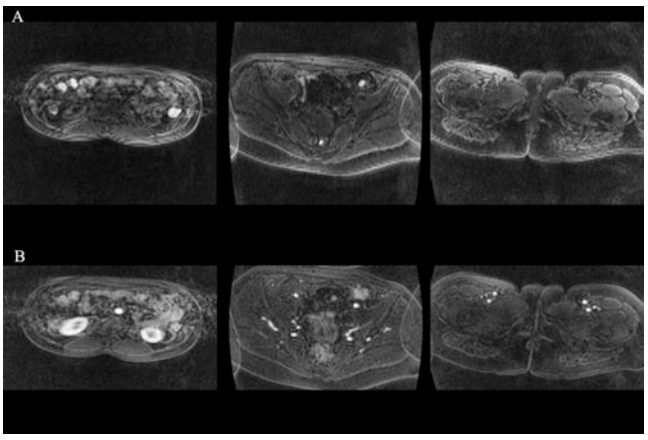

FIG. 1. Axial reformats of a pelvic EZ-STEP coronal MRA acquisition without (A) and with (B) the use of the automatic thickness adjustment algorithm. The use of the algorithm results in an acquisition that covers only the anatomy while avoiding regions with no information supported by the coil (as seen in A), thus eliminating the need of manual volume positioning in the slice direction.

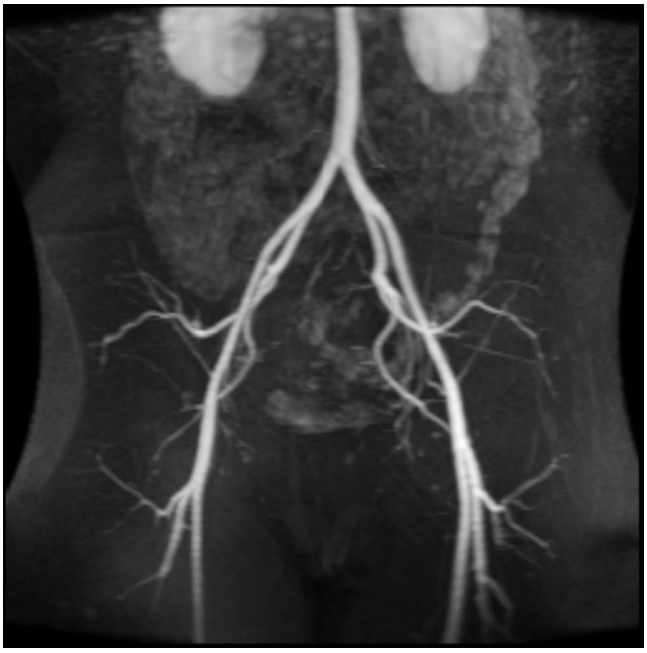

FIG. 2. Maximum intensity projection of the MRA using the volume adjustment algorithm. The vessel tree from the descending aorta to the femoral arteries can be clearly visualized.

acquisition, where the thickness of each station can be detected automatically.

REFERENCES

1. Li W, et al. ISMRM 2005;1709.
2. Li W, et al. ISMRM 2006;565.
3. Prewitt. Object Enhancement and Extraction in Picture Processing and Psycho Pictorics. 75, 149.

339. VISUALIZATION OF EXPERIMENTAL CORONARY MICROEMBOLIZATION USING CONTRAST ENHANCED CARDIAC MRI

Frank Breuckmann, Kai Nassenstein, Ina Konietzka, Christina Bucher, Torleif Sandner, Gernot Kaiser, Christoph Naber, Thomas Konorza, Michael Haude, Stephanie Aker, Andreas Skyschally, Petra Gres, Raimund Erbel, Gerd Heusch, Joerg Barkhausen. ***University Duisburg-Essen, Essen, Germany.***

Introduction: Coronary microembolization (ME) is a frequent event in ischemic heart disease, occurring spontaneously in acute coronary syndromes or artificially resulting from coronary interventions. The experimental pathophysiology and the postmortem morphological alterations of coronary ME are well characterized. In animal models experimental ME results in regional myocardial dysfunction as well as perifocal inflammatory edema and focal scar formation, which can, however, only be detected using postmortem histology.

Purpose: Our study aimed to assess whether the effects of experimental ME can be visualized in-vivo using contrast enhanced cardiac magnetic resonance imaging (CMRI).

Methods: In 12 minipigs, a 2F microcatheter was placed into the distal portion of the left anterior descending coronary artery (LAD) under x-ray guidance, and ME was performed by injection of microspheres (42 μm in diameter, approximately 4500 microphores per mL/min coronary flow). In the first 3 animals, only ex-vivo-measurements of the explanted heart were performed 8 hours after ME. In 9 animals, repetitive in-vivo cardiac exams were performed. The animals were scarified 2, 4 and 8 hours after ME and MR measurements of the explanted heart and histologic examinations were performed.

The in-vivo MR protocol included SSFP-Cine sequences (TR 3 ms, TE 1.5 ms; FA 60°, resolution 1.9 × 1.9 × 6 mm) for the assessment of regional wall motion and T2-weighted TSE sequences (TR 2 × RR, TE 59 ms, FA 180°, resolution1.3 × 1.7 × 5 mm) to visualize myocardial edema. Thereafter, a dose of 0.2 mmol/kg Gd-DTPA (Magnevist, Schering AG, Berlin, Germany) was applied, and IR-turboFLASH sequences (TR 700 ms, TE 4.8 ms, TI 180-300 ms, FA 25°, resolution 1.3 × 1.7 × 5 mm) were performed for the detection of late enhancement. Ex-vivo imaging was performed using high-resolution 2D and

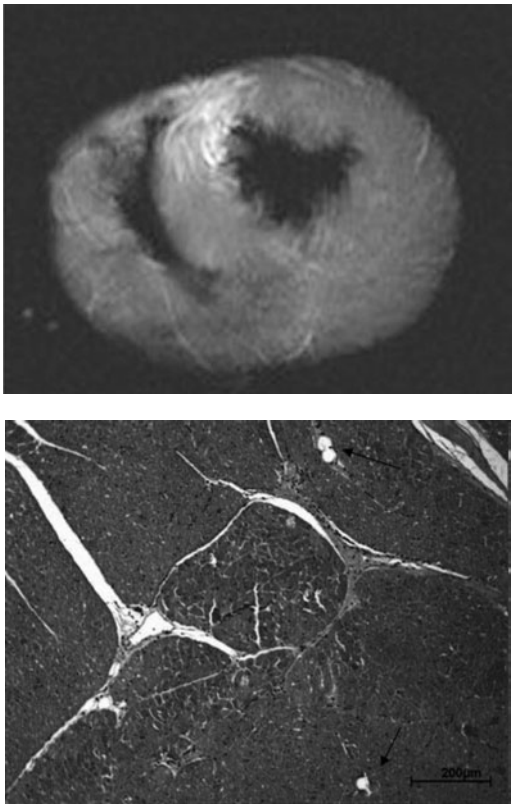

FIG. 1. Ex-vivo demarcation of streaky hyperenhancement 4 hours following experimental ME (a). Corresponding histology demonstrated discrete hypereosinophily and leukocyte infiltration as a hint for oncoming microinfarction close to microspheres [arrows] occluding small vessels (b).

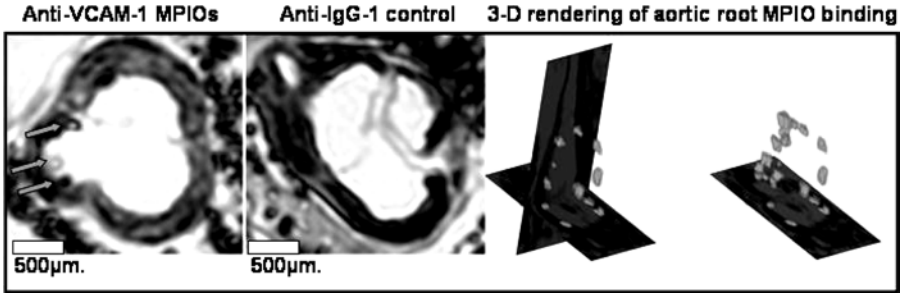

FIG. 1.

3D IR-turboFLASH sequences (TR 800, TE 4.8 ms, TI 300, resolution 0.5 × 0.5 × 3 mm). All experiments were followed by histomorphologic characterization of myocardial damage.

Results: In-vivo cine MRI demonstrated ME-induced regional wall motion abnormalities of the target area in all but one animal (3/3 at 8 hours, 3/3 at 4 hours, 2/3 at 2 hours following ME), whereas myocardial edema was detected in 6 animals (2/3 at 8 hours, 3/3 at 4 hours, 1/3 at 2 hours). In-vivo measurements allowed the visualization of late enhancement in 2 animals only (0/3 at 8 hours, 2/6 at 4 hours, 0/3 at 2 hours). However, high resolution ex-vivo-measurements showed patchy or streaky areas of late enhancement in segments 7/8, 13/14 (Fig. 1a) and/or 17 of the left ventricular myocardium in 11 of 12 pigs (6/6 at 8 hours, 3/3 at 4 hours, 2/3 at 2 hours following ME). Corresponding histology confirmed patchy microinfarcts with leukocyte infiltration in all animals 8 hours after ME. However, in all animals scarified 2 and 4 hours following ME [Fig. 1b] only minor leukocyte infiltrates and beginning evidence of oncoming microinfarction could be detected by histology.

Conclusion: Our data suggest that CMRI permits visualization of experimental ME in an animal model, even prior to histologic demarcation. However, areas of late enhancement could only reliably be detected on ex-vivo images. Due to the lower spatial resolution and blurring caused by respiratory and cardiac movement areas of microinfarctions may only be detected in-vivo if the amount of non-viable myocardium exceeds a certain level. Therefore, high-field MRI resulting in an improved spatial resolution of in-vivo-measurements might be helpful to characterize myocardial damage in-vivo more reliably.

340. MAGNETIC RESONANCE IMAGING OF ENDOTHELIAL ADHESION MOLECULES IN MOUSE ATHEROSCLEROSIS USING DUAL ANTIBODY CONJUGATED MICROPARTICLES OF IRON OXIDE

Martina A. McAteer, Jürgen E. Schneider, Ziad A. Ali, Nicholas Warrick, Christina A. Bursill, Constantin von zur Mühlen, Stefan Neubauer, Keith M. Channon, Robin P. Choudhury. ***Department of Cardiovascular Medicine, University of Oxford, Oxford, United Kingdom.***

Introduction: Superparamagnetic microparticles of iron oxide (MPIO) disrupt magnetic field homogeneity and produce striking contrast effects on MRI which extend over a volume far exceeding their physical size.

Purpose: Our aim was to investigate whether conjugation of monoclonal antibodies to MPIO could enable targeted MRI of endothelial adhesion molecules in mouse atherosclerosis.

Methods and Results: Monoclonal antibodies against VCAM-1 or P-Selectin were covalently conjugated to 4.5 μm MPIO (1×10^7 MPIO/5 μg antibody). Anti-VCAM-1 MPIO bound specifically in a dose-dependent manner to TNF-α stimulated murine endothelial cells *in vitro*, quantified by light microscopy ($R^2 = 0.94$, $p = 0.03$) and by high resolution MRI at 11.7 T ($R^2 = 0.98$, $p = 0.01$). Under simulated blood flow conditions of direct left ventricular injection, both anti-P-Selectin MPIO and anti-VCAM-1 MPIO bound to endothelium overlying atheromatous plaque in aortic roots of $ApoE^{-/-}$ mice. To mimic leukocyte binding, dual antibody conjugated MPIO were constructed, targeting both VCAM-1 and P-selectin. Binding efficiency of dual targeted MPIO increased 6.9 fold *vs.* anti-P-selectin MPIO alone ($p = 0.027$) and 5.5 fold *vs.* anti-VCAM-1 MPIO alone ($p = 0.005$). These high-affinity dual targeted MPIO were then intravenously administered via a tail vein into the normal circulation (approx. 4.5 mg iron/kg body weight). Specific binding of dual targeted MPIO to the aortic root plaque endothelium, as determined by high resolution MRI, was 3.5 fold greater than anti-IgG MPIO control ($p < 0.01$) (Fig. 1).

Conclusions: Dual anti-VCAM-1 and anti-P-Selectin conjugated MPIO bound specifically to endothelium overlying atherosclerotic plaques in the aortic roots of $apoE^{-/-}$ mice following intravenous injection. Bound MPIO showed marked contrast effects which were readily detected by MRI. This approach provides a platform for molecular MRI of endothelial cell markers expressed in a range of vascular pathologies.

341. HIGH RESOLUTION K-T BLAST ACCELERATED DCE-MRI FOR THE ASSESSMENT OF MYOCARDIAL PERFUSION

Aleksandra Radjenovic, PhD,[1] Sven Plein, PhD,[1] Sebastian Kozerke, PhD,[2] John F. Younger,[1] John P. Ridgway,

PhD,[1] John P. Greenwood, PhD.[1] [1]*University of Leeds, Leeds, United Kingdom,* [2]*University and ETH, Zurich, Switzerland.*

Background: Assessment of myocardial perfusion by dynamic contrast enhanced MRI (DCE-MRI) is still an evolving technique and is yet to become a part of standard diagnostic assessment of patients with coronary heart disease (CHD). Despite its advantages over other tomographic methods, the transition of DCE-MRI from a promising research technique into a robust clinical tool has been impeded by the severe spatial and temporal constraints imposed by the nature of this examination. The requirement for rapid collection of signal during the first arterial pass of the contrast agent through the myocardial vasculature limits the maximal achievable spatial resolution. With the spatial resolution currently achieved through conventional fast DCE-MRI, adequate assessment of the subendocardial layer is not possible.

Purpose: k-t BLAST is an acceleration method which differs from other acceleration approaches in that it allows reconstruction from undersampled data based on low resolution training data taking into account similarities in space and among time frames. By exploiting the spatio-temporal correlations in the image series, this technique aims at full recovery of the missing information. We hypothesised that significant improvement in spatial resolution can be achieved through k-t BLAST acceleration of DCE-MRI without loss of image quality or diagnostic information.

Methods: The boundary conditions used in the design of the high-resolution sequence were: a) spatial resolution $\sim$2 mm in plane for a FOV of 400 mm, b) acquisition duration $\sim$100 ms, c) total shot duration $<$200 ms. Temporal requirements b and c allow the imaging of 3 short axis slices through the left ventricle at every heart beat (for heart rates of up to 100 bpm). Scanning was preformed on a whole body 1.5 T MR scanner (Gyroscan Intera CV, Philips Medical Systems) with dedicated k-t BLAST/k-t SENSE acquisition and reconstruction software (GyroTools Ltd, Switzerland).

DCE-MRI with k-t BLAST incorporated a single shot TFE readout (TR/TE/ϕ = 3.6/1.7/15°), k-t acceleration factor = 8, image matrix = 192 × 187 (acquired voxel volume 0.045 mL). Three short axis slices were individually prepared with a saturation recovery prepulse (150 ms prepulse delay). Accelerated DCE-CMRI first-pass studies were acquired within a single breathold.

The regional ethics review board's permission was obtained, and 6 healthy volunteers were scanned at rest and under adenosine induced stress with peripheral venous administration of Gd-DTPA (Magnevist). A 63-year-old male patient with suspected CHD was scanned using a conventional sequence employing a single-shot TFE readout with TR/TE/ϕ =2.7/1.0/15°, SENSE factor = 2 and acquisition matrix of 144 × 144 (acquired voxel volume 0.077 mL, with FOV=400mm and slice thickness = 10mm). Seven weeks later, a repeated examination was performed using the optimised high resolution k-t BLAST sequence and identical geometry settings.

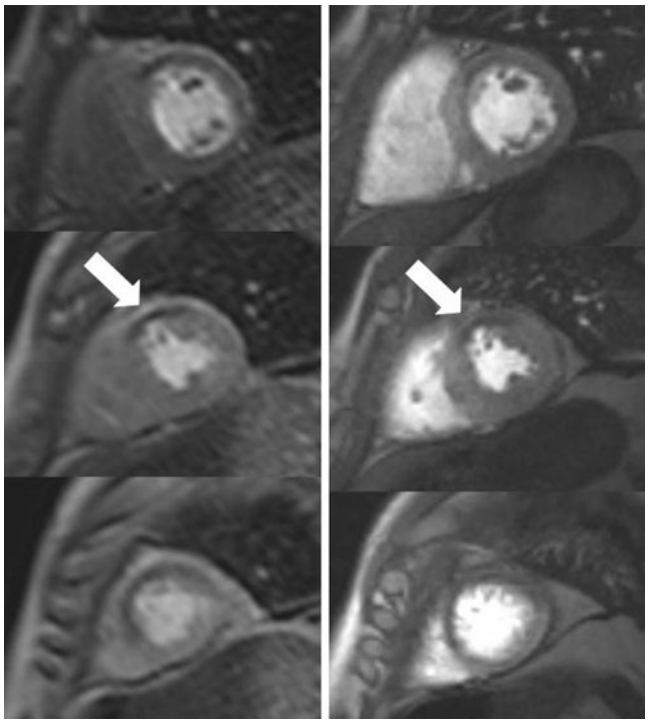

FIG. 1. Conventional (left column) and high resolution k-t BLAST accelerated (right column) DCE-MRI, in a patient with a significant lesion in the LAD territory. The reduction of image voxel size from 0.077 mL to 0.045 mL was achieved through k-t BLAST acceleration.

Results: Images were of consistently high quality, for a range of cardiac, respiratory and haemodynamic conditions.

In a patient with suspected CHD, a lesion in the LAD territory can be seen on both the conventional and k-t accelerated images acquired under adenosine stress (Fig. 1). A significant lesion in the LAD was subsequently confirmed on X-ray angiography.

Conclusion: Myocardial perfusion imaging with the application of k-t BLAST acceleration allows a significant improvement in spatial resolution over other fast MRI acquisition methods. In this pilot study, the feasibility of this approach was demonstrated. Further work is needed to formally investigate the diagnostic utility of this method.

342. MRI CHARACTERIZATION OF A RAT ENDOTHELIAL INJURY MODEL

Kenneth K. Cheung,[1] Manfred J. Ramirez,[1] Pauliina Lehtolainen,[1] David G. Gadian,[2] Roger J. Ordidge,[1] Andrew M. Taylor,[2] Mark F. Lythgoe.[2] [1]*University College London, London, United Kingdom,* [2]*UCL Institute of Child Health, London, United Kingdom.*

Introduction: The vascular endothelium is critical in maintaining normal biological functions such as haemostasis and

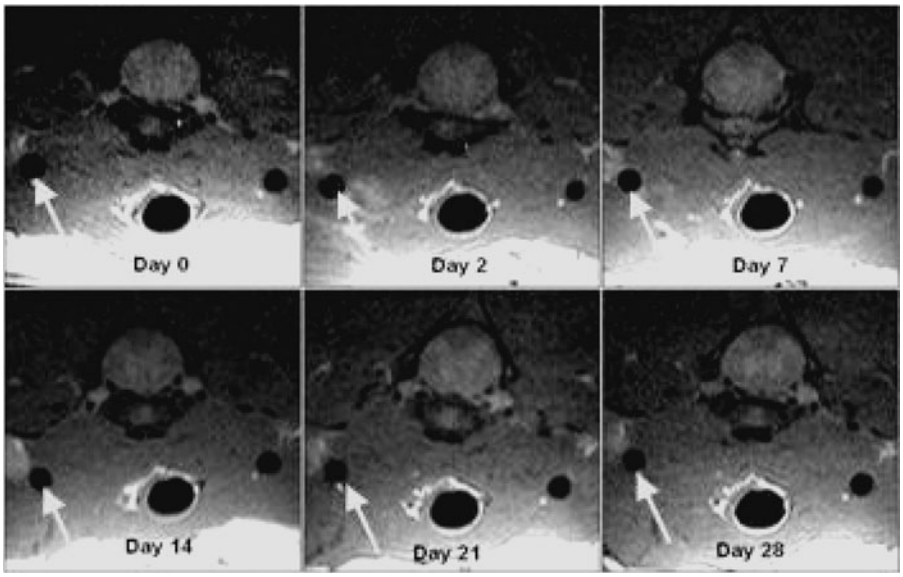

FIG. 1. Typical MR images. (LCCAs indicated by arrows).

inflammatory responses. This layer is often impaired and becomes dysfunctional in cardiovascular diseases. Therefore, the regeneration of a functional endothelium may play a crucial role in end-organ survival. We have established an animal model to investigate angioplasty-induced endothelial injury using the common carotid artery (CCA).

Purpose: This study aims to characterise the development of injury in this model by monitoring changes in lumen area using MRI, in order to provide an initial platform for a longitudinal study incorporating stem cell therapy in the future.

Methods: Study Design: Seven male adult Sprague-Dawley rats were scanned before and after balloon surgery on day 2, 7, 14, 21 and 28.

Surgery Protocol: Animals were anaesthetised with Midazolam (5 mg/mL) and Fentanyl (0.315 mg/mL), and maintained with 2 L/min O_2. A 2F embolectomy catheter was inserted into the left CCA. The balloon was inflated and withdrawn with rotation to denude the endothelium.

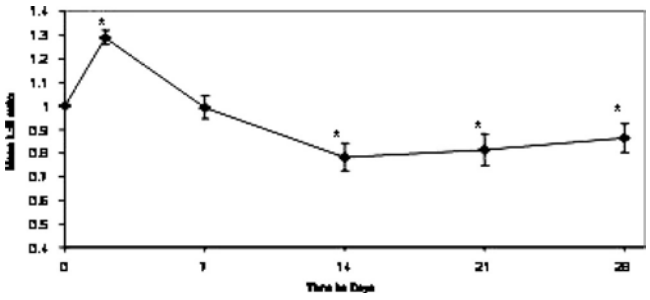

FIG. 2. Diagram showing the mean L:R ratio plotted against time in days. Error bars are +/− SE. ($p < 0.05$ where indicated by *).

MRI Evaluation: Multislice, transverse spin-echo 2DFT images of the CCA were obtained using a 2.35T system, with the first slice positioned immediately proximal to the bifurcation of the CCA. (TR = 1000; TE = 30; FOV = 25 mm; 9 slices; slice thickness = 1.5 mm; 256 × 256 pixels, scan time = 43 minutes). The lumen area of the left CCA across all nine image slices were measured and averaged to obtain the left mean lumen areas (MLA); this is repeated for the control side (right CCA).

Histological Methods: At day 28 ,the LCCAs were extracted, transversely-sectioned and H&E stained. The intima-to-media (I:M) ratio and the ratio of lumen loss due to neointimal hyperplasia (NIH) were calculated.

Data Analysis and Statistics: i) MRI: The ratios between the left and right MLAs (L:R ratio) were calculated for each acquisition and were compared to the pre-injury ratio by paired t-test. ii) *MRI-Histology comparison:* The MRI index (L:R ratio of individual image slices) and histological indices (I:M ratio and lumen-loss ratio) from day 28 were compared on a slice-to-slice basis.

Results: Figure 1 shows typical MR images at various time-points. The mean L:R ratio from all animals plotted against time suggest three stages of luminal change (Fig. 2):

1) Acute lumen gain within 2 days post-surgery, which may be the direct result of balloon expansion, as well as production of vasodilating compounds in response to endothelial denudation (1).
2) Progression of lumen loss after initial gain, with greatest loss at around 14 days postsurgery possibly due to NIH (2).
3) Gradual recovery of lumen patency after day 14.

Figure 3 shows the correlations between the in-vivo MR index (L:R ratio) and ex-vivo histological indices (I:M ratio and lumen loss ratio). Both correlations were statistically significant. (L:R

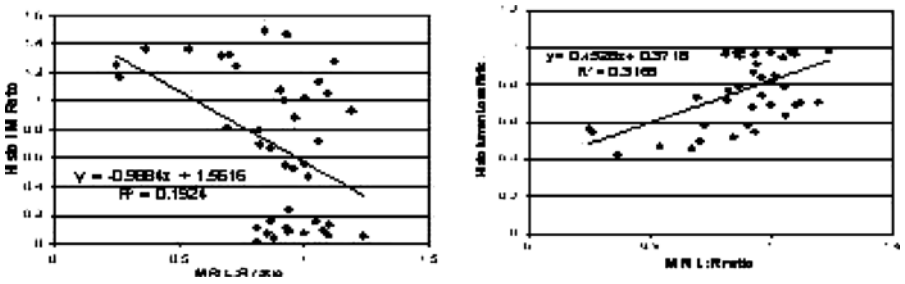

FIG. 3. a & 3b: In-vivo MR L:R ratio plotted against histological (I:M ratio and lumen loss ratio) indices, with r = −0.44 and 0.56 respectively $p < 0.05$.

vs I:M − r = −0.44; L:R vs Lumen loss ratio − r = 0.56; both $p < 0.05$). Comparison between the L:R ratio vs lumen loss ratio demonstrated a moderate correlation between in-vivo and ex-vivo indices, yet the correlation between L:R ratio and I:M ratio is low. This may be due to the methodological differences between MRI and histology, as well as vascular compensatory mechanism in response to the injury in-vivo (3).

Conclusions: We have characterised the pattern of lumen changes of the CCA in this endothelial injury model over a period of 28 days using MRI, in which 3distinct stages of balloon injury development were observed. This characterisation will be useful for assessing the therapeutic effects of stem cells in future studies.

REFERENCES

1. Joly GA, et al. Circulation Research 1992;71:331–8.
2. Gabeler EEE, et al. BMC Cardiovasc. Disorders 2002;2:16–28.
3. Ohlstein EH, et al. Cardiovascular Research 2000;47:759–768.

343. WHOLE HEART CINE MRI USING REAL-TIME RESPIRATORY SELF-GATING

Sergio A. Uribe, Sr, MSc,[1] Vivek Muthurangu, Sr, MD,[2] Redha Boubertakh, Sr, PhD,[1] Tobias Schaeffter, Sr, PhD,[1] Reza Razavi, Sr, MD,[1] Derek L. G. Hill, Sr, PhD,[3] Michael S. Hansen, Sr, PhD.[2] [1] ***King's College London, London, United Kingdom,*** [2] ***UCL Institute of Child Health, Great Ormond Street Hospital, London, United Kingdom,*** [3] ***University College London, London, United Kingdom.***

Introduction: Isotropic nonangulated 3D cardiac MR has previously been investigated as a way of simplifying CMR (1). A fundamental problem with 3D cine techniques is the attendant difficulties with respiratory compensation. Undersampling techniques have been used to acquire 3D cine data sets in a single breath-hold; however, the spatio-temporal resolution available in a clinically feasible breath-hold is inadequate. A static 3D whole heart dataset can be acquired in a free-breathing scan by using navigator beams; however, they disturb the steady state signal in SSFP cine sequences and are time consuming.

In this paper, we present a general approach for 3D cine whole heart imaging using real-time respiratory self-gating from *k*-space center profiles, which has been implemented on a clinical scanner. The results of this respiratory gating approach are compared with nongated free-breathing scan. A preliminary comparison of volume measurements from the new 3D cine and the standard 2D protocol is done.

Method: The breathing motion was derived by using a *k*-space center profile and the acquisition scheme was adjusted in real-time to re-acquire motion corrupted data. A segmented balanced SSFP cine sequence was modified by adding a center profile at the beginning of each *k*-space segment. The respiratory phase was detected by calculating the correlation coefficient between a 1D Fourier Transform of each profile with a reference projection (determined in an initial 4 seconds breath-hold stage). The data were accepted if the correlation coefficient was within a certain acceptance window, defined as a percentage of the range of the correlation coefficient (calculated in a previous learning stage immediately after the breath-hold stage). In order to avoid a long scan due to changes in the breathing pattern, a drift correction was achieved by re-initialization of the reference projection.

Nonangulated isotropic 3D data with and without respiratory gating was acquired and then reformatted into 2D clinical views in five healthy volunteers. The acquired spatial resolution was 2.5 × 2.5 × 2.5 mm^3 with 15 cardiac phases. Flip angle was 60° and TR/TE = 3.1/1.6 ms. A short-axis 2D acquitision with spatial resolution of 2.2 × 2.2 × 10 mm^3 (10 slices), and 30 cardiac phases was acquired for volumetric comparison.

TABLE 1
Volumetric comparison in the left ventricular (LV) and right ventricular

	Median (cine 2D)	Range (cine 2D)	Median (cine 3D)	Range (cine 3D)
LV-EDV [mL]	113.8	94.9–179.9	117.3	96.4–173.6
LV-ESV [mL]	31.9	20.5–56.1	32	22.2–58.3
LV-SV [mL]	83	74.4–123.8	83.3	74.2–115.3
LV-EF [mL]	75.1	68.8–78.4	74.2	68.2–77
RV-EDV [mL]	131.6	114–193.8	133.1	113.3–203.3
RV-ESV [mL]	48.4	34.8–72	47.2	30.1–85.9
RV-SV [mL]	82	73.9–121.8	86	76.5–117.4
RV-EF [mL]	64.8	62.3–69.9	63	57.8–74.2

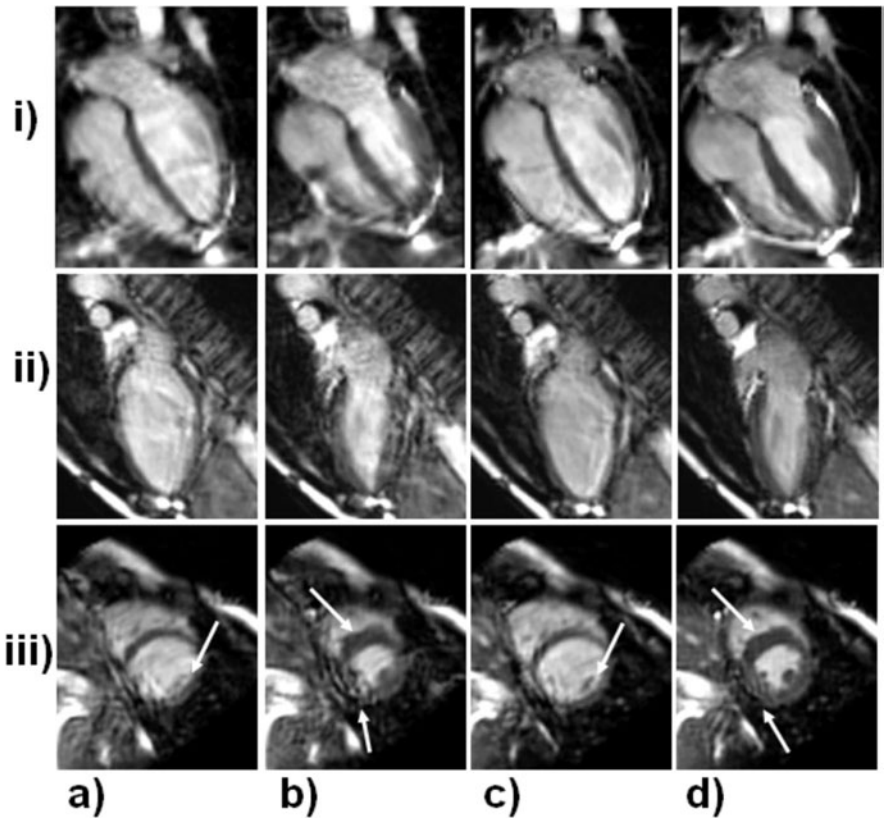

FIG. 1. Representative end-diastolic (a,c) and end-systolic (b,d) frame of 3D reformatted data in i) four chamber, ii) two chamber, and iii) short axis views for one volunteer without (a,b) and with respiratory gating (c,d).

Results: A respiratory gating signal was obtained in all volunteers. Using an acceptance window of 15%, the time required by the gated scans was twice longer than the nongated scans (150 s). Figure 1 shows a comparison of 3D reformatted data with and without this respiratory gating approach. Notice the reduced blurring and the improved delineation of the myocardial border in the gated exams. However, a reduction of image contrast was noticed in 3D cine techniques in comparison to the 2D acquisition (2).

A quantitative analysis between breath-hold multi-slice and 3D reformatted SA data is shown in Table 1. This preliminary result shows a good agreement for all of the functional parameters using both techniques.

Conclusion: The feasibility of real-time respiratory self-navigation for whole heart 3D cine imaging in a clinically reasonable time has been demonstrated in healthy volunteers. Motion artifacts are reduced in free-breathing images by forcing re-acquisition of motion corrupted data. This new technique represents a practical advance for an easier cardiac MR examination, since it reduces time for scan planning and provides patient-friendly free-breathing examination.

REFERENCES

1. Sorensen, et al. Circulation 2004.
2. Nehrke, et al. ISMRM 2006.

344. T2-PREPARED SSFP IMPROVES DIAGNOSTIC CONFIDENCE IN EDEMA IMAGING IN ACUTE MI COMPARED WITH TURBO-SPINECHO

Peter Kellman, PhD, Anthony H. Aletras, PhD, Christine Mancini, Elliot R. McVeigh, PhD, Andrew E. Arai, MD. ***National Institutes of Health, Bethesda, Maryland, USA.***

Introduction: T2-weighted MR imaging of edema in acute MI provides a means of differentiating acute and chronic MI (1)and for assessing the area-at-risk of infarction (2). Standard T2-weighted imaging of edema uses turbo-SpinEcho (TSE) readout with dark-blood preparation. Dark-blood TSE methods are subject to artifacts such as posterior wall signal loss due to cardiac motion (3) and bright subencodcardial rims due to stagnant blood which pose a significant limitation to clinical use. Thus clinical application of T2-weighted CMR is hindered by poor reliability of standard methods (4).

Single-shot imaging with T2-prepared SSFP (true-FISP) readout provides an alternative to dark-blood TSE and may be conducted during free-breathing. This is desirable where patients cannot tolerate breath-holding.

Purpose: We hypothesized that T2-prepared true-FISP would be a more reliable method than dark-blood TSE for imaging of edema in acute MI.

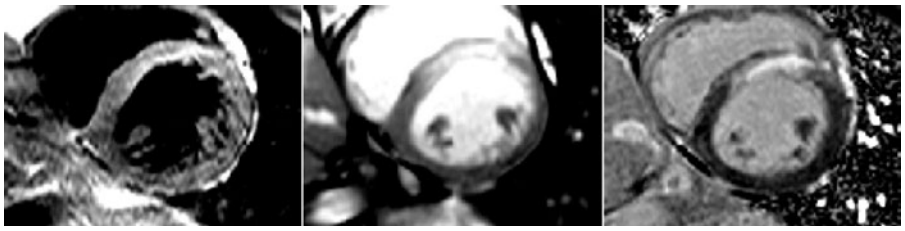

FIG. 1. Acute MI patient exhibiting edema in LAD territory: DIR-TSE (left), T2-prepared true-FISP (center), delayed enhancement (right).

Methods: The proposed approach uses a T2-prepared single-shot true-FISP readout with parallel imaging. Repeated images were acquired, corrected for respiratory motion, and averaged to enhance SNR. The T2-prepared FISP sequence was compared with dark-blood prepared TSE in both normal volunteers and patients with acute MI (within 7 days of acute event).

Images were acquired on a Siemens Espree 1.5T widebore scanner. In-plane resolution was typically 1.9×2.5 mm^2 with 6 mm slice-thickness. ECG triggering used 2 R-R intervals between readouts. TSE images used a double inversion-recovery dark-blood prep with 300% slice-thickness for selective component, BW = 449 Hz/pixel, echo-train-length = 25, TE = 64 ms. Single-shot T2-prepared FISP images used a BW = 977Hz/pixel, TE/TR = 1.6/3.2 ms, flip angle = 90°, T2-prep TE = 60 ms, 8 repetitions. Parallel imaging (rate = 2) was used to obtain the full resolution in a single heartbeat. Delayed enhancement imaging was performed using a segmented turboFLASH sequence.

Results: In normal volunteers (n = 8) where uniform T2-weighted signal intensity is expected, the loss in signal intensity of the posterior wall of the LV (mid-ventricular SAX slice) compared to the septal wall was 22.6 ± 13.7% (mean ± SD) using TSE, and 0.6% ± 4.2% using T2-prepared FISP. Both methods had surface coil intensity correction, and TSE images used timing optimized for minimal cardiac motion. A signal loss of 23% would represent a large fraction of the expected difference in signal intensity between acute MI and normal myocardium.

In patients with acute MI (n = 10), T2-weighted imaging with both methods was performed prior to contrast administration and delayed enhancement imaging of viable myocardium. While the SNR of the edema region for both methods was quite good (Fig. 1), the T2-weighted images using TSE were nondiagnostic in 2-of-10 images, while 1 additional case (Fig. 2) rated diagnostic quality had incorrect diagnosis (incorrect coronary territory). In all 10 cases the T2-prepared FISP was rated diagnostic quality and yielded correct diagnosis.

Conclusions: The proposed bright blood approach overcomes artifacts such as posterior wall signal loss due to cardiac motion and bright sub-encodcardial rims due to stagnant blood which pose a significant limitation to more widely used dark-blood TSE methods. The TSE method was sensitive to RR variation and image quality suffered at higher heart rates, whereas the single shot T2-prepared FISP approach was robust to such variation and enabled non-breathhold imaging. T2-prepared FISP may be used clinically for reliable T2-weighted imaging in acute MI.

REFERENCES

1. Abdel-Aty H, et al. Circulation 2004;109:2411–2416.
2. Aletras AH, et al. Circulation 2006;113:1865–1870.
3. Keegan, J, et al. JMRI 2006;24:563–570.
4. Pennell D. Circulation. 2006;113:1821–1823.

345. OFF-RESONANCE ANGIOGRAPHY: A NEW METHOD TO VISUALIZE VESSELS

Grigorios Korosoglou,[1] Saurabh Shah, MS,[1] Wesley D. Gilson, PhD,[1] Mike Schar, PhD,[1] Lijun Tang, MD,[1] Ioannis Terrovitis, MD,[1] Robert G. Weiss, MD,[1] Ralf Weissleder, MD,[2] Dara L. Kraitchman, VMD, PhD,[1] Matthias Stuber, MD.[1] ***[1]Johns Hopkins University Medical School, Baltimore, Maryland, USA, [2]Massachusetts General Hospital and Harvard Medical School, Charlestown, Massachusetts, USA.***

Introduction: Contrast agent enhanced magnetic resonance angiography (CE-MRA) is a technique with a broad range of

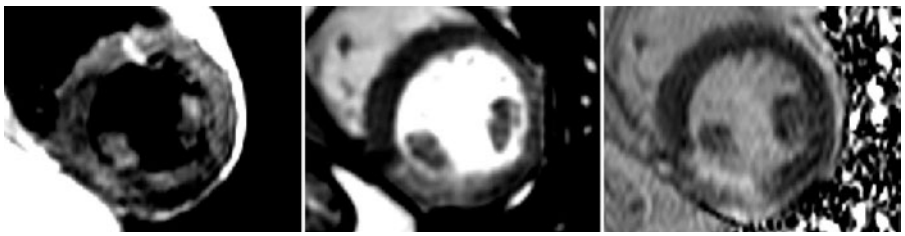

FIG. 2. Acute MI patient exhibiting edema: DIR-TSE (left) with apparent elevated T2 in LAD (incorrect) coronary territory, T2-prepared true-FISP (center) with elevated-T2 in RCA territory, delayed enhancement (right) with MI in RCA territory. Patient had significant RR-variability.

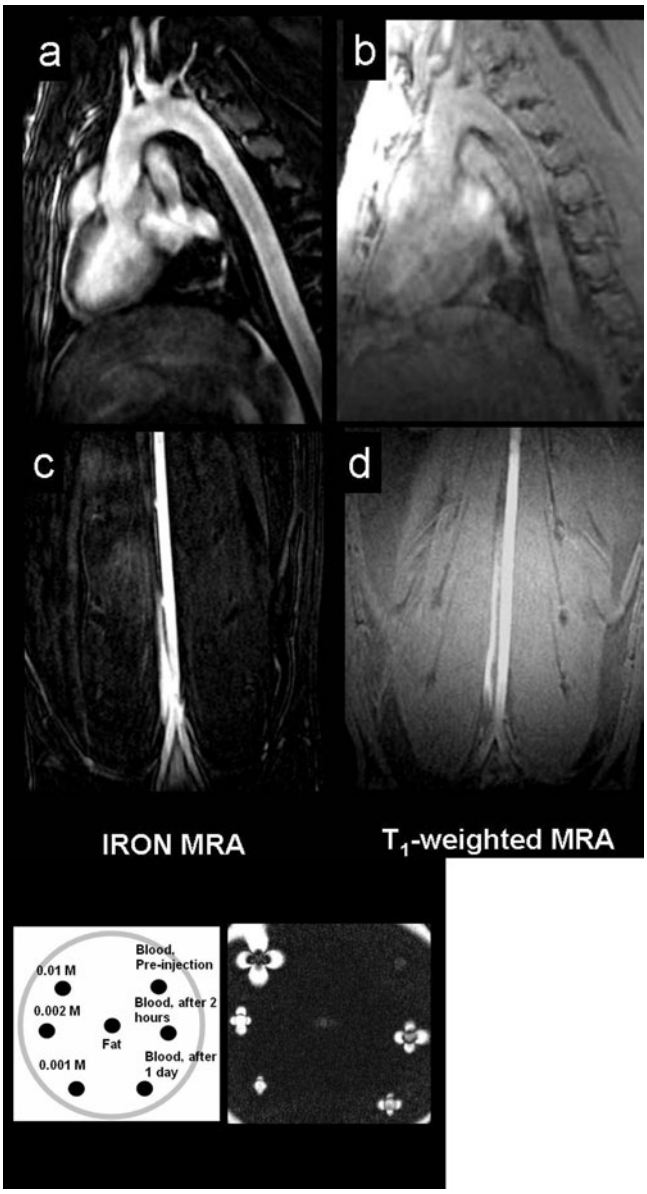

FIG. 1.

cardiovascular applications. Currently, CE-MRA techniques are based upon the T_1 shortening of the blood pool caused by extracellular or intravascular contrast agents. Here, we introduce a new concept in CE-MRA: it combines the use of an iron oxide nanocompound as an intravascular contrast agent together with Inversion Recovery with ON-resonant water suppression (1) for off-resonance angiography (IRON MRA). The positive contrast created by this method is not primarily based on T_1-shortening or on in-flow, but it exploits the shifts in the Larmor frequencies caused by the exposure of superparamagnetic particles to a static magnetic field. By this approach, IRON, for the first time, produces positive contrast within the vessel lumen and simultaneously suppresses signal from on resonant protons and fat contained in surrounding stationary tissue.

Methods: In vivo experiments were performed in 5 rabbits, which received a single intravenous bolus administration of 80 μmol/Kg (n = 3) and 250 μmol/Kg (n = 2) of monocrystalline iron oxide nanocompound (MION-47). Off resonance angiography was implemented on a commercial 3T system (Achieva, Philips Medical Systems, Best, The Netherlands), and a 4 element carotid phased-array coil was used for signal-reception. For IRON MRA, the on-resonant IRON prepulse with a bandwidth of 170 Hz and an excitation angle of 100° was combined with a fat suppressed 3D segmented k-space gradient-echo imaging sequence (field-of-view = 140 × 112 mm, matrix = 288 × 220, TR/TE = 3.9/1.54 ms, α = 15°). IRON MRA from all animals were acquired at baseline pre-contrast, 5–30 minutes, 2 hours, 1 day, and 3 days after MION—47 injection. Pre-contrast, T_1-weighted MRA without IRON pre-pulse was performed for comparison. For validation purposes, *in vitro* experiments were also conducted on agarose gel phantoms containing blood probes from rabbits, fat, and incremental concentrations of MION-47. *In vivo,* the contrast-to-noise (CNR) between the blood and the surrounding tissue was measured on the IRON MRA pre- and serially post contrast.

Results: After the administration of MION-47, *in vivo* off-resonance IRON angiography led to a high quantitative and visual contrast between the blood-pool and the surrounding tissue (Table 1, Figure 1). Vascular enhancement remained unchanged after 2 hours and persisted up to 24 hours after MION-47 injection (Table 1). Maximum CNR was observed 2 hrs post injection for the lower dose, and 1 day after injection for the higher dose (Table 1). Fig. 1 illustrates the high CNR obtained in the thoracic (a) and in the abdominal aorta (c) of a rabbit, 1 day post contrast after the administration of 250 μmol/Kg MION-47. Baseline T_1-weighted precontrast CMRA (images (b) and (d)) are provided for comparison. In vivo findings could be confirmed in phantom experiments. *In vitro*, IRON imaging of blood acquired 2 hours and 1 day after 250 μmol/Kg of MION-47 injection caused strong signal enhancement, consistent with the *in vivo* findings (Fig. 2).

Conclusions: IRON is a new MRI methodology that enables the selective signal enhanced visualization of vascular structures after injection of superparamagnetic nanoparticles. Considering the broad spectrum of potential applications and the fact that contrast enhancement is readily obtained up to 24 h after injection, IRON may provide a versatile adjunct for the investigation of vascular pathologies in several preclinical and clinical settings.

REFERENCE

1. Stuber M, et al. ISMRM. 2005.

346. SIMPLIFIED APPROACH FOR QUANTIFICATION OF AORTIC VALVE AREA BY VELOCITY-ENCODED CARDIAC MAGNETIC RESONANCE IMAGING

TABLE 1
Contrast to noise ratio of the rabbit aorta before and after MION-47 injection.

	Baseline	5–30 minutes	2 hours	1 day	3 days
Rabbit 1	0.5	68	65	23	1
Rabbit 2	0.7	69	64	24	6
Rabbit 3	0.8	54	51	19	1
Mean ± SD of rabbits 1–3	0.7 ± 0.2	63.7 ± 8.4*	60.3 ± 8.1*	22.0 ± 2.7*	2.7 ± 2.8
Rabbit 4	0.7	58	65	86	0.8
Rabbit 5	0.3	38	42	69	0.6

Sing-Chien Yap, MD, Robert-Jan Van Geuns, MD, PhD, Folkert J. Meijboom, MD, PhD, Sharon W. Kirschbaum, MD, Jackie S. McGhie, BsC, Maarten L. Simoons, MD, PhD, Jolien W. Roos-Hesselink, MD, PhD. ***Erasmus MC, Rotterdam, The Netherlands.***

Introduction: The most commonly used clinical method for the quantification of aortic stenosis severity is the continuity equation aortic valve area (AVA) with Doppler velocity-time integral (VTI) data by transthoracic echocardiography (TTE). Most cardiac magnetic resonance (CMR) studies have evaluated planimetry of the stenotic aortic valve; however, little data exist on the use of velocity-encoded CMR for quantification of AVA.

Purpose: To evaluate the accuracy of velocity-encoded CMR for quantifying AVA by a modified continuity equation approach, stroke volume divided by VTI_{Aorta}, in comparison to TTE.

Methods: Eighteen patients with congenital aortic stenosis were examined with CMR and TTE. Velocity-encoded CMR was used to obtain velocity information in the aorta and left ventricular outflow tract (LVOT). CMR AVA was calculated by using a modified continuity equation, dividing stroke volume measured from flow data in the aorta by VTI_{Aorta} (method A), and by using the standard continuity equation, multiplying the VTI ratio by the cross-sectional LVOT area in consistency with TTE (method B).

Results: By TTE, the mean AVA was 1.37 ± 0.46 cm^2. By CMR, the mean AVA was 1.37 ± 0.44 cm^2 (method A) and 1.51 ± 0.53 cm^2 (method B). The measurements of peak velocities and VTIs between modalities correlated well, leading to strong correlations of AVA by either CMR method compared to TTE ($R^2 = 0.78$ and 0.71, for method A and B, respectively). Bland-Altman analysis showed good agreement by both methods (Method A: bias 0.00; limits of agreement −0.42 to 0.43. Method B: bias 0.14; limits of agreement −0.43 to 0.70).

Conclusions: The modified continuity equation using only flow data in the aorta showed a good correlation and agreement with standard TTE, and can be used as an simple, accurate, noninvasive, imaging technique to quantify AVA.

347. MR TISSUE PHASE MAPPING DEMONSTRATES ALTERED DIASTOLIC MYOCARDIAL VELOCITIES IN LEFT VENTRICULAR HYPERTROPHY

Daniela Föll,[1] Christoph Bode,[1] Bernd A. Jung.[2] ***[1] University Hospital, Department of Cardiology, Freiburg, Germany, [2] University Hospital, Department of Radiology, Freiburg, Germany.***

Introduction: An abnormal regional LV wall motion is an important clinical marker for diagnosis and therapy in multiple cardiac pathologies and occurs as diastolic dysfunction for up to one half of the cases of heart failure (1). Especially in patients with left ventricular hypertrophy, regional myocardial relaxation disorders play an important role in the development of heart failure (2). Magnetic resonance high temporal resolution tissue phase mapping (TPM) allows for a quantitative myocardial motion analysis without limitations to certain ventricular regions such as in Tissue Doppler Imaging (3). The aim of this study was to determine whether patients with left ventricular hypertrophy due to arterial hypertension demonstrate changes in diastolic myocardial velocities measured by TPM.

Methods: We examined 10 patients with LV hypertrophy (mean age 56 years) and 6 healthy volunteers (mean age 55 years) by respiratory gated TPM using a 1.5 Tesla CMR Scanner (Siemens Sonata). Three slices were acquired in short axis view of the left ventricle (basal, midventricular, apical) with a black blood prepared gradient echo sequence (TR = 6.9 ms; temporal resolution 13.8 ms; spatial resolution 1.3 × 2.6 mm; *venc* = 15 cm/s in-plane, 25 cm/s through-plane) with prospective ECG-gating, advanced navigator gating (4), view sharing and first-order flow compensation. Global diastolic peak velocities in the longitudinal, radial and circumferential direction of the left ventricle were assessed. Furthermore, time to peak of longitudinal and radial diastolic velocities was calculated, i.e., the time period between the first negative peak as an onset of ventricular expansion/relaxation and the maximal negative diastolic peak velocity.

Results: Patients with left ventricular hypertrophy demonstrated a significant delay in time to peak diastolic longitudinal velocity in all slice locations (t-test; basal: $p = 0.03$, midventricular: $p = 0.01$, apical: $p = 0.003$) and in time to peak diastolic radial velocity in apical slices ($p = 0.03$). Figure 1 shows the time courses of averaged longitudinal velocities in the basal slice location in patients with left ventricular hypertrophy (blue, with standard deviations) compared to the age-matched control group (yellow). No significant differences were encountered in

peak radial and longitudinal velocities in all slices and in time to peak radial velocities in medial and basal slices. In apical slices, peak diastolic rotational velocity was significantly increased in patients in apical slices ($p = 0.003$) compared to age-matched controls.

Discussion: High temporal resolution TPM is a promising method to analyze left ventricular diastolic performance. Our results demonstrate that the temporal evolution of myocardial velocities in patients with left ventricular hypertrophy is substantially altered as indicated by changes in time to peak diastolic longitudinal velocities in all slices and in apical radial velocities. In contrast, the peak velocities, except for apical rotation, were less severely changed compared to age matched normal subjects. It should be noted that TPM offers the possibility for an assessment of left ventricular performance in different myocardial regions. As an example, Fig. 2 shows the longitudinal velocities in the anterior and inferior myocardium of patients with left ventricular hypertrophy (blue) compared to the healthy volunteer group (yellow). As myocardial velocities vary within different segments of the left ventricle diagnostic accuracy might further benefit from a segmental analysis according to the 17 segment model recommended by the AHA.

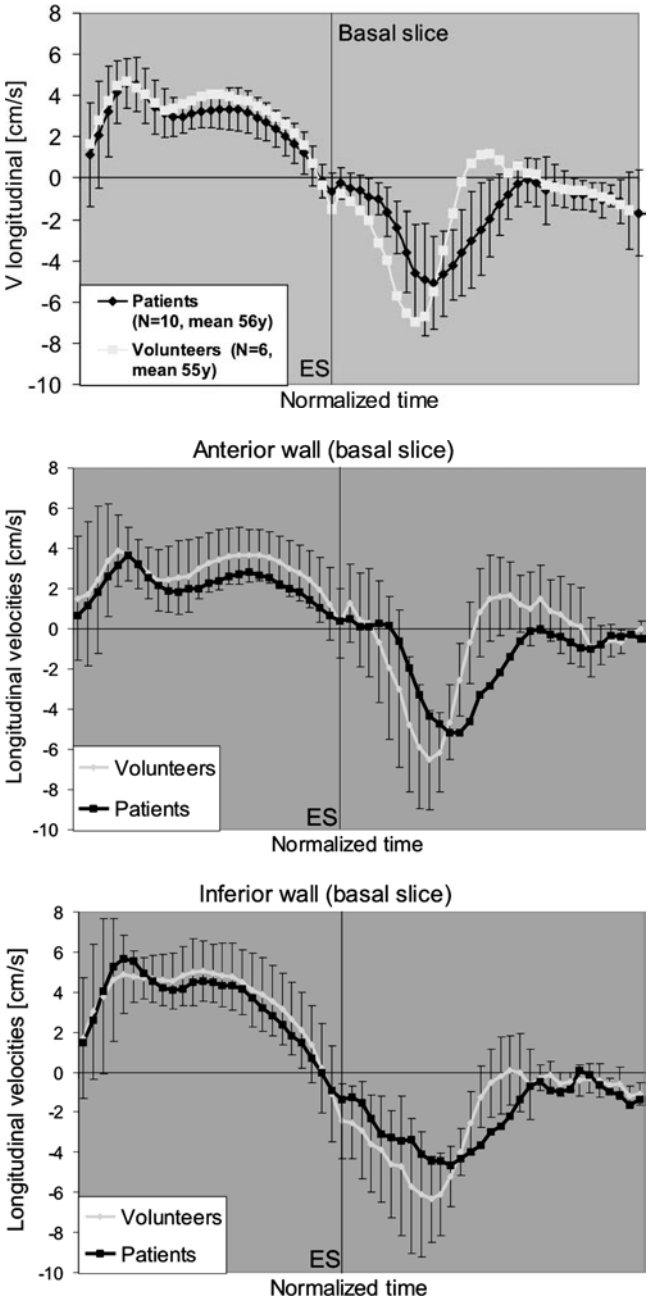

REFERENCES

1. Vasan, et al. Circulation 2000;101:2118–21.
2. Nagueh, et al. Circulation 2001;104:128–130.
3. Jung, et al. J Magn Res Imaging 2007; in press.
4. Jung, et al. Magn Res Med 2005;55:937–942.

348. PERFUSION AND EXCHANGE EFFECTS ON T_1-BASED QUANTIfiCATION OF BLOOD VOLUME

Warren D. Foltz, PhD,[1] Duncan J. Stewart, MD,[1] Graham A. Wright, PhD,[2] Alexander J. Dick, MD.[2] [1]***St. Michael's Hospital, Toronto, Ontario, Canada,*** [2]***Sunnybrook Health Sciences Centre, Toronto, Ontario, Canada.***

Introduction: Blood volume (BV) may be quantified using a two-compartment model of T_1 relaxation assuming fast-exchange (FE) and intravascular contrast. Assuming FE, Bauer demonstrated bias from perfusion under physiological conditions because arterial blood is nonexchanging (1). However, the tissue system should clearly be in intermediate exchange (IE), based on water lifetime measurements in human myocardium in vivo (intravascular lifetime or tau_i of 100 ms and extravascular lifetime or tau_e of 800 ms) which motivates further evaluation of perfusion and exchange contributions to BV (2).

Purpose: The overall purpose is the optimization of BV quantification for monitoring of myocardial viability as well as pathological and therapeutic angiogenesis.

Methods: Perfusion and exchange contributions to BV were evaluated via numerical simulation of the solution of the Bloch equations for a 4 compartment system (arterial and venous blood, intravascular and extravascular water), with bulk transport between vascular spaces and water exchange between tissue spaces. Consistent with our experimental methods, the solution included RF chopping, such that an initial inversion pulse was toggled off on subsequent sequence iterations so that signal subtraction removes the linear additive contribution to T_1. T_1 was then quantified via linear regression of the logarithmically-transformed magnitude data and inversion times. Blood volume was quantified from intravascular and tissue T_1 assuming FE[1]. The simulation was validated using known analytical solutions. The FE equation is directly applicable to the numerical predictions under true FE conditions (tau_i and tau_e of 1 and 7.9 ms, BV = 11.2%). Inclusion of perfusion under FE conditions

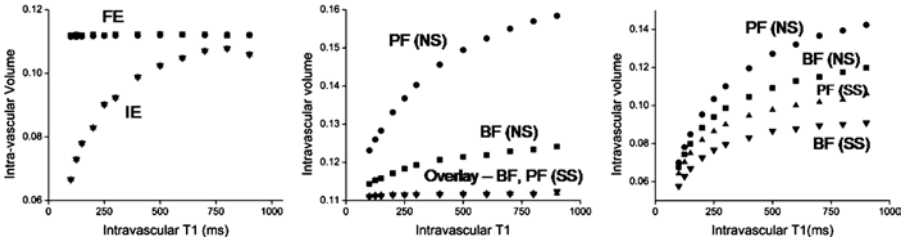

FIG. 1. (left) Overlapping of numerical and analytical solutions for FE and IE exchange without perfusion; (mid) numerical solution with FE following NS and SS inversion with basal (BF) and peak (PF) flow; and (right) numerical solution with physiological parameters for exchange with basal and peak flow. For all cases, the true BV was 11.2%.

results in a linear dependence of BV on T_{1i} when the inversion pulse is nonselective (NS), with the y-intercept representative of the true BV, and an independence of BV on T_{1i} when the inversion pulse is slice-selective (SS). The fidelity of modeling under IE conditions was evaluated using the analytical solution for two-compartment T2 relaxation (tau_i and tau_e of 100 and 792 ms), which is valid because of chopping of the additive T1 contribution. The complete solution with IE and perfusion was tested using reasonable physiological parameters for myocardial measurements (tau_i and tau_e of 100 and 792 ms, BV = 11.2%, basal and peak perfusion lifetimes of 3000 and 750 ms, T_{1i} = 1000 ms, T_{1t} = 1200 ms).[1,2] T_{1t} was evaluated at each flow rate and inversion type for T_{1i} between 100 and 900 ms.

Results: Under FE and IE conditions without perfusion, the simulation mapped identically to the appropriate analytical solutions. Consideration of FE and perfusion resulted in unbiased BV estimates at the y-intercepts of the BV and T_{1t} curves for both NS and SS inversions. A sigmoidal variation of BV at greater T_{1t} was observed following NS inversion. With IE and basal flow, the y-intercept underestimated the true BV by greater than 20% following NS inversion while the plateau of the BV and T_{1i} underestimated the true BV by greater than 10% following SS inversion. Peak flows exacerbated differences from truth.

Conclusions: Numerical modeling predicts that robust BV quantification in vivo must account for both perfusion and IE. This prediction is counter to the results of Bauer and colleagues in rat myocardium, which motivates further evaluation in a porcine myocardial model with gadomer (Schering AG) which has a long intravascular half-life. Possibly, comprehensive compartmental analysis will be requisite for robust quantification of the myocardial blood volume in vivo.

REFERENCES

1. Bauer WR. MRM 1996.
2. Bjornerud A. MRM 2003.

349. MYOCARDIAL PERFUSION CMR IMAGING USING $k - t$ SENSE

Sven Plein, MD, PhD,[1] Aleksandra Radjenovic, PhD,[1] Juerg Schwitter, MD,[2] Peter Boesiger, PhD,[3] Sebastian Kozerke, PhD.[3] [1]***University of Leeds, Leeds, United Kingdom,*** [2]***Unispital Zurich, Zurich, Switzerland,*** [3]***University and ETH Zurich, Zurich, Switzerland.***

Introduction: The simultaneous need for high temporal and spatial resolution as well as multi-slice myocardial coverage makes first pass myocardial perfusion assessment a challenging application of CMR imaging. Echo planar imaging or parallel data acquisition methods, such as SENSE or SMASH, have been successfully employed to approach these challenges. However, for both methods SNR limitations and artifacts limit the achievable acceleration. The recently proposed $k - t$ SENSE method (1) allows accelerating data acquisition further by exploiting data correlations in both space as well as time. However, $k - t$ acceleration is particularly suited to the assessment of cyclical phenomena. The application to myocardial perfusion imaging is possible, but not without challenges because of the large, rapid and nonsynchronous changes in signal intensity in various cardiac compartments during the contrast passage.

Purpose: To assess the feasibility and optimize the use of $k - t$ SENSE accelerated myocardial perfusion CMR imaging.

Methods: In vivo studies were carried out on 1.5 T and 3.0 T Philips MR systems using cardiac phased-array receiver coils. Saturation recovery segmented gradient echo (SAT-GRE) sequences (TR: 2.7 -3.1 ms, TE: 0.9–1.1 ms, flip angle: 15 deg, SAT delay: 150 ms, 62.5% partial Fourier) were employed following intravenous administration of 0.1 mmol/kg Gd-DTPA.

For simulation purposes, fully sampled data were acquired in one subject using nonaccelerated data acquisition (acquisition window 240 ms, spatial resolution: $2.7 \times 2.8 \times 10\text{mm}^3$). Based on these data, 5-, 8- and 10-fold scan acceleration was simulated and images were reconstructed using $k - t$ SENSE without and with training data plug-in (2). Signal intensity (SI) time curves were compared relative to results obtained from fully sampled data (reference). Based on the simulation, it was found that deviations from the reference SI curve increased with increasing acceleration factor as expected for a given training data resolution. To preserve temporal fidelity in the data, the training data resolution was adapted for higher acceleration factors. Good agreement was found when using 11, 17 and 21 training profiles for 5-, 8- and 10-fold acceleration in conjunction with training data plug-in (Fig. 1).

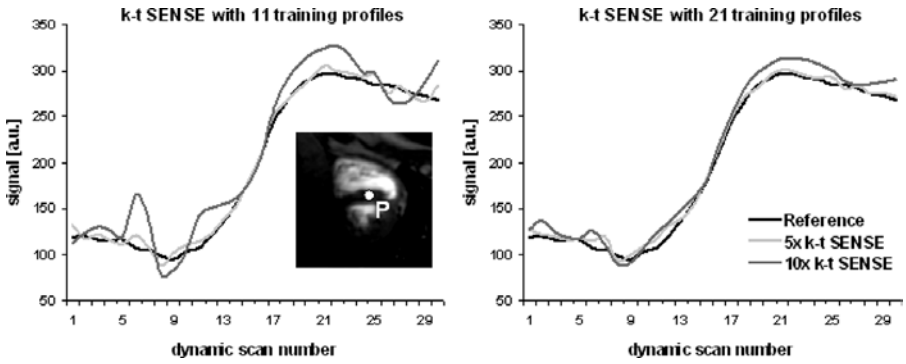

FIG. 1. Simulation results. A fully sampled data set was decimated to simulate 5× and 10× k-t SENSE. Signal-time curves were taken at the point P indicated and compared relative to data from the fully sampled reference. It is seen that at 5-fold acceleration 11 training profiles are sufficient while at 10-fold acceleration 21 instead of 11 training profiles are required to reproduce the signal changes with sufficient accuracy.

Following the insights gained from simulations, high-resolution ($1.5 \times 1.5 \times 10$ mm^3) perfusion imaging using 5-, 8- and 10-fold k-t SENSE was performed in volunteers. The acquisition of the undersampled and the training data required for k-t SENSE was fully interleaved within the same shot. The net acceleration factors, taking into account the number of nonredundant training profiles, were 3.8, 4.3 and 4.5 for 5-fold, 8-fold and 10-fold k-t SENSE, respectively. Accordingly, the acquisition windows were shortened by the respective net acceleration factors. Four slices were acquired with two slices per R-R interval. Representative frames from 5-, 8- and 10-fold accelerated k-t SENSE acquired in the same subject showed no significant differences in image quality (Fig. 2) and mean SI up-slopes (corrected for LV input) were similar (5× k-t: 10.8, 8× k-t: 11.3, 10× k-t: 12.2).

Conclusions: k-t SENSE accelerated myocardial perfusion imaging is feasible. Nominal acceleration factors between 5 and 10 can be used for 2D perfusion assessment if a sufficient training data resolution is selected. The speed-up achieved through k-t SENSE can be used to boost spatial resolution and shorten the acquisition window as demonstrated in this work.

REFERENCES

1. Tsao J, et al. Magn Reson Med 2003; 50: 1031–42.
2. Baltes C, et al.Magn Reson Med. 2005; 54: 1430–8.

350. SERIAL DELIVERY AND ASSESSMENT OF TARGETED ANTI-ANGIOGENIC THERAPY AGAINST ATHEROSCLEROSIS

Patrick Winter,[1] Shelton Caruthers,[2] Ralph Fuhrhop,[1] John Allen,[1] Todd Williams,[1] Thomas Harris,[3] Samuel Wickline,[1] Gregory Lanza.[1] ***[1]Washington University, St. Louis, Missouri, USA, [2]Philips Medical Systems, Cleveland, Ohio, USA, [3]Bristol-Myers Squibb Medical Imaging, Billerica, Massachusetts, USA.***

Introduction: Angiogenesis plays an important role in many stages of atherosclerosis, including plaque growth as well as lesion rupture. $\alpha_v\beta_3$-targeted paramagnetic nanoparticles (NP) can be used to noninvasively detect neovascular expansion of the vasa vasorum and to determine atherosclerotic burden. In addition, targeted NP can deliver anti-angiogenic drugs, such as fumagillin, directly to atherosclerotic plaques in order to intervene in the pathological process. Conventional lipid lowering medications also have anti-angiogenic effects, but they typically require long-term administration making them impractical for acute intervention. Combining the molecular imaging and drug delivery abilities of targeted NP allows localized treatment as well as monitoring of atherosclerosis.

Purpose: This study evaluates the efficacy of repeated doses of targeted therapeutic nanoparticles with and without lipid

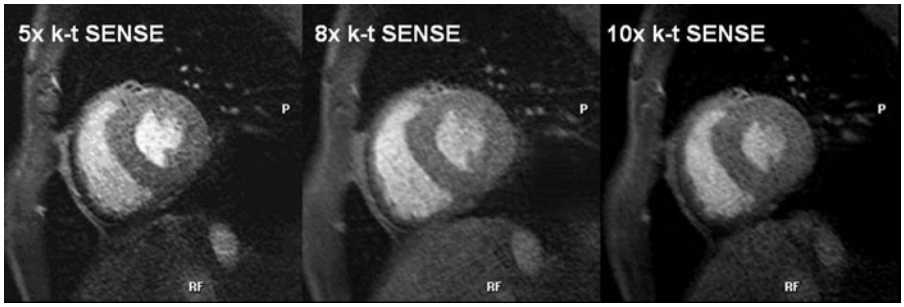

FIG. 2. Comparison of 5×, 8× and 10× k-t SENSE perfusion images acquired in the same subject. Image quality and SI slopes were found to be comparable.

lowering medication (atorvastatin) for inhibiting neovascular proliferation in atherosclerotic plaques.

Methods: Cholesterol-fed rabbits received $\alpha_v\beta_3$-targeted paramagnetic NP with (n = 9) or without (n = 9) fumagillin (30 μg/kg body weight) at weeks 0 and 4 of the study. A portion of the animals (n = 4 per group) was treated with atorvastatin included in the high-cholesterol chow (44 mg/kg feed). Followup assessment of anti-angiogenic response was evaluated at weeks 2, 4, 6 and 8 using $\alpha_v\beta_3$-targeted paramagnetic NP lacking the drug. MRI signal enhancement from the aortic vasa vasorum neovasculature was calculated from transverse black-blood MR images (1.5T) collected before and 4 hours post NP injection (1 mL/kg body weight). The MRI enhancement observed at each followup exam was normalized with respect to the enhancement measured at week 0.

Results: At all timepoints, MRI enhancement in the thoracic aorta of control rabbits was similar to the value observed at week 0 (Figure 1). Enhancement in rabbits receiving $\alpha_v\beta_3$-targeted fumagillin NP with or without statin was lower at week 2 compared with the baseline values. Animals receiving only $\alpha_v\beta_3$-targeted fumagillin NP had decreased enhancement at week 6, which increased at week 8 reflecting recurrence of pathological angiogenesis at this timepoint (4 weeks after the last NP treatment). Treatment with only atorvastatin showed a slow decrease in enhancement reflecting the gradual anti-angiogenic effect of oral statins. Rabbits receiving $\alpha_v\beta_3$-targeted fumagillin NP and atorvastatin showed reduced enhancement at weeks 6 and 8 (Figure 1, *$p < 0.05$), indicating sustained suppression of neovascular proliferation despite the intervening weeks since the last NP injection.

Conclusion: $\alpha_v\beta_3$-targeted paramagnetic NP allow noninvasive quantification of atherosclerotic disease progression and are able to effectively deliver fumagillin for anti-neovascular therapy. While fumagillin NP provide rapid suppression of angiogenesis, this effect is only transient, lasting for 3 to 4 weeks.

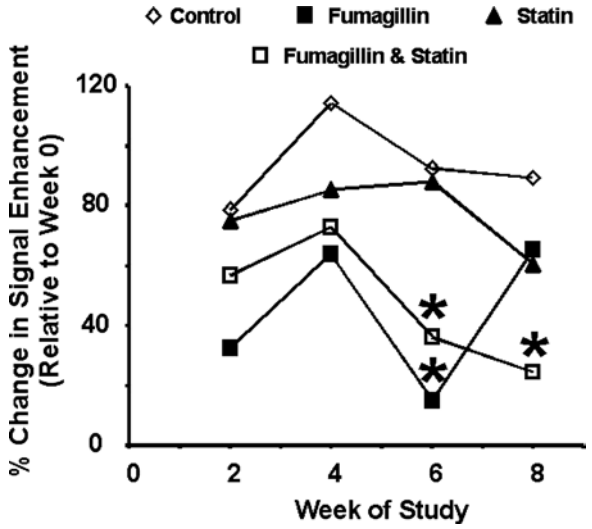

FIG. 1.

The anti-angiogenic effect of lipid lowering drugs, on the other hand, is much slower but provides sustained treatment. Combining the fast acting nature of targeted fumagillin NP with the long lasting benefits of atorvastatin could allow rapid and persistent inhibition of angiogenesis associated with atherosclerosis. These data illustrate the potential of molecular imaging and targeted therapy to improve the treatment and monitoring of atherosclerosis, which may prevent subsequent myocardial infarction or stroke.

351. HIGH-RESOLUTION 11.7 TESLA MRI FOR THE DETECTION OF ACTIVATED PLATELETS USING AN ACTIVATION-SPECIFIC PLATELET CONTRAST AGENT IN AN EX VIVO MOUSE MODEL

Constantin von zur Muehlen,[1] Juergen Schneider, PhD,[1] Ziad Ali, MD,[1] Martina McAteer, PhD,[1] Stefan Neubauer, MD,[1] Keith Channon, MD,[1] Christoph Bode, MD,[2] Karlheinz Peter, MD,[3] Robin Choudhury, MD.[1] [1]***University of Oxford, Oxford, United Kingdom,*** [2]***University Hospital Freiburg, Freiburg, Germany,*** [3]***Baker Heart Institute, Melbourne, Australia.***

Introduction : Combining Magnetic Resonance Imaging (MRI) with targeted contrast agents provides an important opportunity to detect thrombosis/thromboembolism and to identify unstable atherosclerotic plaques. The surface of ruptured atherosclerotic plaque is lined with activated platelets, constituting an attractive molecular contrast target. We evaluated whether (1) microparticles of iron oxide (MPIO) coupled to single-chain antibodies against ligand-induced binding-sites (LIBS) specific for the activated conformation of glycoprotein IIb/IIIa could be targeted to platelets in a mouse angioplasty model and (2) whether bound MPIO could be quantified by MRI.

Methods and Results: One μm sized MPIOs were conjugated to anti-LIBS single-chain antibody (LIBS-MPIO) or a non-specific antibody (cont-MPIO). Twenty-four hours after femoral artery wire injury in mice, dense platelet adhesion was present at the site of injury. Mice were killed and perfused with cont-MPIO or LIBS-MPIO via the left ventricle. *Ex vivo* MRI was performed at 11.7 T using a 13 mm ^{1}H birdcage radiofrequency coil (RAPID Biomedical, Würzburg, Germany). A 3D gradient echo sequence (TE = 4 ms/TR = 90 ms, field of view 13 × 13 × 19.5 mm, matrix size 256 × 256 × 384, two averages, imaging time ~ 7 h per sequence) was used in an unattended overnight run. Data reconstruction was performed off-line with a final isotropic resolution of 25 μm^3. Bound beads appeared as circular, intensely low signal areas in the lumen (Fig. 1, arrows). Quantified by MRI low signal areas were more frequent with LIBS-MPIO than cont-MPIO (23.7 vs. 6.2; $p < 0.01$). Histology confirmed significantly greater binding of LIBS-MPIO (9.98 vs. 0.5 beads/section; $p < 0.01$). Low signal zones on MRI and MPIOs in the histological sections correlated strongly,

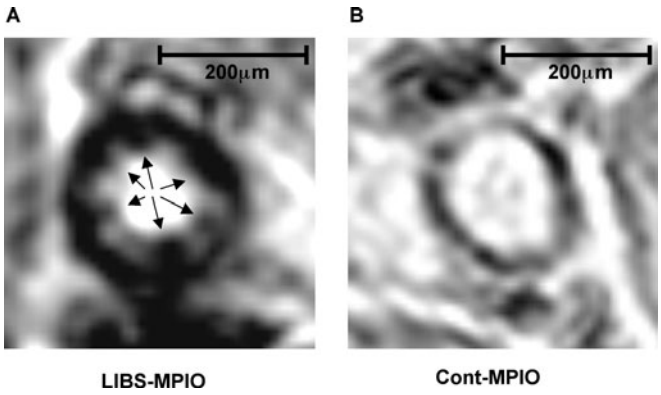

FIG. 1.

indicating accurate quantification with MRI ($R^2 = 0{,}72$; $p < 0.001$).

Conclusions: (1) LIBS-MPIO specific for *activated* platelets provide a functional molecular MRI contrast agent. (2) Bound MPIOs are readily identified with MRI. (3) MRI provides quantitative data on bead binding. (4) These results provide a promising basis for the use of this contrast imaging strategy to identify activated platelet thrombi in a range of pathologies.

352. VISUALIZATION AND TRACKING OF A CONVENTIONAL PASSIVE CORONARY GUIDEWIRE IN A SWINE WITH REAL-TIME FLAPS

Ioannis Koktzoglou, MS, Richard Tang, MD, Kathleen R. Harris, BA, Debiao Li, PhD, Rohan Dharmakumar, PhD.
Northwestern University, Chicago, Illinois, USA.

Introduction: 'Positive contrast' imaging (PCI) has emerged as a way to visualize off-resonant spins neighboring magnetically labeled cells and catheters (1, 2). Recently, Fast Low Angle Positive contrast with Steady-state free precession imaging (FLAPS) has been proposed as a time-efficient PCI technique for generating bright signals from off-resonant spins (3). FLAPS may allow for tracking of conventional (i.e., radio-opaque), passive endovascular devices that, relative to active devices, are more accessible and offer better mechanical properties with reduced risk of heating.

Purpose: To examine whether a FLAPS technique, modified to highlight magnetic field deviations, enables the visualization and tracking of a conventional passive coronary guidewire in a controlled phantom and in a swine.

Materials and Methods: All MRI experiments were performed in a 1.5 T scanner (Siemens, Erlangen, Germany). Phantom experiments were performed using a 4 channel head coil, and animal experiments were performed using a spine array coil and a 6-element cardiac coil. *Phantom Protocol:* Visualization and tracking of a 0.018 inch diameter coronary guidewire (Glidewire Gold, Terumo Medical Co., Tokyo, Japan) was performed in a thoracic aortic phantom (Elastrat, Geneva, Switzerland) filed with tap water. In the phantom experiments, the guidewire was advanced to the aortic root outside of the MRI scanner, and retracted under real-time FLAPS MRI to the inferior descending thoracic aorta. Imaging parameters for the real-time FLAPS protocol were: oblique sagittal slice orientation yielding a 'candy cane' view of the thoracic aorta, TR/TE = 2.8/1.4 ms, flip angle = 20°, FOV = 22.5 × 30 cm^2, matrix = 144 × 256, slice thickness = 15 mm, BW = 1530 Hz/pixel, frame rate = 2.5 s^{-1}. *Animal Protocol:* Another 0.018 inch diameter coronary guidewire (Glidewire Gold, Terumo Medical Co.) was introduced into the femoral artery of one 30 kg domestic pig and advanced into the abdominal aorta under x-ray guidance. The animal was transferred into the MR suite and, under real-time MRI guidance with the FLAPS technique, the guidewire was advanced through the thoracic aorta and into the left ventricle. Imaging parameters for the FLAPS protocol were: oblique sagittal slice orientation, TR/TE = 2.7/1.4 ms, flip angle = 20°, FOV = 25 × 25 cm^2, matrix = 192 × 192, half partial Fourier, slice thickness = 15 mm, BW = 1530 Hz/pixel, and frame rate = 3.6 s^{-1}.

Results: Visualization and tracking of the guidewire with positive contrast FLAPS was readily visible in the thoracic aortic phantom (Fig. 1) and *in-vivo* (Fig. 2). Figure 1 shows FLAPS images of a realistic phantom of the thoracic aorta displaying the retraction of the guidewire from the aortic root (ar) and through the ascending aorta (asc), aortic arch (aa), and the descending aorta (des). The guidewire's length (hollow arrows) and tip (white arrows) are visible. Figure 2 shows FLAPS images acquired in a live swine displaying the passing of a 0.018 inch diameter guidewire from the abdominal aorta into the left ventricle. The guidewire's length (hollow arrows) and tip (white arrows)

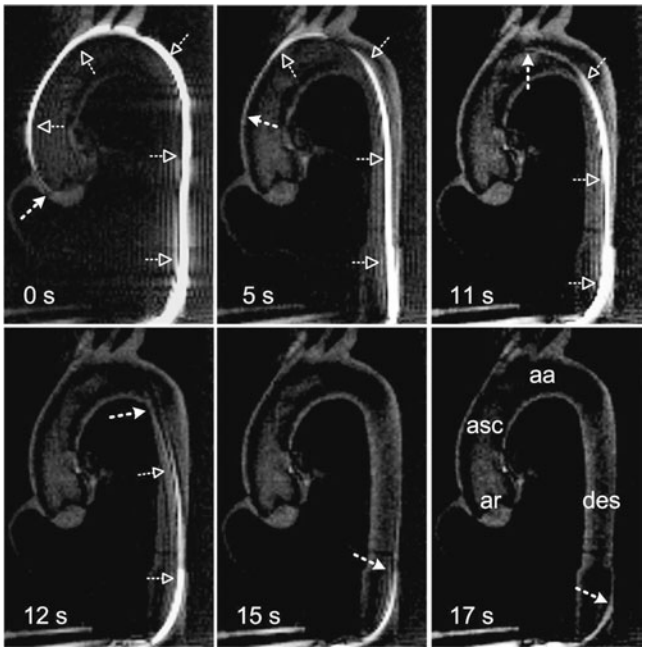

FIG. 1.

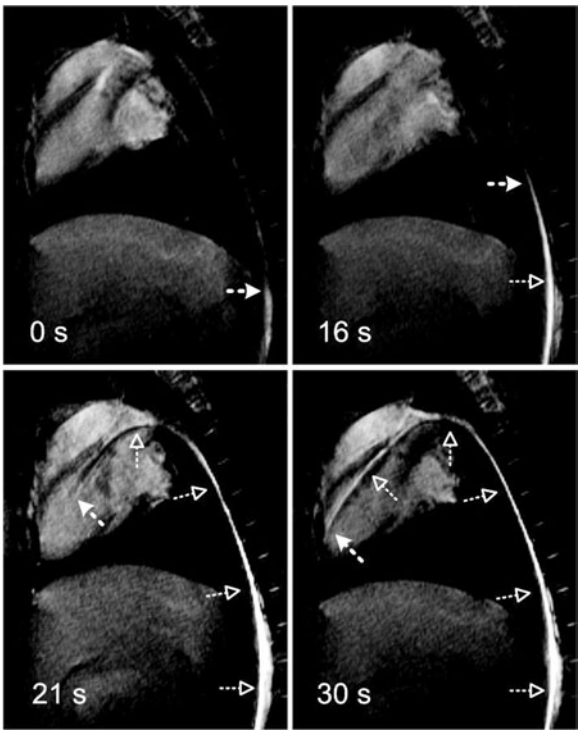

FIG. 2.

are visible. For both figures, time is given in the bottom left corner.

Conclusion: Passive guidewire visualization and real-time tracking is feasible with FLAPS *in-vivo*. Real-time FLAPS appears to be a promising technique for interventional MR applications seeking to track passive endovascular devices.

REFERENCES

1. Cunningham, et al. Magn Reson Med 2005;53:999–1005.
2. Seppenwoolde, et al. Magn Reson Med 2003;50:784–790.
3. Dharmakumar, et al. Phys Med Biol 2006;51:4201–4215.

353. STRONG PROGNOSTIC IMPLICATION OF LEFT ATRIAL CONDUIT AND PUMP FUNCTIONS ASSESSED BY CARDIAC MAGNETIC RESONANCE IN HYPERTENSIVE PATIENTS AT RISK OF DIASTOLIC DYSFUNCTION

Matthew Kaminski, MD, Sui Tsang, BSc, Thomas H. Hauser, MD, Rodney Falk, MD, Raymond Y. Kwong, MD, MPH.
Brigham and Women's Hospital, Boston, Massachusetts, USA

Introduction: Patients with hypertensive cardiomyopathy are at increased risk of major adverse cardiac events (MACE) despite preserved systolic left ventricular (LV) function. Left atrial (LA) size has been proposed to be a load-insensitive marker of hemodynamic diastolic impairment of the LV.

LAV by Geometric Assumption Method (GEO)		
	HR (95% CI)	p-value
LAV at ventricular end-diastole* (ml/m^2)	1.001 (1.00–1.002)	0.09
LAV at ventricular end-systole* (ml/m^2)	1.00 (0.99–1.00)	NS
LAV before atrial contraction* (ml/m^2)	1.00 (0.99–1.00)	NS
Percent of LA emptying by conduit function	0.98 (0.95–1.02)	0.36
Percent of LA emptying by pump function	0.94 (0.91–0.98)	0.003
Direct 3-Plane LA Area Measurement (DIRECT)		
LAV at ventricular end-diastole* (cm^2/m^2)	1.07 (1.01–1.13)	0.02
LAV at ventricular end-systole* (cm^2/m^2)	1.04 (0.98–1.11)	NS
LAV before atrial contraction* (cm^2/m^2)	1.06 (1.00–1.12)	0.06
Percent of LA emptying by conduit function	0.92 (0.85–0.99)	0.03
Percent of LA emptying by pump function	0.93 (0.88–0.98)	0.005

*Indexed to body surface area (BSA).

Purpose: We tested the hypothesis that impaired conduit and pump functions of the LA during ventricular diastole assessed by cardiac MR (CMR) are associated with MACE. We further examined the prognostic association between 2 LA sizing methods, one with and one without geometric assumptions.

Methods: One hundred eighty-five hypertensive patients without evidence of prior myocardial infarction underwent a clinically-indicated CMR. We assessed the LA size by direct area measurements in 3 radial planes (DIRECT) and by a standard geometric model (GEO) which calculated LA volume (LAV). LA size was assessed at three time phases during ventricular diastole to determine the conduit and pump functions.

Results: During a median follow up of 19 months, 35 patients experienced MACE, including 16 deaths. LA conduit and pump functions by the DIRECT method were highly correlated to the GEO method ($r = 0.85$, $p < 0.0001$ and $r = 0.83$, $p < 0.0001$, respectively). LA conduit function by the DIRECT method was also inversely correlated to LV mass ($r = -0.19$, $p = 0.01$). Decreased LA conduit and pump functions by the DIRECT method demonstrated strong association with MACE and provided more prognostic information than the GEO method (Table 1).

Conclusions: CMR assessment of LA mechanics without any geometric assumption provides strong prognostic information in hypertensive patients.

354. THE INFLUENCE OF RENAL MRI/MRA DIAGNOSED RENAL ARTERY STENOSIS ON GLOMERULAR FILTRATION RATE AND RENAL

PARENCHYMAL VOLUME IN PATIENTS WITH ATHEROSCLEROTIC RENOVASCULAR HYPERTENSION

Rajiv Agarwal, MD,[1] Samir Amin, BA,[2] Raja Muthupillai, PhD,[3] Scott D. Flamm, MD.[1] [1]***Cleveland Clinic Foundation, Cleveland, Ohio, USA,*** [2]***Baylor College of Medicine, Houston, Texas, USA,*** [3]***Philips Medical Systems, Cleveland, Ohio, USA.***

Introduction: Atherosclerotic renovascular hypertension is a common clinical entity with considerable implications if left undiagnosed or untreated. Appropriate therapy must be implemented early to avoid irreversible ischemic death of the affected kidney. MRI/MRA has become a robust noninvasive imaging modality to diagnose renal artery stenosis (RAS) and simultaneously can accurately assess renal parenchymal volume. However, the relationship among the severity of RAS, renal volume, and renal function (as measured by glomerular filtration rate [GFR]) is unknown.

Purpose: To determine the relationship among RAS, renal parenchymal volume, and renal function as measured by glomerular filtration rate using the Modification of Diet in Renal Disease (MDRD) equation.

Methods: From January 2002 to November 2005, 1050 patients (518 males, 532 females) underwent renal MRI/MRA on a 1.5 T Philips MR system for suspected renovascular hypertension. T1 and T2 weighted axial and coronal images were obtained pre and post gadolinium administration. Additionally, contrast enhanced 3D MRA and 3D phase contrast MRA were performed. Main renal arteries were assessed for degree of RAS. The severity of RAS was graded as mild, moderate, or severe (includes occluded). Patient charts were reviewed for demographic and laboratory data. GFR (mL/min per 1.73 m^2) was calculated by the widely accepted MDRD equation (incorporating the patient's age [years], race, gender, and concentrations of serum creatinine [mg/dL], urea nitrogen [mg/dL], and albumin [g/dL]). Individual kidney volumes were calculated from MRI by the disc-summation method. Similar data was obtained for an additional 200 patients with suspected renovascular hypertension but without evidence for RAS (control group).

Results: Twenty-four and two tenths percent of patients (252/1050) who underwent renal MRI/MRA had evidence for RAS. Laboratory data necessary to calculate GFR by the MDRD equation was available for 108 (52 males, 56 females) of these patients, as well as 75 (32 males, 43 females) of the 200 patients without RAS. In patients with severe stenosis or occlusion of at least one renal artery (n = 50), GFR was 29.2 mL/min per 1.73 m^2 and volume of the affected kidney 107 mm^3 (Table 1). In patients with moderate RAS (n = 29), GFR was 31.2 mL/min per 1.73 m^2 and volume of the affected kidney 130 mm^3. Similarly, in patients with mild RAS (n = 29), GFR was 41.7 mL/min per 1.73 m^2 and volume of the affected kidney 135 mm^3. Finally, in patients without RAS, GFR was 54.8 mL/min per 1.73 m^2 and volume was 164 mm^3. As expected, females had lower GFR and kidney volumes compared to males in all groups.

Conclusions: In our study of patients with suspected renovascular hypertension, calculated MDRD GFR correlates inversely with the severity of RAS. The decrease in GFR is statistically significant even for patients with mild RAS compared to those without RAS. Similar differences are also seen in patients with moderate RAS compared to those with mild RAS. However, GFR is not significantly different between moderate and severe RAS groups. Renal volumes are significantly reduced in patients with mild RAS compared to those without RAS, and in patients with severe RAS compared to those with moderate RAS. However, there was no significant difference in renal volumes between patients with mild and moderate degrees of RAS. Our study suggests that there is a substantial decline in renal function when the severity of RAS progresses from none to mild and from mild to moderate; however, MDRD GFR plateaus once moderate RAS develops. On the other hand, decline in renal volumes is seen primarily at both ends of the spectrum of RAS. These findings suggest that with mild RAS calculated renal parenchymal volumes are reflective of declines in renal function. With moderate or greater RAS, renal parenchymal volumes demonstrate greater changes than MDRD GFR.

TABLE 1
Severity of RAS vs. MDRD GFR and Renal Parenchymal Volume

Severity of RAS by CMR/CMRA	n	Age (years)	Serum Creatinine (mg/dL)	Serum Urea Nitrogen (mg/dL)	Serum Albumin (g/dL)	Calculated GFR (mL/min per 1.73 m^2 ± SD)	Affected Kidney Volume (mm^3)
Severe	50	76	2.4	47	3.6	29.2 ± 15.9	107
Moderate	29	74	2.3	47	3.5	31.2 ± 16.8	130
Mild	29	69	1.8	33	3.8	41.7 ± 20.4	135
None	75	61	1.7	32	3.6	54.8 ± 33.3	164

For GFR: p =< 0.05 for none vs. mild and mild vs. moderate; p = NS for moderate vs. severe.
For Volume: p =< 0.05 for none vs. mild and moderate vs. severe; p = NS for mild vs. moderate.

355. AN OPERATOR-INDEPENDENT 3D WHOLE HEART MRI TECHNIQUE FOR CARDIAC FLOW ESTIMATIONS

Lau Brix, MSc,[1] W. Yong Kim, MD, PhD,[2] Steffen Ringgaard, MSc, PhD,[2] Thomas S. Sørensen, MSc, PhD.[3]
[1]Department of Biomedical Engineering, Aarhus University Hospital, Aarhus N, Denmark, [2]MR Research Centre, Aarhus University Hospital, Aarhus N, Denmark, [3]Centre for Advanced Visualization and Interaction, University of Aarhus, Aarhus N, Denmark.

Introduction: Cardiac MRI (CMR) is a well-established imaging technique for measuring blood flow in the large vessels surrounding the heart. Currently, standard operator-dependent 2D CMR techniques are being used clinically for volumetric flow measurements. By measuring the 3D velocity field in a 3D volume, the blood flow can be determined in any imaging plane. This 3D approach may facilitate quantitative flow measurements in patients suffering from congenital or acquired heart disease.

Purpose: To compare flow values from an operator-independent, respiratory gated, 3D CMR technique, which enable quantification of aortic and pulmonary blood flow with flow values obtained by a conventional 2D flow technique.

Methods: The applied 3D flow technique was an isotropic 3D segmented k-space phase-contrast gradient echo sequence (4 *k*-lines per heart-phase) with a short EPI readout (EPI factor = 5). The protocol had a spatial resolution of 3.0 × 3.0 × 3.0 mm^3, a SENSE factor of 2.6, a flip angle of 10°, a matrix size of 128 × 128 and a velocity encoding of 150 cm/s.

A conventional segmented k-space (3 *k*-lines per heart-phase) 2D navigator gated flow sequence was run with a resolution of 1.41 × 1.41 × 5.0 mm^3, a flip angle of 25°, a matrix size of 256 × 256 and 2 signal averages. The 2D slices were placed approximately 3 cm above and perpendicular to the aortic and the pulmonary valves respectively.

Both techniques used a navigator gating window of 8 mm which yielded an efficiency of approximately 50%. Both sequences were evaluated in 10 healthy subjects (age 29 ± 7, 2 females and 8 males). All data were acquired in each individual during the same examination session to ensure comparability. Quantitative data analyses were performed retrospectively with dedicated software developed by a co-author. The software enabled automatic alignment of the 2D flow slice in the 3D flow volume (Fig. 1A). Thus, 2D and 3D scans could be compared directly. Statistical analyses were done by Wilcoxon matched pairs signed rank test and by Bland & Altman plots.

Results: Statistical analyses did not reject the null hypothesis indicating that the 2D and the 3D techniques yielded similar flow results (*Aortic flow:* 2D = 101.1 ± 17.4 mL and 3D = 92.5 ± 19.8 mL, p = 0.20, *Pulmonary flow*: 2D = 85.0 ± 11.4 mL and 3D = 79.5 ± 19.4 mL, p = 0.64). However, Bland & Altman plots of the data suggest that the 3D technique underestimates flow compared to 2D flow (Fig. 1B).

Discussion: Our results suggest that the two blood flow measurement methods provide similar flow results. However, the 3D method had a tendency to underestimate the flow values as compared to the 2D method.

Operator-independent 3D acquisition allows for convenient off-line flow quantification in any imaging plane. Furthermore, it is possible to automatically reformat a slice in the 3D flow acquisition that matches the imaging plane of an arbitrary

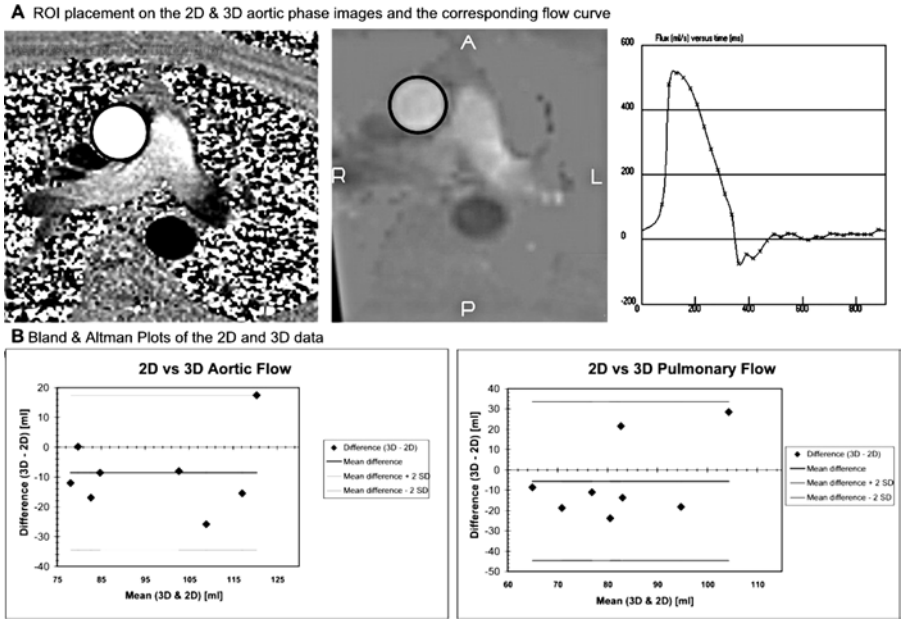

FIG. 1. (A) ROI placement on the 2D & 3D aortic phase images and the corresponding flow curve. (B) Bland & Altman Plots of the 2D & 3D data.

morphological or functional acquisition. Therefore, isotropic 3D whole heart flow measurements may facilitate integration of flow and anatomy in evaluation of complex congenital heart disease as well as acquired heart diseases.

Conclusions: Three dimensional whole heart flow measurements allows for quantitative flow estimation in the aorta and pulmonary artery. Further evaluation is needed in patients with heart disease to establish the clinical potential.

356. INVESTIGATION OF THE PATHOLOGIC BASIS OF Q WAVES WITH MR IMAGING AS REFERENCE METHOD

Minna B. Carlsson, BSc,[1] Henrik Engblom, MD,[1] Erik Hedstrom, PhD,[1] Einar Heiberg, MSc, PhD,[1] Martin Ugander, MD, PhD,[1] Galen S. Wagner, MD,[2] Hakan Arheden, MD, PhD.[1] [1]***Lund University, Lund, Sweden,*** [2]***Duke University Medical Center, Durham, North Carolina, USA.***

Background: Historically, Q waves on ECG have been associated with transmural myocardial infarction (MI). It has, however, been difficult to establish the pathologic basis for Q waves in humans, due to lack of accurate *in vivo* methodology for differentiation between infarcted and noninfarcted myocardium. Recently, delayed contrast enhanced cardiovascular magnetic resonance imaging (DE-MRI) has been shown to have great ability to detect infarcted myocardium and is, therefore, a good reference method for ECG studies. Histopathology and imaging studies have shown that the relation between Q waves and transmurality is not as close as previously reported. Considering the fact that the first part of the QRS complex reflects depolarization of subendocardial myocardium, endocardial extent of MI might be predictive of pathological Q waves. Since the terms Q-wave MI and nonQ-wave MI are well established clinical entities, it is of clinical importance to increase the understanding of the pathologic basis of Q waves. The aim of this study was therefore to test the hypothesis that endocardial extent of MI is more predictive of pathological Q-waves than is infarct transmurality. We also sought to investigate the relation between QRS scoring and different MI characteristics.

Methods: Twenty-nine patients (27 men, 41–83 years) with reperfused first-time acute MI were prospectively included. One week after admission, DE-MRI was performed, and a 12 lead ECG was recorded. Infarct size, MI transmurality and endocardial extent of MI were measured on the DE-MRI images. Q waves were identified according to Minnesota coding, and MI size was estimated by QRS scoring.

Results: A significant difference was found between patients with and without Q waves with regard to MI size ($p = 0.03$) (Fig. 1A) and endocardial extent of MI ($p = 0.01$) (Fig. 1B), but not with regard to mean and maximum MI transmurality

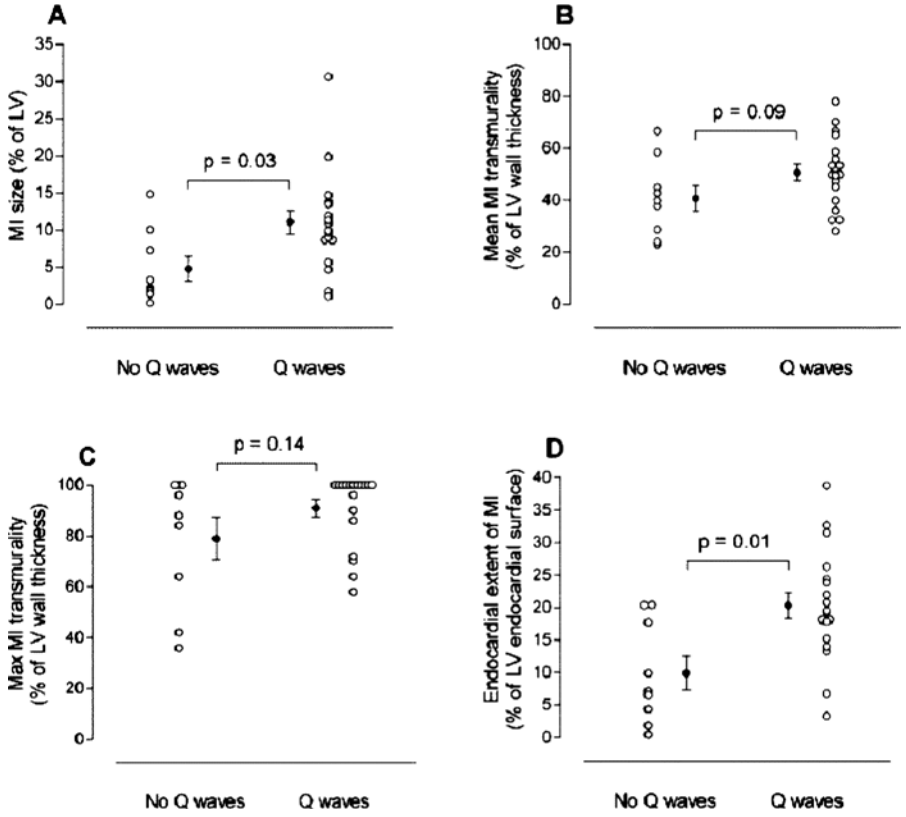

($p = 0.09$ and $p = 0.14$) (Fig. 1C and D). Multivariate logistic regression analysis showed that endocardial extent was the only independent predictor of pathological Q waves. Of the MI characteristics investigated, QRS score was most strongly correlated to endocardial extent of MI ($r_s = 0.86$, $p < 0.001$).

Conclusion: The endocardial extent of reperfused first-time acute MI is more predictive of pathological Q waves than is MI transmurality, and QRS scoring is most strongly correlated to endocardial extent of these infarcts.

357. NEW INSIGHTS INTO PULMONARY REGURGITATION: CONSEQUENCES FOR VENTRICULAR PERFORMANCE AND EXERCISE CAPACITY

Louise Coats, MRCP,[1] Sachin Khambadkone, MD, MRCP,[1] Graham Derrick, MRCP,[1] Marina Hughes,[1] Rod Jones, MSc,[1] Bryan Mist, PhD,[2] John E. Deanfield, FRCP,[1] Philipp Bonhoeffer, MD,[1] Andrew M. Taylor, MD, MRCP FRCR.[1]
[1]Great Ormond Street Hospital for Children, London, United Kingdom, [2]The Heart Hospital, London, United Kingdom.

Background: Chronic pulmonary regurgitation (PR) is associated with an adverse prognosis. Percutaneous pulmonary valve implantation (PPVI) can treat this condition without cardiopulmonary bypass and provides a model with which to study the potential for right ventricular recovery.

Method: We selected 17 patients (age 21.2 ± 8.7 years) from our total population of 125 who had undergone PPVI for various indications because they had important PR (regurgitant fraction >25% on magnetic resonance [MR]) and an echocardiographic gradient < 50 mmHg across the right ventricular (RV) outflow tract. Cardiopulmonary exercise testing and CMR were performed before and within 3 months of PPVI.

Results: Following PPVI, MR showed a reduction in PR (40.7 ± 7.3 to 4.1 ± 6.1%, $p < 0.001$), a fall in RV end diastolic volume (115.4 ± 33.1 to 98.9 ± 32.0 mL/m^2, $p = 0.001$) and an increase in effective RV stroke volume (34.3 ± 7.8 to 44.4 ± 9.3 mL/m^2, $p < 0.001$). Left ventricular end diastolic volume (66.6 ± 18.0 to 73.4 ± 16.5 mL/m^2, $p = 0.014$), stroke volume (38.4 ± 11.1 to 46.4 ± 10.2 mL/m^2, $p = 0.001$) and ejection fraction (57.8 ± 8.1 to 63.5 ± 5.2 mL/m2, $p = 0.001$) increased. Though patients felt better, there was no change in oxygen consumption at the anerobic threshold or at maximal exertion.

Conclusion PPVI relieves PR and restores compensatory cardiac performance. The lack of improvement in standard exercise parameters suggests that, in contrast to pressure overload, the contractile reserve of chronically volume-overloaded myocardium may be limited.

358. COMPREHENSIVE EVALUATION OF PERIPHERAL ARTERIAL DISEASE USING MULTI-MODALITY MAGNETIC RESONANCE

Justin D. Anderson, MD, Frederick H. Epstein, PhD, Craig H. Meyer, PhD, Patrick Norton, MD, Nancy Harthun, MD, Klaus D. Hagspiel, MD, David C. Isbell, MD, Stuart S. Berr, PhD, Arthur Weltman, PhD, Joseph M. DiMaria, BA, Jennifer R. Hunter, RN, John Christopher, RT, Christopher M. Kramer, MD. ***University of Virginia, Charlottesville, Virginia, USA.***

Introduction: Current diagnostic techniques for peripheral arterial disease (PAD) rely on angiography, which is insensitive to vessel wall plaque and its effect on downstream muscle microcirculation and metabolism. We have recently developed a comprehensive MR approach to PAD, including vessel wall imaging for plaque volume and peak-exercise calf muscle perfusion and phosphocreatine (PCr) recovery time. These techniques may improve upon angiography for characterizing disease severity and progression. Thus, we examined the feasibility of completing all of these measures in patients with PAD.

Methods: Patients with mild to moderate symptomatic PAD by ankle-brachial index (ABI) were recruited and had one leg imaged. Gadolinium-DTPA (0.2 mM/kg) enhanced MR angiography from the abdominal aorta to the foot was performed with a moving table/bolus chase technique in 3 stations (64–104 slices, FOV 500, TR 2.5–3.0, TE 1.0–1.1, flip 20–25°, voxel

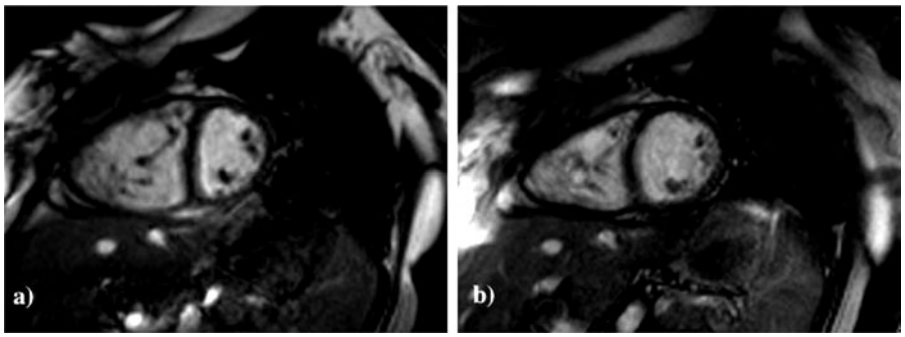

FIG. 1. Balanced steady-state free precession short axis cine MR image a) before and b) after PPVI.

size 1.6–2.0 × 1.0–1.3 × 1.0–1.5 mm) (Fig. 1A, tight stenosis in proximal left superficial femoral artery [SFA]). For analysis, a 16 arterial segment model and five point ordinal scale (0–4, 4 = occluded) was used to grade severity of disease by segment and was then indexed to all 16 segments (MRA score) and to the 7 SFA inflow segments only (inflow score). Plaque volume (PV) in the SFA was assessed using a custom-built flexible, linear four-element surface coil array and a fat suppressed multi-slice turbo-spin-echo pulse sequence with blood suppression and spatial presaturation (TR 715 ms, TE 7.6 ms, echo spacing 7.5 ms, voxel size 0.5 × 0.5 × 3 mm, 3 mm thick, 4 signal averages) (Fig. 1B, same patient, same level as stenosis on MRA). PV was defined as (Total vessel area—lumen area) × slice thickness and analyzed with VesselMASS software. Calf muscle perfusion was measured at peak exercise performed on an MR-compatible ergometer using first pass gadolinium-DTPA enhanced imaging (0.1 mmol/kg). A GRE pulse sequence imaged muscle perfusion in the mid-calf (inversion recovery, TI 320 ms) with FOV 180 × 180, matrix = 64 × 64, flip 15°, TR 900, TE 1.8 (Figure 1C, same patient, bottom arrow points to high signal in soleus which is perfused at peak exercise). Tissue function (TF) was measured from time intensity curves in regions of interest in calf muscle. PCr recovery time was analyzed by ^{31}P MRS during recovery from peak exercise using a single-pulse, surface coil localized, 512 ms free induction decay acquisition centered on the mid-calf and a monoexponential fit of PCr versus time, beginning at cessation of exercise (Fig. 1D, same patient, PCr recovery time 122 seconds). Data are presented as mean ± S.D.

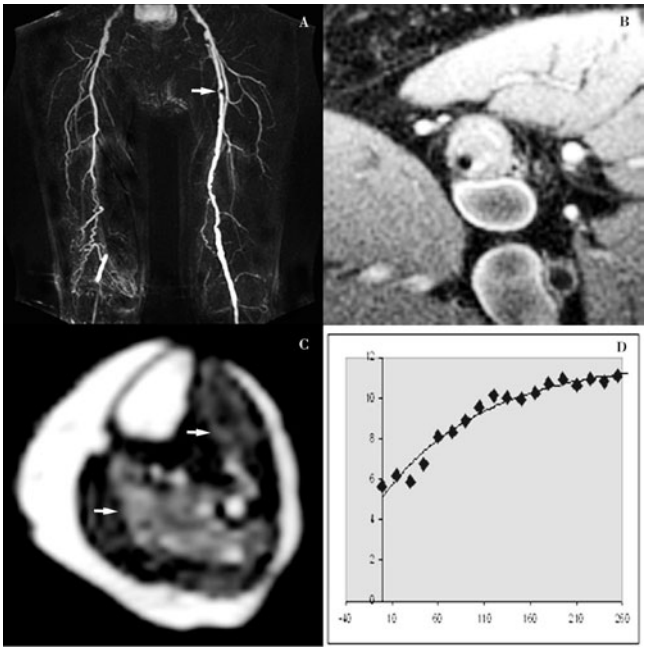

FIG. 2. A. MR angiogram of the SFA. Note the tight stenosis in the proximal SFA. B. T1-weighted black blood vessel wall image at the site of the maximal obstruction on the MRA. C. Image of post-exercise peak perfusion of the calf. Note the heterogeneity of signal inensity in the calf muscle depending in part on the muscles used to exercise. D. PCr recovery time plot. The PCr recovery time constant in this patient was 122 sec (normal = 34 sec).

Results: Fifteen patients (age 65 ± 10 years) with mild to moderate PAD (mean ABI 0.68 ± 0.12) completed the study except for 3 with technically inadequate perfusion imaging. Twelve left and 3 right legs were imaged. Mean PV was 10.2 ± 5.2 cm^3, and PV/total vessel volume (TVV) was 0.73 ± 0.12. Mean work performed during exercise was 164 ± 113 joules. Mean TF slope was 2.15 ± 0.65 (normal = 3.14 ± 0.54) and PCr recovery time 89 ± 71 seconds (normal = 34 ± 17 seconds). Mean inflow score was 1.13 ± 0.47 and MRA score was 1.40 ± 0.66. Plaque volume (PV) correlated with calf tissue perfusion (TF) in the 12 patients with perfusion measurements ($p = 0.05$, $r = 0.553$). In all 15 patients, PV/TVV correlated with both inflow score ($p < 0.001$, $r = 0.773$), and CMRA score ($p < 0.05$, $r = 0.527$). A trend towards a relationship was observed between TF and PCr recovery time ($p = 0.08$, $r = 0.501$).

Conclusion: We have demonstrated the feasibility of a comprehensive approach to PAD using multi-modality MR. Plaque volume in the SFA wall correlates with both calf muscle perfusion and MRA findings. These techniques used in concert have the potential to improve the ability to characterize and risk stratify PAD patients, as well as monitor disease progression and response to novel therapies.

359. FEASIBILITY STUDY OF 3D CARDIAC TISSUE ENGINEERING FOR EMBRYONIC CELL THERAPY AFTER MYOCARDIAL INFARCTION

Matthieu Lepetit-Coiffe, PhD, Mathieu Hauwel, PhD, Jean Pascal Jacob, MS, Jean Luc Daire, PhD, Jean Noel Hyacinthe, PhD, Marisa Jaconi, PhD, Jean Paul Vallee, Pr.
Geneva University Hospital, Geneva, Switzerland.

Introduction: To study the feasibility and accuracy of 3D cardiac tissue engineering for the cell therapy of heart failure.

Material and Methods: Animal preparation: Three dimensional cardiac tissue consisted in fibrin matrix in which was incorporated 300000 iron oxide particles magnetofected Embryonic Stem Cells derived cardiomyocytes. Sixteen rats weighted 200–300 g, have been included in this study. Under general anesthesia, chest of the animal was opened: heart failure was induced by left coronary occlusion and then 3D cardiac tissue was engrafted with fibrin glue on the heart in place of the suspected infarcted area. Four conditions (N = 4 rats/conditions) were studied: 1) normal heart with fibrin matrix containing only iron oxide particles (NFe); 2) normal heart with 3D cardiac tissue (NFeESC); 3) infarcted heart with fibrin matrix containing only iron oxide particles (MIFe); and 4) infarcted heart with 3D cardiac tissue (MIFeESC).

MR imaging: Each rats were imaged under 1.5 T MR magnet (Intera, Philips) 6 hours after surgical intervention, 3 days (D3), 7 days (D7) and 45 days (D45) later. The 2 hours/animal MR protocol consisted in 12 slices FFE sequence (TE/TR/FA

= 7 ms/350 ms/50°, acquired pixel size = 0.2 × 0.3 mm^2, slice thickness = 2 mm), SE sequence (TE/TR/FA = 22 ms /375 ms/90°, acquired pixel size = 0.2 × 0.3 mm^2, slice thickness = 2 mm) for iron oxide particles repairing; a C-SPAMM TAG preparation segmented cine FFE sequence (interTAG spacing = 1.25 mm, acquired pixel size = 0.6 × 1.8 mm^2, slice thickness = 3 mm) was also used for quantitative regional function study. After 0.6 mL injection of contrast agent (Dotarem, Guerbet), a 7 slices FFE cine sequence (acquired pixel size = 0.4 × 0.4 mm^2, slice thickness = 2 mm) and with same geometry a delayed enhancement inversion recovery T1 weighted FFE sequence (TE/TR/TI/FA = 7.6 ms/12 ms/300 ms/45°, acquired pixel size = 0.3 × 0.3 mm^2, slice thickness = 2 mm) were acquired for Left ventricular Ejection Fraction (EF), End-systolic volume (ESV) and End-diastolic volume (EDV) and Infarct zone evaluation. Fifty days after engraftment, animals were sacrificed and heart taken out for histology Prussian Blue staining preparation.

Statistical analysis: Statistical relationship between animals were performed over time and conditions for EF, ESV, EDV and Infarct zone with a Bonferroni and Dunnett ANOVA test (SPSS software). Measure of wall thickening (WT) was performed in 6 sectors and values for MIFe and MIFeESC groups compared.

Results: Histological results confirmed presence of infarcted zone at D45. Prussian Blue staining is in good correlation with CMR hyposignal related to iron oxide particles observed along the 45 days post engraftment. Infarct area remained stable along time as assessed by delayed enhancement MRI, and no significative difference was observed between groups at D3. The global function and LV volumes were significantly different between the normal an infarct groups, and there was a trend toward improvement in the cell treated MI group. EF, ESV and EDV of MIFe and MIFeESC groups presented same time evolution (Fig. 1); at D 45 there was a significant improvement of the regional function in the infarct zone of the cell therapy group by comparison to the nontreated group.

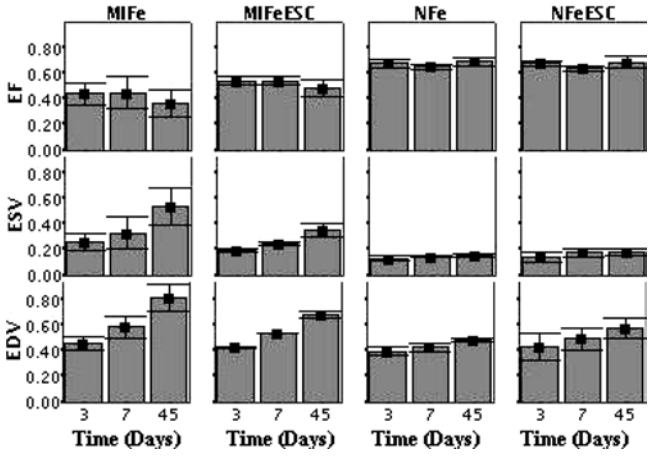

FIG. 1. Time evolution of ejection fraction (EF), end systolic volume (ESV) and end diastolic volume (EDV) for each conditions (Normal heart with fibrin matrix containing only iron oxide particles (NFe), normal heart with 3D cardiac tissue (NFeESC), infarcted heart with fibrin matrix containing only iron oxide particles (MIFe), and infarcted heart with 3D cardiac tissue (MIFeESC)MIFe heart failure , MIFeESC, NFe, NFeESC).

Conclusion: In this study, we demonstrated the feasibility and the potential benefice of the 3D cardiac tissue engineering for the cell therapy using embryonic stem cells after the myocardial infarct. Further experiments are needed to confirm this preliminary results.

360. VARIATION IN RIGHT VENTRICULAR OUTFLOW TRACT MORPHOLOGY FOLLOWING REPAIR OF CONGENITAL HEART DISEASE

Silvia Schievano, Louise Coats, Wendy Norman, Philipp Bonhoeffer, Andrew Taylor. ***UCL Institute of Child Health, London, United Kingdom.***

Introduction: Recently, we have introduced a novel procedure that can relieve both regurgitation and/or stenosis in the right ventricular outflow tract (RVOT) by a minimally invasive approach. Percutaneous pulmonary valve implantation (PPVI) involves transcatheter placement of a valved stent within the existing degenerated valve or conduit and can be performed without cardiopulmonary bypass or residual pulmonary regurgitation. Selection of patients for this exciting new technique depends on the presence of an appropriate site for implantation within the RVOT that will ensure device stability. The currently available device is composed of a bovine jugular venous valve sutured into a balloon-expandable platinum-iridium stent. It has an unexpanded length of 35 mm and can be deployed to a maximum diameter of 22 mm. The diameter of deployment is determined by the balloon size of the delivery system.

Purpose: Our aim was to identify subgroups of RVOT morphology that relate to suitability for PPVI and to document their prevalence in our patient population.

Methods: Eighty-three consecutive patients with RVOT dysfunction (5–41 years, 76% tetralogy of Fallot) referred to our center for magnetic resonance imaging were studied. A morphological classification was created according to visual assessment of 3D reconstructions and detailed measurement. Diagnosis, RVOT type, surgical history and treatment outcomes were documented.

Results: RVOT morphology was heterogeneous; nevertheless, 5 common types were identified. Type I, a pyramidal morphology, was most prevalent (49%) and related to the presence of a transannular patch. Other types (II-V) were seen more commonly in patients with conduits. Two patients had unclassifiable morphology. Ninety-five percent of patients were assigned to the correct morphological classification by visual assessment alone. PPVI was performed successfully in 10 patients with Type II-V morphology and in 1 patient with unclassifiable morphology. Percutaneous implantation was not performed in patients with

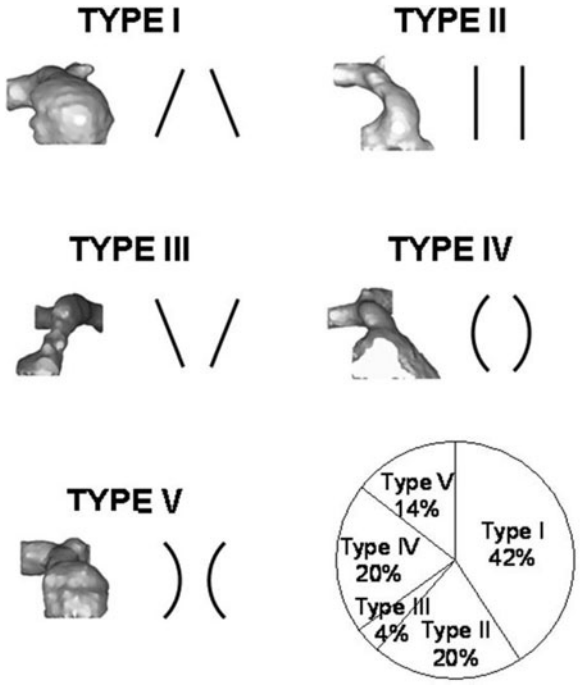

FIG. 1. Five types of RVOT morphology and their frequency in our patient population.

Type I morphology. Only RVOT diameters < 22mm in diameter were suitable for the current device.

Conclusions: Three-dimensional imaging and measurement of the outflow tract is essential to identify patients who are most appropriate for PPVI. Though only 13% of our patients underwent percutaneous implantation, >50% of outflow tract morphologies may be suitable for this approach, in particular with the development of new devices appropriate for larger outflow.

361. COMBINED STEAM AND DELAYED CONTRAST ENHANCEMENT FOR IMPROVED MR IMAGING OF INFARCTED MYOCARDIAL TISSUE

El-Sayed H. Ibrahim, MSE, Matthias Stuber, PhD, Dara L. Kraitchman, PhD, DVM, Robert G. Weiss, MD, Nael F. Osman, PhD. ***Johns Hopkins University, Baltimore, Maryland, USA.***

Introduction: The ability to identify myocardial infarction (MI) is important for therapeutic decision-making (1). Inversion-Recovery (IR) MRI is considered the gold-standard for obtaining delayed enhancement (DE) images. One problem with IR-DE is the low blood-infarct contrast, especially shortly after contrast-injection.

Stimulated-echo acquisition-mode (STEAM) imaging is used in many applications (2). Recently, a method was proposed for black-blood STEAM cardiac imaging (3). In this work, the STEAM pulse-sequence is modified to simultaneously acquire both black-blood viability and anatomical cardiac images.

Methods: Three STEAM images are simultaneously acquired within the same cardiac cycle with different modulations or tunings: low-tune(LT), high-tune(HT), and no-tune(NT). The LT and HT images are combined as described in reference 3 to construct anatomical heart image. The NT image is acquired

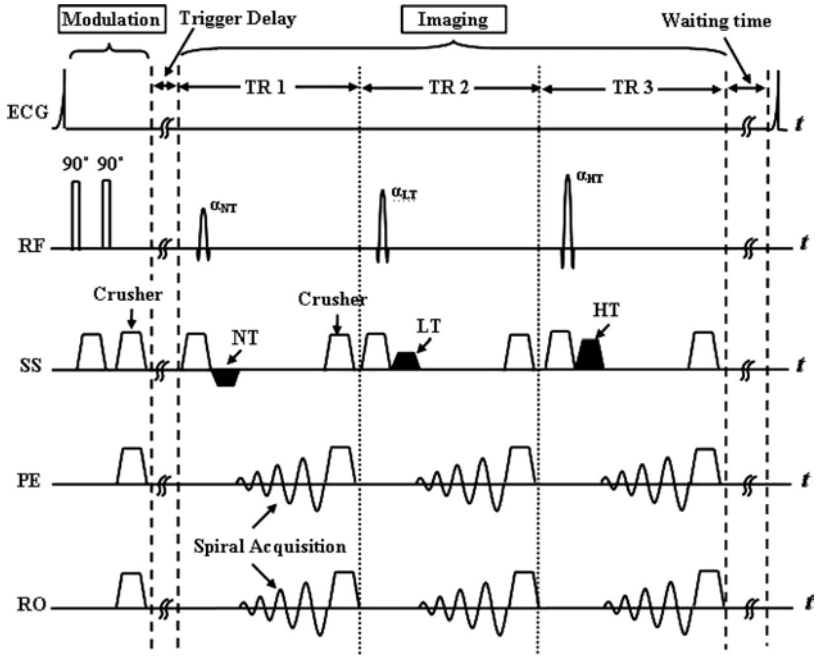

FIG. 1. Pulse sequence diagram.

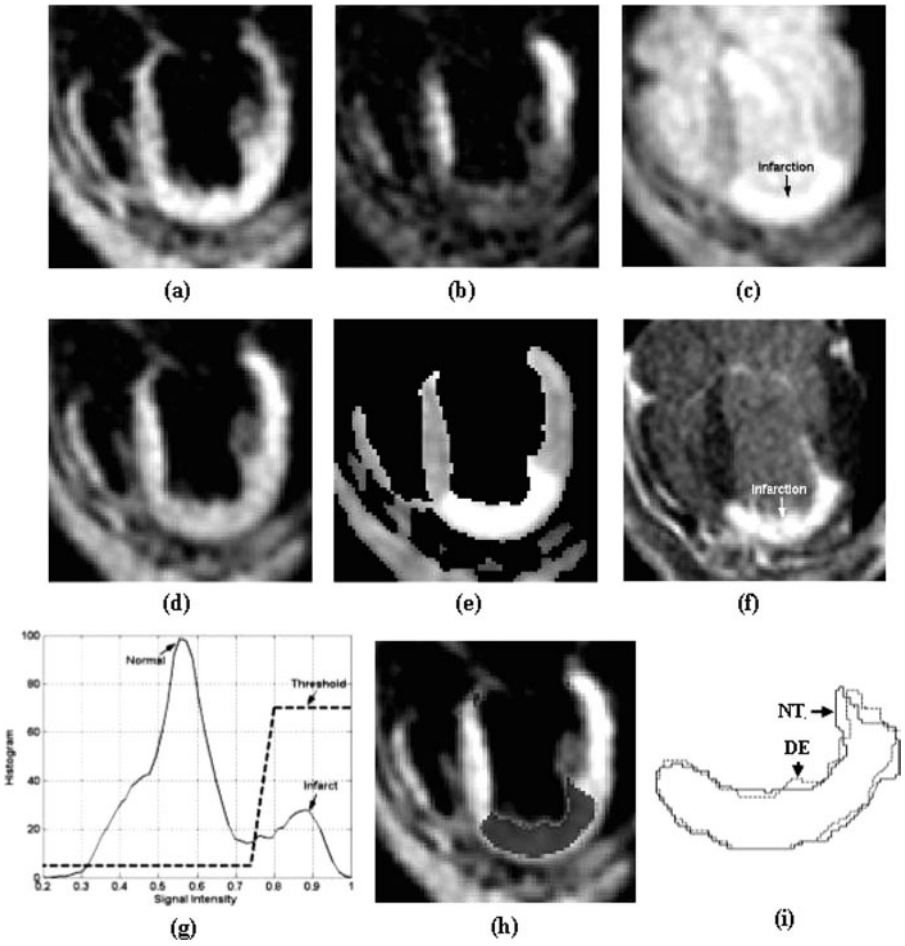

FIG. 2. Long-axis images of an infarcted dog. (a) LT image, (b) HT image, (c) NT image, (d) Anatomy image, (e) NT image masked by the anatomy image. (f) IR-DE image, (g) Intensity histogram of image (*e*). (h) The infarct in image (*e*) is segmented based on intensity histogram, (i) The infarcts extracted from the NT and DE images.

with zero modulation-frequency, which after contrast injection, results in T_1-weighted viability image. Fig. 1 shows the pulse-sequence used. Notice that the scan time is the same as acquiring single image as the 3images are interleaved.

Four dogs and 9 patients with MI were scanned on 1.5T and 3T Philips scanners, respectively. STEAM images were acquired 10-15 minutes post-injection using spiral acquisition. The dog experiments parameters: TR/TE = 23/4.9 ms; heart-rate = 100–140 bpm; trigger-delay (TD) $\approx$ 200 ms; FOV = $350 \times 350\,mm^2$; and Gd-DTPA dose = 0.2 mmol/kg. The patient experiments parameters were same as the dog experiments except: TR/TE =1 8/2.6 ms; heart-rate = 60–90 bpm; and TD $\approx$ 300 ms. Conventional IR-DE images were immediately obtained after STEAM imaging. IR-DE parameters were similar to STEAM parameters, except: TR/TE = 4.13/1.2 ms. The inversion-time was visually selected to achieve good myocardium-infarct contrast.

The low blood-infarct contrast in the NT image was resolved by masking the image with threshold of the anatomical image. The blood-infarct contrast-to-noise ratio (CNR) was computed from the STEAM and IR-DE images. CNR was computed as the difference between the tissues signal means, divided by standard-deviation of the background noise. The infarcted regions were extracted from the IR-DE and NT images using the full-width at half-maximum (FWHM) method, and then compared on a pixel-by-pixel basis. In addition, Bland-Altman analysis was performed between the two methods.

Results: Figure 2 shows results from a dog experiment. Figure 2 also shows the reconstructed anatomical image and the NT viability image masked by a threshold of the anatomy image. The corresponding IR-DE image is also shown. The intensity histogram of the masked NT image shows two signal peaks representing normal and infarcted myocardium. The threshold signal-intensity between the normal and infarcted myocardium, determined by FWHM method, is displayed as dashed-line. Pixels with intensities above this threshold were considered infarction and colored in red. The infarcted regions extracted from the NT and IR-DE images are shown overlaid on each other. Figure 3 shows similar results from a patient experiment. Figure 4 shows an example where the proposed method surpassed the IR-DE

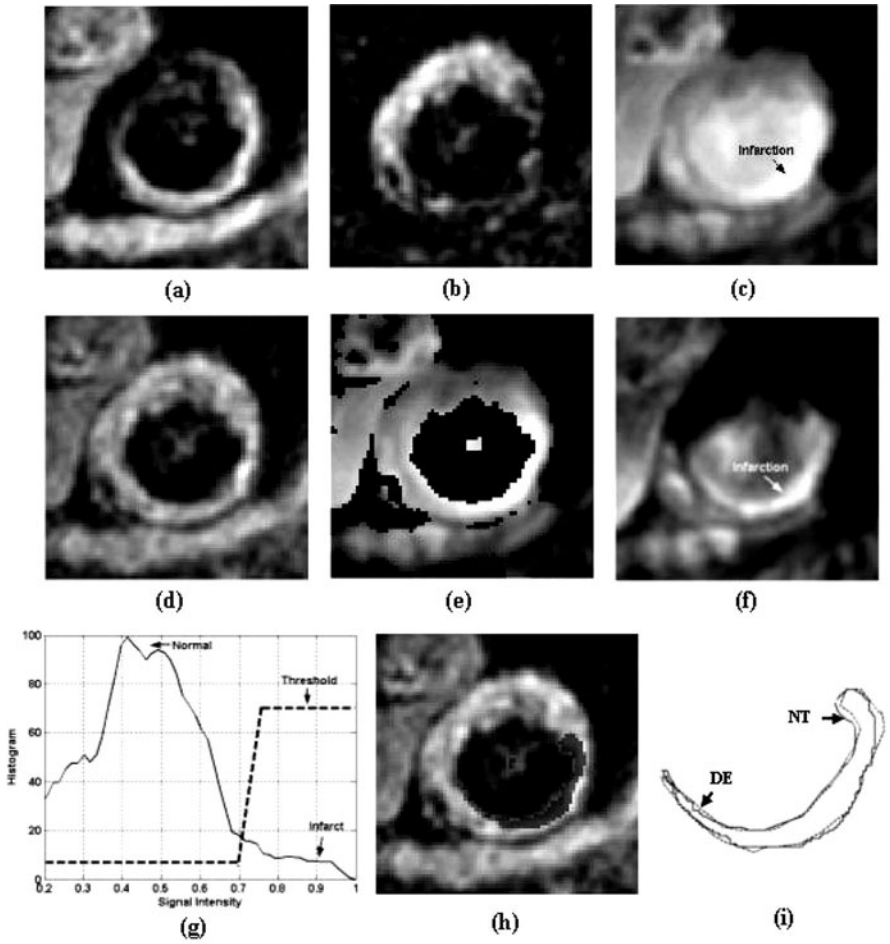

FIG. 3. Short-axis images of a patient with MI. (a) LT image, (b) HT image, (c) NT image, (d) Anatomy image, (e) NT image masked by the anatomy image, (f) IR-DE image, (g) Intensity histogram of image (*e*). (h) The infarct in image (*e*) is segmented based on intensity histogram. (i) The infarcts extracted from the NT and DE images.

method. In this example, the blood in the right-ventricle cavity could be mistakenly interpreted as extension of the infarction, due to its high signal-intensity in the IR-DE image. However, this did not occur in the STEAM image.

The STEAM blood-infarct CNR (33 ± 4.8) was significantly ($p < 0.002$) higher than that from IR-DE images (11 ± 3.5). The STEAM myocardium-infarct contrast was sufficient for accurate delineation of infarcts. The infarcted regions extracted from the STEAM images showed sensitivity and specificity of $87 \pm 6\%$ and $85 \pm 5\%$, respectively, when compared to those extracted from the IR-DE images. The Bland-Altman analysis showed no bias between the 2 methods for determining infarcts-sizes. *Conclusions:* An MRI technique is proposed for myocardial viability imaging. A single image is obtained with bright infarct

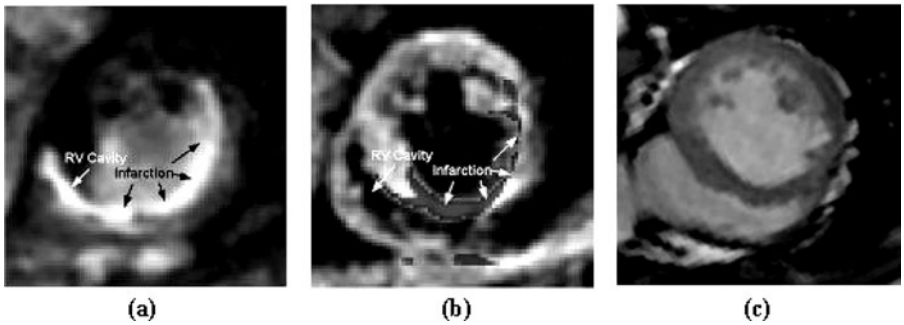

FIG. 4. Results of a patient with MI. (a) IR-DE image. (b) Segmented NT viability image. (c) SSFP image for reference.

and black blood. The proposed technique supports the delineation of endocardium, enabling accurate measurement of the infarct-size.

ACKNOWLEDGMENTS

Grants: Donald W. Reynolds Foundation, R01-HL072704,R01-HL073223,R01-HL61912,K02-HL05193.

REFERENCES

1. Kim RJ, et al. Circulation 100:1992–2002.
2. Frahm J, et al. J Magn Reson 64:81–93.
3. Fahmy AS, et al. Magn Reson Med 55:404–412.

362. REAL-TIME MR IMAGING OF MYOCARDIAL REGIONAL FUNCTION WITH THROUGH-PLANE MOTION CORRECTION USING SLICE-FOLLOWING

El-Sayed H. Ibrahim, MSE, Ahmed S. Fahmy, PhD, Tetsuo Sasano, MD, PhD, Khaled Z. Abdel-Moneim, MSE, Roselle Abraham, MD, Matthias Stuber, PhD, Nael F. Osman, PhD.
Johns Hopkins University, Baltimore, Maryland, USA.

Introduction: Strain-encoding (SENC) MRI provides direct imaging of myocardial strain through the acquisition of two images with different phase-encodings: low-tuning (LT) and high-tuning (HT) images (1). A technique has recently been proposed for real-time SENC imaging (2). However, the SENC technique, like other motion tracking techniques, suffers from the heart's through-plane motion, which may make the resulting images not completely accurate.

In this work, we propose a modification of the SENC technique for real-time myocardial strain imaging while tracking the original prescribed slice in the through-plane direction. This is accomplished by combining SENC and slice-following techniques. We refer to the conventional SENC technique, the technique in reference 2, and the proposed technique as SENC, fast-SENC, and sf-fast-SENC, respectively.

Methods: In slice-following, thin slice is tagged and then thicker slab, that encompasses the tagged slice, is imaged. Three-dimensional selective-excitation is implemented to reduce FOV, thus reduce scan time, while implementing slice-following. The tagged magnetization is confined to thin disk, encompassing the heart, inside the imaging-plane. To cut scan time into half in sf-fast-SENC, the two sets of LT and HT images are acquired in interleaved way in a single breath-hold. Spiral acquisition is implemented to reduce scan time to one heartbeat.

All experiments were conducted on a 3T Philips scanner. Two gel phantoms with cylindrical shapes were scanned while moving in and out of the imaging-plane. Ten healthy pigs and 10 healthy volunteers (32 ± 5 years-old) were also scanned. The imaging parameters for sf-fast-SENC: 3 spirals $\times$ 8 ms; TR/TE = 11/1.2 ms; FOV = 210×210 mm^2; diameter of the cylindrical excitation-FOV = 160 mm; scan-matrix = 64×256; flip-angle = 40°; tagged slice-thickness = 8 mm; imaging slice-thickness = 30 mm. For fast-SENC: imaging slice-thickness = 8 mm; reduced excitation FOV = 160×160 mm^2. For SENC: 12 spirals $\times$ 12 ms; FOV = 300×300 mm^2; TR/TE = 20/1.2 ms. The pulse-sequence is shown in Fig. 1. Because only one cardiac cycle is required for fast-SENC or sf-fast-SENC imaging, the whole cardiac cycle, till end-diastole, could be imaged, which is not applicable in SENC.

Standard grid-tagged SPAMM images were acquired. The strain curves from the different SENC images were compared to those computed from the orthogonal tagged images with and without tracking the tag intersection-points in the direction orthogonal to the SENC imaging-plane, which in SENC corresponds to applying and not applying slice-following, respectively. Strains from tagged images were computed as described in reference 3.

Results: Figure 2 shows the setup and results of the moving phantom experiment. One gel phantom totally disappeared after selective-excitation. The cross-section of the other phantom changed as the phantom moved forward and backward in the slice-selection direction when imaging with fast-SENC. The imaged cross-section changes agreed with those calculated based

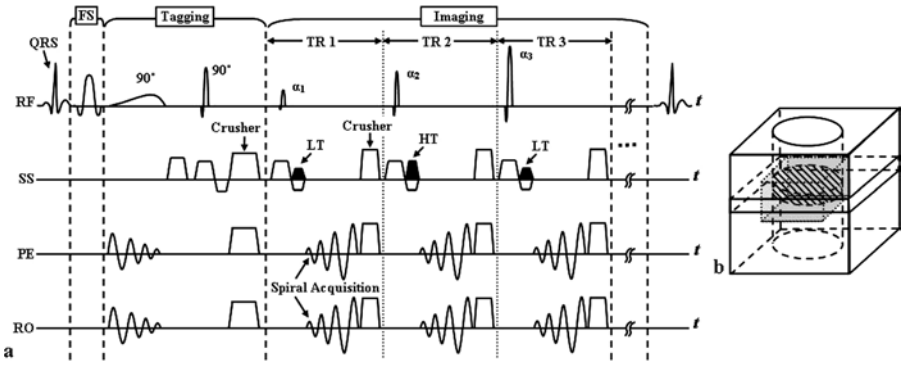

FIG. 1. (a) Pulse sequence diagram for sf-fast-SENC. (b) The tagged (dashed thin disk) and imaged (gray thick slab with reduced in-plane FOV) regions in sf-fast-SENC. RF, SS, PE, RO, FS, LT, and HT stand for radiofrequency, slice-selection, phase-encoding, read-out, fat-suppression, low-tuning, and high-tuning, respectively.

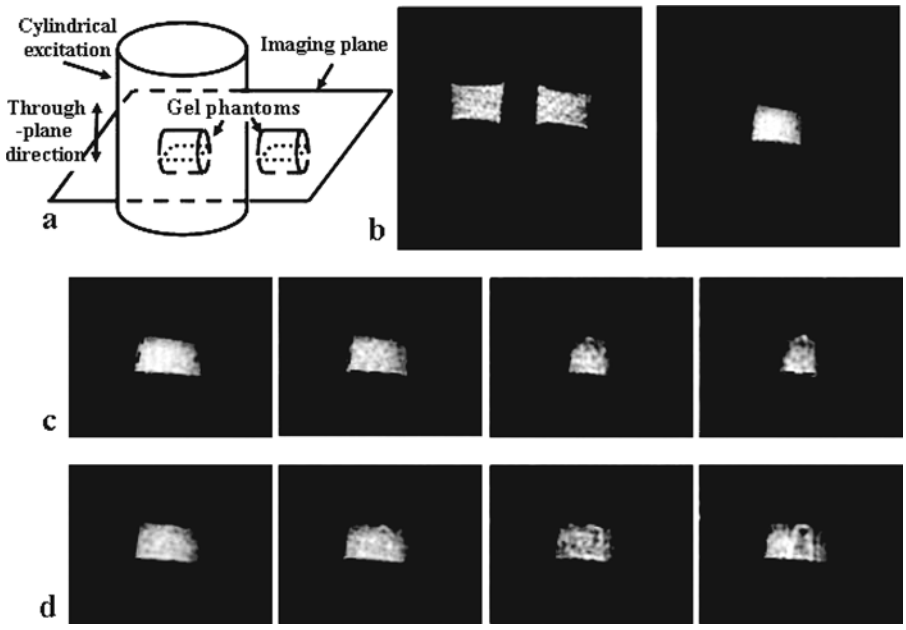

FIG. 2. The moving phantom experiment. (a) Setup of the moving phantom. (b) The resulting images before and after applying selective excitation. One of the two gel phantoms disappeared after applying selective excitation. (c) A sequence of fast-SENC images acquired during phantom motion. The cross-section of the cylindrical gel phantom changes from one frame to another. (d) A corresponding sequence of sf-fast-SENC images acquired during phantom motion. The phantom cross-section is kept the same.

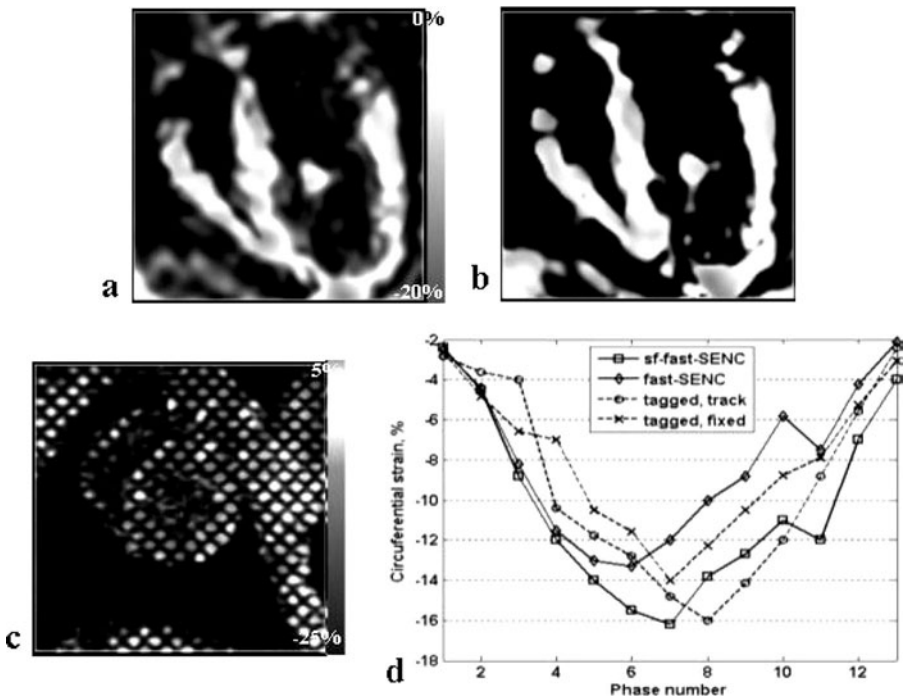

FIG. 3. Results from a pig experiment. (a) Sf-fast-SENC circumferential strain image. (b) The corresponding fast-SENC circumferential strain image. (c) The orthogonal short-axis SPAMM tagged image. (d) Circumferential strain curves from different SENC and SPAMM images for a ROI on the basal-lateral L V wall.

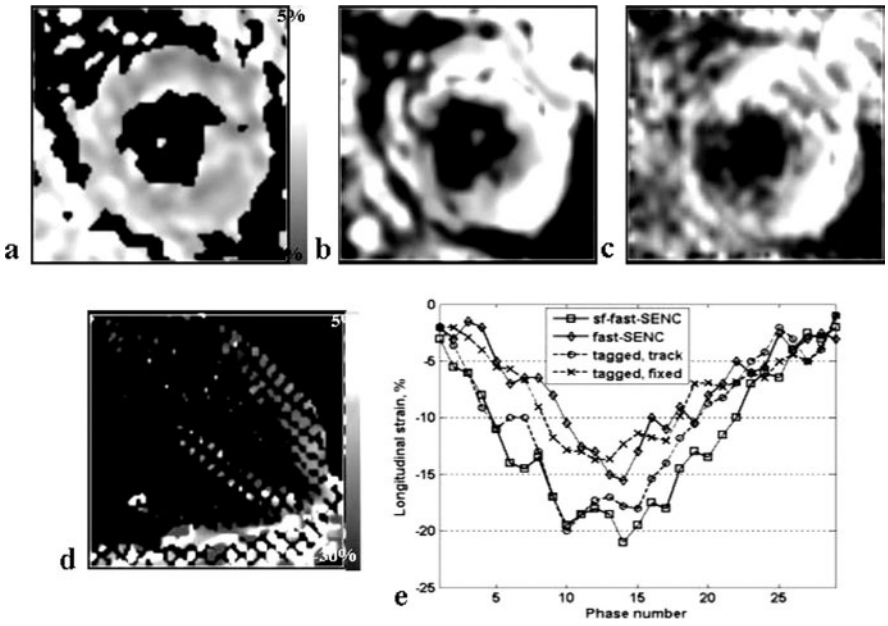

FIG. 4. Results from a volunteer experiment. (a) Sf-fast-SENC longitudinal strain image. (b) The corresponding fast-SENC longitudinal strain image. (c) SENC longitudinal strain image. (d) The orthogonal long-axis SPAMM tagged image. (e) Longitudinal strain curves from different SENC and SPAMM images for a ROI on the mid-septal LV wall.

on phantom dimensions and setting. The cross-section was kept constant in sf-fast-SENC because of slice-following.

Figure 3 shows circumferential strain images from pig experiment. The figure shows sf-fast-SENC and fast-SENC images of long-axis slice. The orthogonal short-axis SPAMM image is shown. Figure 3 shows strain curves computed for small region-of-interest (ROI) on the basal-lateral LV wall. Figure 4 shows longitudinal strain images from volunteer experiment. Figure 4 shows sf-fast-SENC, fast-SENC, and SENC images of short-axis slice. The orthogonal long-axis SPAMM image is shown. Figure 4 shows strain curves computed for small ROI on the mid-septal LV wall.

The results showed significant ($p < 0.01$) difference between the strain values from sf-fast-SENC and fast-SENC(or SENC) images, especially at end-systole. In addition, there was similarity between the strain values from sf-fast-SENC and fast-SENC images and those from corresponding SPAMM images with and without tracking the tag intersection-points, respectively.

Conclusions: A method is proposed for real-time black-blood myocardial functional imaging while considering the tissue through-plane motion. The method could be used for dynamic imaging such as contrast-agent bolus-tracking or stress-test monitoring.

REFERENCES

1. Osman NF, et al. Magn Reson Med 46:324–34.
2. Pan L, et al. Magn Reson Med 55:386–95.
3. Osman NF, et al. Magn Reson Med 42:1048–60.

363. FREE-BREATHING COMBINED FUNCTIONAL AND VIABILITY MRI CARDIAC IMAGING

El-Sayed H. Ibrahim, MSE, Amy E. Spooner, MD, Matthias Stuber, PhD, Robert G. Weiss, MD, Nael F. Osman, PhD.
Johns Hopkins University, Baltimore, Maryland, USA.

Introduction: Composite strain-encoding (C-SENC) MRI provides simultaneous myocardial functional and viability imaging (1). Breath-holding is commonly used to minimize respiratory motion. However, breath-holding can be difficult in some patients such as those with severely impaired ventricular function or respiratory disease. Reducing the breath-hold duration restricts the image resolution and signal-to-noise ratio (SNR). Reduced temporal-resolution could result in misregistration between the acquired functional and viability images. Also, reduced spatial-resolution could affect the accuracy of determining the infarcted region.

Real-time diaphragm monitoring through navigator-echo (NE) solves the respiratory motion problem. It requires little patient cooperation and produces high-quality images. In this work, the navigator-echo technique is combined with C-SENC for free-breathing C-SENC imaging. The resulting images are found to be superior to those acquired with breath-holding.

Methods: In C-SENC imaging, tagging is applied in the slice-selection direction after the R-wave detection. At the imaging timepoint, 3 images are consecutively acquired with different phase-encodings: low-tuning (LT), high-tuning (HT), and no-tuning (NT) images. The LT and HT images are combined to construct strain image (2). The NT image is a T_1-weighted viability image which, after contrast-injection, shows bright infarction. The functional and viability images are color-coded and combined into one composite image (1).

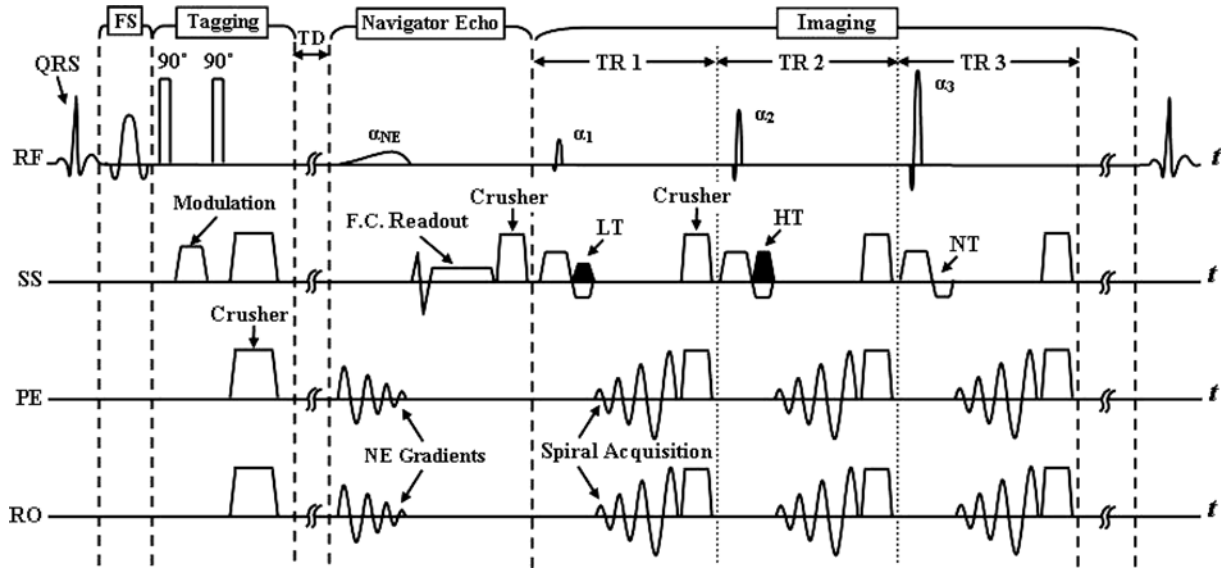

FIG. 1. Pulse sequence diagram for navigator-echa C-SENC, RF, SS, PE, RO, FS, FC, LT, and HT stand for radiofrequency, slice-selection, phase-encoding, read-out, fat-suppression, flow-comprnsated, low-tuning, and high-tuning, respectively.

Because the heart bulk motion is mainly in the craniocaudal direction, a 1D navigator image, obtained across the liver-lung interface, is a good indicator of the diaphragm position (3). Navigator position is prospectively calculated before image-acquisition using cross-correlation. Changes in the cardiac position, within the gating-window limit, are corrected by adjusting the imaging-plane.

Figure 1 shows the pulse-sequence diagram used. The navigator-echo consists of spiral cylindrical excitation followed by flow-compensated readout along the long-axis of the cylindrical excitation. A shallow NE flip-angle is used to avoid saturation effects.

Five human subjects with and without myocardial-infarction (MI) (age $= 45 \pm 8$) were scanned on 3T Philips scanner. The imaging parameters for breath-hold (BH) C-SENC: spiral acquisition $= 12$ spirals $\times$ 12 ms; TR/TE $= 18/2.6$ ms; scan-duration ≈ 13 s; FOV $= 350 \times 350$ mm^2; scan-matrix $= 128 \times 256$; trigger-delay (TD) ≈ 300 ms;GD-DTPA $= 0.2$ mmol/kg; images acquired 10–15 minutes post-injection. The imaging parameters for NE C-SENC are the same as BH C-SENC imaging, except: spiral acquisition $= 14$ spirals $\times$ 14 ms; scan matrix $= 256 \times 256$; navigator gating-window $= 7$ mm; scan-duration $= 36$ s; acquisition-efficiency $= 40\%$. Also, standard inversion-recovery delayed enhancement (DE) images were acquired to determine the existence of MI.

Results: Figure 2 shows the resulting images from a subject who showed a thin myocardial region of enhanced signal-intensity in the DE image (arrows). This enhanced region could represent MI or fibrosis. With BH C-SENC imaging, the acquired spatial resolution is not sufficient for detection of the enhanced myocardium as shown in the C-SENC composite image. The corresponding NE C-SENC image shows higher resolution and SNR, which enabled the detection of the enhanced region (blue region in the image). White and red represent minimum and maximum strains, respectively. Figure 3 shows the results from a patient without MI. The NE C-SENC image has higher

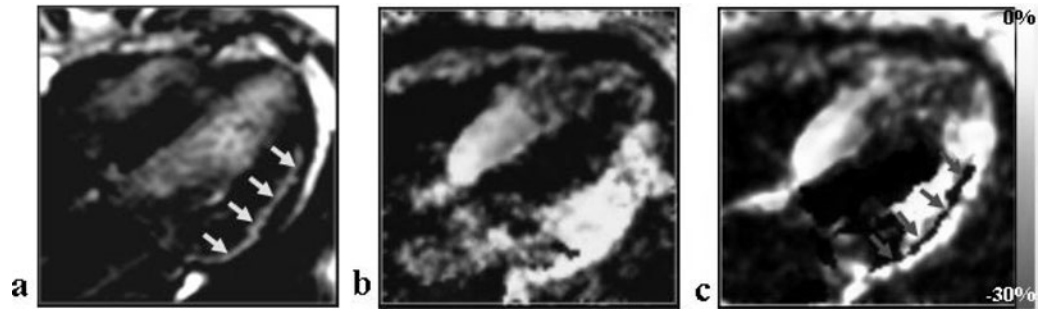

FIG. 2. Results from a subject who showed a thin region of enhanced myocardial signal-intensity in the DE image (arrows). (a) DE image. (b) Composite C-SENC circumferential strain image acquired with breath-hold. The thin bright myocardial region is missed with this resolution. (c) Corresponding navigator-echo C-SENC image. With this better image quality, the enhanced myocardium is detected (blue). White and red represent min. and max. strains.

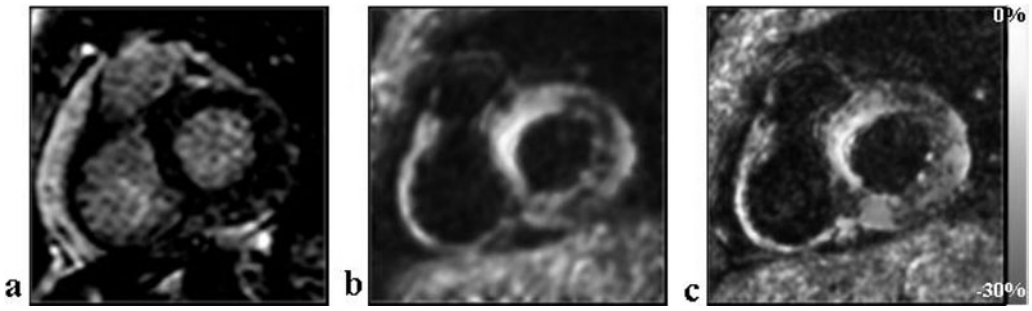

FIG. 3. Results from a patient without MI. (a) DE image showing no infarction. (b) Composite C-SENC longitudinal strain image acquired with breath-hold. The image has low spatial resolution. (c) The corresponding navigator-echo C-SENC image has higher SNR and spatial resolution. White and red represent min. and max. strains.

resolution (double) and SNR (40% more) than the BH C-SENC image, which allows for accurate computation of strain values.

From all the experiments, the total scan time of NE C-SENC imaging, including NE prescan (39 $\pm$ 8 seconds), was similar to that of BH C-SENC imaging, including the breath-holding instructions and patient recovery-time (35 $\pm$ 6 seconds). However, the difference in the calculated infarct size was significant ($p < 0.01$).

Conclusions: The navigator-echo technique is successfully combined with C-SENC for free-breathing combined viability and functional cardiac imaging. NE C-SENC imaging results in higher spatial resolution, higher SNR, and easier imaging setup without noticeable increase in the total scan-time. This supports accurate calculation of infarct size and strain values.

ACKNOWLEDGMENTS

Grants: Johns Hopkins Cardiovascular Reynolds Center and NIH-grant:HL61912.

REFERENCES

1. EI Ibrahim, et al. J Cardiovasc Magn Reson 8: 299–300.
2. Osman NF, et al. Magn Reson Med 46:324–334.
3. Wang Y, et al. Radiology 198:55–60.

364. ROLE OF CARDIAC MAGNETIC RESONANCE IN THE DIAGNOSIS OF CORONARY ARTERY DISEASE IN PATIENTS WITH COMPLETE LEFT BUNDLE BRANCH BLOCK

Erick Alexanderson, MD,[1] Patricio Cruz, MD,[2] Jose A. Talayero, MD,[2] Carlos Sierra, MD,[2] Leonardo García-Rojas, MD,[2] Aloha Meave, MD.[1] [1]***Instituto Nacional de Cardiología Ignacio Chavez, Mexico D.F., Mexico,*** [2]***Universidad Nacional Autónoma de México, Mexico D.F., Mexico.***

Introduction: Coronary Artery Disease (CAD) seems to be the predominant etiology of left bundle branch block (LBBB). However, noninvasive diagnosis of CAD in patients with LBBB continues to be a challenge. Basal and stress electrocardiography have low sensitivity and specificity. The LBBB may cause frequently wall motion and myocardial perfusion abnormalities, especially at septum level reducing the sensitivity of echocardiography and nuclear scan for the diagnosis of ischemic heart disease. Cardiac Magnetic Resonance (CMR) delayed enhancement gadolinium-based contrast technique distinguishes reversible form irreversible myocardial damage.

Purpose: The aim of this study was to evaluate the role of CMR-delayed enhancement technique in the diagnosis of CAD in patients with LBBB.

Methods: We studied 17 consecutive patients with diagnosis of LBBB and suspicion of CAD. CMR scan was performed in a 1.5 T Magnetom Sonata Siemens scanner. Intravenous gadolinium contrast was administrated and a first pass and delayed images with inversion-recovery sequences were obtained in short axis, delayed enhancement was found. A coronary angiography was performed in all the patients. A sensitivity, specificity and kappa concordance were obtained.

Results: We studied 17 patients with a mean age of 63 years, 82% with history of hypertension. Eleven patients had abnormal coronary arteries with significative obstruction ($\geq$ 50 stenosis) in the left anterior descending artery; normal coronary arteries were found in 6 patients. Positive delayed enhancement was found in 10 patients mostly located at septal and inferoseptal level, 7 patients did not have late enhancement. When CMR and coronary angiography results were compared, the 10 patients with delayed enhancement had abnormal coronary arteries while 6 patients without delayed enhancement had normal coronary arteries and only 1 patient of this group showed coronary lesion (90% sensitivity, 100% specificity, $p < 0.05$).

Conclusions: CMR delayed enhancement gadolinium technique has a high sensitivity and specificity for the diagnosis of coronary artery disease in patients with LBBB. The results seem to be superior to other non-invasive cardiac techniques.

365. MEASUREMENT OF END DIASTOLIC VOLUME AND EJECTION FRACTION IN PATIENTS WITH DILATED OR SYSTEMIC RIGHT VENTRICLES-AXIAL OR SHORT AXIS IMAGE ACQUISITION?

Andrew M. Crean, MRCP FRCR, John F. Younger, MB FRACP MRCP, John P. Greenwood, MD, MRCP. ***Leeds General Infirmary, Leeds, United Kingdom.***

Purpose: To ascertain the most reproducible method for volume and ejection fraction measurement of the dilated, impaired or systemic right ventricle.

Methods: Twenty-one patients were studied (13 tetralogy of Fallot; 6 primary pulmonary hypertension; 1 transposition of the great arteries with Mustard correction; 1 double outlet right ventricle). Axial and short axis cine stacks of the right ventricle were acquired (slice thickness 10 mm with 0 mm interslice gap) using a steady state free precession sequence on a 1.5T system (CV/i Signa, GE Medical, Milwaukee, Wisconsin, USA). A single observer performed contour tracing on both cine stacks at each slice level to generate measurements of end diastolic volume and ejection fraction for the right ventricle. All measurements were made in random order to eliminate tracing recall bias and using dedicated off line analysis software (QMass v6.1.6, Medis, Netherlands). Measurements were repeated a second time by the same observer on both cine stacks for all patients after an interval of 2 weeks, again in random order.

Statistical analysis was performed using a paired t test (SPSS v12 for Windows) to interrogate variability between measurements made in the axial versus short axis orientation as well as intra-observer variability for each method.

Results: Twenty-one full patient data sets were analysed. All variables conformed to a normal standard distribution and did not require transformation prior to analysis. Results are presented as mean (standard deviation).

There were significant differences in observed end diastolic volumes between measurements made in axial vs short axis orientation :

a) read one—mean difference 23 mL (SD 21 mL), 95% CI of difference 14–33 mL $p < 0.0001$
b) read two—mean difference 21 mL (SD 19 mL), 95% CI of difference 13–30 mL $p < 0.0001$

Differences in observed ejection fraction were not, however, significant:

a) read one—mean difference 1.5% (SD 3.4%), 95% CI of difference -3.1 to $+0.02\%$, p = ns.
b) read two—mean difference 0.7% (SD 4.6%), 95% CI of difference -2.8 to $+1.4\%$, p = ns.

Intra-observer variability analysis showed high levels of repeatability for measurement of EDV and EF with no statistically significant differences regardless of orientation of original slice acquisition:

a) Axial EDV: 1.3% variability in measurement 95% CI -3.3% to $+0.6\%$
b) Short axis EDV: 2.2% variability in measurement 95% CI -5.1% to $+0.7\%$
c) Axial EF: 2.1% variability in measurement 95% CI -5.1% to $+1.2\%$
d) Short axis EF: 0.58% variability in measurement 95% CI -0.03% to $+4.4\%$

Conclusion: Measurement of right ventricular size and function can be obtained reliably and repeatedly using either method of slice acquisition in the pathological right ventricle. There is a significant tendency to observe a larger end diastolic volume if axial slice measurement is used. However, since the mean difference is only in the order of 20 mL this is unlikely to impact on clinical management. Nevertheless, this study suggests it may be preferable to make sequential measurements (eg, follow up studies in tetralogy of Fallot) from the same cine orientation. There is no difference (statistical or clinical) in measurement of ejection fraction irrespective of slice orientation chosen for contour tracing.

366. DESIGN OF AN ACTIVATABLE NANOPARTICULATE CONTRAST AGENT WITH A UNIQUE FLUORINE SIGNAL FOR CARDIOVASCULAR MOLECULAR IMAGING

Anne M. Neubauer, MS,[1] Patrick Winter, PhD,[1] Shelton Caruthers, PhD,[2] Junjie Chen, PhD,[1] Frank Hockett, MS,[1] Gregory Lanza, MD,[1] PhD, Samuel Wickline, PhD.[1] ***[1]Washington University, St. Louis, Missouri, USA, [2]Philips Medical Systems, Best, The Netherlands.***

Introduction: Certain pathological conditions, such as atherosclerosis, are exacerbated by enzymatic activity. For example, metalloproteinases (MMPs) can cause degradation of the atherosclerotic plaque cap, leading to rupture and subsequent thrombosis. Molecular imaging of enzyme activity with MRI via an "activateable" contrast agent could thus be useful for characterizing this process. Liquid perfluorocarbon nanoparticles containing gadolinium have recently been utilized as an effective targeted contrast agent for MR imaging of such biomarkers as fibrin and $\alpha_v\beta_3$-integrins (1). These particles also contain a large amount of fluorine nuclei (19F), which can be used for MR imaging with the added advantage of essentially zero background signal. This unique signature has been used for

EDV axial 1st read	EDV axial 2nd read	EDV sao 1st read	EDV sao 2nd read	EF axial 1st read	EF axial 2nd read	EF sao 1st read	EF sao 2nd read
265 (103)	269 (107)	242 (92)	247 (98)	32.8 (9.9)	33.5 (9.7)	34.4 (9.7)	34.2 (11.1)

imaging and quantification of the bound agent (2), as well as a blood pool signal for 19F MR angiography at clinical field strengths (3). The ability to include gadolinium in the outer lipid shell provides an opportunity to design an activateable agent based upon 19F MR imaging such that cleavage of the gadolinium would cause a change in the signal obtained.

Methods: Perfluorocarbon (perfluoro-15-crown-5 ether) nanoparticles were formulated to contain approximately 50,000 lipophilic paramagnetic chelate molecules (Gd-DTPA-BOA) per particle or an inert lipid layer (1). The relaxation times of both were compared at three different MR field strengths (1.5T Philips Intera Clinical Scanner, 4.7 and 11.7T Varian small-bore scanners) using inversion recovery spectroscopy for T1 on the same samples at room temperature and ambient oxygenation. The gadolinium effect on 19F T1 was further analyzed through transmetallation studies (5). Zinc chloride and phosphate were added to the nanoparticle suspension to induce replacement of the gadolinium on the DTPA-BOA chelate with zinc and allowed to proceed to equilibrium (9 days at room temperature). Zinc to gadolinium ratios of 0, 0.1, 0.5, 0.75, 1, and 10 were used to obtain variable levels of gadolinium replacement, mimicking cleavage. Finally, MR imaging of both nanoparticle samples (+Gd and -Gd) were performed using a balanced steady state free precession sequence (bSSFP) at 1.5 T over a range of flip angles to characterize the signal and contrast behavior ($1 \times 1.25 \times 5$ mm resolution, TR = 4 ms, TE = 2 ms, 64 signal averages).

Results: Relaxation time measurements indicate that the gadolinium has a significant influence on the fluorine nuclei, particularly at lower field strengths (Table 1). Transmettalation studies further verified this conclusion in that increasing the zinc to gadolinium ratio resulted in increased 19F T1 times (Fig.). This indicates that the incremental removal of gadolinium from the surface of the particle results in a measurably different 19F T1 time. Testing the influence of the gadolinium on the signal generated using a clinically applicable imaging sequence indicates that its removal via enzyme cleavage may increase the signal obtained using a bSSFP sequence (Fig. 1).

Conclusions: When located in close proximity to the fluorine nuclei, gadolinium can be used to shorten the T1 times for 19F imaging with perfluorocarbon nanoparticles, particularly at 1.5 T. Removal of gadolinium from the particle surface results in a measurable change in 19F T1 relaxation time so that design of an activateable agent based upon 19F imaging is feasible. Finally, this change in T1 translates into a difference in signal intensity on MR images when using a clinically applicable fast scanning sequence. We propose that this data may be used to manufacture a perfluorocarbon nanoparticle for 19F imaging which utilizes an enzyme-cleavable gadolinium linker for MR molecular imaging of pathological enzyme activity.

REFERENCES

1. Winter, et al. Circulation 2003;108:2270–4.
2. Morawski, et al. Magn Reson Med 2004;52:1255–62.
3. Neubauer, et al. J Cardiovasc Magn Reson 2007 (in press).
4. Thomas, et al. J Magn Reson Imaging 1994;4:631–5.
5. Lorent, et al. Invest Radiol 2001;36:115–22.

TABLE 1

	Field Strength		
	1.5 T	4.7 T	11.7 T
NP -Gd	945	992	764
NP +Gd	237	492	612

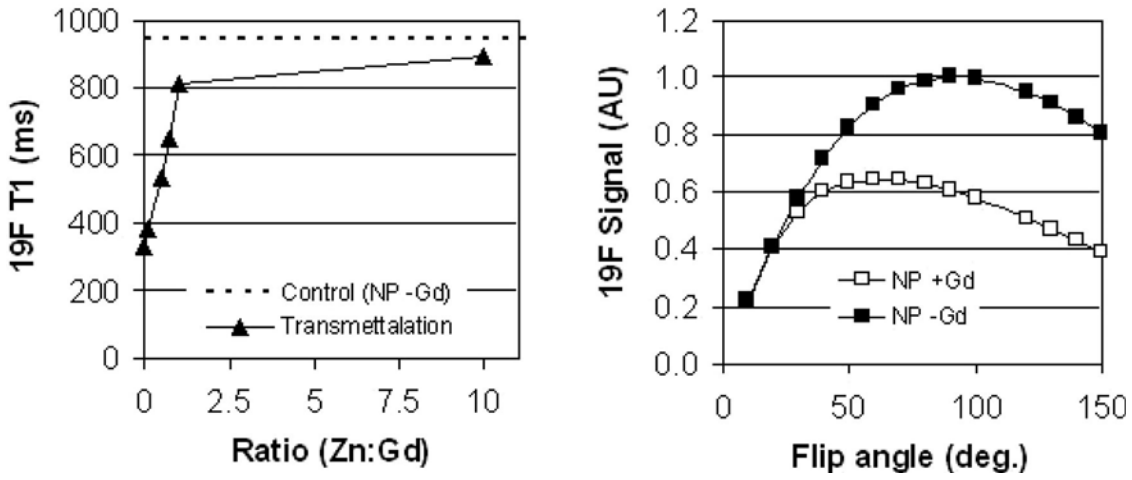

FIG. 1. (Top) Table of 19F T1 relaxation times (ms) of PFC nanopartides which either did (+Gd) or didnot (-Gd) contain a gadolinium chelate in their outer lipid layer. (Left) This graph demonstrates how release of gadolinium from the particle surface results in a drastic alteration in 19F relaxation time, providing a mechanism for generating an activateable signal. (Right) Data demonstrating that the signal generated from PFC NP can be increased by removal of gadolinium from the particle surface using a balanced stady state free precession sequence. A range of flip angles was used to demonstrate the signal and contrast behavior.

367. AUTOMATIC DATA ACQUISITION WINDOW DETERMINATION FOR CORONARY MRA

Xiaoming Bi, PhD,[1] Yiu-Cho Chung, PhD,[1] Peter Weale, BA, DCR(R),[1] Gary McNeal, MS,[1] Sven Zuehlsdorff, PhD,[1] Debiao Li, PhD,[2] Renate Jerecic, PhD.[1] [1]***Siemens Medical Solutions, Chicago, Illinois, USA,*** [2]***Northwestern University, Chicago, Illinois, USA.***

Introduction: Coronary motion during a cardiac cycle varies substantially from subject to subject (1). Typically, cine images are acquired and visually assessed prior to coronary MRA to identify the appropriate data acquisition window (2). Such procedure is highly subjective and requires user experience. Automated post-processing methods were developed (3) where substantial user interaction is required.

The purpose of this work is to develop an automated method without user interaction for the objective selection of the optimal data acquisition window in coronary MRA.

Method: Fourteen healthy volunteers were scanned on a 1.5 Tesla scanner (Sonata, Siemens, Erlangen, Germany). For each subject, cine images were acquired in the 4 chamber orientation with the following protocols: 2D TrueFISP triggered-retrospective-gated with both high ($1.3 \times 1.3 \times 6\ mm^3$) and low ($1.7 \times 1.7 \times 6\ mm^3$) spatial resolution during free-breathing (3 averages) and breath-holding. Small field-of-view was used to minimize signal contribution from regions outside of the heart by oversampling in the readout and phase-encoding directions (4).

Forty cardiac phases were acquired and the correlation coefficient (CC) for adjacent cardiac phases was calculated inline for each measurement. The maximal (CC_{max}) and minimal (CC_{min}) coefficients were identified and neighboring phases of the CC_{max} within a user-defined threshold value α were defined as cardiac diastasis if $CC > (CC_{max} - \alpha \cdot [CC_{max} - CC_{min}])$. The correlation curve was generated inline as part of the reconstruction and instantly available for display.

To choose an appropriate acceptance threshold, cardiac diastasis was calculated with α equaled 1%, 5%, 10%, and 15%, respectively. Since the motion of the right coronary artery (RCA) was more significant than the left, the cross-section of RCA in the 4 chamber view was visually assessed by 2 experienced reviewers independently to select the quiescent period. The mid-point and width of the calculated diastasis from the CC were compared to the visually determined quiescent period assessed by the reviewers. In this study, the visual assessment was taken as standard reference. Therefore, the mid-point of the data acquisition window should correlate using two-tailed, paired t-test. Since the width of the calculated acquisition window should not exceed the observed width to accommodate minor heart rate variations, one-tailed, paired t-test was used.

Results: Selected acquisition window from 2 reviewers agrees with each other (p values = 0.38/0.08 for the mid-point/width). The comparison results of the observed (reviewer) and automatically calculated data acquisition window are summarized in Table 1. Although $\alpha = 0.01$ yields results in agreement with the reviewers (p value >0.05 for both the mid-point and width of the window), the acceptance window is small (mean width = 44 ms) and not practical. With $\alpha = 0.05$, good correlation between visual assessment and automatic selection is achieved with reasonable acquisition window width (mean value = 107 ms).

Discussion: The study demonstrates that objective data acquisition window for coronary MRA can be automatically determined from cine images without user interactions. A threshold value of $\alpha = 0.05$ is appropriate for both breath-holding and free-breathing techniques. High-resolution ($1.3 \times 1.3\ mm^2$) is recommended for breath-holding cine scans and low resolution ($1.7 \times 1.7\ mm^2$) is appropriate for free-breathing cine acquisitions. This technique can potentially be used for other MR imaging techniques requiring data acquisition in the quiescent period of the cardiac cycle. This method needs to be validated in patients with abnormal wall motions in the future.

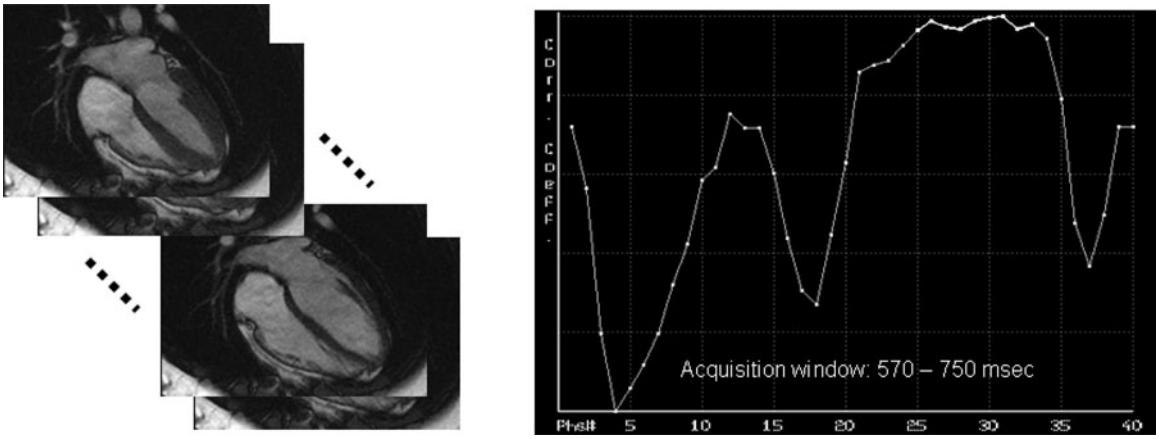

FIG. 1. Exemplary small FOV cine images (end-systole ard mid-diastole) and automatically generated correlation curve with recommended acquisition window. No manual cropping or interactions were involved. For this subject, cardiac phase number 26 to 33 were identified as diastasis, corresponding to an acquisition window from 570 to 750 msec.

TABLE 1
Correlation results (p-value) of the selected data acquisition window (mid-point and width) based on visual assessment (reviewer) and automatic calculation with different imaging protocols and acceptance thresholds α. Note α value of 0.05 yields results in good agreement with the visual assessment and provides

		p-values with various acquisition window thresholds (α)							
		$\alpha = 0.01$		$\alpha = 0.05$		$\alpha = 0.10$		$\alpha = 0.15$	
Breath-hold/free-breath	In-plane resolution	Mid	Width	Mid	Width	Mid	Width	Mid	Width
breath-hold	1.3 × 1.3	0.27	1	0.28	0.99	0.01	0.23	0.01	0.01
	1.7 × 1.7	0.27	1	0.05	0.99	0.01	0.78	1E-5	0.01
Free-breathing	1.3 × 1.3	0.33	1	0.02	0.99	7E-5	0.63	2E-5	8E-5
	1.7 × 1.7	0.49	0.99	0.06	0.96	9E-6	0.02	3E-6	1E-5

REFERENCES

1. Wang Y, et al. Radiology 1999;213:751–8.
2. Weber OM, et al. MRM 2003;50:1223–8.
3. Jahnke C, et al. JCMR 2005;7:395–9.
4. Bi X, et al. ISMRM 2006:2163.

368. AUTOMATIC MOTION COMPENSATION ALGORITHM (MAG) IMPROVES SCAN COMPLETION RATE FOR FREE BREATHING WHOLE HEART CORONARY MRA

Robson Macedo, MD,[1] Ashkan A. Malayeri, MD,[1] Seth Berkowitz, BSEE,[1] Kakuya Kitagawa, MD, PhD,[1] Vibhas S. Deshpande, PhD,[2] Steven Shea, PhD,[1] David A. Bluemke, MD, PhD.[1] [1] *Johns Hopkins Hospital, Baltimore, Maryland, USA,* [2] *Siemens Medical Solution, Los Angeles, California, USA.*

Purpose: Coronary MR Angiography (CMRA) using navigator echos reduces motion artifact by triggering the CMRA sequence based on the position of the diaphragm. During lengthy CMRA acquisitions associated with whole heart technique, there is considerable diaphragm drift and/or change in breathing patterns that may be encountered. An automatic motion compensation algorithm combining diaphragm tracking with slice following has not been previously evaluated for whole heart CMRA.

Materials and Methods: The whole-heart CMRA approach consisted of a magnetization-prepared, 3D, centric-ordered, segmented, refocused SSFP sequence using a 1.5 T MRI system (Siemens, Avanto). A navigator technique with using real time slice following (MAG) and respiratory gating window of ± 2.5 mm was applied to suppress motion artifacts from respiratory change in diaphragm position. Motion adaptive gating (MAG) is an algorithm designed to adapt and select the optimal respiratory navigator-gating window continuously throughout a scan. The algorithm searches for the end expiratory position, and changes the respiratory gating window such that data are acquired only during this breathing phase. To prevent erroneous tracking, the breathing data is checked for consistency before an adaptation occurs. The reference position for slice following remains unchanged throughout the scan. Both whole heart CMRA (average 1.5 × 1.1 × 1.1 mm resolution) a) using conventional navigator gating and b) with automatic motion compensation algorithm (MAG) pulse sequence were performed in random order in 20 participants (11 males and 9 females with mean age of 41.5 ± 15.4). The average scan duration and scan efficiency were calculated for both motion compensation algorithms. The scan was considered nondiagnostic if whole heart CMRA was not complete after 15 minutes. Signal-to-noise (SNR), contrast-to-noise (CNR) ratio, and image quality scores of the right coronary artery (RCA), left main coronary artery (LMCA), left anterior descending coronary artery (LAD) and circumflex coronary artery (CX) were compared in a paired analysis for both whole heart pulse sequences. Vessel sharpness measurements obtained from cross sectional views of the RCA were also analyzed for both techniques.

Results: Mean scan time for the conventional navigator was 843.1 ± 597.6 s; the MAG mean time was 706.5 ± 367.0 s ($p = 0.2$). The conventional navigator technique was nondiagnostic due to irregular breathing patterns in 4/20 (20%) cases compared to 1/20 (5%) using the MAG pulse sequence. The average scan efficiency was similar for the MAG technique compared to the conventional navigator (29.3 ± 20.1% vs. 32.9 ± 13.4%, respectively, $p = 0.3$). There was no significant difference in image quality scores for the RCA, LCMA, LAD and CX

TABLE 1

	Conventional (Mean ± SD)	MAG (Mean ± SD)	p value
SNR values			
RCA	32.4 ± 11.6	31.2 ± 13.3	0.6
LMCA	33.3 ± 13.5	36.0 ± 13.9	0.3
LAD	30.4 ± 13.7	33.3 ± 17.3	0.4
CX	28.4 ± 12.8	32.3 ±15.7	0.1
CNR values			
RCA	21.7 ± 9.8	20.4 ±10.4	0.5
LMCA	21.3 ± 12.2	24.1± 12.6	0.2
LAD	18.6 ± 11.2	20.5 ±12.8	0.5
CX	12.8 ±8.8	17.2 ± 9.7	0.07

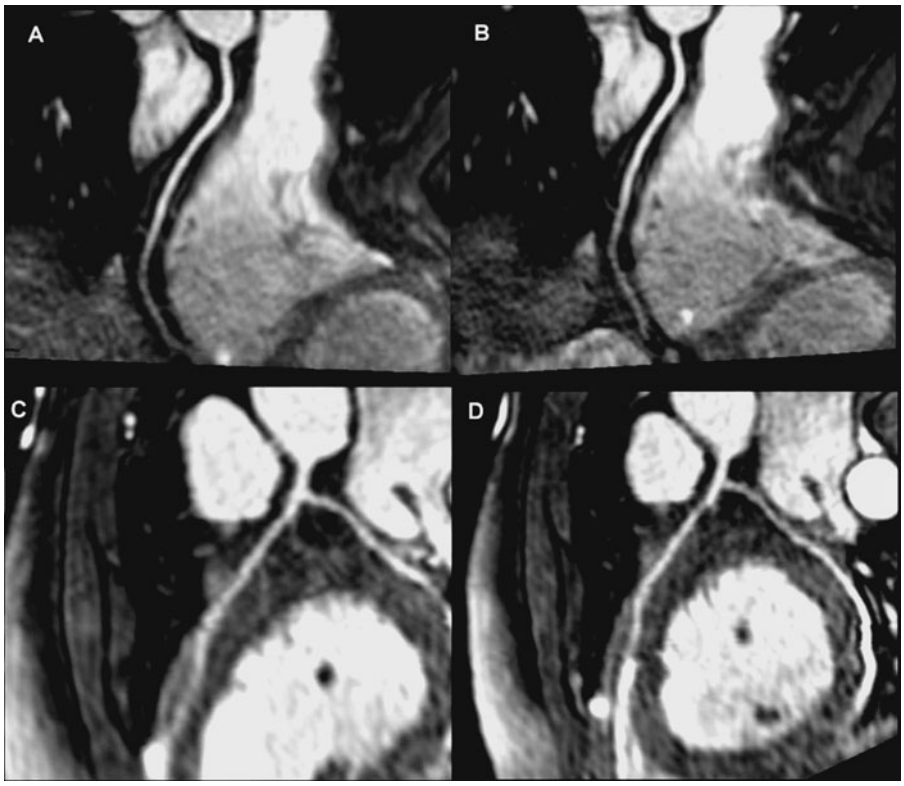

FIG. 1. Examples of coronary artery images acquired without (left; A + C) and with (right; B + D) MAG. No significant difference in image quality was found.

($p = 0.79$, 0. 13, 0.14, 0.63, respectively) (Fig. 1). There was also no significant difference in SNR and CNR values for the RCA, LMCA, LAD and CX (Table 1). Vessel sharpness measurements for the RCA were similar for both methods (0.40 ± 0.21, 0.41 ± 0.16, $p > 0.5$).

Conclusion: Automatic motion compensation algorithm achieved a higher completion rate for whole heart CMRA compared to conventional navigator CMRA with similar image quality.

369. LATE CONTRAST ENHANCED CMR IN THE EVALUATION OF INFARCT SIZE AND MICROVASCULAR OBSTRUCTION IN OPTIMALLY TREATED PATIENTS AFTER ACUTE MYOCARDIAL INFARCTION

Robin Nijveldt, MD,[1] Aernout M. Beek, MD,[1] Mark B. M. Hofman, PhD,[1] Victor A. W. M. Umans, MD, PhD,[2] Paul A. Algra, MD, PhD,[2] Cees A. Visser, MD, PhD,[1] Albert C. van Rossum, MD, PhD.[1] [1]***VU University Medical Center, Amsterdam, The Netherlands,*** [2]***Medical Center Alkmaar, Alkmaar, The Netherlands.***

Background: Infarct size (IS) and microvascular obstruction (MVO) are strong predictors of prognosis following acute myocardial infarction (AMI). However, their time course and significance in optimally treated patients is not well known. In this study we investigated the change of IS over time, and the incidence and significance of MVO in an optimally treated, homogeneous patient group after reperfused AMI.

Methods: Forty patients with first AMI who were treated within 6 hours with primary stenting, abciximab, aspirin, heparin and clopidogrel underwent cine and contrast enhanced (ce)CMR at 4–7 days and 4 months after admission. Left ventricular volumes and ejection fraction (LVEF), infarct size (IS) and size of

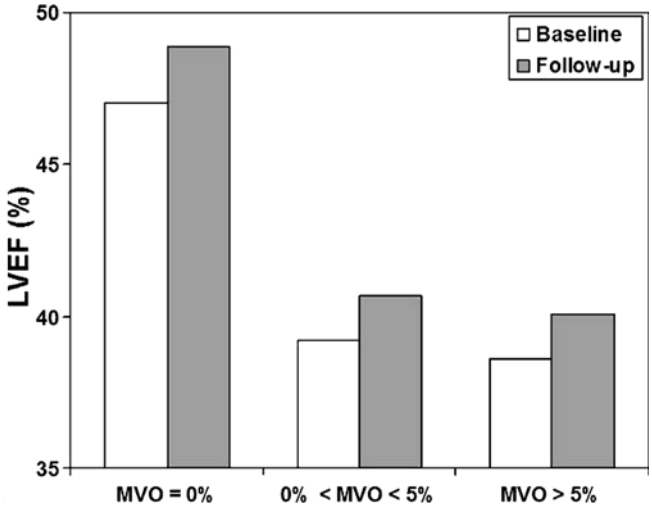

FIG. 1.

MVO were determined in short axis views covering the whole left ventricle. MVO was defined as subendocardial areas of hypoenhancement within the hyperenhanced area on ceCMR images, 10–15 minutes after injection of Gd-DTPA, and calculated as percentage of IS.

Results: IS decreased with 18.1% at follow-up ($p < 0.01$). The 23 (57.5%) patients with MVO had larger IS, lower LVEF at baseline, and more involution of IS at follow-up. LVEF, IS and IS reduction did not differ between patients with small and large areas of MVO. Overall, LVEF improved from $42.3 \pm 9.8\%$ to $44.0 \pm 9.8\%$ ($p = 0.06$), and the degree of change was similar in patients with no, small and large areas of MVO.

Conclusions: IS reduces over time by 18.1% in optimally treated patients after AMI. Despite optimal reperfusion, MVO was found in the majority of patients. Although patients with MVO had larger infarcts and lower LVEF, functional change at follow-up was comparable to patients without MVO. Importantly, our data suggested that the mere presence of MVO might be more relevant than its extent.

370. MR VECTOR FIELD MEASUREMENT AND VISUALIZATION OF NORMAL AND PATHOLOGICAL TIME-RESOLVED THREE-DIMENSIONAL CARDIOVASCULAR BLOOD flOW PATTERNS

Gert Reiter, PhD,[1] Ursula Reiter, PhD,[2] Bernhard Kainz,[3] Andreas Greiser, PhD,[4] Horst Bischof, Prof.,[3] Rainer Rienmüller, Prof.[2] [1]***Siemens Medical Solutions, Graz, Austria,*** [2]***University Hospital Graz, Graz, Austria,*** [3]***Technical University Graz, Graz, Austria,*** [4]***Siemens Medical Solutions, Erlangen, Germany.***

Introduction: Assessment of blood flow properties is crucial in the understanding and diagnosis of many cardiovascular diseases. Usual MR through-plane phase contrast methods provide a lot of useful information via the possibility to determine flow through cross sections or velocities in preferred directions. Its usefulness in complex fluid dynamical situations—as for example in the cardiac chambers—is limited, because main directions of flow are neither known nor constant in time.

Purpose: The purpose of the present work is to study time-resolved three-dimensional blood flow patterns in the cardiac chambers via different phase contrast measurement procedures and visualized as color encoded vector fields by suitable software.

Methods: Conceptually the easiest way to acquire three-dimensional blood flow data is to measure through-plane and both in-plane velocity components via phase contrast method. Alternatively an orthogonal grid of through-plane phase contrast measurements can be placed across a volume of interest. In both cases velocity vectors are determined on each imaging plane: In the case of the combined through-plane and in-plane measurement for each pixel and in the grid case for each intersection point of planes.

A generic way of representing the measured velocity fields is to represent each velocity vector as color encoded vector in three-dimensional space: length and color of the vector represent the magnitude of velocity, the direction of the vector the direction of the velocity. Suppression of noisy pixels (which can be done automatically via a signal-to-noise threshold in the anatomical phase contrast images) as well as the provision of anatomical landmarks (canonically via projection of the vectors onto corresponding anatomical phase contrast images) are additional necessary steps to provide interpretable images.

MR flow measurements were performed on a 1.5 Tesla scanner (Magnetom Sonata) with a six-channel cardiac array coil employing standard ECG-gated Flash-based two-dimensional phase contrast sequences. All images were loaded to a dedicated software package ("4D Flow") providing the above described vector field visualization.

Results: Both, the combined through-plane and in-plane measurement as well as the grid measurement produced the following typical normal blood flow patterns in the cardiac chambers: During early diastole E-wave flow through mitral and tricuspid valve was directed apically and high velocities appeared homogeneously across both orifices. The mitral and tricuspid inflows reached their maximum fast, decreased during middle diastole

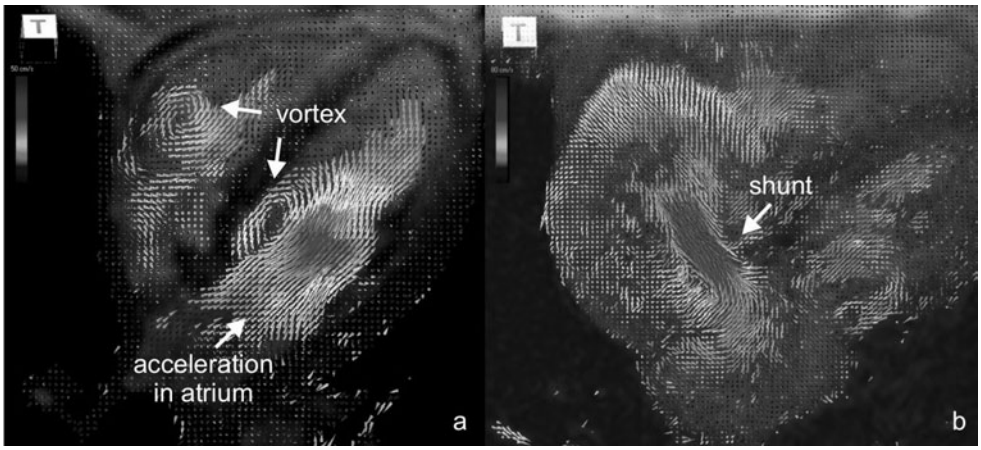

FIG. 1.

and reached a second maximum in end diastole (A-wave). In contrast to E-wave blood was accelerated in the atria during A-wave (Fig. 1a). Already early after the onset of diastolic filling small vortices were formed at all valvular leaflets. Especially the vortex at the anterior leaflet of the mitral valve increased towards end diastole and a larger part of the inflowing blood discharged into this vortex (Fig. 1a). When mitral and tricuspid valve closed, blood was accelerated towards aortic and pulmonic valve, respectively. The large vortex at the anterior leaflet of the mitral valve passed over to a flow uniformly directed towards the aorta.

Apart from normal blood flow patterns various blood-flow related pathologies including valvular regurgitation and stenosis, shunts (Fig. 1b) as well as flow patterns around valvular prostheses could be visualized in accordance with results of reference measurements.

Conclusions: Measurement of time-resolved three-dimensional blood flow patterns via different phase contrast methods and their visualization as color encoded vector fields is a promising tool in the analysis of cardiovascular diseases.

371. REGURGITANT VOLUME BY CARDIAC MRI IS SUPERIOR TO ECHOCARDIOGRAPHIC PARAMETERS IN PREDICTING VALVE REPLACEMENT IN PATIENTS WITH CHRONIC AORTIC REGURGITATION

Arun Abraham, MBBS, Colin Edwards, MBBCh, FRACP, FCP(SA), Tony Scott, MBChB, FRACP, FACC, Hitesh Patel, MBChB, FRACP, Guy Armstrong, MBChB, FRACP, FESC, Hamish H. Hart, Jonathan P. Christiansen, MBChB, FRACP, FACC, MD. ***North Shore Hospital, North Shore, New Zealand.***

Introduction: Aortic valve replacement (AVR) after LV decompensation may result in suboptimal outcomes. Echocardiographic (TTE) dimensions are used to determine timing of AVR in asymptomatic patients with aortic regurgitation (AR). Cardiac MRI (CMR) can quantify ventricular volumes, regurgitant volume (R_{vol}) and fraction (R_{fr}), and image valvular and aortic anatomy. We investigated the role of CMR in the evaluation of patients with AR, the value of R_{vol} and R_{fr} in predicting subsequent need for AVR, and their correlation with TTE measurements.

Methods: Twenty-nine patients with AR (age 57 $\pm$ 19; 20 male; 28/29 asymptomatic at the end of follow up) were reviewed prospectively following CMR. Average follow up was 14.5 $\pm$ 6.6 months. Ventricular measurements were made by standard imaging techniques for both TTE and CMR. R_{vol} and R_{fr} were measured by CMR using velocity-encoded phase contrast imaging. The decision to recommend AVR was made independent of the CMR result.

Results: Aortic valve morphology was tricuspid (21), bicuspid (7) or quadricuspid (1). CMR and TTE assessment of valve morphology was concordant in all cases. Ascending aortic dilation was noted in 13 patients (4.7 $\pm$ 0.5 cm). Average R_{vol} was 39 $\pm$ 21 mL and R_{fr} 24 $\pm$ 14%. R_{vol} correlated with CMR-derived LV end-diastolic and end-systolic volumes ($R = 0.8$ and 0.54, $p < 0.05$), but R_{fr} correlated poorly with both ($R = 0.27$ and 0.29, p = ns). TTE measurements of LV end-diastolic (EDD) and end-systolic (ESD) dimensions correlated acceptably with R_{vol} ($R = 0.41$ and 0.53, $p < 0.05$) but not R_{fr} ($R = 0.23$ and 0.07, p = ns). Six patients were listed for surgery, and only one was symptomatic. An $R_{vol} > 67$mL predicted the need for AVR with 83% sensitivity and 100% specificity (ROC area = 0.96). R_{vol} was more predictive of AVR than either R_{fr} (0.77) or TTE indices: EDD (0.71), ESD (0.82) and Ejection Fraction (0.42).

Conclusions: R_{vol} was superior to both TTE parameters and R_{fr} as a predictor of subsequent need for AVR. TTE dimensions correlated acceptably with R_{vol} but poorly with R_{fr} assessed by CMR. CMR can provide a comprehensive and accurate assessment of AR, and has the potential to be the optimal imaging modality for these patients.

372. RELATION BETWEEN REGIONAL AND GLOBAL SYSTOLIC FUNCTION IN PATIENTS WITH ISCHEMIC CARDIOMYOPATHY AFTER β-BLOCKER THERAPY OR REVASCULARIZATION

Theodorus A. M. Kaandorp, MD,[1] Jeroen J. Bax, MD, PhD,[1] Joost Doornbos, PhD,[1] Sacha E. Bleeker, PhD,[2] Eric P. Viergever, MD,[1] Don Poldermans, MD, PhD,[3] Ernst E. van der Wall, MD, PhD,[1] Albert de Roos, MD, PhD,[1] Hildo J. Lamb, MD, PhD.[1] ***[1]Leiden University Medical Center, Leiden, The Netherlands, [2]Erasmus MC-Sophia Rotterdam, Rotterdam, The Netherlands, [3]ThoraxCenter Rotterdam, Rotterdam, The Netherlands.***

Introduction: We hypothesized that a differential effect on regional myocardial segments occurs depending on the type of therapy. Systemic medical therapy is expected to have a more global effect on both ischemic, dysfunctional myocardial segments and on non-ischemic, remote myocardium, whereas revascularization will have a more local effect on the ischemic, dysfunctional myocardium depending on the territory of the revascularized vessels.

Purpose: To assess the relationship between improved regional and global myocardial function in patients with chronic ischemic cardiomyopathy in response to β-blocker therapy or revascularization.

Methods: Cardiac MRI was performed in 32 patients with ischemic cardiomyopathy before and 8 $\pm$ 2 months after therapy. Patients were assigned clinically to β-blocker therapy (n = 20) or revascularization (n = 12). MRI at baseline was performed to assess regional and global LV function at rest and under low-dose dobutamine. Wall thickening was analyzed in dysfunctional, adjacent, and remote segments. Follow-up MRI included rest function evaluation.

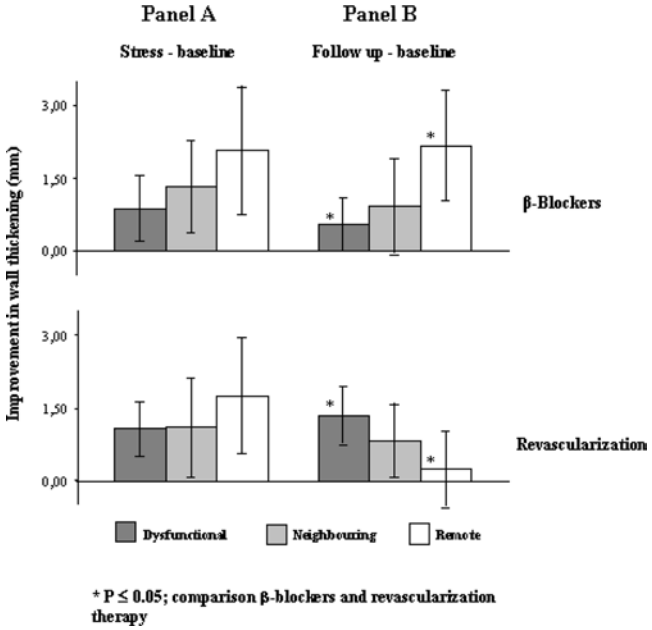

FIG. 1.

Results: Augmentation of wall thickening during dobutamine at baseline was similar in dysfunctional, adjacent and remote segments in both patient groups. Therefore, baseline characteristics were similar for both patient groups. In both patient groups resting LV ejection fraction and end-systolic volume improved significantly ($p < 0.05$) at follow-up. Stepwise multivariate analysis revealed that improvement in global LV ejection fraction in the β-blocker treated patients was significantly related to improved function of remote myocardium ($p < 0.05$), whereas in the revascularized patients improved function in dysfunctional and adjacent segments was more pronounced ($p < 0.05$).

Conclusions: In patients with chronic ischemic LV dysfunction, β-Blocker therapy or revascularization resulted in a similar improvement of global systolic LV function. However, after β-blocker therapy, improved global systolic function was mainly related to improved contraction of remote myocardium, whereas after revascularization the dysfunctional and adjacent regions contributed predominantly to the improved global systolic function.

373. IMPROVED CARDIAC SHIMMING IN A CLINICAL SETTING BY MULTI-FRAME FIELDMAP ACQUISITION AND AUTOMATIC ROI EXTENSION

Andreas Greiser, PhD,[1] Oliver Weber, PhD,[2] Vibhas Deshpande, PhD,[3] Edgar Mueller, PhD.[1] [1]***Siemens AG Medical Solutions, Erlangen, Germany,*** [2]***Siemens Medical Solutions Bern, Switzerland,*** [3]***Siemens Medical Solutions, Los Angeles, California, USA.***

Introduction: Performance of cardiac shimming procedures in a clinical environment is often limited by either required user interaction or insufficient convergence of the shim algorithm. Both temporal and spatial side conditions are critical to allow calculation of optimal shim settings. Assuming that some areas within the myocardium with strong local suscepitibility changes (i.e., veins, lung interface) cannot be shimmed and the attempt might even impair the overall shim convergence, it may be advantageous to restrict the input to the "benign" pixels with limited frequency difference.

Purpose: To generate accurate field maps in the heart and facilitate workflow for shim ROI definition.

Methods: A method for acquiring time-resolved 2D fieldmaps with high spatial resolution in the heart was implemented (gradient echo cine with Cartesian sampling, 2 excitations with echo time shifted in 2nd acq. (ΔTE 2.37 ms at 1.5T, 4.74 ms at 3T). On various clinical scanners (Siemens Magnetom Avanto, Espree, Trio), field maps were acquired in triggered, multiple breath held acquisitions on healthy volunteers ($n = 5$, matrix 128×70, FoV 400×320 mm, slice 8 mm, temp. res. 42 ms) covering the whole heart from base to apex. Based on a rectangular standard adjustment volume positioned inside the ventricle, anatomical regions of interest (ROI) were calculated: a region growing algorithm was applied that adds neighbouring pixels to the initial volume which have a local frequency value within the frequency range of the initial adjustment volume. Linear shim terms were calculated and the resulting frequency distribution was analyzed. From the single slice cine fieldmap, the time interval with least changes was determined and used for the full coverage fieldmap acquisition.

Results: In all cases dynamic fieldmaps with high image quality could be acquired (Fig. 1A). The application of automatic ROI extension resulted in a markedly increased shim volume (Fig. 1B, C). The dynamic analysis allowed the determination of an individual acquisition window, resulting in shortest possible shim acquisitions with full heart coverage, typically 3 slices per breathhold, acquisition window 234 ms (Fig. 1D, E).

Conclusions: The use of automated ROI extension and motion analysis reduces the user interaction to simply place one

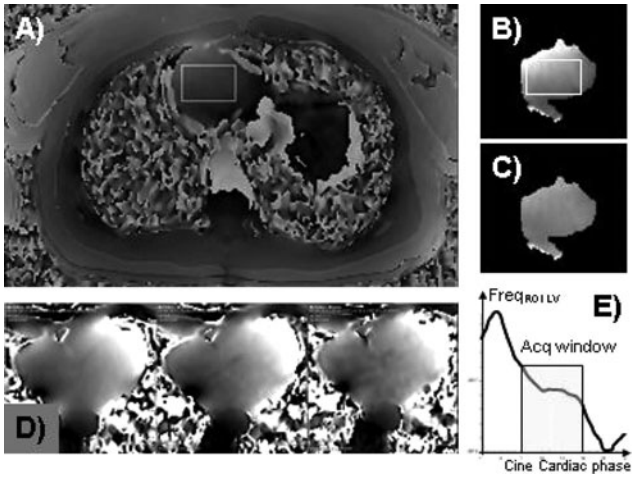

FIG. 1.

initial shim volume in the heart and run a single breathhold cine fieldmap to determine the optimal acquisition interval and ROI. Dynamic analysis of fieldmap cine data can directly show the temporal compliance of shim settings and can either be used to determine optimal time window for stable shim settings or to calculate shims for specific acquisition windows as required by the various following imaging sequence to be optimized. The remaining goal is to investigate the impact of this cardiac shimming method to CMR applications that will profit from a better shim.

374. POSITIVE CONTRAST (IRON) IMAGING: CORRECTION MECHANISMS FOR MAGNETIC FIELD INHOMOGENIETIES

Saurabh S. Shah, MS,[1] Ronald Ouwerkerk, PhD,[2] Michael Schär, PhD,[3,4] Grigorios Korosoglou, MD,[2] Wesley D. Gilson, PhD,[2] Dara L. Kraitchman, VMD, PhD,[2] Matthias Stuber, PhD.[5,6] ***[1]Department of Biomedical Engineering, Johns Hopkins University, Baltimore, Maryland, USA, [2]Russell H. Morgan Department of Radiology and Radiological Science, Johns Hopkins University School of Medicine, Baltimore, Maryland, USA, [3]Philips Medical Systems, Cleveland, Ohio, USA, [4]Russell H. Morgan Department of Radiology and Radiological Science, Johns Hopkins University, Baltimore, Maryland, USA, [5]Russell H. Morgan Department of Radiology and Radiological Science, Department of Medicine, John Hopkins University, Baltimore, Maryland, USA, [6]Deprtment of Electrical Engineering, Johns Hopkins University School of Medicine, Baltimore, Maryland, USA.***

Introduction: Inversion Recovery with ON-resonant water suppression (1) (IRON) is a positive contrast imaging method that hyperenhances the signal from susceptibility induced local field variations. It has been used to improve visualization of magnetically labeled stem-cells and endovascular devices (2, 3). However, if amplitude modulated radiofrequency (RF) pulses are used for suppressing tissue and fat, B_1-inhomogeneities can lead to non-uniform suppression and reduction in CNR. B_0-inhomogeneities can also compromise performance of the IRON method. Mechanisms are required to minimize these undesired effects.

Purpose: To theoretically and experimentally investigate correction schemes for field inhomogeneities that adversely affect IRON imaging.

Methods: Adiabatic RF pulses are characterized by simultaneous modulation of RF-amplitude and phase. By properly manipulating the modulation functions, spins that experience different B_1-fields can be excited with the same flip angle, thereby adequately dealing with B_1-variations.

MATLAB simulations were performed to compare a selective *sech* adiabatic inversion pulse with a selective *sinc-gaussian* RF pulse. A modified IRON method—Adiabatic IRON—was proposed, which utilized adiabatic inversion pulses for signal suppression. Additionally, a shimming tool developed by Schär et al (4) was evaluated for calculating localized shimming corrections.

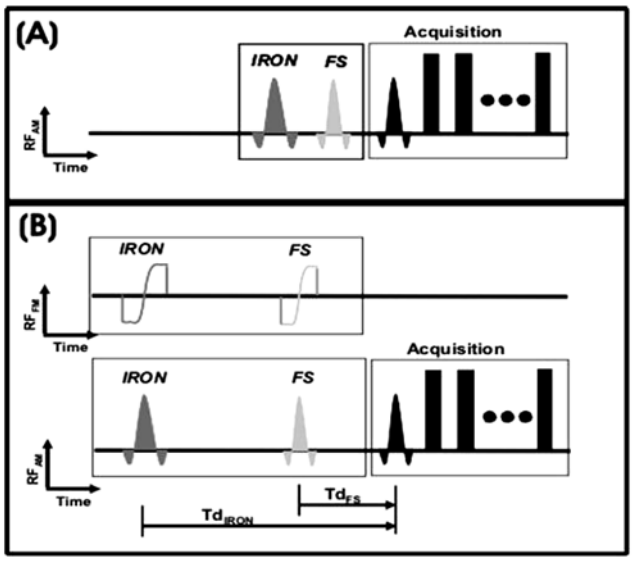

FIG. 1. Pulse sequence diagrams for two IRON methods. (A) *Conventional IRON:* this method utilizes two conventional frequency selective suppression pulses, the IRON pulse and the FS pulse, for the suppression of the background and fat, respectively. There is no time delay, either between the IRON and the FS pulse, or between the FS pulse and the excitation pulse. *(B) Adiabatic IRON:* this method utilizes two selective adiabatic pulses, similar to the Conventional IRON method, however, because these pulses invert the magnetization, additional time delays (Td_{IRON} and Td_{FS}) are required for nulling their signal at the time of the excitation pulse. In both IRON methods, a spoiling gradient (not shown) is played out immediatelyafter the FS pulse.

The conventional and the adiabatic IRON methods were implemented on Philips Achieva 3T system. For the *in vitro* experiment, two 750 mL Eppendorf tubes containing 0.01M Feridex and mineral oil were embedded in a gelatin phantom. Coronal images were obtained using the IRON methods and a TSE acquisition (TE/TR = 6.4 ms/2000 ms, FA = 90°, FOV/matrix = 180 mm/256 × 256, RFOV = 100%, slice thickness = 3 mm, echo train = 24). For the conventional IRON, positive contrast was achieved by appropriately adjusting the flip angle, bandwidth and center frequency of the saturation pulses. For the adiabatic IRON, adiabatic inversion pulses with adjustable bandwidth, center frequency and delay time were applied for signal suppression (Table 1). SNR/CNR were measured by selecting ROIs within the two tubes.

For the *in vivo* measurements, 250 μL Feridex (450 μg Fe/mL) was injected intramuscularly into a hind-limb of a rabbit. Similar to the *in vitro* experiment, coronal slices were obtained using both IRON methods together with a TSE acquisition. ROIs were manually selected within the injection site and background tissue for SNR/CNR calculations.

TABLE 1
In vitro and in vivo paramameters for the suppression pulses used in the two IRON methods

		Suppresion Pulse	Flip Angle (deg)	Bandwidth (Hz)	Center Freq (Hz)	Time Delay (ms)
In Vitro	Conventional IRON	IRON pulse	95*	254	0	0
		FS pulse	100*	510	−550	0
	Adiabatic IRON	IRON pulse	180*	249	0	650
		FS pulse	180*	499	−550	125
In Vivo	Conventional IRON	IRON pulse	100*	204	0	0
		FS pulse	105*	510	−550	0
	Adiabatic IRON	IRON pulse	180*	5	0	450
		FS pulse	180*	4	−550	200

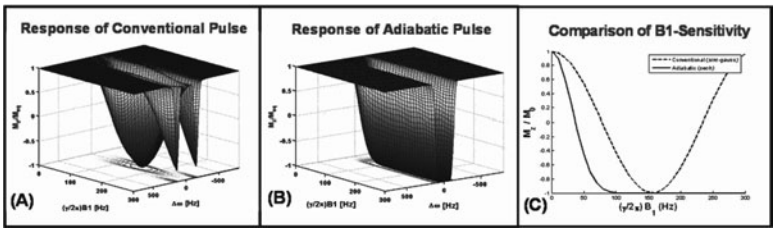

FIG. 2. Comparison of a conventional pulse with an adiabatic pulse. A) Response of a *sinc-gaussian* pulse with a bandwidth of 250 Hz. The normalized magnetization is plotted in 3D against a range of frequencies and a range of B_1 values. B) Response of a *sech* adiabatic pulse. C) Comparison of B-sensitivity for ihe conventional and ihe adiabatic pulse The flip angle of an amplltudfi modulated conventional pulse depends on the B_1-sensitivity. Therefore, conventional pulse is highly sensitive to variations in B_1. In contrast, with simultaneous modulation of amplitude and phase the adiabatic pulse remain insensitive to.

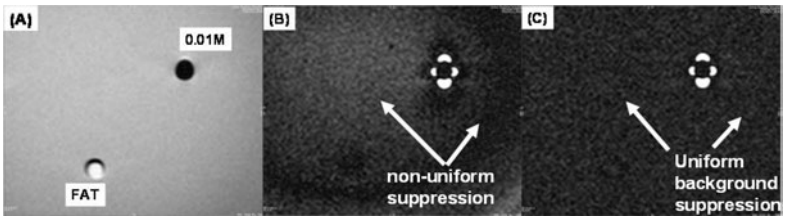

FIG. 3. In vitro comparison of the two IRON methods. A) TSE image shows the location of two Eppendorfs containing 0.01 M Feridex solution in 1% agar gel and fat, respectively. B) The *Conventional IRON:* the conventional suppresion pulses are sensitive to inhomogeneities present in the B_1-field, which prevents uniform suppression of the background signal. Therefore, some of the background regions appear less saturated than others. C) The *Adiabatic IRON*: the use of adiabatic inversion pulses reduces B_1-sensitivity, thereby providing uniform suppression of the background and the fat signal. (Images are cropped to ROI).

Results: Figure 2 provides a comparison of B_1-sensitivity for a conventional and an adiabatic RF pulse. In contrast to the conventional pulse, the adiabatic pulse is insensitive to B_1-variations above a threshold value of B_1-envelope.

Figure 3 shows that both IRON methods are successful *in vitro* for suppression of the background and fat signal, and provide identical positive enhancement in the area of Feridex. The conventional pulses fail to attain uniformity in the background suppression due to B_1-inhomogeneities (Fig. 3B, solid arrows), whereas the adiabatic inversion pulses successfully achieve homogeneous suppression, increasing CNR (Table 2). Similarly, the background suppression varies from the medial to lateral regions of the hind-limb *in vivo* (Fig. 4), with the conventional IRON. Whereas, the adiabatic IRON provides more uniform background suppression and improved visualization of superparamagnetic material.

Conclusions: In positive contrast IRON imaging, adiabatic *sech* inversion pulses were successfully utilized for B_1-independent suppression of the background tissue and fat signal *in vitro* and *in vivo*. The long delay times associated with inversion recovery make it less suitable for rapid imaging and may emphasize T_1 differences. Nevertheless, the adiabatic inversion leads to an improved background signal suppression *in vitro* and *in vivo*. Together with sophisticated higher-order shimming algorithms, this helps to minimize ambiguous signal enhancement in positive contrast IRON imaging which improves the specificity of the method.

TABLE 2
In vitro and in vivo comparison for the two IROM methods. White SNR in the enhanced region is similar in both the IRON methods, the adiabatic IRON method improves background suppression (reduced background SNR) resulting in an increase in CNR.

		$SNR_{(Feridex)}$	$SNR_{(Agar)}$	$CNR_{(Feridex/Agar)}$
In Vitro	Conventional IRON	17.35	6.94	10.41
	Adiabatic IRON	17.45	5.05	12.40
		$SNR_{(Feridex)}$	$SNR_{(Tissue)}$	$CNR_{(Feridex/Tissue)}$
In Vivo	Conventional IRON	36.40	5.36	31.04
	Adiabatic IRON	36 .6B	4.36	32.31

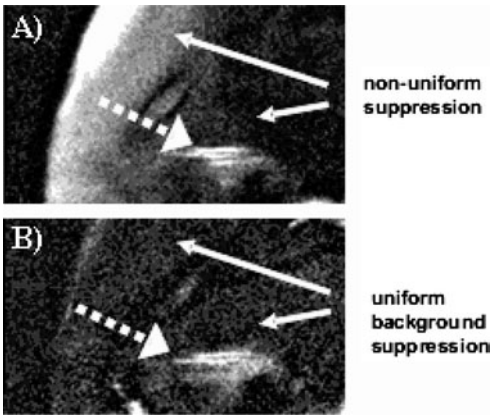

FIG. 4. In vivo comparison of the two fat suppressed IRON methods. The site of Feridex injection is marked with dotted arrows. The use of conventional suppression pulses results in non-uniform background suppression pulses results in non-uniform background suppression across the ROI (A). Whereas, the adiabatic inversion pulses attain a comparatively more uniform suppression of the background.

REFERENCES

1. Stuber et al. Proc. ISMRM 2005; 13.
2. Gilson et al. Proc. ISMRM 2006; 14.
3. Shah et al. Proc. ISMRM 2006; 14.
4. Schär et al. MRM 2004; 51: 799-806.

375. CARDIAC FUNCTION DURING AGEING IN ENERGETICALLY COMPROMISED GUANIDINOACETATE N-METHYLTRANSFERASE (GAMT)-KNOCKOUT MICE—A ONE YEAR LONGITUDINAL MRI STUDY

Jurgen E. Schneider, PhD, Lee-Anne Stork, Craig A. Lygate, PhD, Michiel ten Hove, PhD, Julie Wallis, PhD, Liam M. Sebag-Montefiore, Kieran Clarke, PhD, Hugh Watkins, MD, PhD, Stefan Neubauer, MD. ***Oxford University, Oxford, United Kingdom.***

Introduction: High-resolution magnetic resonance imaging (cine-MRI) is a highly attractive tool to determine global cardiac function in normal, genetically or surgically manipulated mice. In hearts of a mouse model of guanidinoacetate N-methyltransferase (GAMT)-deficiency (the second essential step in creatine synthesis)), which consequently lack creatine as noninvasively confirmed by ^{1}H-MRS (2), we previously showed normal function at rest but a a reduced inotropic reserve under acute stress (3). In the present study, we subjected male and female normal and GAMT-ko mice to a longitudinal cine-MRI study over a time period of one year to systematically investigate the hypothesis that the lack of creatine would be detrimental for resting cardiac performance during aging.

Methods: Twenty-eight mice (male and female wild type (WT) and GAMT-ko mice, n = 7 per group) were subjected to high-resolution cine-MRI as described previously (4) at the age of 6 weeks, 4, 8 and 12 months, respectively. All experiments were performed on a vertical 11.7 T MR scanner (Bruker) using dedicated quadrature-driven birdcages (ids 28 mm and 40 mm). End-diastolic and end-systolic frames were segmented using AmiraTM 2.3, and cardiac functional parameters such as end-diastolic (EDV), end-systolic (ESV) and stroke volume (SV),

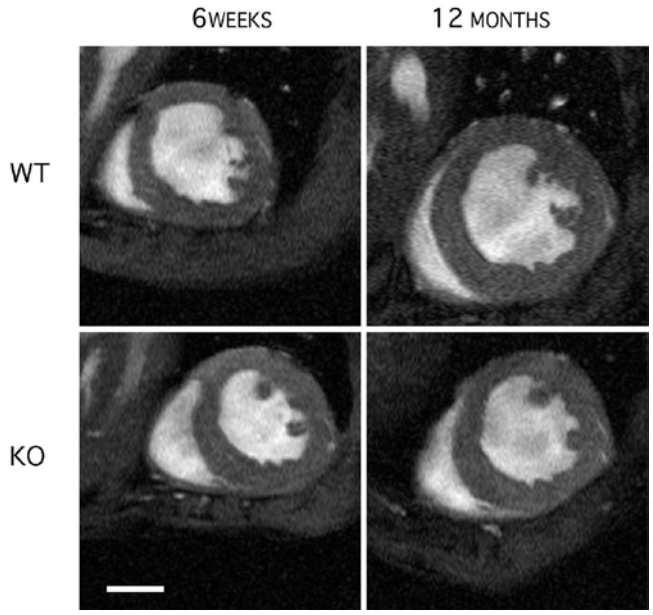

FIG. 1.

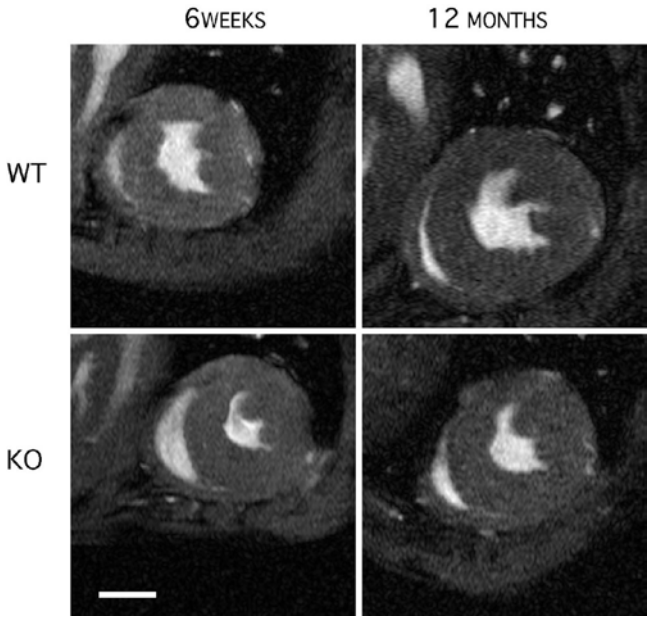

FIG. 2.

ejection fraction (EF) and left-ventricular mass (LVM) calculated. Furthermore, LV volumes of a mid-ventricular slice were segmented in all cine-frames, normalised to EDV of this slice and fitted to obtain maximum rates of contraction and relaxation i.e. $\pm$ dV/dt. Statistical analysis was performed using an unpaired t-test and an ANOVA-test for repeated measures. A value of $p < 0.05$ was considered significant.

Results: Figure 1 shows end-diastolic frames of a WT (top row) and of a GAMT-ko mouse at 6 weeks (left column) and at 12 months (right column), respectively. Figure 2 shows the corresponding end-systolic frames (scale bar: 2 mm). Figure 3 depicts the EF for all four groups as a function of time. Statistical analysis revealed no significant differences between the genotypes, except for body weight (females—from 4 months onwards; males—all time points) and LVM (males only—and 8 months), which disappeared when normalised to the body weight.

The ANOVA-test revealed no statistical significant difference for heart rate, SV and EF within each group, between genders or genotypes over time. It showed a group effect for male ko and WT for larger EDV ($p = 0.012$) and ESV ($p = 0.009$), which disappeared when normalised to the body weight. Maximum rates of contraction and relaxation showed no difference between the genotypes.

Discussion: Creatine plays a crucial role in the energy metabolism of the heart and a loss of creatine, as characteristically observed in the failing heart, has been postulated as one major mechanism leading to contractile dysfunction due to energetic derangement. It is therefore surprising that despite the lack of creatine in the hearts of GAMT-ko mice, this study did not reveal a cardiac phenotype under baseline conditions between the different genotypes, even at the age of 12 months. Since the GAMT-ko mice are already creatine-deficient during gestation, it seems likely that compensatory mechanisms may have developed during embryonic development. More experiments are under way to investigate this further. However, this study demonstrates the power of the MR-technique to accurately quantify cardiac functional parameters in genetically modified mice in a longitudinal fashion. Importantly, each animal served as its own control, providing a more powerful statistical analysis and substantially reducing the number of mice required to conduct such a study.

Acknowledgement: This work was supported by the British Heart Foundation (BHF).

REFERENCES

1. Hum Mol Genet 2004;13:905.
2. Magn Reson Med 2004;52:1029.

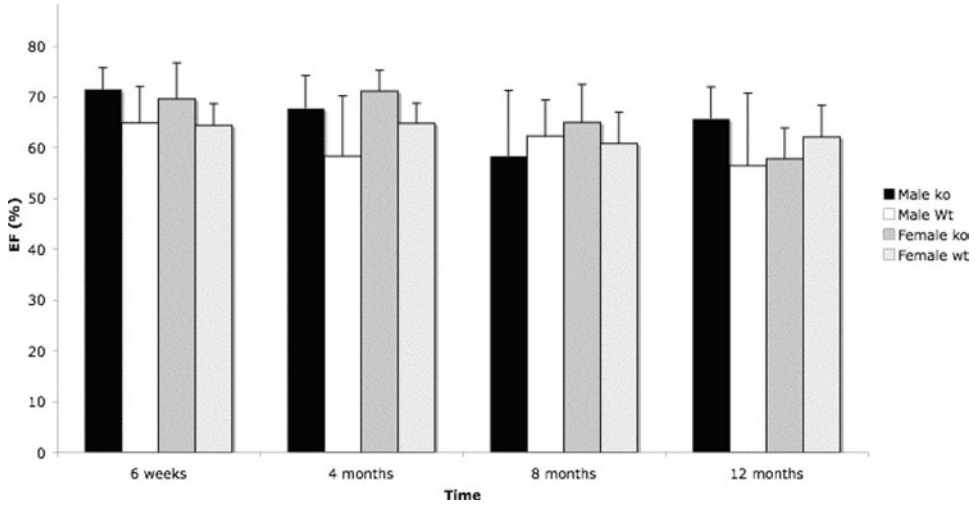

FIG. 3.

3. Circulation 2005;111:2477.
4. J Magn Reson Imaging 2003;18:691.

376. COMPARISON OF CARDIAC CONTRAST ENHANCED MRI AND CT IN SUB-ACUTE MYOCARDIAL INFARCTION

Balazs Ruzsics, MD,[1] Pal Suranyi, MD,[1,2] Pal Kiss, MD,[1,2] Brigitta C. Brott, MD,[3] Silvio H. Litovsky, MD,[4] Tamas Simor, MD, PhD,[1,2] Steven G. Lloyd, MD, PhD,[5] Gabriel A. Elgavish, PhD,[1,2] Himanshu Gupta, MD, FACC.[6] ***[1]Department of Biochemistry and Molecular Genetics, University of Alabama at Birmingham, Birmingham, Alabama, USA, [2]Elgavish Paramagnetics Inc., Birmingham, Alabama, USA, [3]Department of Cardiology, University of Alabama at Birmingham, Birmingham, Alabama, USA, [4]Department of Anatomic Pathology, University of Alabama at Birmingham, Birmingham, Alabama, USA, [5]Department of Medicine, University of Alabama at Birmingham, Birmingham, Alabama, USA, [6]Division of Cardiovascular Disease,University of Alabama at Birmingham, Birmingham, Alabama, USA.***

Introduction: Delayed contrast hyperenhancement (DE) on MRI may overestimate infarct size, probably due to partial volume effects that are inherent to the in vivo practicable slice thickness. Previous ex vivo reports that used signal-intensity(SI) threshold of 2 SD above normal myocardium demonstrated excellent correlation of MRI DE with TTC staining. DE CT may have an important role to assess myocardial viability in those patients where an MRI exam is contraindicated. In this work, in one week old pig infarcts, we carried out a quantitative comparison of viability assessment using the following modalities: in vivo DE MRI and cardiac CT, and ex vivo MRI and TTC-staining. Infarct quantification was semi-automated to reduce observer bias.

Methods: In five pigs (n = 5), one week following reperfused infarction, conventional delayed contrast enhanced (DE) images were acquired on a 1.5 T MRI-System after injecting 0.2 mmol/kg Gd (DTPA): FOV = 300 mm, image matrix = 256 × 256, slice thickness = 10 mm, read-out flip-angle = 25°, echo-time (TE) = 3.32 ms, repetition-time (TRp) = 7.18 ms, and recycle-time (TR) of one or two R-R intervals. The inversion time was set to the optimal value (between 225–325 ms) to null the signal of healthy myocardium. For DE image analysis, mean SI of a remote, normal myocardial region was measured (about 100 pixels). Mean SI_{remote} plus 2, 4 or 6 times the standard deviation was used to define threshold limits. Hyperenhanced pixels, and hypoenhanced pixels surrounded by hyperenhanced regions were considered infarcted and counted. The ratio of infarcted to total area of a slice, the Percent-Infarcted-area-per-Slice(PIS_{DE}) was calculated. Cardiac CT imaging was performed using a 64 detector CT scanner. After slice prescription, a 5 mL/kg bolus of iodixanol (Visipaque) was injected at rate of 4 mL/s, followed by 30 mL saline chaser. When signal in the ascending aorta reached a predefined threshold of 150 Hounsfield units, respiration was suspended and imaging performed with retrospectively gated cardiac MDCT protocol. After initial first-pass contrast scan, the post-contrast imaging protocol was repeated every 5 minutes for 40 minutes. True short-axis slices (1.4 mm) of MDCT images were reconstructed by multiplanar reconstructions of axial slices at 75% of cardiac phase on a Philips workstation, matching the orientations of short-axis postmortem myocardial slices were. MDCT images were analyzed automatically after manual contour tracing of endo-epicardial borders. Similar to MRI DE, myocardial hyperenhancement (nonviable) was delineated using SI_{remote}+2SD as threshold, and PIS_{CT} was calculated. Ex-vivo DE MRI images were generated using TI = 225–325 ms and a 3mm slice thickness (same as for TTC). TTC-staining was done at the end of the study, followed by hematoxyllin-eosin stained light microscopy.

Results: Correlations of PIS, using different DE-MRI thresholds, versus TTC are shown in Fig. 1a. Of the three thresholding methods, using 2SD resulted in the largest overestimation of infarct size, while using 6SD yielded results closest to the line of identity when compared to TTC. Quantitative assessment

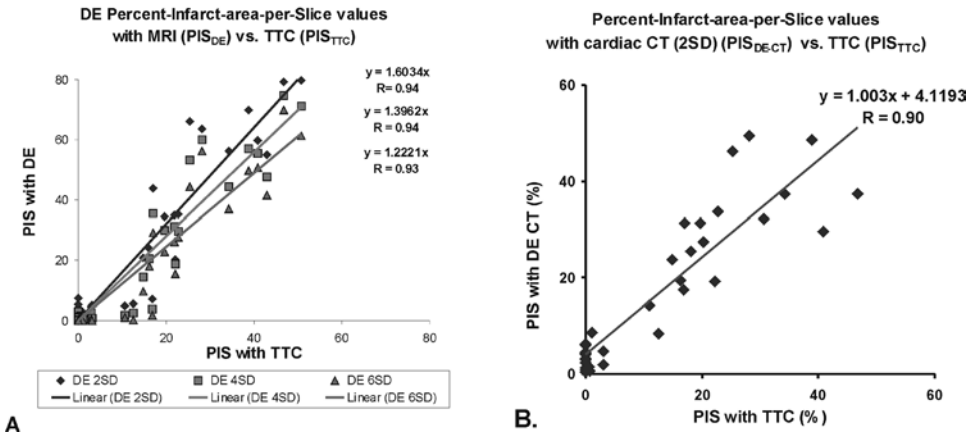

FIG. 1.

of infarct size using CT (PIS_{CT}) yielded significant correlation with that determined with TTC (Fig. 1b). Agreement among all modalities was excellent in visualizing the no-reflow zone (hemorrhage or non-digested, non-viable myocardium) in the center of the infarct.

Conclusion: In vivo CT, mainly due to high spatial resolution yielded the most accurate noninvasive quantification of myocardial infarction compared to gold standard TTC staining. Thresholding limits described in DE-CMRI and CT may have important clinical implications in quantifying sub-acute infarct. The overestimation of infarct size in DE-CMRI is probably due to partial volume effects that are inherent to in vivo imaging. Both CT and ex vivo CMRI identified the no-reflow zone as detected with TTC and microscopy.

377. NEGATIVE PREDICTIVE VALUE OF ADENOSINE-STRESS CARDIAC MAGNETIC RESONANCE IMAGING IN COMPARISON TO CORONARY ANGIOGRAPHY

Günter Pilz, MD, FESC, Markus Klos, MD, Susanne Eierle, Eman Ali, Berthold Höfling, MD, FESC, Peter Bernhardt, MD. ***Agatharied Teaching Hospital, University of Munich, Hausham, Germany.***

Background: Adenosine-stress cardiac magnetic resonance imaging (CMR) is increasingly proposed for non-invasive detection of relevant coronary artery disease (CAD). Given the clinical impact of underdiagnosing significant CAD, the CMR exam's negative predictive value seems particularly important. Aim of our study was to show the negative predictive value of CMR in comparison to invasive coronary angiography (CA) on a prospective basis.

Method: Ninety-five consecutive patients with suspected or known CAD who were referred for CA were additionally scanned in a 1.5 T whole-body scanner (GE Signa Excite) including adenosine-stress perfusion and delayed enhancement (DE) before undergoing catheterization. Patients without myocardial ischemia and no DE by CMR were included into the study. CA was performed within 48 hours after CMR. Both CMR and CA data were independently analyzed by experienced investigators. Significant CAD was regarded as luminal narrowing of $\geq$70% in CA.

Results: Seventy-two patients without ischemia and without evidence of DE in CMR were included into the study. Nineteen (26.4%) presented with CCS I, 42 (58.3%) with CCS II and 11 (15.3%) with CCS III. Fifty-three (73.6%) patients had no previous diagnosis of CAD. 19 (26.4%) patients had previously undergone PCI of one or more coronary vessels. In CA, significant coronary stenoses could be excluded in 67 (93.1%) of study patients. Coronary stenosis ($\geq$70%) was found in 5 (6.9%) patients, with a luminal narrowing of 70% in 3 cases (4.2%) and of 95% in two cases (2.8%). Four out of these 5 patients had known CAD and a history of PCI, one patient with a stenosis of 95% had no previously known CAD. Hence, negative predictive value of CMR for stenosis $\geq$ 70% in patients without previously known CAD was 0.98 and in patients with previous PCI 0.79. Exploratory analysis for stenosis $\geq$90% gave values of 0.98 and 0.95, respectively.

Conclusion: Adenosine-stress CMR allows for noninvasive exclusion of significant coronary stenosis in patients without previously known CAD with a very high and in patients who previously underwent PCI with an acceptable predictive value. Thus, CMR based decision making could reduce the rate of purely diagnostic CA. Further studies are warranted to clarify the rare false negative CMR results.

378. COMPARISON OF STRESS CMR WITH STRESS SPECT FOR THE ASSESSMENT OF CORONARY ARTERY DISEASE

John F. Heitner, MD,[1] Igor Klem,[2] Ijaz Ahmad,[1] Frederick Meine,[2] Michele Parker,[2] Robert M. Judd,[2] Michael W. Hanson,[2] Salvatore Borges-Neto,[2] Raymond J. Kim.[2] [1] ***New York Methodist Hospital, Brooklyn, New York, USA,*** **[2]** ***Duke University Medical Center, Durham, North Carolina, USA.***

Background: Single positron emission scintigraphy (SPECT) imaging is the most utilized outpatient procedure in the United States. The diagnostic accuracy of SPECT can be limited by soft tissue attenuation and low resolution. Cardiac magnetic resonance imaging (CMR) can also assess myocardial perfusion with a much higher spatial resolution and without the susceptibility to soft tissue attenuation.

Objectives: To compare stress CMR to stress SPECT in the assessment of coronary artery disease (CAD) in patients who present with chest pain.

Methods: We prospectively enrolled 65 patients with chest pain who were at intermediate risk for CAD. Exclusion criteria included; pregnancy, age <35, prior CAD, caffeine within 16 hours, pacemaker or defibrillator, aneurysm clips, morbid obesity and claustrophobia. Patients who met entry criteria for the study had a comprehensive evaluation including: physical exam, serum lipid profile, C- reactive protein (CRP), ECG, and a chemistry profile. All patients underwent both a stress CMR and stress SPECT. CMR included cine, adenosine- stress and rest perfusion, and delayed enhancement. Stress SPECT included stress and rest perfusion (a dual isotope protocol) and assessment of wall motion and ejection fraction. Both studies were interpreted in a blinded fashion. If either of the two stress tests were positive patients were referred for coronary angiography. Patients were followed for myocardial infarction (MI), revascularization, or cardiac death.

Results: There were two patients excluded from the study due to technical issues in retrieving the SPECT images from archive.

Baseline Characteristics			
Characteristics	Entire Group (n = 63)	CAD (n = 13)	No CAD (n = 50)
Age (years)	58.1	58.5	58
Males	41 (65%)	11 (85%)	30 (60%)
Diabetes	12 (19%)	5 (38%)	7 (14%)
Hypertension	38 (60%)	10 (77%)	28 (56%)
Hypercholestrolemia	32 (51%)	8 (61%)	24 (48%)
Statins	28 (44%)	8 (61%)	20 (40%)
Beta Blocker	18 (29%)	6 (46%)	12 (24%)
Aspirin	30 (48%)	9 (69%)	21 (42%)
C-reactive Protein	0.4	0.58	0.36

Of the remaining 63 patients, 37 patients were referred for cardiac angiography. There were 13 patients who had significant CAD (≥70%). The mean follow up was 30 months. Two patients had a myocardial infarction/cardiac death and one patient had noncardiac death (metastatic prostate cancer) on follow-up. The sensitivity, specificity, positive predictive value (PPV) and negative predictive value (NPV) of CMR are 71%, 83%, 56%, and 91%, respectively. The sensitivity, specificity, PPV, and NPV of stress SPECT are 64%, 87%, 60%, and 89%, respectively.

Conclusion: In patients being evaluated for the presence of CAD, stress CMR has similar diagnostic accuracy as stress SPECT.

379. SIMULATION OF BANDING ARTIFACTS RESULTING FROM REALISTIC CARDIAC MOTION DURING SINGLE SHOT MYOCARDIAL PERFUSION IMAGING

Michael Salerno, MD, PhD,[1] Wolfgang G. Rehwald, PhD,[1,2] Robert M. Judd, PhD,[1] Raymond J. Kim, MD.[1] [1]***Duke University, Durham, North Carolina, USA,*** [2]***Siemens Medical Solutions, Durham, North Carolina, USA.***

Introduction: Banding artifacts often corrupt first pass myocardial perfusion images. An edge moving at constant velocity can create banding artifacts (1). Contraction and relaxation of the heart during systole and early diastole produce time varying displacements of the myocardial border which vary significantly from constant velocity motion. The appearance of banding artifacts is affected by the resolution, sequence timing parameters, and the imaging time within the cardiac cycle. The effect of such nonlinear motion on artifact appearance during systole and early diastole using clinical pulse sequence parameters has not been explored.

Purpose: To simulate the effects of motion during single shot perfusion imaging using a realistic model of cardiac motion with clinically relevant pulse sequence parameters, and to verify the results in humans.

Methods: The radii of the epicardial and endocardial borders were measured from a short axis cine of a healthy volunteer, and fit with one cycle of a cosinusoidal wave (Fig. 1). For the simulation, the heart was represented as circles of these radii which varied according to this cosinusoidal model. Data collection was simulated by sampling the k-space representation of these two circles (the sum of two Jinc functions) at each k-space location according to the pulse sequence timing. The following parameters were used: FOV 350 × 262 cm, MAT 192 × 91, Resolution 1.8 × 2.9 mm, TR 2.3-3, BW 420–680 Hz/Pixel, sequential PE order. The contrast between the left ventricle (LV) and myocardium was set to 3:1. Parallel imaging with 24 phase correction lines (corresponding to 59 PE lines collected) was simulated with the same parameters to show the effect of reduced image acquisition time.

The appearance of the motion artifacts in a volunteer was visualized using a nonselective T_2-prepared GRE pulse sequence to achieve a contrast ratio of 3:1 between the LV and myocardium without requiring a contrast agent. The T_2 preparation time was 80 ms, and the remaining pulse sequence parameters were identical to those of the simulation. The trigger time was varied in 50 ms intervals to create images throughout the cardiac cycle. Imaging was performed on a 1.5T Siemens SONATA.

Results: The cosinusoidal model reasonably fit the myocardial radii during systole and early diastole (Fig. 1). Fig. 2 shows the volunteer images (a-d), and simulated images without (e-h) and with (i-l) parallel imaging at acquisitions centered at 150, 200, 250, and 300 ms from end diastole. During systole (150–250 ms) the myocardial border is less distinct, and the "banding" artifact appears mid-myocardial. In the images near peak systole (300 ms) where the heart wall is moving more slowly but changing direction, the myocardial border is sharper, but a "band" artifact appears at the endocardial border which is more pronounced. At this resolution, these "bands" are only

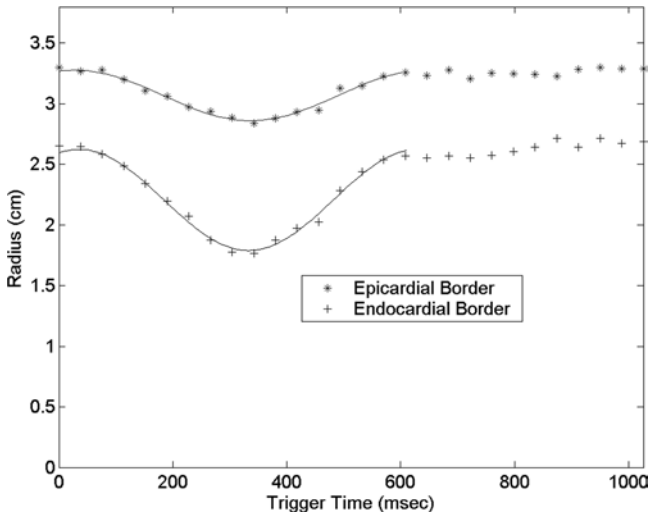

FIG. 1. Fit of Cosine Model to Myocardial Radius

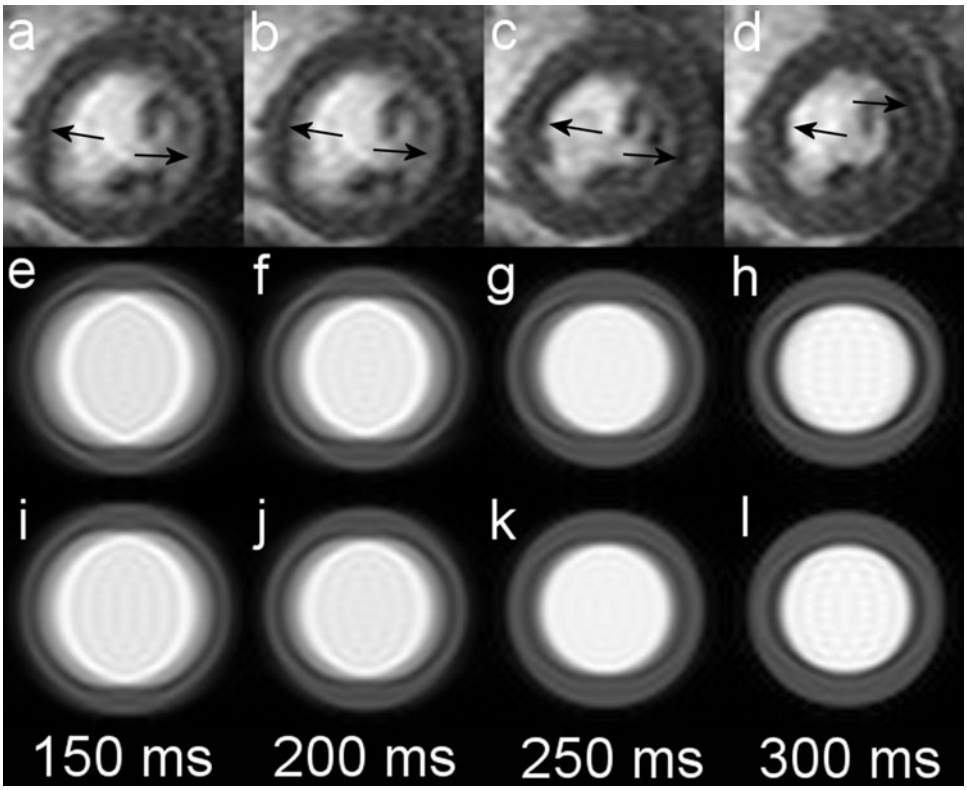

FIG. 2. Conventional Volunteer images (a–d) and conventional (e–h) and parallel (i–l) simulated images. PE direction is L–R.

1–2 pixels wide. The artifact seen near peak systole is conceptually similar to the case of centric reordering of an edge moving at constant velocity, due to the effective change in the direction of the displacements at the center of k-space. This has been shown to cause a darker "band" artifact (1). When the image is acquired over a shorter time interval, the heart exhibits a smaller range of positions during data collection and a less severe motion artifact results. This is evident when comparing the simulated images with and without parallel imaging (acquisition times 135 ms and 210 ms respectively).

Conclusions: Banding artifacts occur not just during times of peak motion but throughout systole and early diastole for current myocardial perfusion pulse sequences. Decreasing total sampling time and reordering PE lines may reduce the artifacts.

REFERENCE

1. Storey et al. MRM 2002;48:1028.

380. CARDIAC MRI REVEALS ENHANCED DOBUTAMINE RESPONSIVENESS IN ADJACENT ZONES EARLY AFTER MYOCARDIAL INFARCTION IN iNOS KNOCKOUT MICE

Frederick H. Epstein, PhD, R. Jack Roy, Yaqin Xu, MD, PhD, Christopher M. Kramer, MD, Brent A. French, PhD. ***University of Virginia, Charlottesville, Virginia, USA.***

Introduction: Previous studies have shown reduced post-infarct left ventricular (LV) remodeling 28 days after myocardial infarction (MI) in inducible nitric oxide synthase knockout ($iNOS^{-/-}$) mice. However, the mechanisms that underlie the reduction in functional and structural remodeling remain unknown.

Purpose: We sought to test the hypothesis that, early after MI, $iNOS^{-/-}$ mice would display alterations in dobutamine (dob) response as compared to wild type (WT) mice. *Methods:* Six $iNOS^{-/-}$ and 6 wild-type (WT) C57Bl/6 mice were studied by cardiac MRI (CMR) at baseline and at 1 and 7 days after MI. MI was induced by a 1-hour occlusion of the left anterior descending coronary artery followed by reperfusion. All imaging was performed on a small-bore 4.7 T scanner equipped with a high-performance gradient system and using a 25 mm diameter cylindrical Litz RF coil. In addition to cine CMR of the entire LV, at baseline and on day 7 post-MI, myocardial tagging was used to quantify regional circumferential shortening (E_{cc}) in 2 mid-ventricular slices at rest and during dob infusion (20 μg/kg/min). On day 1, gadolinium-enhanced CMR was used to determine infarct size, location, and borders, thereby defining each of 6 sectors per slice as infarcted, adjacent, or remote. Contractile reserve (ΔE_{cc}) was defined as peak E_{cc} at dob minus peak E_{cc} at rest.

Results: Before MI, resting E_{cc} was similar between groups (WT: 0.16 ± 0.02 vs. $iNOS^{-/-}$: 0.17 ± 0.02, p = NS). Infarct size (% LV mass) at day 1 was also similar for WT and $iNOS^{-/-}$ mice (WT: $34 \pm 9\%$ vs. $iNOS^{-/-}$: $36 \pm 5\%$, p = NS). On day

7 in remote zones, resting E_{cc} (WT: 0.14 ± 0.03 vs. iNOS$^{-/-}$: 0.14 ± 0.03, p = NS) and dob response (WT: 0.02 ± 0.03 vs. iNOS$^{-/-}$: 0.01 ± 0.02, p = NS) were similar for both groups. For adjacent zones on day 7, resting E_{cc} was similar between groups (Fig. 1) and was reduced vs. remote zones ($p < 0.05$). No dob response was measured in WT adjacent zones whereas a normal dob response was measured in iNOS$^{-/-}$ adjacent zones (Fig. 1).

Conclusions: CMR demonstrates a normal dob response in the adjacent noninfarcted zones of iNOS$^{-/-}$ mice 7 days after MI compared to a completely absent response in WT mice. This difference in beta-adrenergic responsiveness may be one factor contributing to the attenuation of maladaptive structural and functional LV remodeling previously observed post-MI in iNOS $^{-/-}$ mice.

381. QUANTIFYING MITRAL VALVE REGURGITATION WITH CARDIAC MRI AND ECHOCARDIOGRAPHY

Jason T. Su, DO, LuAnn L. Minich, MD, Michael D. Puchalski, MD, Alice Olson, Lloyd Y. Tani, MD. ***University of Utah, Salt Lake City, Utah, USA.***

Background: Mitral regurgitation (MR) is commonly seen in both acquired and congenital heart disease. MR results in volume overload of the left heart and if left untreated, may lead to myocardial dysfunction, heart failure, and rhythm abnormalities. Echocardiography is the most widely used imaging modality for the evaluation of MR because it is both noninvasive and readily available for serial examinations. Despite its ubiquitous use, quantifying MR by echocardiography continues to be challenging. Therefore, most pediatric echocardiography laboratories use a subjective assessment based on the size of the regurgitant MR jet. Since cardiovascular magnetic resonance (CMR) has been well validated as the gold standard for quantification of ventricular volumes and for quantifying pulmonary valve regurgitation with phase contrast imaging, the quantification of mitral valve regurgitation using a combination of the CMR methods should yield the most accurate results.

Purpose: Using CMR as the gold standard, we sought to: 1) determine whether subjective echocardiographic assessment of MR severity is accurate, and 2) identify the best echocardiographic method of quantifying MR.

Methods: This is an IRB approved prospective cohort study of patients with congenital and/or acquired heart disease who had isolated MR previously graded at least mild in severity. All patients were at least 8 years of age to avoid the need for sedation for the CMR. A complete echocardiogram and CMR were performed on the same day. All CMRs were performed by a pediatric cardiologist who was blinded to the echo data. MR was quantified by obtaining the left ventricular volumes using the standard technique and subtracting the forward flow, determined by phase contrast imaging across the ascending aorta. Images were post-processed on an independent workstation for analysis by MASS and FLOW (Medis, Inc.) Subjective quantification of MR was obtained from the cardiologist who provided the report for clinical use. A designated sonographer performed all of the studies and made the all measurements. Information obtained included: functional analysis, left atrial and MR area, vena contracta, regurgitant volume by proximal isovelocity surface area (PISA) and Doppler methods, and provided measurements for effective regurgitant orifice area (ERO).

Results: Ten patients (6 congenital) were enrolled with the mean age of 17.5 years (range 9.7–26.5). The average regurgitant volume/ejection fraction by CMR was 30.2%. There was excellent correlation with CMR regurgitant volume and regurgitant volume by PISA ($p = 0.0008$, $r = 0.965$) and the Doppler method ($p = 0.005$, $p = 0.803$). There was also a strong correlation with indirect indices such as: ERO ($p = 0.0003$, $r = 0.971$), left atrial area ($p < 0.0001$, $r = 0.965$), MR jet area ($p = 0.022$, $r = 0.71$) and vena contracta ($p = 0.003$, $r = 0.829$). There was no correlation between CMR regurgitant volume and subjective assessment of MR severity, LV EDV or LV function indicies.

Conclusions: Despite its widespread use, subjective assessment of MR severity by echocardiography does not correlate with regurgitant volume and/or regurgitant fraction determined by CMR, and may be misleading when used to guide clinical management. Using CMR as a reference, there is strong correlation with echocardiographically determined MR volume (PISA and Doppler methods) and vena contracta. Further study is warranted to determine the predictive value and clinical utility of echocardigraphic parameters in assessing MR severity.

382. EFFECTS OF AGE AND GENDER ON RIGHT VENTRICULAR STRUCTURE AND FUNCTION

Suzanne White, MD, Saadi Siddiqi, MD, Chizor Iwuchukwu, MD, William Schapiro, RT, Nora Ngai, PhD, Michael Passick, RDCS, Jing Han, PhD, Nathaniel Reichek, MD. ***Research Department, St. Francis Hospital, Stony Brook University, SUNY, Roslyn, New York, USA.***

Background: The complex shape of the right ventricle has made accurate and reproducible quantitation difficult using common clinical imaging techniques. Cardiac magnetic resonance (CMR) has emerged as a valuable 3D imaging modality for right ventricular assessment. We sought to determine the effects of age and gender on right ventricular structure and function using CMR.

Methods: One hundred fifty-six (82 females, 74 males) healthy normotensive, nonobese (BMI < 28), nondiabetic volunteers aged 20-90 (mean 51 ± 15) underwent volumetric CMR (Siemens Sonata). Volunteers were excluded for any condition or medication likely to affect cardiovascular function or body size and composition. A screening echocardiogram was performed on each participant to exclude subjects with cardiovascular

	Gender			Age		
Variable	Female (n = 82)	Male (n = 74)	p	Pooled (n = 156)	Female (n = 82)	Male (n = 74)
RVEF (%)	57 ± 8*	51 ± 7	<.0001	0.08 (0.32)**	0.07 (0.53)	0.08 (0.50)
RVEDVi (mL/m2)	65 ± 14	74 ± 14	<.0001	−0.31 (<0.0001)	−0.42 (<0.0001)	−0.22 (0.06)
RVESVi (mL/m2)	28 ± 9	36 ± 9	<.0001	−0.25 (0.002)	−0.29 (0.008)	−0.21 (0.07)
RVMi (g/m2)	21 ± 7	24 ± 6	0.007	−0.17 (0.03)	−0.15 (0.17)	−0.19 (0.10)
RVSP (mmHg)	24 ± 7	26 ± 7	0.26	0.25 (0.0025)	0.32 (0.0034)	0.18 (0.15)

*Mean + SD

**Correlation coefficient (p value).

abnormalities. CMR data was obtained by imaging contiguous 8 mm slices through the entire cardiac volume using a TrueFISP breath-hold segmented cine sequence in the left ventricular short axis plane. Images were segmented at the right and left ventricular endocardium and epicardium by a highly experienced image analyst and ventricular volumes at end-diastole and end-systole determined. Right ventricular free wall mass as well as left ventricular mass were determined.

Results: Women have higher ejection fractions and lower end diastolic volume indices, end systolic volume indices, and mass indices than men. As age increases, end diastolic volume indices and end systolic volume indices decrease, but there is no age related difference in ejection fraction and mass indices. The relationship between age and end diastolic and end systolic volume indices was statistically significant in women but not in men, despite a similar downward trend. Right ventricular systolic pressure also increased slightly but significantly with age in women. There was no relationship between right ventricular systolic pressure and right ventricular mass index in this normal population.

Conclusions: Increasing age results in concentric right ventricular remodeling with reductions in right ventricular volume, constant mass and ejection fraction. These changes are more evident in women than in men and associated with an age-related increase in pulmonary artery pressure. Similar age and gender effects on the left ventricle have been previously described. The underlying mechanism remains unknown but may be related in part to physical inactivity with resultant deconditioning.

383. ULTRAFAST VIABILITY IMAGING IN LESS THAN 10 MINUTES

Lincoln Diniz, MD,[1] Karin Dill, MD,[1] Jessica Hung, BS,[1] John Sheehan, MD,[1] Ed Wu, MD,[1] Al Zhang, PhD,[2] James Carr, MD.[1] [1]***Northwestern University, Chicago, Illinois, USA,*** [2]***Siemens Medical Systems, Chicago, Ilinois, USA.***

Introduction: Delayed enhanced cardiovascular magnetic resonance (DE-MRI) is increasingly being recognized as the gold standard for myocardial viability assessment (1, 2). Conventional viability protocol typically involves scanning the heart from base to apex, first with segmented cine steady-state free precession (SSFP) imaging and then with segmented inversion recovery TurboFLASH (IR-TFL) post contrast injection. The entire protocol can take 30–40 minutes per patient thus limiting the patient throughput in a busy cardiac imaging practice. Acceleration strategies, such as iPAT, can now be implemented with conventional cine SSFP resulting in significant improvements in acquisition speed. Similarly, single-shot techniques such as inversion recovery TrueFISP (IR TrueFISP) (3), can be used instead of segmented IR-TFL to further reduce the scan times. By combining real-time cine SSFP with delayed enhanced IR-TrueFISP, it may be possible to drastically reduce the overall length of time to carry out a viability study.

Purpose: To evaluate an ultrafast viability protocol using real time cine TrueFISP and single shot IR TrueFISP and compare it to the conventional segmented viability techniques.

Methods: Twenty-two patients with suspected myocardial scar underwent assessment of left ventricular viability on a 1.5T Siemens Avanto. Initial functional imaging of the heart was carried in the short axis plane from base to apex using segmented cine TrueFISP (TR/TE 3.0/1.5; flip angle 70^0; matrix 144 × 192; pixels 2.8 × 2.1 mm^2; 55 ms per frame). GRAPPA, with acceleration factor of 2, was used to reduce acquisition time to 5 seconds per slice. Real-time short axis cine TrueFISP images (TR 2.3/TE 1.0; flip angle 55^0; FOV 250 × 340 mm; matrix 86 × 192; pixels 3.0 × 1.6 mm^2; 65 ms per frame) were then obtained from base to apex in one 20 second breath-hold. TSENSE, with acceleration factor of 3, was used to speed up the acquisition. Gadolinium-DTPA (0.2 mmol/kg) was injected via an 18 G intravenous cannula. Approximately 10 minutes post contrast injection, single-shot IR TrueFISP (TR/TE: 3.2/1.6; flip angle 55^0; TI 250–350 ms; 6 mm thick slice) images were obtained in a short axis orientation from base to apex. The entire stack of images was acquired in a 20 second breath-hold. The entire

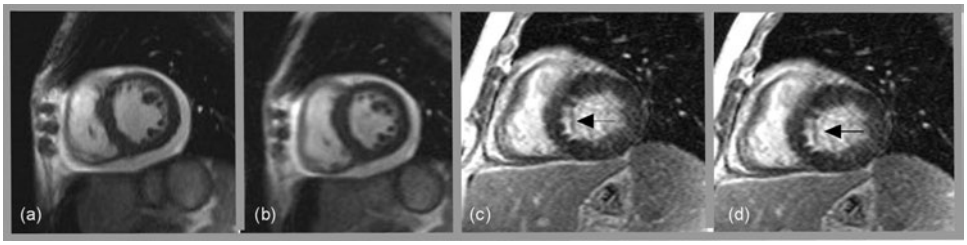

FIG. 1. (a) Short axis segmented cine TrueFISP showing pericardial effusion. (b) Short axis real-time cine TrueFISP with TSENSE showing pericardial effusion (c) Short axis IR TurboFLASH showing subendocardial infarct in septal wall (arrow) (d) Short axis IR True FISP also showing subendocardial infarct in spetalwall (arrow). Conspicuity of abnormality and image quality are similar to IR TurboFLASH.

left ventricle was then imaged with segmented IR TurboFLASH (TR/TE: 8.0/4.0; flip angle 25^0; TI 250–350 ms). Each slice was acquired in a 10 second breath hold.

For the purposes of analysis, a 16 segment model was used according to the American Heart Association classification. Two experienced observers evaluated each short axis image separately. For the cine images, each segment was scored for wall motion (1 = normal; 2 = mild/moderate hypokinesia; 3 = akinesia; 4 = dyskinesia) and wall thickness (1= normal; 2 = thinning). For the delayed enhanced imaged, each segment was assessed for the presence of hyperenhancement and the transmural extent of myocardial enhancement was noted. The acquisition time was noted for each sequence.

Results: The average total acquisition time for real-time cine TrueFISP (Fig. 1b) was 19 sand segmented cine TrueFISP (Fig. 1a) was 49 s. The average total acquisition time for single-shot IR TrueFISP (Fig. 1d) was 21 sand segmented IR-TFL (Fig. 1c) was 88 s. There was high correlation between real time cine TrueFISP and segmented cine TrueFISP for wall motion (r = 0.82) and wall thinning (r = 0.79). Single-shot IR TrueFISP identified 95% of the hyperenhancing regions detected with segmented IR TurboFLASH.

Conclusion: Ultrafast viability imaging using real-time cine TrueFISP and delayed-enhanced IR TrueFISP is considerably faster than a conventional viability protocol and can produce comparable results. This strategy may have significant impact on patient workflow in a busy cardiac MRI practice.

REFERENCES

1. Kim RJ, et al. NEJM 2000;343:1445–1453.
2. Simonetti OP, et al. Radiology 2001;218:215–223,
3. Carr JC, et al. ISMRM 2003.

384. CORONARY MICROVASCULAR DYSFUNCTION: CMR PERFUSION ABNORMALITIES OF ACTIVE VASOMOTION IN WOMEN WITH CHEST PAIN AND NORMAL CORONARY ANGIOGRAMS

Chizor Iwuchukwu, MD,[1] Saadi Siddiqi, MD,[1] Aracely Norales, RN,[2] Nora Ngai, PhD,[2] William Schapiro, RT,[2] John Abela, RT,[2] Marguerite Roth, RN,[2] Jing Han, PhD,[1] Yi Wang, PhD,[1] Nathaniel Reichek, MD, FACC, FAHA.[1] [1]*St. Francis Hospital, Stony Brook University, SUNY, Roslyn, New York, USA,* [2]*St. Francis Hospital, Roslyn, New York, USA.*

Background: Microvascular dysfunction can cause chest pain in women without epicardial coronary artery stenoses, but the optimal strategy for detection of microvascular dysfunction is unclear. We examined the relative value of stressors which detect impaired maximal coronary conductance to that of stressors causing active vasomotion in the detection of microvascular dysfunction.

Methods: Myocardial perfusion reserve was assessed noninvasively using cardiovascular magnetic resonance first pass perfusion imaging (CMR) in 13 women (m = 53.9 yrs, range 43–66 yrs, 9 post-menopausal) with chest pain, abnormal stress tests and no stenoses on invasive (12) or CT (1)coronary angiograms. CMR was performed at rest and during adenosine (A, n = 11) maximal coronary vasodilation, and hand grip (G, n = 13) and cold pressor testing (CPT, n = 4) which evoke β adrenergic vasodilation in normals, dilating epicardial coronary arteries and increasing myocardial perfusion. Rotational long axis CMR imaging was performed with a saturation recovery partial Fourier TrueFISP sequence and 0.05 mmol/kg Gd chelate, with 20 minute washout periods. CMR data was evaluated for myocardial contrast uptake upslope, normalized by the aortic input function, using MASS, (Medis) with manual tracing (Fig. 1a,b). A global myocardial stress/rest perfusion slope reserve index was calculated and results compared to normal controls.

Group	Stress	N	Mean Flow Reserve	Std Dev
Chest Pain	Grip	13	0.65	0.22
	Adenosine	11	1.49	0.36
	Cold Pressor	4	**1.00***	0.15
Control	Grip	2	0.55	0.26
	Adenosine	7	1.66	0.76
	Cold Pressor	8	**1.61***	0.36

*$p < 0.01$

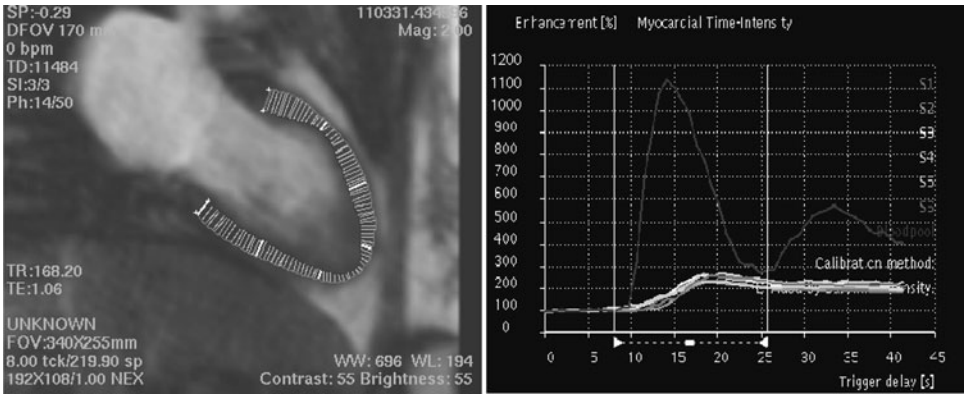

FIG. 1. (a) Manually traced cardiac borders on first pass perfusion. (b) Upslope graph of first pass myocardia1 contrast uptake.

Results: (Table) Mean adenosine perfusion slope ratio did not differ between patients and controls and fell at the lower end of the reported range. Mean hand grip perfusion slope ratio was reduced similarly in both groups. However, there was a significant difference in cold pressor perfusion slope ratio between the two groups, with abolition of reserve in women with chest pain.

Conclusion: In women with chest pain and no coronary stenoses, the cold pressor test demonstrates abnormalities of sympathetically mediated β adrenergic vasodilation, which may be more sensitive than adenosine induced abnormalities of maximal vasodilation. In contrast, hand grip does not appear to discriminate between patients with microvascular dysfunction and normals in this setting.

385. INFARCT-RELATED ECG CHANGES RESOLVE IN CORRESPONDENCE WITH INFARCT RESORPTION OVER TIME AFTER FIRST-TIME INFARCTION ASSESSED BY DELAYED CONTRAST-ENHANCED MRI

Henrik Engblom, MD,[1] Erik Hedström, PhD,[1] Einar Heiberg, PhD,[1] Galen S. Wagner, MD,[2] Olle Pahlm, MD, PhD,[1] Håkan Arheden, MD, PhD.[1] [1]***Lund University Hospital, Lund, Sweden,*** [2]***Duke University Medical Center, Durham, North Carolina, USA.***

Introduction: Infarct-related changes in the electrocardiogram (ECG) seen after acute myocardial infarction (MI) have previously been shown to resolve over time. The pathologic correlate of these resolving ECG changes is not completely understood.

Purpose: Therefore, the aim of this study was to explore the relationship between infarct resorption as assessed by delayed contrast-enhanced cardiovascular magnetic resonance (DE-MRI) and QRS scoring of the ECG after reperfused first acute MI.

Methods: Eighteen patients with reperfused first-time myocardial infarction were prospectively enrolled. Delayed contrast-enhanced cardiovascular magnetic resonance imaging (DE-MRI) imaging for infarct visualization was performed 1 day, 1 week, 6 weeks, 6 months and 1 year after admission. Infarct size by DE-MRI, expressed as a percentage of the left ventricle, was compared to relative infarct size estimated by QRS scoring of the ECG if there was an ECG recorded at the day of the MR examination.

Results: The timing and magnitude of decrease in relative infarct size was similar for the two methods (Fig. 1). Both showed the most pronounced decrease during the first week and 1-year decreases of 35% and 40% for QRS score and DE-MRI, respectively. There was, however, a significant overestimation of infarct size by QRS scoring compared to DE-MRI, except at day 42. A significant correlation ($p < 0.05$) between the methods was found at all time-points with R-values ranging from 0.63–0.80.

Conclusions: The timing and the magnitude of decrease in relative infarct size is similar by DE-MRI and QRS scoring after reperfused first-time infarction. There is, however, a systematic overestimation of infarct size by QRS scoring as compared with DE-MRI.

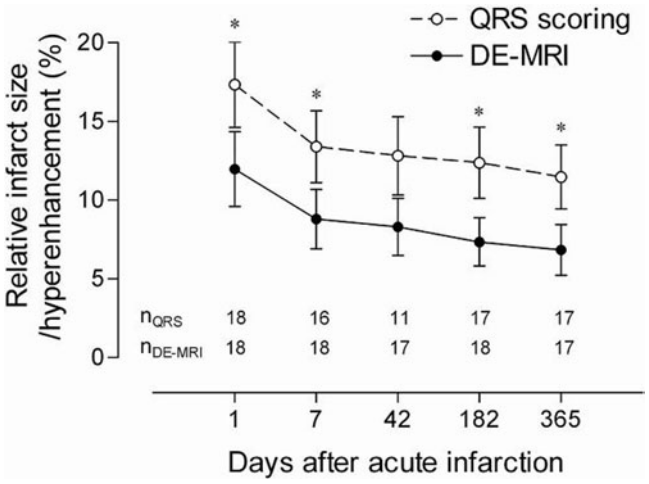

FIG. 1.

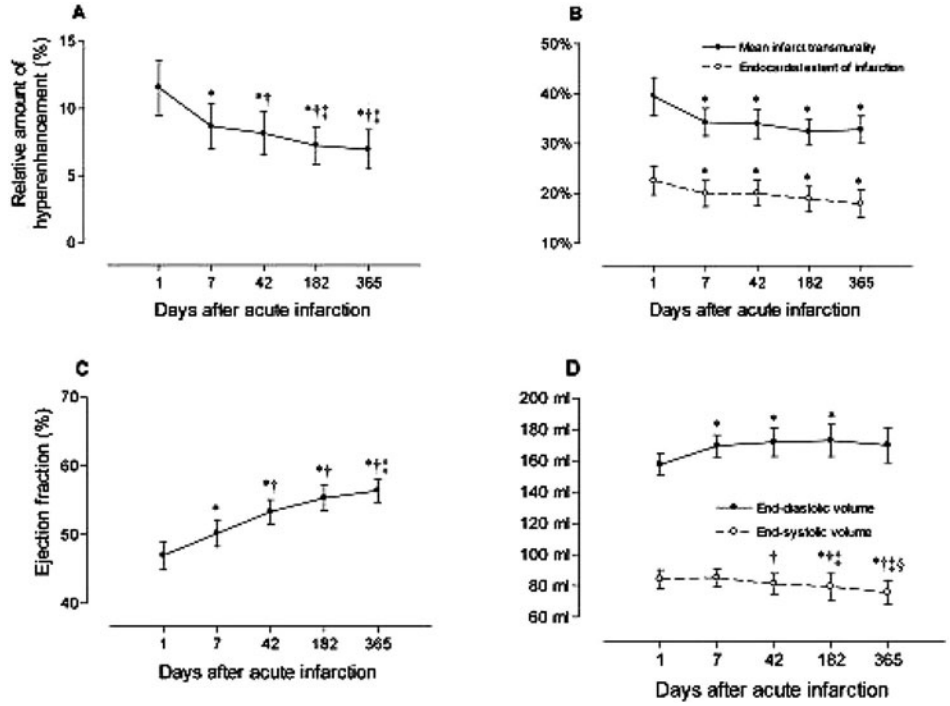

FIG. 1.

386. EARLY AND LATE TIME COURSE OF INFARCT RESORPTION AND RECOVERY OF GLOBAL LEFT VENTRICULAR FUNCTION IN PATIENTS WITH REPERFUSED FIRST MYOCARDIAL INFARCTION

Henrik Engblom, MD,[1] Erik Hedström, PhD,[1] Einar Heiberg, PhD,[1] Galen S. Wagner, MD,[2] Olle Pahlm, MD, PhD,[1] Håkan Arheden, MD, PhD.[1] [1]*Lund University Hospital, Lund, Sweden,* [2]*Duke University Medical Center, Durham, North Carolina, USA.*

Introduction: The time course of myocardial infarct (MI) resorption after reperfused acute infarction and its relationship to recovery of left ventricular (LV) function has been studied in animal models. This has also partly been described in humans, using delayed contrast-enhanced magnetic resonance imaging (DE-MRI). These studies have, however, offered limited coverage of the acute changes occurring during the first week after MI.

Purpose: The aim of this study was therefore to explore the changes in infarcted myocardium and the left ventricular function in patients with reperfused first-time infarction at multiple points in time during the first year after admission, starting day 1 after the acute event.

Methods: Twenty-two patients with reperfused first-time myocardial infarction were prospectively enrolled. Cardiac magnetic resonance imaging (MRI), including cine imaging and delayed contrast-enhanced (DE) imaging for infarct visualization, was performed 1 day, 1 week, 6 weeks, 6 months and 1 year after admission. Left ventricular ejection fraction, end-diastolic volume and end-systolic volume were assessed from the cine images. Infarct size, transmurality and endocardial extent of infarction, expressed as a percentage of the total endocardial surface, were determined from the DE-MRI images.

Results: Infarct size decreased, especially during the first week after infarction (Fig. 1A). Both infarct transmurality and endocardial extent of infarction contributed to the decrease in infarct size (Fig. 1B). The LV ejection fraction increased gradually over time (Fig. 1C), reflected by an early increase in end-diastolic volume and a gradual decrease in end-systolic volume (Fig. 1D). Vertical bars indicate standard error of the mean. $^{*}P < 0.05$ versus Day 1; $^{\dagger}p < 0.05$ versus Day 7; $p < 0.05$ versus Day 42; $p < 0.05$ versus Day 182.

Conclusions: Infarct size decreases mostly during the first week after infarction in patients with small to moderate sized reperfused first-time infarcts. The global left ventricular, however, increases gradually during the first year after infarction.

387. HIGH-RESOLUTION MRI FOR IDENTIFICATION OF VARIOUS COMPONENTS OF HUMAN CAROTID ARTERY PLAQUE USING DIFFERENT WEIGHTINGS AND FAT SUPPRESSION

Bernard C. M. Te Boekhorst, MD,[1] Maarten-Jan J. M. Cramer, MD, PhD,[2] Matthijs van Oosterhout, MD, PhD,[2] Gerard Pasterkamp, MD, PhD,[2] Pieter A. F. M. Doevendans, MD, PhD,[2] Cees J. A. van Echteld, PhD.[2] *ICIN, Utrecht, The Netherlands,* [2]*UMCU, Utrecht, The Netherlands.*

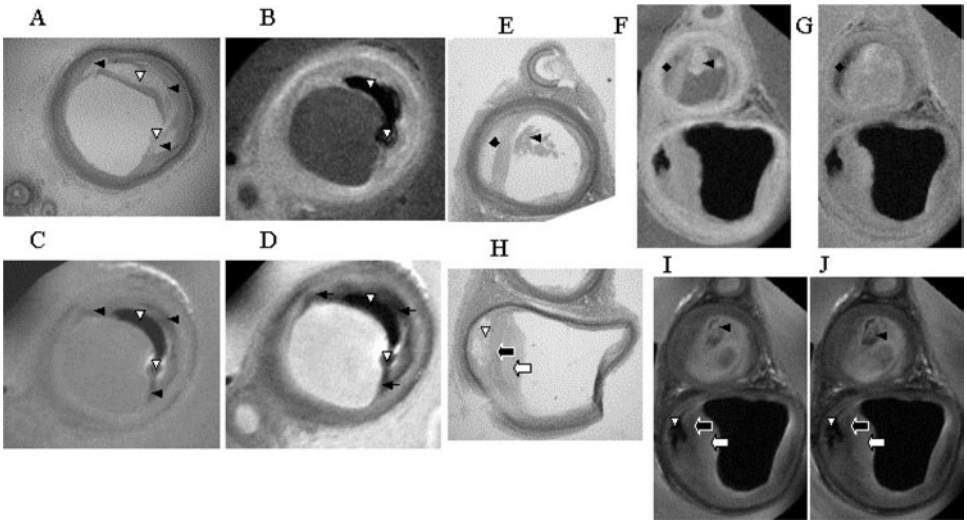

FIG. 1. Plaque in human carotid artery.

Purpose : Carotid atherosclerotic plaque composition rather than lumenal vessel obstruction determines the risk of plaque rupture and subsequent stroke. Multicontrast-weighted MRI for classification of carotid lesions is feasible, however not all plaque constituents are visualized at microscopic detail thus far.

Methods: Formaldehyde-fixed autopsy human carotid artery specimens were imaged. MRI measurements were performed on a 9.4 T Bruker Avance system. T1-weighted images (FLASH) with (Fig. 1G)/without (Fig. 1B, F) fat suppression and T2- and PD-weighted images (FSE) were acquired. Slice thickness was 0.5 mm and in-plane resolution 90 × 90 ìm (T2w) and 70 × 70 ìm (T1w). Corresponding plaque levels were embedded in paraffin and stained with EvG and HE.

Results: Calcification was black on all MRI weightings (Fig. 1A-D, H-J, white triangles). Intra-plaque hemorrhage and thrombus were dark on T2- and PD-weighted images, whereas T1-weighted images showed heterogeneous and high signal (Fig. 1B, F, black triangles). On fully T2-weighted images (Fig. 1I) the fibroblast layer/fibrous cap (EvG, Fig. 1H, double white arrow) had higher intensity than the smooth muscle cell layer (EvG, Fig. 1H, double black arrow). Lipid core gained conspicuity on T1-weighted images after fat suppression (Fig. 1G, black diamond).

Conclusions: Multicontrast-weighted MRI of human carotid plaque has come close to histology and allows for discrimination between smooth muscle cell layers and fibrous cap as well as between lipid core and intercellular fat deposits.

Also, old intra-plaque bleeding and thrombus can be identified clearly.

388. ASSESSMENT OF RECENT MYOCARDIAL INFARCTION USING PRECONTRAST T1 WEIGHTED (T1W) CMR IMAGING

James W. Goldfarb, PhD, Sheeba Arnold, Marguerite Roth, Jeanette McLaughlin, Jing Han. ***St Francis Hospital, Roslyn, New York, USA.***

Introduction: Recent myocardial infarction (MI) is known to have local edema that normally resolves over time. Myocardial edema of this type can be increased or created through mechanical interventions. Myocardial edema or more generally body fluid (for example, pericardial effusion or cerebrospinal fluid) has both long T1 and T2 MR relaxation times. T2-weighted CMR of myocardial edema has been used to detect acute myocardial infarction (MI) and has been shown to define the myocardial "area at risk," a zone of reversibly and irreversibly injured myocardium. T2-weighted MR image quality often suffers from long breathhold times, image artifacts and poor contrast between myocardium and the LV bloodpool.

Early attempts to detect MI with precontrast T1-weighted CMR yielded highly variable results. Postcontrast imaging of the myocardium with T1-weighted inversion recovery (IR) techniques has been refined for delayed hyperenhancement (DHE) imaging. Inversion recovery CMR pulse sequences are heavily T1 sensitive and capable of providing excellent contrast between tissues with only small differences in T1 relaxation times.

Purpose: In this study, use of a T1-weighted technique for the detection of myocardial edema resulting from recent MI or intervention was investigated. The precontrast T1 relaxation times of injured and adjacent myocardium were measured and compared for a range of infarct ages.

Methods: Sixteen subjects participated in this study (15 men; mean age, 57.8 years ± 11.5; age range, 43-85 years). The inclusion criteria were a prior MI documented by serum cardiac markers and/or positive nuclear stress testing. Eight subjects had experienced an MI within two months of CMR (MI age, 0.05 years ±0.03; range, 0.03-0.13) and eight subjects had older MIs (MI age, 1.7 years ± 1.2 range, 0.4–3.5). Imaging was performed

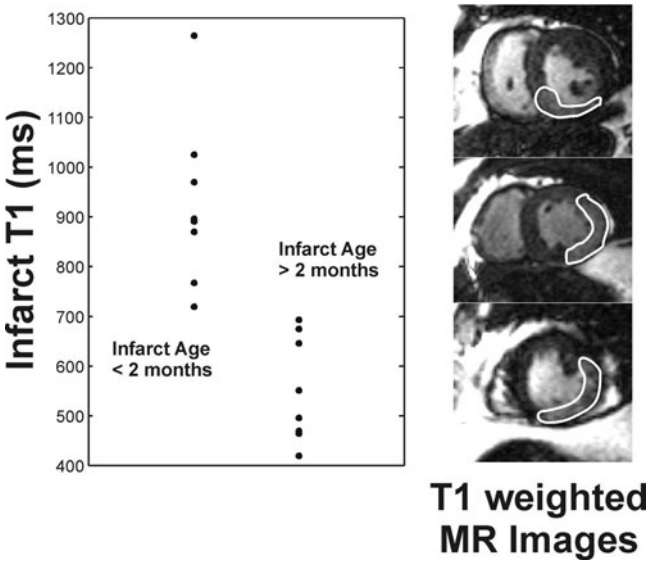

FIG. 1.

using a 1.5T clinical scanner (Siemens Magnetom Sonata, Erlangen, Germany). Subjects underwent precontrast T1 weighted imaging using an IR-TrueFISP CINE technique. This was followed by contrast injection (0.2 mmol/kg gadodiamide) and DHE infarct imaging. Regions of MI were identified on DHE images and the T1 relaxation times of the regions were measured using the precontrast T1-weighted images. Infarct and adjacent myocardial T1 relaxation times were evaluated for associations with age.

Results: For patients having MIs within the last two months, areas of myocardial edema were well depicted using T1 weighted images (Fig. 1). The precontrast T1 relaxation times were significantly ($p = 0.0005$) different between the infarcted region and the adjacent myocardium for recent MIs, but were only slightly significantly ($p = 0.0498$) different for older MIs. The recent infarct T1 relaxation times (< 2 months) were significantly ($p = 0.0001$) longer than those of the older MIs (925 ± 169 ms vs 551 ± 107 ms)(Fig.). For both recent and chronic MI groups, there were no significant correlations (p values ≥ 0.05) between infarct and adjacent T1 relaxation times and infarct age.

Conclusions: As a result of local edema, the T1 relaxation time of infarcted myocardium is increased and may remain high up to two months after MI. This allows imaging of myocardial edema using T1-weighted MR techniques that can provide image quality that may be difficult to achieve with T2-weighted techniques. The detection and characterization of myocardial infarction on a segmental basis can be performed using precontrast T1-weighted CMR imaging.

389. ANATOMY IMAGE RECONSTRUCTION FROM STRAIN-ENCODED (SENC) TUNING IMAGES

Tamer A. Yousef, Nael F. Osman, PhD. ***Johns Hopkins University, Baltimore, Maryland, USA.***

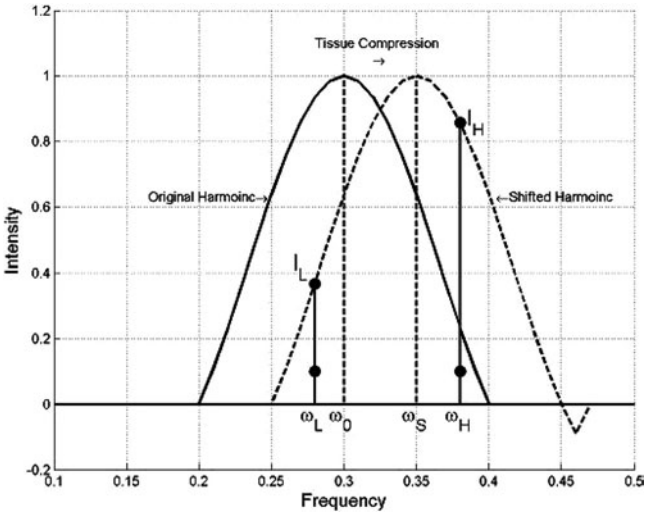

FIG. 1. Detection of harmonic peak shift (during tissue compression) through low and high turnings.

In strain Encoding (SENC), two images are acquired for the same slice with two different z-encoding gradients in order to calculate the through-plane strain map. Neither of these two images completely represents the anatomy of the heart in this slice. In this abstract, a fast algorithm is presented for constructing the anatomical image from these two images.

Introduction: Strain-Encoding (SENC) is a new technique for calculating the through-plane strain in MR images of the heart (1). The technique applies sinusoidal tagging of frequency ω_o in the normal plane to the selected slice. By changing the gradient in the normal direction during the acquisition, two images are acquired at two different frequencies (tunings), a low-tuning image I_L at tuning frequency ω_L and a high tuning image I_H at ω_H as shown in Fig. 1. The local strain at each voxel can be calculated by detecting the shift happened to the harmonic peak using the strain Eq. given in 1. However, the anatomy image is not directly obtained by this SENC pulse sequence and extra processing is needed in order to reconstruct it.

Theory: Three methods are represented in order to reconstruct the anatomical image:

A. Simple Addition: By noticing that I_L is directly proportional to the local stretching while I_H is directly proportional to the local compression in the tissue (Fig. 1), the anatomy image can be estimated by directly adding the two images.

B. Peak Location: Due to the stretching/compression that occurs in the tissue, the harmonic peak is shifted either to higher or lower frequency (ω_S). So, the harmonic peak location is determined using strain Eq. in 1 then a linear interpolation between I_L and I_H is calculated to obtain the values of the anatomy images at ω_S.

C. Sinc Interpolation: Since both A and B are variations of linear interpolation methods, the slice profile shape is totally neglected. However, this can highly affects the generated anatomy image since the normal anatomy image is acquired exactly at the center point of the slice profile. So, after the peak location

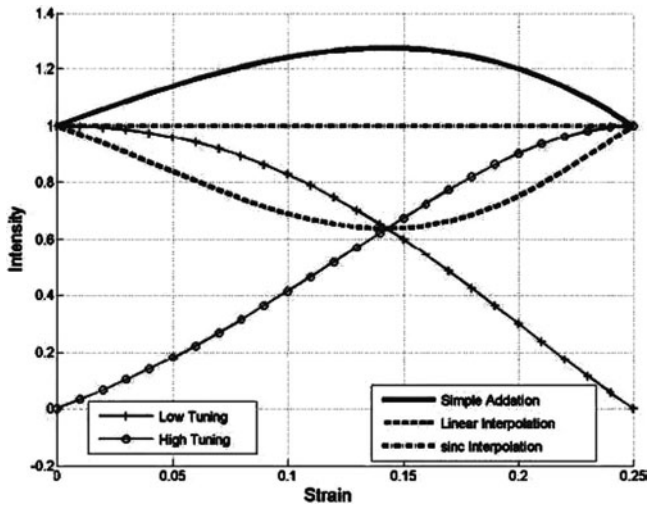

FIG. 2. Intensity of the generated anatomy images for different strain values.

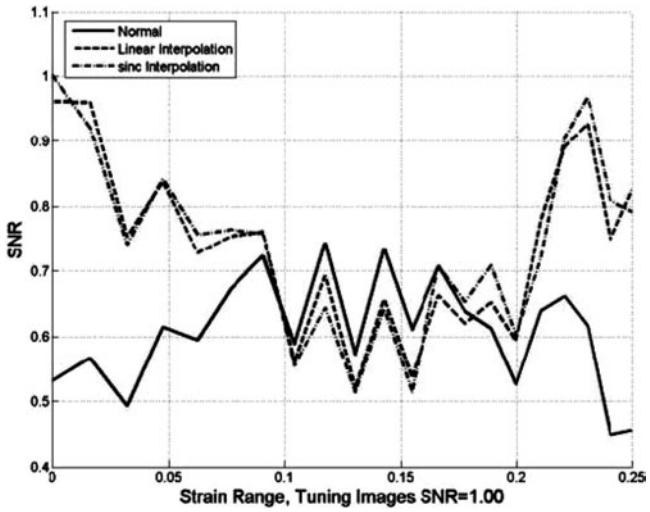

FIG. 3. SNR of a generated anatomy pixel using simulated data for different strain values. Note that SNR for both methods B, C are nearly the same and is higher than method A especially at low and high frequencies.

frequency is calculated, a non linear curve fitting for the slice profile (which is usually sinc profile in SENC technique) is applied between I_L and I_H in order to obtain the peak value of the slice profile at each pixel.

Methods: Numerical simulation data for SENC were generated at different SNR (by adding different noise level to the simulated slice profile then shifting the harmonic peak profile in the frequency domain by multiple steps). The strain values for these shifts were estimated using (1). The anatomy images were generated using the proposed methods then the SNR of the generated anatomy images is calculated for different strain values. Also, a study was conducted on a normal volunteer using Philips 3T clinical scanner. Short- and long-axis cardiac images were acquired using the SENC pulse sequence. For each imaging view (short axis or long axis), two sets of images were acquired with two different demodulation frequencies. Then, the anatomy images were calculated using the proposed algorithms.

Results: Figures 2 and 3 shows the SNR for the numerical simulation results. While both methods B, C have higher SNR compared to method A (especially at the low and high

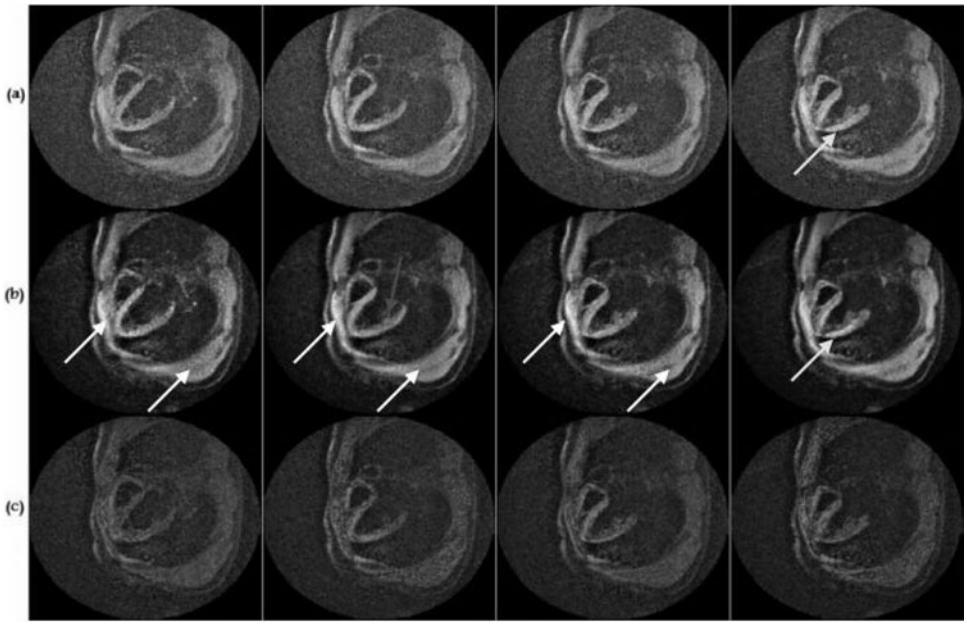

FIG. 4. (a, b) Generated anatomy images at different 4 cardiac phases at 36, 148, 261, 373 ms starting from the R wave (in columns). (a) using method A, (b) using method C. Note the difference in voxel intensity between the two series in the low strain areas (e.g. static tissues) and in the high strain areas (e.g. the myocardial during contraction in the last 2 frames) while the intensity remains nearly in the same level for average strain values (e.g. the myocardial in the first 2 frames). Also, the noise effect on the background is slightly suppressed due to the inherited noise suppression in the nonlinear interpolation used in method C. (c) Strain values computed from SENC and mapped on the generated anatomy image using metod C.

frequencies), method C is shown to maintain constant intensity along the whole strain range.

Conclusion: Anatomy image can be generated from the SENC tuning images. This is helpful in mapping the strain values generated originally from the SENC into its corresponding anatomical positions.

REFERENCE

1. Osman NF, et al. Imaging longitudinal cardiac strain on short-axis images using strain-encoded MRI. Magn Resn Med 2001;46:324–10.

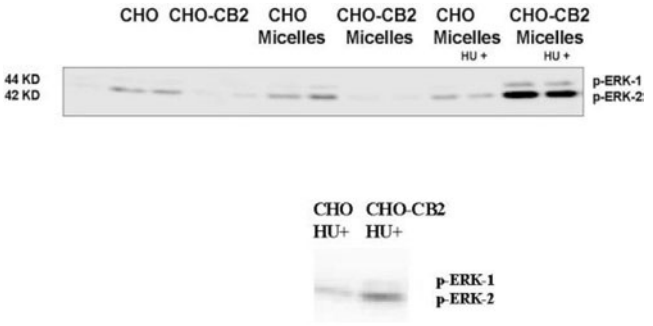

FIG. 1. West Blot.

390. CHARACTERIZATION OF MICELLE-BASED CONTRAST AGENT TARGETING PERIPHERAL CANNABIS RECEPTORS AND ITS POTENTIAL USE FOR ATHEROSCLEROTIC PLAQUE VISUALIZATION BY MRI

Bernard C. M. Te Boekhorst,[1] Juan Rodrigues-Feo, MD, PhD,[2] Sandra M. Bovens,[2] Toon I. P. M. de Kroon, MD, PhD,[3] Maarten-Jan J. M. Cramer, MD, PhD,[2] Gerard Pasterkamp, MD, PhD,[2] Pieter A. F. M. Doevendans, MD, PhD,[2] Cees J. A. van Echteld, MD, PhD.[2]
[1] ICIN, Utrecht, The Netherlands, [2] UMCU, Utrecht, The Netherlands, [3] Institute of Biomembranes, Utrecht, The Netherlands.

The peripheral cannabis (CB2) receptor is expressed by inflammatory cells in human atherosclerotic lesions (1). Administration of CB2 agonist in mice reduces plaque size. Production of a micelle-based contrast agent specifically targeting CB2 might have a diagnostic potential.

Materials & Methods: HU-308-PEG-ylated micelles were formed after dispersion of a lipid film of di-oleoyl-phosphoethanolamine PEG1000 (75 M%), gadolinium-bistearylamide (10 M%), lissamine-rhodamine-PE (5 M%) and HU-308 (10 M%) in buffer (alfa-MEM).

The hydrodynamic diameter of the micelles was measured with dynamic light scattering. Control and CB2 expressing Chinese hamster ovary cells (CHO cells) were grown at 37°C, 5% CO2 and stimulated with control or HU-308 micelles for 10 minutes (western blotting) or 1.5 hours (MRI) and confocal fluorescence microscopy.

The ratio between phosphorylated and total MAP kinases (determined by western blotting) was used as read out of stimulation of the CB2 receptor by HU-308 micelles. MRI measurements

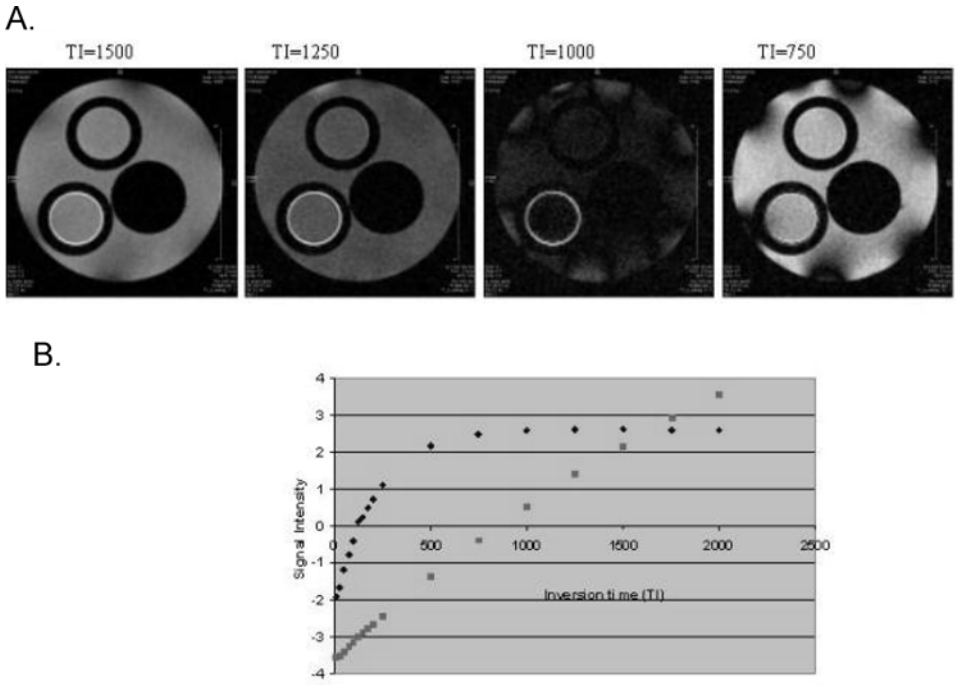

FIG. 2. MRI: IRSE, T1 measurement of untargeted paramagnetic micelles.

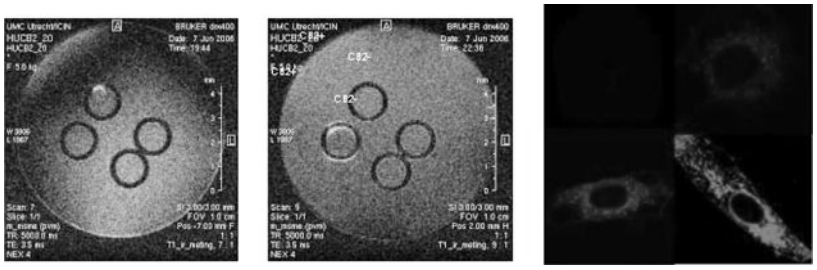

FIG. 3. A and B. MRI of adjacent transverse slices of capillaries with CHO cells, C. CFM of CHO cells.

were performed in a 9.4 T magnet. Inversion recovery spin echo (IRSE) was used for T1 measurement of a micellar solution (2.5 micromole/L Gd-BSA) and for T1-weighted images of the CHO cells grown on glass capillaries. Confocal fluorescence microscopy was performed on CHO cells grown on cover slips.

Results: The hydrodynamic diameter of the micelles was 8–14 nm. There was an obviously increased level of expression of phosphorylated MAP kinases in the CB2 expressing CHO cells after stimulation with HU-308 micelles, as observed with western blotting (Fig. 1) and verified by an increased ratio between phosphorylated and total MAP kinases.

The T1 of the micellar solution (2.5 micromole/L Gd-BSA) was 2050 ms as compared to 3600 ms for the alfa-MEM without micelles at 9.4T (Fig. 2A/B). CB2 expressing CHO cells incubated with HU-308 micelles showed paramagnetic enhancement at T1-weighted IRSE images, whereas control CHO cells incubated with these micelles did not (Fig. 3A/B). Also CB2 expressing and control CHO cells incubated with respectively control and HU-308 micelles, did not show paramagnetic enhancement.

Confocal fluorescence microscopy (CFM) of CHO cells showed increased uptake of HU-308 micelles by CB2 expressing CHO cells (Fig. 3Civ) when compared to control CHO cells (Fig. 3Ciii). Control micelles were not uptaken by both control and CB2 expressing CHO cells (Fig. 3Ci/ii resp.).

Conclusion: Successful in-vitro targeting and MR enhancement of the peripheral cannabis receptor with micelles promises great diagnostic potential for atherosclerosis.

REFERENCE

1. Steffens et al, Nature 2005.

391. MRI CHARACTERIZATION OF AGAROSE 'COCOONS'

Warren D. Foltz,[1] Mark Ormiston,[1] Duncan J. Stewart,[1] David Courtman,[1] Alexander J. Dick.[2] [1]*St. Michael's Hospital, Toronto, Ontario, Canada,* [2]*Sunnybrook Health Sciences Centre, Toronto, Ontario, Canada.*

Introduction: Early and severe cell attrition in vivo may limit the efficacy of stem cell therapy. Strategies which promote cell survival include tissue angiogenic pre-treatment, cell transformation, and cell encapsulation. Agarose encapsulation strategies, in which single cells are 'cocooned' ex vivo in agarose matrices, have strong prosurvival properties because of matrix supplementation with provisional matrix proteins. MRI should be effective for tracking capsule fate in vivo because agarose gels have long served as tissue-mimicking phantoms. Furthermore, capsule imaging may be facilitated by transient loading with paramagnetic contrast.

Purpose: The overall purpose is the design and pre-clinical optimization of strategies for stem cell therapy.

Methods: Capsules (mean diameter 50 μm) were constructed according to the methodology of Courtman. T_1 and T_2 were modulated by varying agarose content (2.5% and 1.8%). Some capsules were also incubated for 20 minutes ex vivo in 5 mM Gd-DTPA. Sets of encapsulated cell pellets were also constructed, using a density of rabbit fibroblasts which optimizes single cell loading. Post-aspiration, capsule pellet relaxation times ($\sim$150 μl in eppendorf tube) were quantified using the head coil of a 1.5 Tesla GE Signa, with validated magnetization-prepared spiral imaging sequences.

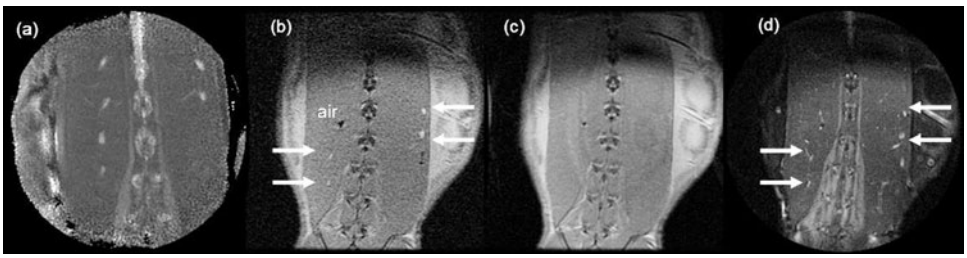

FIG. 1. (a) coronal T_2 image including 6 discrete lumbar injection sites (no Gd-DTPA); (b, c) early and late spgr (+1 and 4 hours) depicting 4 Gd-DTPA sites with white arrows; and (d) corresponding late fse (+4 hours).

Capsule pellets were injected directly (50 μl target volume) using a precision Hamilton syringe (250 μl volume) and at discrete locations into the lumbar muscles of rabbits (n = 4, New Zealand White, 2–5 kg). The spatial distributions of T_2 were evaluated using stacks of spiral images (TE of 11 and 54 ms, TR = 3000 ms, 0.8 × 0.8 × 1.7 mm^3, 24 nex) while T_1 scanning was performed in select slices using a Look-Locker method (train of 9 small-tip angle pulses separated by 160 ms, same resolution and TR). The persistencies of contrasts from agarose and Gd-DTPA were tracked via repetitive imaging over the first five hours post-injection, using heavily T_1-weighted spgr imaging (TR of 50 ms), which should highlight Gd-DTPA capsules only, and T_2-weighted fse or spiral imaging (TR of 3000 ms), which should highlight all capsules. One animal was imaged two days later to evaluate the persistencies of contrasts. Capsule distribution volumes (DV) and relaxation times were evaluated on a per-region-of-interest basis using custom software (xcinema, Stanford University).

Results: Ex vivo, reducing agarose content increased T_2 (2.5%: 70 ± 15 ms; 1.8: 107 ± 15 ms; p = 0.018, n = 5). Gd-DTPA reduced T_2 to 59 ± 5 ms (p = 0.003) and 64 ± 9 ms (p = 0.009, n = 4). Gd-DTPA immersion reduced T_1 from 2764 ± 303 to 122 ± 8ms (n = 6, p = 0.0003). Cell encapsulation may increase T_2 slightly (1.8%: 111 ± 20 ms to 117 ± 20 ms, p = 0.046, n = 3).

In vivo, 1.8% capsules presented with DV of 47 ± 16 mm^3, T_2 elevation of 53 ± 26% (n = 9) from remote T_2 of 29 ms, and T_1 elevation of 70 ± 24% from remote T_1 of 1150 ms (n = 9). Two and five tenths percentcapsules presented with DV of 30 ± 26mm^3, T_2 elevation of 39 ± 10% (n = 9), and T_1 elevation of 67 ± 10% (visible n = 3). Propagation of T_2 measurements through a slow exchange model suggests DV filling with agarose by 22 ± 7mm^3 at 1.8% and 14 ± 13mm^3 at 2.5%. Consistently, Gd-DTPA contrast in short-TR images had disappeared by 4 hours, while contrast in long-TR images persisted throughout the experimental time course and out to day 2.

Conclusions: MRI can effectively visualize agarose 'cocoons' following direct muscular injection in vivo. Capsule visualization in short TR images is facilitated transiently by immersion in paramagnetic contrast agents. We anticipate that matrix incorporation of large paramagnetic molecules such as Gd-dextran (Gadomer, Schering AG) will prolong T_1 enhancement. Some dilution of the pellet appears necessary for robust injection, because of pellet viscosity and often associated air injection.

392. ANGULAR DEPENDENCE OF MYOCARDIAL VELOCITY IN PATIENTS WITH CONGENITAL HEART DISEASE

Michael D. Taylor, MD, PhD, Rajesh Krishnamurthy, MD, Taylor Chung, MD, G. Wesley Vick, III, MD, PhD. ***Baylor College of Medicine/Texas Children's Hospital, Houston, Texas, USA.***

Introduction: Tissue Doppler imaging (TDI) is a useful technique to analyze both systolic and diastolic function in patients with congenital heart disease. TDI is limited by interrogating only the velocity vector component parallel to the incident ultrasound beam. During both systole and diastole, the myocardial velocity vector direction (V/|V|) traces a complex path in three dimensions.

Purpose: The objective of this work was to quantify the relationship between the longitudinal velocity component (similar to the TDI geometry) and the three-dimensional velocity vector as measured with 3D tissue velocity encoded MRI.

Methods: Six patients with repaired congenital heart disease (tetralogy of Fallot) and two normal subjects were evaluated using magnetic resonance phase contrast with velocity encoding in three dimensions. A single plane of tissue velocity mapping data was acquired in the four-chamber orientation. The data were acquired using a standard phase contrast sequence with velocity encoded in three orthogonal directions. One velocity component was aligned to the ventricular septum from base to apex, termed the longitudinal component ($\theta = \pi/2$). This is the analogous direction to echo based TDI. The other two directions are termed circumferential ($\phi = \pi/2$) and radial ($\phi, \theta = 0$). Parametric images of the three-dimensional magnitude and direction of the velocity vector were created for each image. Regions of interest encompassing ~125 mm^3 were interrogated on the lateral mitral annulus, interventricular septum, and lateral tricuspid annulus. The data were compared to echocardiography tissue Doppler tracings acquired at the same locations.

Results: The velocity encoded MR data replicated with high fidelity the tissue Doppler tracings. The peak E, A, and S wave myocardial velocities calculated with each modality were statistically correlated with p-values < 0.05 [correlation coefficients, R(E) = 0.91, R(A) = 0.79, and R(S) = 0.72]. Even in two of the patients with marked right ventricular systolic dysfunction secondary to their repaired congenital heart disease, MR was able to generate accurate velocity information. During systole the longitudinal velocity component does not represent the predominant direction of the cardiac motion. As seen in Fig. 1, in a normal subject, the longitudinal component represents only ~50% of the total vector magnitude. There are significant components of circumferential and radial velocity that contribute to the total velocity during systole. In contrast, during diastole the longitudinal component represents a significant fraction of the total velocity vector, representing ~75% of the total magnitude. The radial component is only responsible for ~10% of the total velocity vector magnitude. This relationship between the longitudinal component and the total magnitude is not a linear function of vector direction or a function of disease state. In the normal subjects, the longitudinal component at the lateral tricuspid valve annulus represents the primary direction of diastolic relaxation. Conversely, the data for tetralogy patients suggests the circumferential component represents the primary velocity component.

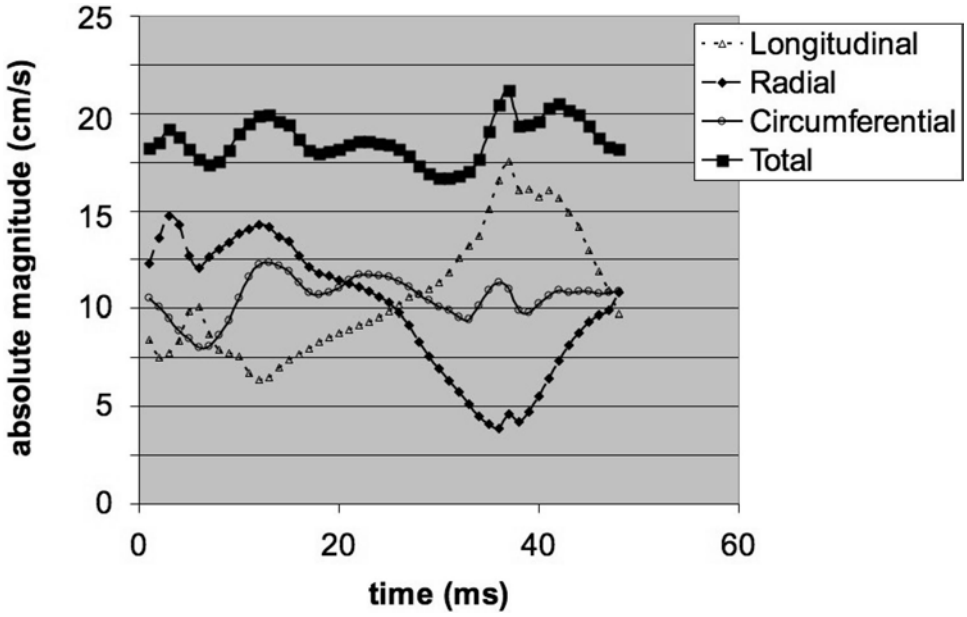

FIG. 1.

Conclusions: The angle between the total velocity vector and the longitudinal component is a complex temporal function. These data show that the echocardiography-based tissue Doppler measurement does not fully describe the complex 3D nature of myocardial velocities. Discrepancies between the total velocity vector and the longitudinal component appear to depend on disease state—an important finding as TDI is used increasingly for functional assessment of patients with congenital heart disease.

393. QUANTITATIVE GLOBAL AND REGIONAL CARDIAC WALL MOTION ANALYSIS WITH A 3-DIMENSIONAL RECONSTRUCTION CARDIAC IMAGE MODELING (CIM) TOOL

Jessica Hung, BS,[1] Christopher Francois, MD,[1] Nicole A. Nelson, MD,[1] Karin Dill, MD,[1] Ed Wu, MD,[1] Alistair Young, PhD,[2] Brett R. Cowen, BE MBChB,[2] Renate Jerecic, PhD,[3] James Carr, MD.[1] [1]***Northwestern University, Chicago, Illinois, USA,*** [2]***University of Auckland, Auckland, New Zealand,*** [3]***Siemens Medical Systems, Chicago, Ilinois, USA.***

Introduction: Cardiac function is currently assessed using a visual analysis of wall motion in short axis at the base, middle, and apex of the heart. This visual analysis is a subjective, qualitative evaluation and can have high interobserver variability (1). In order to minimize the amount of subjective input, a semi-automated 3D reconstruction Cardiac Image Modeling tool (CIM 4.6, University of Auckland, New Zealand) has been developed to quantitatively assess global and regional cardiac function (2). CIM is a semi-automated tool that creates a 3Dreconstruction of the heart, based on user-defined guidepoints to customize endocardial and epicardial computer generated tracings on long and short axis magnetic resonance (MR) time series images (Fig. 1a) (3). Using CIM, it is possible to calculate regional, segmental ejection fractions (EF) based on the 16-segment model of the heart according to the American Heart Association (AHA) classifications. If it were possible to accurately quantify regional wall motion abnormalities (RWMA), this may be useful in clinical assessment of cardiac patients pre- and post- therapy.

Purpose: To evaluate the ability of the CIM tool to assess global and regional cardiac function in comparison to the current manual contour tracing and qualitative assessment of wall motion.

Methods: Thirty-three patients (23 males, 10 females) referred for assessment of left ventricular cardiac viability were scanned on a 1.5T Siemens Avanto. Cardiac function was assessed using cine TrueFISP technique in a short axis orientation from base to apex in all patients. Based on global EFs as calculated by a standard post-processing tool (Argus, Siemens), the study group was divided into three categories (normal = EF $\geq$ 50%; moderate = 30% $<$ EF $<$ 50%; severe = EF $\leq$ 30%). The studies were randomized and underwent quantitative analysis with CIM and qualitative analysis by three blinded reviewers. The heart was divided into the 16-section AHA defined cardiac model. Each of the reviewers independently scored the sections as normal or abnormal. CIM calculated quantitative regional EFs (Fig. 1b). The quantitative EFs were then classified as normal and abnormal (normal = EF $\geq$ 50% and abnormal = EF $<$ 50%).

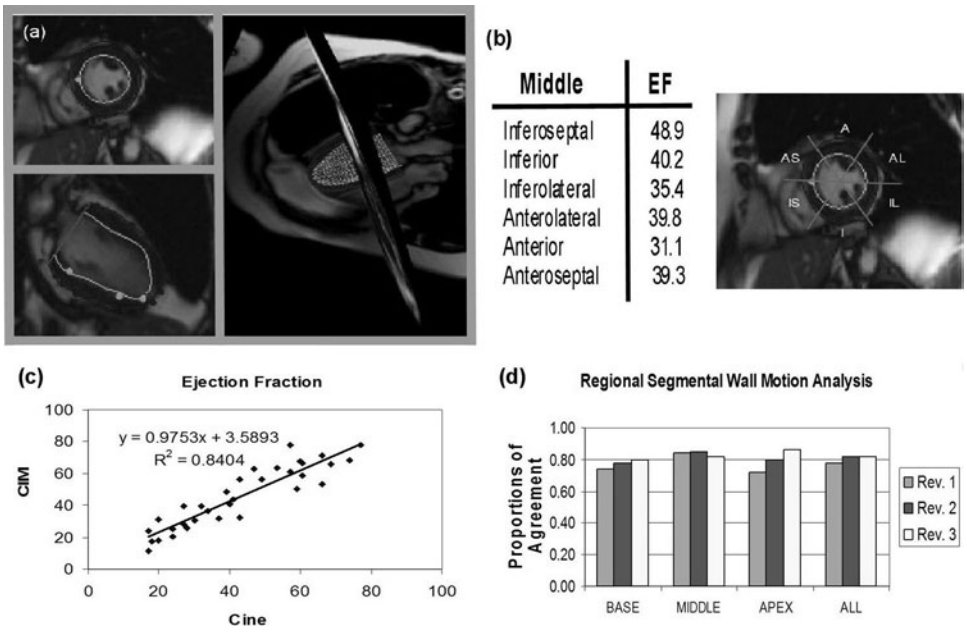

FIG. 1. (a) CIM interface. User defined guidepoints in short and long axis views for 3D reconstruction. (b) Middle axial slice divided according to the regional AHA guidelines and analyzed by CIM. (EF = Ejection Fraction) (c) Linear regression of global ejection fraction of all 33 patients for assessing correlation between visual analysis and CIM analysis ($R^2 = 0.84$). (d) Total proportions of agreement for the segments within the short axial slices (base middle, apex), and the overall proportions of agreement for all the segments in all the 33 patients.

Proportions of agreement (pa) were used to determine the agreement between the readers and CIM. Proportion of agreement was defined as the number of sections that the reader and CIM tool both scored a section as normal or both scored a section as abnormal, divided by the total number of sections.

Results: There was a high correlation ($r^2 = 0.84$) between the manual contour tracing method and CIM for global EF (Fig. 1c). On an individual segment basis, there was moderate agreement with all segments showing a pa > 0.6, with the exception of the Base-Inferoseptal and the Base-Anteroseptal segments. Regional wall motion analysis of the sections in the base, middle, and apex separately showed a moderate-high agreement (pa > 0.7). Overall regional wall motion analysis of all the sections from all the patients combined showed a high proportion of agreement (pa $= 0.8$) (Fig. 1d).

Conclusions: CIM accurately calculated global EF and other left ventricular parameters compared to other post-processing techniques. Furthermore, CIM is able to calculate regional EF on a segmental basis. Our studies show a moderate agreement with qualitative analysis of RWMA. CIM has the potential to quantify regional improvements in patients throughout the course of therapy.

REFERENCES

1. Hoffman R, et al. J Am Coll Cardiol 2006;47:121–128.
2. Swingen CM, et al. J Magn Reson Imaging 2003;17:528–537.
3. Young AA, et al. Radiology 2000;216:597–602.

394. AN ENDOCARDIAL TO EPICARDIAL MYOCARDIAL CONTRACTION GRADIENT IS PRESENT IN SEVERE COMPENSATED AORTIC STENOSIS: DOES IT REVERSE AFTER AORTIC VALVE REPLACEMENT?

Robert W. W. Biederman, MD,[1] June Yamrozik,[1] Ronald Williams,[1] Vikas K. Rathi, MD,[1] Diane A. Vido,[1] Ketheswaram Caruppannan, MD,[1] Nael Osman, PhD,[2] Saundra Grant,[1] Geetha Rayarao,[1] Sunil Mankad, MD,[1] James A. Magovern, MD,[1] Mark Doyle, PhD.[1] [1]***Allegheny General Hospital, Pittsburgh, Pennsylvania, USA,*** [2]***Johns Hopkins University, Baltimore, Maryland, USA.***

Introduction: Experimental animal aortic stenosis (AS) induced by supravalvar constriction exhibits decreased subendocardial coronary blood flow as defined by microspheres, and decreased subendocardial shortening as demonstrated by piezoelectric crystal techniques. Such abnormalities have been shown by us and others to rapidly normalize following relief of stenosis. In late, but compensated human AS, a subendocardial to subepicardial gradient (S_{endo}/S_{epi}) in strain as measured by CMR radio-frequency (RF) tissue tagging is present.

Hypothesis: We hypothesize that an S_{endo}/S_{epi} myocardial strain gradient is present in severe AS but will reverse following aortic valve replacement (AVR) in concert with LVH regression.

Methods: Thirty-two patients with late, but compensated, AS underwent MRI (GE, 1.5T, EXCITE HD, Milwaukee, Wisconsin, USA) with 3D quantification of LV metrics. Two dimensional strain via radio-frequency tissue tagging was performed

with analysis via HARP (Palo Alto, California, USA) of the endocardial and epicardial shell for 8-12 contiguous short-axis slices pre, 6 months and 12 months following AVR.

Results: Eighteen of 24 patients had full 2D strain available and of high quality for HARP analysis. Following AVR, there was marked regression of LV mass (91 ± 39 vs 77 ± 32 g/m^2, LVEDVI and LVESVI [79 ± 25 vs 69 ± 11 mL and 37 ± 29 vs 23 ± 8 mL, respectively] while EF increased [58 ± 18 vs $67 \pm 10\%$] [$p < 0.001$ for all]). For the group composed of CAD+ and CAD- patients, S_{endo}/S_{epi} strain was markedly abnormal pre AVR 0.52 ± 0.33, was 0.56 ± 0.51 at 6 mo and $0.59 \pm 0.49\%$ by 12 mo (all p = NS) and remaining below historic controls ($1.20 \pm 40\%$). However, there was marked improvement in absolute strains when defined by endo, midwall and epi segments, both over time ($p < 0.05$) and from base to mid ($p < 0.05$), excluding the apex. In those with concommitant CAD and AS, the improvements in LV metrics post AVR were further blunted ($p < 0.05$) despite CABG in all. However, CAD- patients never fully approached historic control absolute strain or S_{endo}/S_{epi} strain ratios despite their marked improvements.

Conclusion: Representing another pathologic feature of severe AS, abnormalities beyond standard strain can be elucidated by MRI at the level of the subendocardium and subepicardium that rapidly improve in parallel post-AVR. However, in contrast to animal models where S_{endo}/S_{epi} strain ratios rapidly improve *and* normalize, human strain and strain ratios do not. The rapid time course for experimental AS with its comparative lack of fibrosis, as compared with decades of afterload excess leading to extensive myocardial hypertrophy, fibrosis and perturbation of the extracellular matrix, may be much more easily reversed as compared to humans. This human strain pattern is further perturbed in those with CAD and its improvement post-AVR is markedly blunted, favoring considerations for earlier AVR.

395. CAN EJECTION FRACTION PREDICT SEX?

Robert W. W. Biederman, MD, Diane A. Vido, Geetha Rayarao, June Yamrozik, Ronald Williams, Saundra Grant, Mark Doyle, PhD. ***Allegheny General Hospital, Pittsburgh, Pennsylvania, USA.***

Introduction: Historically, it has been assumed that the mechanical contraction parameter ejection fraction (EF) is identical across the sexes. Until recently, however, the fidelity and reproducibility of imaging techniques guaranteed virtual superimposition of EF, nullifying any differences were they to be present in nature.

Hypothesis: Using high resolution CV MRI, we hypothesized that there would be decreased EF in females as compared to males when examined on a population basis.

Methods: A database composed of consecutive patients who underwent CV MRI scanning (GE, EXCITE HD 1.5T, Milwaukee, Wisconsin, USA) enrolled between Aug 2002 and May 2006 was interrogated to yield all normal pts classified by strict criteria: EF > 55%, no valvular disease >1+, no evidence of CAD, HTN, or cardiomyopathy. EF was determined primarily by standard FIESTA 3D methodology or 2D when available. RVEF was also evaluated, but only in those whose LVEF >55%. Patients were stratified only by sex.

Results: One thousand one patients were evaluated, from which 481 were classified as normal, comprising of 226 males and 255 females (mean age 50 ± 9 yrs). All normals passed the Kolmogorov-Smirnov test for Normality. The mean EF for men was 63.5 ± 4.9; range: 58.6–68.4%, while for women it was 64.5 ± 4.6; range: 59.9–69.1%, $p < 0.05$. Under the assumption that EF > 55% may not be appropriate for normal thresholding, EF > 60 and 65% were also stratified but did not yield significant differences between sexes. Similarly, the RVEF was lower in males as compared to females thresholded for EF > 55%, (56.3 ± 4.2 vs $59.0 \pm 4.4\%$), respectively, $p < 0.001$. A subset of 150 patients with clinical CV disease, representing the entire range of EF (5%–81%), underwent intra and interobserver reproducibly for LVEF and was 0.13 and 0.85%, respectively.

Conclusion: Contrary to conventional doctrine, LV ejection performance (EF) as measured clinically, using highly reproducible and accurate CV MRI, is lower for males than females as determined in the largest CV MRI database (>1500 patients) to our knowledge to date examining this subject. This finding is also true for the RVEF. Beyond establishing normal ranges for LV and RV EF's, these observations have far reaching clinical implications in defining thresholds of normality, as well as belying intrinsic differences in contractile mechanisms.

396. CALCULATION OF AORTIC PRESSURE WAVEFORM FROM MRI BLOOD FLOW VELOCITY MEASUREMENTS

Yu Ding, PhD, Subha V. Raman, MD, MS, FACC, Orlando P. Simonetti, PhD. ***The Ohio State University Medical Center, Columbus, Ohio, USA.***

Introduction: Aortic pulse pressure is an important clinical parameter. It can be measured invasively by catheterization or estimated by brachial cuff pressure. However, brachial pressure has not been shown to be a consistently accurate estimate of central aortic pressure (1). Phase contrast magnetic resonance imaging (PC-MRI) can accurately measure aortic blood flow and pulse wave velocity. According to the mathematical model presented here, blood flow velocity and pressure are related by two differential equations. Using PC-MRI blood flow data as input, with proper boundary conditions, the aortic pressure waveform can be generated from the mathematical model.

Purpose: Generate pressure waveforms at any location in aorta from PC-MRI blood flow velocity measurements in patients.

Methods: This method is based on a one-dimensional model considering both the Windkessel effect and the traveling wave

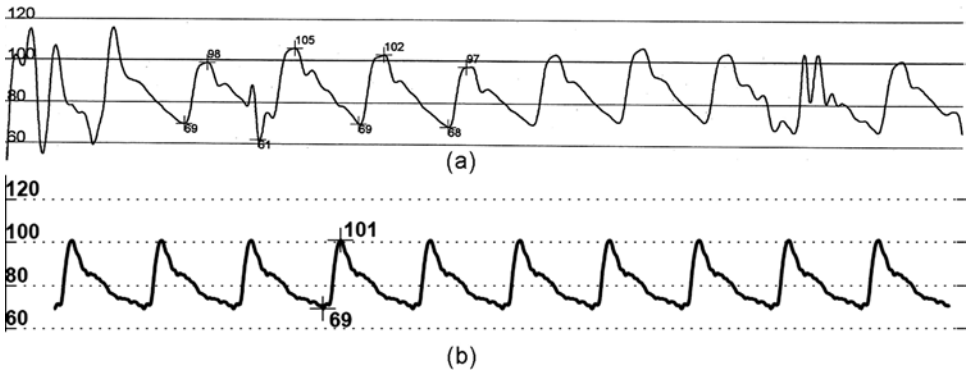

FIG. 1. Pressure waveform (mmHg vs. time) directly transduced inthe ascending aorta via fluid-filled catheter system (a) versus aortic pressure waveform generated through model calculation in a 42 year-old male who underwent CMR and cardiac catheterization ont he same day.

properties of pulsatile blood flow in aorta (2). Similar to the Windkessel model, this model has an electrical circuit analogy, which has a uniform distribution of capacitors and resistors along two parallel conducting lines. Therefore, telegraph equations are proposed to describe the relation between blood flow velocity and pressure. Mathematically, the telegraph equations can be derived from linearized one-dimensional Navier-Stokes and continuity equations with the additional assumption that aorta cross-sectional area is a function of pressure only (3). Since blood flow is partially reflected by the iliac bifurcation, we adopt a partial reflecting boundary condition. We assume that there is only one reflection site somewhere in the distal aorta, but the exact location of reflection site is not important. The complex side-wall boundary condition is avoided.

Our method requires only two blood flow velocity measurements as input. From one aorta para-sagittal view with in-plane one-dimensional velocity encoding along the primary direction of flow, blood flow velocity and pulse wave velocity are measured. A second measurement is made in the common carotid artery axial view with through-plane one-dimensional velocity encoding. The time delay between incident and reflected blood flow and the reflection coefficient can be estimated from these measurements.

The blood flow velocity waveform is separated into incident and reflected waveforms and the characteristic impedance which relates velocity to pressure is calculated. The only free model parameter, the characteristic impedance phase angle, was empirically adjusted to 15 degrees.

TABLE 1
Pulse pressure comparisons between Mean and SD of cath data vs. model calculation

Subject	1	2	3	4
Mean (mmHg)	55.3	35.0	35.1	37.5
SD (mmHg)	3.5	3.0	4.9	2.9
Model Calculation (mmHg)	52.7	35.6	31.9	40.8

The experimental study was done on a 1.5T MRI system (Avanto, Siemens, Germany) in the Ross Heart Hospital at The Ohio State University. Four patients (age range from 27 to 76 with mean age 50) who had both CMR and catheter-based pressure measurements (three on the same day and one five days before) were included. The blood flow velocity waveforms were measured in aorta and carotid arteries and the corresponding aortic pressure wave was calculated. The imaging parameters were: 192 × 144 or 192 × 120 matrix, 5.0 mm thick slice, flip angle 15 or 25 degrees, TR =14 ms, TE = 3.1 ms, pixel bandwidth = 355 Hz.

Results: Mean aortic pressures measured by a fluid-filled catheter system, averaged over 5 cardiac cycles vs. estimated mean aortic pressures using the mathematical model in four patients are summarized in the Table. Compared to direct pressure transduction, the aortic pressure waveforms generated by the model are of similar shape and amplitude (Fig. 1).

Conclusions: Based on a mathematical model describing the blood flow velocity and pressure relation in aorta, a new method was developed to calculate blood pressure from flow velocity measured by PC-MRI. Future work will be to include nonlinear terms and to collect additional validation data.

REFERENCES

1. Pauca AL, et al. Chest 1991;102:1193–1198.
2. Anliker M, et al. Z Ang Math Phys 1971;22:217–246.
3. Westerhof N, et al. J Biomechanics 1969;2:121–143.

397. DYNAMIC CMR CARDIAC ANATOMY: THE 'CYPRESS TREE' PAPILLARY MUSCLE ROOT

Robert W. W. Biederman, MD,[1] Mark Doyle, PhD,[1] Leon Axel, MD.[2] [1]*Allegheny General Hospital, Pittsburgh, Pennsylvania, USA,* [2]*NYUMC, New York, New York, USA.*

Introduction: The understanding of gross cardiac anatomy has been relatively stable over the last 80 yrs, reliant on well-established autopsy findings. The advent of dynamic imaging by

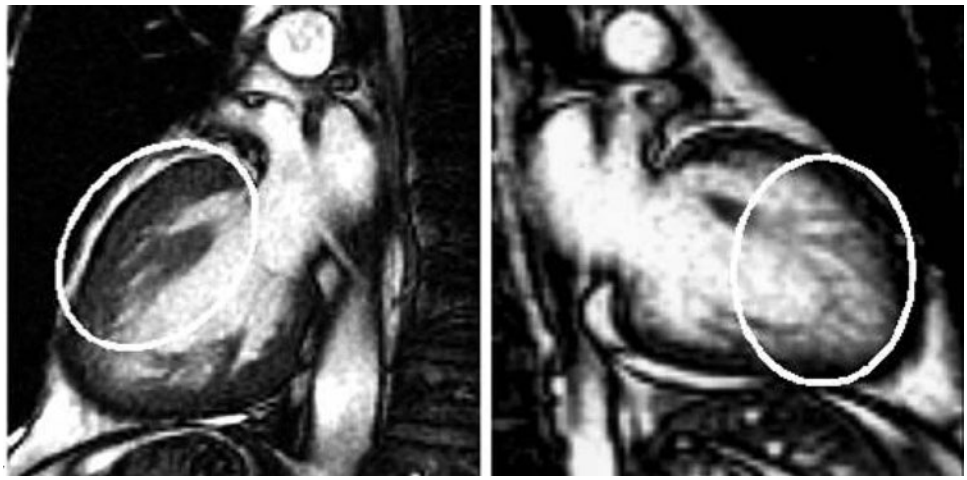

FIG. 1.

cardiovascular MRI (CMR) and CT provides a window to view anatomic features *in vivo*, providing insights typically masked at autopsy due to death.

Hypothesis: We hypothesize that CMR with its high spatial and temporal resolution allows detection of anatomic features not previously appreciated at autopsy.

Methods: Four hundred one (401) patients underwent CMR (GE, 1.5T) examinations with 255 retrospectively and 146 prospectively examined to determine anatomic features of the LV papillary muscles (PM). Specifically, the basal origins of the PM were defined.

Results: The insertion of the PM was seen in 401/401 patients (100%). In 392 out of 401patients (97.8%), the appearance of the PM was not a uniform appearing muscle arising from the inner face of the LV endocardium, but was a finger-like series of long, root-like slender trabeculae carnae traversing >1cm before inserting into the main body of PM, challenging our previous understanding of PM anatomy (Fig. 1).

Conclusion: The capabilities of CMR to view cardiac features *in vivo* non-invasively affords a useful tool to study living cardiac anatomy. Unlike the widely accepted belief that papillary muscles uniformly arise from the LV floor, they resolve into a 'cypress tree' root-like structure with multiple thin projections before coalescing into a thick muscle head. Such observations have far reaching clinical implications in areas such as mitral regurgitation, post MI remodeling and electrical transmission of the His-Purkinje system while challenging our classic teachings.

398. CAN IMPROVEMENTS IN DYSSYNCHRONY OCCUR VIA NON-PACEMAKER TECHNIQUES; UTILIZATION OF A MINIMALLY INVASIVE LV WRAP: DETECTION OF DYSSCHRONY BY CMR

Robert W. W. Biederman, MD,[1] Frank Grothues, MD,[2] Helmut Klein, MD,[2] Ronald Williams,[1] June Yamrozik,[1] Geetha Rayarao,[1] Diane A. Vido,[1] Christof Huth, MD,[2] Mark Doyle, PhD.[1] ***[1]Allegheny General Hospital, Pittsburgh, Pennsylvania, USA, [2]University Hospital Magdeburg, Magdeburg, Germany.***

Introduction: In patients presenting with dilated cardiomyopathy (CMX), the efficacy of dyssynchrony reduction by placing a Nitinol wrap around the heart is unknown.

Hypothesis: We hypothesize that the HeartNetTM (Paracor Medical Inc, Sunnyvale, CA) surgically placed in patients with severe dilated CMX reduces dyssynchrony.

Methods: At baseline, 18 subjects, 8 patients (47 ± 9 yrs) with mean NYHA Class 2.3 ± 0.5 on optimal medical therapy (maintained throughout the study) and 10 normal controls (44 ± 7 yrs) underwent 3D cardiovascular MRI to assess LV function. Using Medis Mass software (Leiden, The Netherlands), endocardial and epicardial boundaries were outlined in contiguous short-axis slices. Circumferentially, the myocardium was divided into 16 equally spaced segments and end-systolic (ES) time automatically identified as time of maximal wall thickening. End-systolic times were analyzed to assess progression towards normal ES time and the dyssynchrony index taken as the dispersion of ES times. All treated patients underwent minimally invasive L thoracotomy with deployment of the HeartNet^{TM}designed to conform to the epicardium. Follow-up CMRI was performed at 6 months in all pts.

Results: All patients survived HeartNet^{TM} placement and were available for follow-up. NYHA class decreased to 1.9 ± 0.6 ($p < 0.04$). One patient was admitted for CHF in the first month. Global LV wall thickening improved ($129 \pm 29\%$ vs. $136 \pm 35\%$, $p < 0.001$) but remained lower than controls ($169 \pm 39\%$, $p < 0.001$) and ES wall thickness increased (10.2 ± 2.7 mm vs. 10.8 ± 3.0 mm, $p < 0.001$). For the mid and apical regions, indices of ES dyssynchrony showed no significant change pre to post. The basal region demonstrated a reduction in the LV dyssynchrony index (254 ms vs. 220 ms, $p < 0.05$, $f = 12.8$). At baseline, the ES time of the base was higher than controls (363 ± 254 ms vs. 311 ± 75 ms, $p < 0.0001$) and at follow-up,

ES time at the base was comparable to controls (331 ± 220 ms vs. 311 ± 75 ms, p = 0.09).

Conclusion: Given the general paucity of novel therapies available for the treatment of dilated CMX, minimally invasive placement of the HeartNet^{TM}LV wrap improved global myocardial function, and in the basal region the ES time was restored to near normal values, with a concomitant improvement in synchrony. The singular advantage of this approach is the ease of a minimally invasive approach. A registered clinical trial in USA and Europe is now under way.

399. AN MRI MECHANISTIC INSIGHT INTO THE PATHOGENESIS OF NONISCHEMIC CARDIOMYOPATHY

Robert W. W. Biederman, MD, Srinivas Murali, MD, June Yamrozik, Ronald Williams, Geetha Rayarao, Diane A. Vido, Saundra Grant, Mark Doyle, PhD. ***Allegheny General Hospital, Pittsburgh, Pennsylvania, USA.***

Introduction: Differentiating between ischemic and nonischemic cardiomyopathy (CMX) is important for optimal patient management. Detection of endocardial and/or transmural MRI delayed hyperenhancement (DHE) identifies nonviable tissue, classifying the patient as ischemic. However, by MRI, classification of a dilated nonischemic CMX is currently largely a diagnosis of exclusion and no subclassifications exist.

Hypothesis: In addition to a binary decision regarding the etiology of CMX, nonischemic CMX can be further characterized using the MRI myocardial DHE signal pattern.

Methods and Results: Review of consecutive patient records referred for CV MRI (GE, 1.5T, EXCITE HD, Milwaukee, Wisconsin, USA) presenting with EF < 35% over the preceding 12 months yielded 117 patients. Mean EF 24%, mean EDVI 129 mL. All patients received CMRI contrast (Magnevist, Berlex, Montville, New Jersey, USA or MultiHance, Bracco, Princeton, New Jersey, USA) with standard DHE. The majority, 80 (68%) were classified as ischemic CMX, with 37 nonischemic CMX; 24 of these (65%) had a DHE pattern; 9 with myocarditis characterized by a patchy and/or punctate DHE pattern and an acute and/or fulminant presentation; 13 with no DHE signal and 15 with a distinct DHE linear midwall septal stripe, confined to the basal to mid LV myocardium (Fig. 1). This stripe is associated with fatty-fibrosis on histopathology.

Conclusions: Delayed enhancement MRI can identify ischemic CMX. It can also stratify nonischemic CMX based on the DHE pattern: 1) lack of enhancement 2) patchy appearance 3) or a striking midwall septal stripe distinct from the first two with histopathologic/CMR correlation appearing to define a zone of depleted myocardial cellular structure replaced with fibro-fatty tissue. This pattern may be pathogneumonic for those with a viral etiology to their non-ischemic presentation. Whether this latter pattern further defines clinical response to pharmacologic therapy and/or prognosis remains a tantalizing prospect.

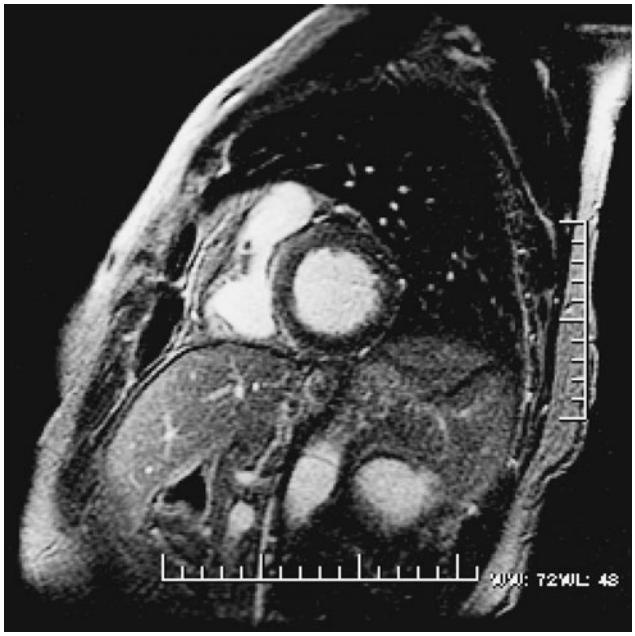

FIG. 1.

400. IS THERE AN ALTERNATIVE EXPLANATION FOR POST-MI MITRAL REGURGITATION: INSIGHTS FROM CMR

Robert W. W. Biederman, MD, Ronald Williams, June Yamrozik, Ketheswaram Caruppannan, MD, Vikas K. Rathi, MD, Geetha Rayarao, Diane A. Vido, Saundra Grant, Mark Doyle, PhD. ***Allegheny General Hospital, Pittsburgh, Pennsylvania, USA.***

Introduction: Multiple explanations exist for the etiology of LV annular dilatation post-myocardial infarction (MI). The current assumptions suggest an active process reflecting remodeling of adjacent myocardium. However, nongeometric, passive mechanisms have not been considered, yet are important. Cardiovascular MRI (CMR) delayed hyperenhancement (DHE) postcontrast techniques describe a myriad of LV myocardial histopathology such as infarct, infiltrative and inflammatory perturbations within the LV but may also be sensitive to nonmyocardial pathology.

Hypothesis: We hypothesize that DHE may detect occult LV annular and/or mitral valvar enhancement in postMI patients, and its presence might predict progression of unfavorable changes in annular geometry that lead to progression of mitral regurgitation (MR).

Methods: One hundred sixty-four (164) patients; 111 S/P MI (43 F, 37 acute, 74 chronic) underwent CMR (1.5T GE, Milwaukee, Wisconsin, USA) with 0.2 mmol/kg of Magnevist (Berlex, Wayne, New Jersey, USA) or 0.1 mmol/kg MultiHance (Bracco,Princeton, New Jersey, USA). Notation of presence or absence of a DHE pattern involving the mitral annulus and/or

valve was made. Patients were specifically excluded if MI pattern involved basal myocardium to avoid confounding signal etiology. NonMI patients (53) referred for contrast CMR served as controls. A subset of patients in whom follow-up data was available was analyzed for geometric changes of the mitral annulus and degree of MR while related to presence or absence of DHE (+DHE, −DHE).

Results: All postMI patients demonstrated an area of infarct by functional analysis, confirmed by DHE (100%). Additional DHE was present involving the mitral annulus in 49/111 (44%) and in 84/111 (76%) the mitral valve. Lesser amounts of DHE signal was also seen in adjacent valves: aortic 25/111 (22%), tricuspid 33/111 (30%) while virtually no DHE signal was seen along the tricuspid annulus 5/111 (5%). Only 6/53 (11%) of controls demonstrated any degree of valvar enhancement and 3/52 (6%) had annular enhancement with the majority of these in myocarditis pts.

In the subset of 12 postMI patients available at baseline (3 ± 2 days), 6 weeks and 6 months, there was progressive mitral annular dilation present in 10/12 (83%) +DHE but only 2/6 (33%) −DHE patients. As well, the degree of mitral annular dilation trended higher in those with +DHE vs. −DHE (3.0 × 2.9 × 4.5 mm vs. 2.5 × 2.0 × 4.2 mm, p = NS). Finally, the progression of MR underwent greater deterioration at a faster pace in those with +DHE vs. −DHE ($p < 0.05$). Indeed, MR progressed in all patients except for one in whom DHE decreased and in one patient who remained unchanged. MR remained unchanged in all patients who were −DHE.

Conclusion: CMR DHE depicts focal annular and/or valvar enhancement in large number of post MI patients, suggesting a specific, as yet unknown reactive process may contribute to annular dilatation and/or mitral leaflet pathology. Preliminary data supports a deleterious impact in the postMI remodeling pattern in those with mitral annular or valvar delayed enhancement. This passive phenomena is currently not a suspected contributor to the postMI phenotype but may portend late LV dilatation and either primary or secondary progessive mitral regurgitation.

401. CMR DETERMINED REGIONAL MYOCARDIAL PERFUSION UPTAKE RATE PREDICTS EVENTS IN WOMEN WITHOUT OBSTRUCTIVE CORONARY ARTERY DISEASE: THE NHLBI-SPONSORED WOMEN'S ISCHEMIA SYNDROME EVALUATION (WISE) STUDY

Mark Doyle, PhD,[1] Gerald M. Pohost, MD,[2] Leslee J. Shaw, PhD,[3] George Sopko, MD,[4] Eduardo Kortright, PhD,[5] Diane A. Vido,[1] Sheryl F. Kelsey, PhD,[6] B. Delia Johnson, PhD,[6] William J. Rogers, MD,[7] Steven E. Reis, MD,[8] Marian B. Olson,[8] Barry L. Sharaf, MD,[9] Carl J. Pepine, MD,[10] C. Noel Bairey-Merz, MD,[11] Sunil Mankad, MD,[1] Robert W. W. Biederman, MD.[1] ***[1]Allegheny General Hospital, Pittsburgh, Pennsylvania, USA, [2]University of Southern California, Los Angeles, California, USA, [3]ACRI, Atlanta, Georgia, USA, [4]National Institutes of Health, National Heart, Lung, and Blood Institute, Washington, DC, USA, [5]University of New Orleans, New Orleans, Louisiana, USA, [6]Epidemiology Data Center, Pittsburgh, Pennsylvania, USA, [7]University of Alabama at Birmingham, Birmingham, Alabama, USA, [8]University of Pittsburgh Medical Center, Pittsburgh, Pennsylvania, USA, [9]Rhode Island Hospital, Providence, Rhode Island, USA, [10]University of Florida, Gainesville, Florida, USA, [11]Cedars Sinai Medical Center, Los Angeles, California, USA.***

Introduction : Previously, we showed that low uptake of gadolinium contrast by magnetic resonance myocardial perfusion imaging (MPI) predicted adverse events in women without significant angiographic obstructive coronary artery disease (CAD). Others have indicated that gradients in the transmural perfusion pattern may be present, but these signals can be contaminated by blood-pool-myocardial susceptibility artifacts.

Hypothesis: We postulate that base to apex gradients in normalized MPI uptake slope may better predict adverse events in women without significant epicardial CAD.

Methods: Women (n = 116), mean age 57 ± 11 yrs, with symptoms suggestive of acute myocardial ischemia and without significant obstructive CAD as assessed by angiography (<70% stenosis) underwent MR MPI. During follow-up (34 ± 16 months), time to first adverse event (death, myocardial infarction or hospitalization for worsening anginal symptoms) or first serious adverse event (death or myocardial infarction) was analyzed using basal and mid-level MPI data of normalized uptake-slope and uptake level, together with ejection fraction (EF).

Results: Adverse events occurred in 27 (23%), and serious adverse events occurred in 6 (5%). By univariate Cox regression modeling, parameters predictive of adverse events were the average MPI uptake level, the average MPI uptake slope and EF ($p < 0.005$ for each). Assessment of the MPI uptake level requires establishment of normal values for each site, and when restricting analysis to self-normalized variables, myocardial uptake slope and EF were combined to predict adverse events ($p < 0.001$). Further, the normalized uptake slope at the mid-LV was a better predictor than the basal-LV ($p < 0.001$). A positive value of the Cox model regression variable for the uptake slope at the mid-LV and EF identified high-risk patients. High vs. low risk patients experienced annualized event rates of 9% vs. 3%, $p < 0.001$, and serious adverse events at annualized rates of 2.3% vs. 0.4%, respectively.

Conclusions: Among women with suspected myocardial ischemia but no significant obstructive CAD, mid-LV measures of MPI normalized uptake slope better predicted prognosis compared to basal-LV measures. Combination with EF further improved prediction of prognosis.

402. PASADENA: A NOVEL TOOL TO IMAGE ATHEROSCLEROTIC PLAQUE

Eduard Y. Chekmenev, PhD,[1] Siu Kei Chow, BS,[2] Pratip K. Bhattacharya, PhD,[1] Daniel P. Weitekamp, PhD,[3] Brian D. Ross, MD, PhD.[1] [1] *Huntington Medical Research Institutes, Pasadena, California, USA,* [2] *University of California, San Diego, La Jolla, California, USA,* [3] *California Institutes of Technology, Pasadena, California, USA.*

Introduction: The PASADENA (Parahydrogen And Synthesis Allows Dramatically Enchanced Signal Alignment) method offers a promise of increasing the sensitivity of magnetic resonance (MR) over 10,000 times through hyperpolarization of target ^{13}C nucleus during molecular hydrogenation (1-3). Here, we present a study of a new class of agents, which target binding to atherosclerotic plaque by means of fluoro-carbon moiety and utilize a moiety for PASADENA signal enhancement. ^{13}C magnetic resonance imaging (MRI) and magnetic resonance spectroscopy (MRS) with signal enhancement over 10,000 fold offer multiple advantages including sub-second experimental time, which is especially attractive for cardiac applications. This class of agents potentially enables the subsecond noninvasive MRI study of cardiac plaque formation with increased spatial resolution and high chemical specificity.

Purpose: We identify a lipid targeted atherosclerotic plaque binding molecule(s), that will bind to vessels of small caliber like coronary artery, employing binding assays to dimyristoylphosphatidylcholine (DMPC) by ^{19}F solid-state nuclear magnetic resonance (ssNMR) spectroscopy to satisfy the following requirements: PASADENA moiety with C=C double bond for parahydrogen molecular addition, solubility in aqueous buffers, and high affinity for atherosclerotic plaque.

Methods: We utilized acrylate moiety for PASADENA, which has been shown very successful in *in vitro* and *in vivo* application. Hydrofluorocarbon moiety was inserted as corresponding arcylate ester. ^{19}F NMR spectroscopy was employed for binding assays utilizing ssNMR. ^{19}F spectroscopy provides high sensitivity silimar to ^{1}H. In addition, fluorinated methyl group has a distinct ^{19}F chemical shift. When fluorinated molecule binds lipid membrane mimicking atherosclerotic plaque, ^{19}F resonance of its fluorinated methyl group shifts by up to few ppm and becomes broader due to non-zero chemical shift anisotropy typical for solids, Figure 1. Binding assays were performed in Bruker Avance data acquisition system at 4.7T.

Results: Out of many commercially available candidates two molecules were selected for lipid binding studies to DMPC membranes: 4,4,5,5,6,6,7,7,8,8,9,9,9-tridecafluoro-2-hydroxynonyl acrylate (TDHA) and 2,2,3,3-tetraflroro-propyl acrylate (TFPA) after preliminary screening for solubility in water. While both candidates demonstrated significant binding to hydrated DMPC membranes, TDHA has very low solubility of <0.2 mM and thus unattractive. TFPA, on the other hand, has solubility of $\sim$20 mM in phosphate buffer at physiological pH $\sim$7. The kinetics experiment demonstrated that this class of fluorocarbon acrylates binds to the lipid membrane within the first minute of mixing. TFPA binds to DMPC bilayers in 5:1 molar distribution ratio corresponding to $\sim$5% enrichment of DMPC membranes by TFPA by weight at 45°C (Fig. 1). Thirty-three percent of all TFPA molecules are partitioned in lipid membranes.

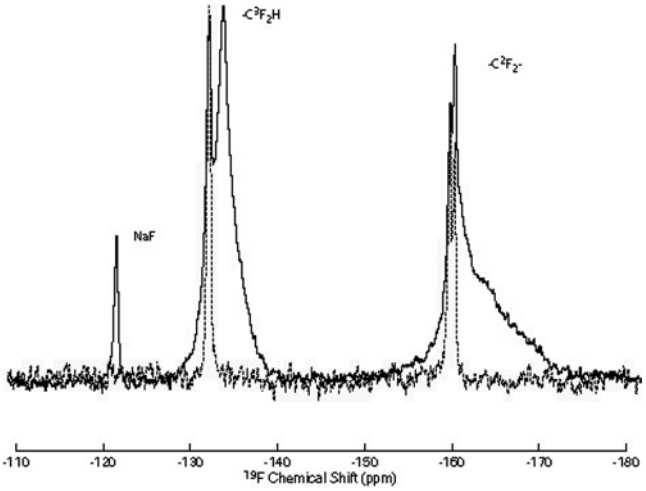

FIG. 1. Solid trace corresponds to the binding experiment of TFPA to DMPC lipid membrane while dashed trace corresponds to the spectrum recorded from 20 mM TFPA solution in water.

Conclusion: Our results demonstrated efficient and rapid binding of TFPA to the lipid membranes mimicking atherosclerotic plaque accompanied by its higher solubility in aqueous buffer, which shows an excellent prospect of employing this class of molecules for *in vivo* hyperpolarized studies on atherosclerotic plaque formation. Experiments with the hyperpolarized ^{13}C spectroscopy and imaging are underway.

ACKNOWLEDGEMENT

EYC and BDR thank RSRI for generous support. SKC is American Heart Association (AHA) undergraduate summer fellow and thank Daniel Tofan for designing TDHA. PB is grateful to AHA, ABTA, SURF & James G. Boswell Foundation for support. DPW thank Beckman Institute Pilot Award. Additionally, we acknowledge Prof. Peter Dervan, Prof. William Perman and Dr. William Opel for the support of PASADENA program.

REFERENCES

1. Bhattacharya P, et al. Magnetic Resonance Materials in Physics Biology and Medicine 2005;18:245–256.
2. Bowers CR, et al. Journal of the American Chemical Society 1987;109:5541–5542.
3. Fayad et al. Magn Reson Imag Clin N Am 2003;11:101–113.

403. STRAIN ANALYSIS OF TAGGED MRI USING GABOR FUNCTIONS

Leon Axel, PhD, MD, Sohae Chung, PhD, Ting Chen, PhD.
NYU Medical Center, New York, New York, USA.

Introduction: Cardiac cine MRI with magnetization tagging produces images with tag lines that move with the underlying muscle. However, practical quantitative analysis of this motion requires automated tracking of the tags. One previous approach to tag tracking has involved the use of HARP analysis, which is essentially phase analysis of a single side band demodulation of the tags, carried out in the Fourier domain. We here report on a related but different fully automated tag analysis approach, using Gabor filters.

Purpose: To describe and demonstrate the use of Gabor filter banks for automated analysis of regional cardiac function from tagged MRI.

Methods: Gabor filters are sinusoidally modulated Gaussians that can be convolved with an image to extract the local periodic "stripe" content. The response to a pair of filters with sine and cosine modulations can be used to find the local tag phase. The filtering operation can be efficiently carried out in the Fourier domain. After the heart starts to contract, the local tag spacing and orientation may change. The response to a bank of Gabor filters with different spacing and orientation can be used to recover corresponding information on the local tag pattern. From the response to the filter bank, we can estimate the local position (phase) relative to the tag pattern; as the tags move, the corresponding changing phase gives an Eulerian description of the motion component orthogonal to the initial tags. Alternatively, the phases at each position at a given reference time can be tracked to their corresponding new positions over the cardiac cycle, to provide a Lagrangian description of the motion. As long as the motion between frames is less than a tag spacing, we can readily overcome problems of phase aliasing. Combining such data from two sets of images with orthogonally oriented tags, or from one set of images with two sets of tags in a grid pattern, we can generate a full description of the in-plane motion. The Lagrangian motion data can then be used to calculate the corresponding local strain deformation of the heart wall. In addition, the output of the filter bank can be used to generate a tag-free filtered image, with the (untagged) blood suppressed, which can be used in segmentation of the heart wall. Although the Gabor filtering and subsequent analysis steps can be carried out automatically without segmentation, masks derived from cardiac segmentation can be used to suppress undesired analysis results from outside the heart wall.

Results: Representative automatic analysis results on grid-tagged short axis images of a normal volunteer (initial tag spacing 5.6 pixels) are shown in the Figure, including: (*a*) midsystolic image, (*b*) corresponding extracted motions of initially tagged positions, (*c, d*) corresponding displacement fields (units of pixels) in vertical (c) and horizontal (d) directions, shown in masked LV region, (*e*) corresponding local principal strains (red greatest and blue least), (*f*) time course of principal strains in representative inferolateral region of interest (red circle marked in e).

Conclusions: Gabor filter banks provide an attractive alternative to HARP analysis of tagged MRI. While both approaches provide rapid and automated analysis methods, the Gabor filter banks are relatively robust to the changes in tag spacing and orientation that may occur during the cardiac cycle, and

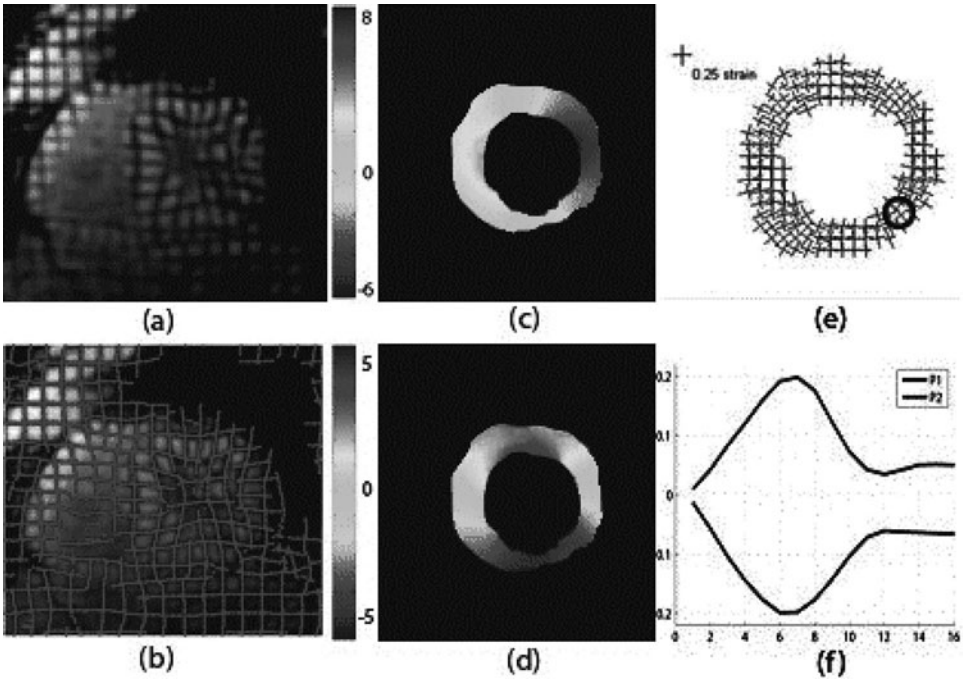

which may cause problems for the usual fixed spatial frequency HARP approach. In addition, the effective double side band approach of the Gabor filters should provide a relative SNR advantage over the single side band HARP method. In both cases, however, we need a sufficient density of tags, as both methods rely on finding the regional phase of a locally periodic tag pattern.

404. ROLE OF CORONARY MAGNETIC RESONANCE ANGIOGRAPHY IN EVALUATION OF ANOMALOUS CORONARY ARTERIES

Vikas K. Rathi, MD,[1] Ronald M. Razmi, MD,[2] Mark Doyle, PhD,[1] Agostino Meduri, MD,[3] Tony G. Farah, MD,[1] Benigno Soto, MD,[4] Gerald M. Pohost, MD,[5] Robert W. W. Biederman, MD.[1] [1] ***Allegheny General Hospital, Pittsburgh, Pennsylvania, USA,*** [2] ***Heart Center of Indiana, Indianapolis, Indiana, USA,*** [3] ***Universita Cattolica del S. Cuore, Rome, Italy,*** [4] ***University of Alabama at Birmingham, Birmingham, Alabama, USA,*** [5] ***University of Southern California, Los Angeles, California, USA.***

Background: X-ray cineangiography (CATH) has been the imaging modality of choice for assessment of the coronary arteries. However, due to its two-dimensional nature, it does not reliably delineate the proximal course of anomalous coronary arteries in relation to the aorta or pulmonary artery. This information is often critical to the management of these patients. CT angiography is three-dimensional, with excellent spatial resolution but high radiation and contrast side effects. Preliminary data indicate that coronary magnetic resonance angiography (CMRA) is an effective tool in defining the origin and proximal course of these arteries where identification of intraluminal stenosis is not the primary aim. We compared the accuracy of CMRA to CATH in 37 consecutive patients referred with a diagnosis of anomalous coronary arteries.

Methods: A retrospective evaluation of the charts of patients referred to CMRA for evaluation of anomalous coronary arteries was performed. Each patient underwent CMRA on a 1.5T magnet (GE Signa CVi; Milwaukee, Wisconsin, USA) After scout images were obtained, axial T1-weighted spin echo sequences were used to determine the location of the aortic root and pulmonary artery (PA), as well as the ostial origin of the coronaries. This was followed by series of cardiac-gated, FIESTA double oblique slices (slice thickness: 5 mm, matrix 224 × 240, FOV 30 X 30, NEX − 0.8) during breath holding. In addition, double oblique breathhold SE with thin slices and dedicated coronary 3D FIESTA block imaging (TR: 3.8, TE − 1.8, TI − 86, martrix 224 × 160, FOV 30 × 30, NEX − 0.5) was also performed where required. All the coronary acquisitions were performed without administration of contrast agent.

Results: After initial review of the results of the CMRA, blinded comparison was made with CATH and consensus was reached regarding the exact course of these anomalies. A second blinded review by two CATH experts with over 70 years of cumulative angiography experience was performed on a subset of 61% (n = 22) cases where CATH films was available for second review. CMRA independently delineated the origin and proximal course of the coronary vessels in all 36 patients. Coronary anomalies diagnosed by CMRA included right-sided origin of left coronary artery (n = 10), right-sided origin of circumflex artery (n = 8), slight anterior or posterior displacement of left coronary artery (n = 2), left-sided origin of right coronary artery (RCA) (n = 12), posterior displacement of RCA (n = 3), common ostium of left and right coronary artery (n = 2), left coronary from non coronary cusp (n = 1), and normal coronaries (n = 3). One patient was determined to have right coronary origin from main pulmonary artery with collaterals from left. More importantly, there was only 27.7% agreement between CATH and CMRA, thereby CMRA completely changing the findings of the CATH regarding the course of the anomalous arteries. The most fatal anomaly, such as interarterial course of the major vessel, was present in 16 patients by CMRA, out of which only 6 were identified by CATH (concordance 37.5%). Therefore, a 62.5% rate of new diagnosis of interarterial course delineation was made and these patients were referred for timely surgical intervention. On the other hand, 5 patients were incorrectly classified by CATH as having an interarterial course and appropriate CMRA diagnosis of non-interarterial course was made thereby avoiding needless surgical intervention.

Conclusion: To our knowledge this is the largest case series of independent anomalous CMRA simultaneously compared to X-ray angiography. CMRA is a noninvasive, nonionizing, devoid of radiation and accurate technique for diagnosis of patients with anomalous coronary arteries. In this series, it correctly identified every anomaly and prevented many needless surgeries, while identifying appropriate candidates for surgery in many life-threatening instances. This degree of accuracy qualifies CMRA as the imaging modality of choice for assessing proximal course of the anomalous coronaries in a safe and expedient manner.

405. IS THE LEFT VENTRICLE SPARED FROM RIGHT VENTRICULAR FAILURE IN SEVERE PULMONARY HYPERTENSION?

Vikas K. Rathi, MD, Srinivas Murali, MD, Madhavi Akkineni, MD, Ketheswarm Caruppannan, MD, June Yamrozik, RT(MR), Ronald B. Williams, Carrie Melegari, Diane Vido, MS, Mark Doyle, PhD, Robert W. W. Biederman, MD. ***Allegheny General Hospital, Pittsburgh, Pennsylvania, USA.***

Introduction: In patients with long standing pulmonary hypertension (PHTN) the right ventricle (RV) is the primary organ to withstand the increased pressure and volume which overtime leads to insidious right heart failure. However, the effect of decreased preload due to pulmonary hypertension and failing

right heart on the left ventricular (LV) function and geometry is unknown. Theoretically, the left ventricular function should be spared; however, the 2D and 3D geometry could change due to the interventricular dependence and remodeling contributing to impaired LV mechanics. Clinically, it is often noted that, despite a small LV, the perception of a hypertrophied LV with abnormal geometry by 1D and 2D techniques is present.

Hypothesis: We hypothesize that in PHTN, there will be abnormal LV volumetrics and geometry due to the impaired preload due to RV dysfunction and that a 3D evaluation will confirm or refute the 1D and 2D observations. We further speculate that RV volume overload due to intracardiac shunting (secondary PHTN) will overload the RV to a greater extent than RV failure due to primary PHTN.

Methods: We analyzed 19 subjects (age: 52 ± 19) with severe pulmonary hypertension by CMR to understand the pathophysiology of RV and LV function and geometry. The patients were divided in two groups, 7 subjects with idiopathic pulmonary arterial hypertension (IPAH) and 12 subjects with secondary pulmonary arterial hypertension (SPAH) due to congenital left to right shunting ($n = 5$), ASD ($n = 4$), VSD ($n = 1$), connective tissue disorder ($n = 4$), ischemic heart disease ($n = 1$) and primary lung disease ($n = 2$). All patients underwent standard CMR imaging on (GE 1.5T EXCITE HD, Milwaukee, Wisconsin, USA). To display anatomy, standard fast spin-echo images in transverse axis were obtained along with double oblique contiguous FIESTA images to obtain 3D RV and LV volumes (EDV, ESV, EF, MASS, relative wall thickness [RWT]) indexed to body surface area. Tricuspid annular plane systolic excursion (TAPSE) was also measured.

Results: Patients with PHTN had a markedly elevated RVEDVI relative to LVEDVI (120 ± 78 mL/m^2) vs. (66 ± 26 mL/m^2) representing very opposite ends of the normal volume spectrum. RVEDV was $\geq$2 standard deviations (SD) above normal while LVEDVI was just below normal. Distinguishing IPAH from SPAH demonstrated that RVEDV trended much higher (147 ± 116 mL/m^2 vs. 105 ± 42 mL/m^2 while there was virtual superimposition of LVEDVI independent of mechanism of PHTN (72 ± 29 mL/m^2 vs. 68 ± 16 mL/m^2 $p = NS$). Evaluation of LV geometry revealed by 1D normal septal and posterior wall thickness that translated into normal RWT: 0.35 ± 0.09, while LVMI was low normal: 55 ± 22g/m^2 (normal: 59 ± 11). Finally, 3D mass/volume ratio was normal for the LV: 0.83 (normal: 0.74 ± 0.15) as it was for 3D RV mass/volume ratio: 0.24 ± 0.11(normal: 0.22 ± 0.15). TAPSE, as expected was positively correlated with the RVEF ($r = 0.59$, $p < 0.05$).

Conclusion: The effect on LV volumetrics in long standing severe PHTN have long been debated. Using 3D CMR, despite the concept that the LV is smaller and possesses abnormal geometry by 1D and 2D interrogations, the 3D LV metrics are entirely normal. Unexpectantly, the LV, despite markedly impaired preload, especially in IPAH relative to SPAH, regulates normal volumetrics independent of the etiology of PHTN. Paradoxically, IPAH appears to have limited ability to withstand pressure overload as compared to volume overload resulting in marked dilation while it is known that for the LV, the exact opposite is true. This incriminates the RV in IPAH as possessing a defect in its ability to appropriately hypertrophy in the face of pressure overload, implicating a myocardial defect at the level of mRNA.

406. TIME COURSE OF REGIONAL FUNCTIONAL RECOVERY OF INFARCTED, ADJACENT AND REMOTE MYOCARDIAL SEGMENTS IN PATIENTS WITH REPERFUSED MYOCARDIAL INFARCTION

Henrik Engblom, MD,[1] Erik Hedström, PhD,[1] Einar Heiberg, PhD,[1] Galen S. Wagner, MD,[2] Olle Pahlm, MD, PhD,[1] Håkan Arheden, MD, PhD.[1] [1]***Lund University Hospital, Lund, Sweden,*** [2]***Duke University Medical Center, Durham, North Carolina, USA.***

Introduction: The transmurality of infarction has been shown to affect the probability of regional functional improvement of the left ventricle (LV) after acute myocardial infarction. The time course of this functional improvement, however, is not completely known.

Purpose: Therefore, the aim of this study was to explore how regional LV function change over time in infarcted, adjacent as well as in remote myocardial segments after acute infarction.

Methods: Twenty-two patients with reperfused first-time myocardial infarction were prospectively enrolled. Cardiac magnetic resonance imaging (MRI), including cine imaging and delayed contrast enhanced (DE) imaging for infarct visualization, was performed 1 day, 1 week, 6 weeks, 6 months and 1 year after admission. Regional wall thickening was determined in 72 LV segments (6 slices, 12 segments in each) derived from the cine images. These segments were categorized into different groups based on the infarct transmurality assessed by DE-MRI at day 1.

Results: For all time points, there was a progressive decrease in wall thickening as infarct transmurality increased ($p < 0.001$) (Fig. 1). There were varying patterns of regional recovery of wall thickening depending on the localization and the initial infarct

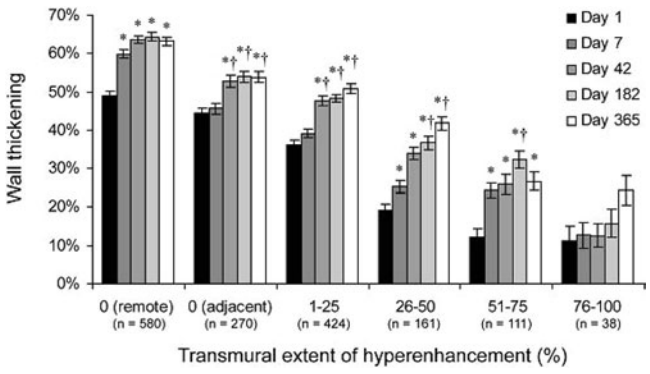

FIG. 1.

transmurality of the segments. Note that the remote LV segments improved in wall thickening, especially during the first week. Note also the late recovery of function in segments showing 76-100% transmurality on the initial examination. Vertical bars indicate standard error of the mean. $^{*}p < 0.05$ versus Day 1; $^{\dagger}p < 0.05$ versus Day 7.

Conclusions: The time course of recovery of regional LV function after reperfused myocardial infarction is dependent of infarct transmurality in the region, but also of the myocardium surrounding it.

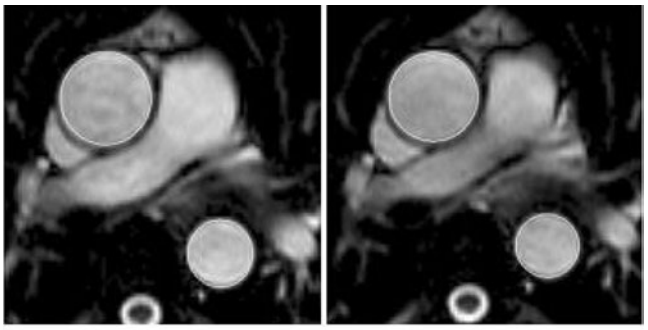

FIG. 1.

407. CHANGES OF AORTIC SIZE AND DISTENSIBILITY WITH AGE MEASURED BY SSFP CINE IMAGING IN HEALTHY VOLUNTEERS

Elisabeth D. Burman, Philip J. Kilner. ***Royal Brompton Hospital, London, United Kingdom.***

Introduction: Aortic size increases and aortic distensibility decreases with age. Normal values for aortic size are relevant to the assessment of abnormalities of the aorta, for example in Marfan's disease. They have previously been obtained using spin-echo and gradient echo imaging. Steady state free precession (SSFP) breathhold cine imaging is now widely used in CMR, giving cine acquisitions with good blood-tissue contrast.

Purpose: To establish normal ranges of aortic root size and distensibility in healthy volunteers by SSFP imaging in specified planes of acquisition with respect to gender and age.

Methods: Sixty healthy normotensive volunteers were investigated (31 M, 29 F, age range 20–80, average age 49 M, 47 F) comprising three groups aged 20–40, 40–60, 60–80 years, with ten subjects of each gender in each age range. CMR was performed using a 1.5T Siemens Sonata scanner. An oblique coronal view of the left ventricular outflow tract was acquired from transaxial and coronal multislice scouts. From this plane, an orthogonal SSFP cine with voxel dimensions $6 \times 1.7 \times 1.4$ mm, was obtained transecting the ascending and descending aorta at the level of the right pulmonary artery. This acquisition was used to measure systolic and diastolic cross sectional areas and diameters. The% systolic distension was calculated as [(maximum area–minimum area) $\times$ 100 $\div$ minimum area]. The% distensibility was then calculated as the% systolic distension $\div$ pulse pressure.

Results: The means $\pm$ standard deviations (and 95% confidence intervals) for respective groups are shown in the tables. Aortic cross sectional areas and dimensions were found to increase with age and were found to be larger in men than women.

Aortic area measurements (cm^2) with distension (%) and distensibility (%/mmHg), $\pm$ SD

Male	Ascending aorta-systole	Ascending aorta-diastole	% dist	%/ ΔP	Descending aorta-systole	Descending aorta-diastole	% dist	%/ ΔP
20–40	5.7 ± 1.3 (3.2–8.2)	4.5 ± 1.0 (2.5–6.5)	27.2	0.57	3.0 ± 0.6 (1.8–4.2)	2.5 ± 0.5 (1.6–3.5)	19.4	0.42
40–60	7.0 ± 1.5 (4.0–10)	6.2 ± 1.5 (3.2–9.2)	14.0	0.35	4.3 ± 0.8 (2.7–6.0)	3.9 ± 0.9 (2.2–5.6)	11.9	0.30
60–80	7.5 ± 1.5 (4.6–10)	6.8 ± 1.4 (4.0–9.6)	10.2	0.22	4.4 ± 0.5 (3.3–5.5)	4.0 ± 0.6 (2.8–5.2)	9.9	0.20
All subjects	6.7 ± 1.6 (3.6–9.8)	5.8 ± 1.6 (2.6–9.0)	17.1	0.38	3.9 ± 0.9 (2.1–5.7)	3.5 ± 0.9 (1.6–5.3)	13.7	0.31
Female	Ascending aorta-systole	Ascending aorta-diastole	% dist	%/ ΔP	Descending aorta-systole	Descending aorta-diastole	% dist	%/ ΔP
20–40	4.8 ± 0.7 (3.4–6.1)	3.7 ± 0.5 (2.6–4.8)	29.7	0.80	2.5 ± 0.5 (1.5–3.5)	2.1 ± 0.4 (1.3–2.9)	18.4	0.48
40–60	6.5 ± 1.0 (4.5–8.5)	5.8 ± 1.1 (3.7–7.9)	13.1	0.31	3.3 ± 0.7 (1.8–4.7)	2.9 ± 0.7 (1.6–4.2)	11.9	0.28
60–80	7.2 ± 1.4 (4.5–9.9)	6.6 ± 1.4 (3.9–9.3)	9.0	0.18	3.7 ± 0.5 (2.7–4.7)	3.4 ± 0.5 (2.4–4.3)	10.3	0.20
All subjects	6.1 ± 1.5 (3.3–9.0)	5.4 ± 1.6 (2.2–8.5)	17.3	0.43	3.2 ± 0.8 (1.6–4.7)	2.8 ± 0.7 (1.3–4.3)	13.5	0.32

Aortic% distension and distensibility (%/mmHg) were found to decrease with age by very similar amounts in both groups. Comparing the 20 40-year-olds with the 60–80-year-olds, systolic ascending aortic areas increased by 1.8 cm^2 in males and 2.4 cm^2 in females over the 40 year period.

Systolic ascending aortic diameters increased by 4 mm in males and 6 mm in females over the same period.

Conclusions: We provide age-related values for aortic root size and distensibility in healthy volunteers by SSFP imaging.

408. T2-WEIGHTED CMR IN SYSTEMIC LUPUS ERYTHEMATOSUS: RELATION TO DISEASE ACTIVITY

Hassan Abdel-Aty, Natalie Siegle, Rainer Dietz, Jeanette Schulz-Menger. ***Franz-Volhard-Klinik, Kardiologie, Charité Campus Buch, Universitätsmedizin Berlin, Helios-Klinikum, Berlin, Germany.***

Background: Systemic lupus erythematosus (SLE) is a multiorgan inflammatory disorder mainly affecting women and is associated with high cardiovascular morbidity and mortality. Little is known about the myocardial tissue characteristics in SLE and their relation to disease activity. T2-weighted cardiovascular magnetic resonance (CMR) is sensitive to myocardial edema, which is shown pathologically to be a component of the myocardial inflammatory response in SLE. We hypothesized that global myocardial T2 signal abnormalities relate to disease activity in SLE.

Methods: We studied 18 SLE patients (17 females, 35 $\pm$ 11 y) and 10 healthy volunteers (9 females, 30 $\pm$ 11 y). Diagnosis followed the criteria of American Rheumatism Association; assessment of SLE activity was based on the European Consensus Lupus Activity Measurement (ECLAM) index. Patients were classified into active ($n = 8$, ECLAM > 5) or inactive ($n = 10$, ECLAM < 5). CMR was performed on 1.5T scanner. Using a body coil, breath hold triple inversion recovery T2-weighted (STIR) images were acquired in 3 short axis slices (TR: 2RR, TE: 61). Corresponding spin echo T1-weighted images were acquired in the same slice positions to facilitate identification of the skeletal muscle. SSFP Cine images were acquired in short and long axis views. Using a dedicated software (MASS®, Medis, Netherlands), endo- and epicardial contours were drawn in each slice and the absolute T2 SI was measured and related to that of the latissmus dorsi muscle in the same slice to calculate the relative T2 ratio. This was averaged in all slices to obtain the global relative T2 ratio.

Results: Ejection fraction (EF) was not significantly different between groups (controls: 65 $\pm$ 5, inactive: 66 $\pm$ 6, active 62 $\pm$ 9; $p =$ ns for all groups). In contrast relative T2 ratio was significantly higher in active SLE (controls: 1.7 $\pm$ 0.2, inactive: 1.9 $\pm$ 0.2, active: 2.1 $\pm$ 0.2; $p < 0.001$ for all). Relative T2 ratio tended to correlate with the ECLAM score ($p = 0.059$) but not with EF or age. SLE activity could be identified using a relative T2 cutoff value of 1.9 (AUC = 0.91, $p < 0.001$).

Conclusion: Our data shows that global myocardial T2 is elevated in active SLE, which may represent subclinical myocardial involvement.

409. GENDER-RELATED DIFFERENCES IN LEFT VENTRICULAR REMODELING AND FIBROSIS IN HYPERTROPHIC CARDIOMYOPATHY: INSIGHTS FROM CMR

Hassan Abdel-Aty,[1] Andre Rudolph,[1] Thomas Elgeti,[2] Bernd Hamm,[2] Rainer Dietz,[1] Jeanette Schulz-Menger.[1] ***[1] Franz-Volhard-Klinik, Kardiologie, Charité Campus Buch, Universitätsmedizin Berlin, Helios-Klinikum, Berlin, Germany, [2] Institut für Radiologie, Charite Campus Mitte, Universitätsmedizin Berlin, Berlin, Germany.***

Background: Population studies show that gender is an independent risk factor for heart failure mortality in hypertrophic cardiomyopathy (HCM). Yet, the interaction between gender, myocardial fibrosis and remodeling in HCM whether obstructive (HOCM) or non-obstructive (HNCM) remains poorly understood. Cardiovascular magnetic resonance (CMR) is the current noninvasive gold standard to assess myocardial mass, volumes and fibrosis making it the suitable candidate to explore this interaction.

Methods: We studied 64 HCM patients (28 females, 51 $\pm$ 16 y) who were categorized into HNCM ($n = 31$) or HOCM ($n = 33$) based on LVOT obstruction (LVOT area <2.7 cm^2). Sixty healthy subjects (31 females, 34 $\pm$ 10 y) served as our control group. We applied SSFP cine imaging and late enhancement (LE) after iv gadolinium injection covering the left ventricle in short axis slices on a 1.5T scanner. End-diastolic volume and total myocardial mass were quantified and the LV remodeling index (LVRI = EDV/mass) was calculated. LE was manually traced and expressed as percentage of the total LV mass using a dedicated software (MASS, Medis, Netherlands).

Results: Females had a lower LVRI in the control (0.7 $\pm$ 0.1 vs. 0.9 $\pm$ 0.2, $p < 0.001$) and HNCM (1.1 $\pm$ 0.2 vs. 1.5 $\pm$ 0.5, $p < 0.001$) groups compared to males. In contrast, HOCM females had a similar LVRI compared to males (1.8 $\pm$ 0.5 vs. 1.7 $\pm$ 0.4, $p =$ ns). The mean LVRI difference between HOCM females and female controls was higher (1.1; CI: 0.8 to 1.3) than that between HOCM males and male controls (0.8; CI: 0.6 to 1.0). Regression analysis showed a significant interaction between gender and LVRI ($p = 0.008$). LE indicating myocardial fibrosis was noted in 58% of the patients. No significant relation was found between myocardial fibrosis and gender in any of the patient subgroups (Chi square, $p =$ ns). Percentage myocardial fibrosis was not significantly different between HOCM (8 $\pm$ 5 vs. 6 $\pm$ 6% $p =$ ns) and HNCM (8 $\pm$ 9 vs. 9 $\pm$ 12%; $p =$ ns) gender subgroups.

Conclusion: Our data suggest a complex interaction between gender, obstruction and LV remodeling in HCM in which HOCM females exhibit a disproportionate degree of remodeling. This

	Females			Male		
	Control	HNCM	HOCM	Control	HNCM	HOCM
EF	68 ± 5	71 ± 12	82 ± 7	62 ± 6	72 ± 7	75 ± 10
LVMI	0.6 ± 0.1g/cm	0.8 ± 0.2g/cm	1.3 ± 0.4 g/cm	0.8 ± 0.2 g/cm	1.3 ± 0.3 g/cm	1.5 ± 0.4 g/cm
EDV	127 ± 20 mL	117 ± 25 mL	120 ± 29 mL	164 ± 38 mL	160 ± 42 mL	159 ± 56 mL
LVRI	0.7 ± 0.1	1.1 ± 0.2	1.8 ± 0.4	0.9 ± 0.2	1.5 ± 0.5	1.7 ± 0.4

confirms recent epidemiological studies showing that HOCM women have a high risk of heart failure mortality. Gender does not appear to influence the development or the quantity of fibrosis in HCM.

410. CMR STUDIES IN PATIENTS WITH CHRONIC TOTAL OCCLUSION OF A CORONARY ARTERY

Sandra Pujadas,[1] Francesc Carreras,[1] Carlos Cotes,[1] Ruben Leta,[1] Xavier Alomar,[2] Victoria Martin,[1] Manel Sabate,[1] Guillem Pons-Llado.[1] [1] *Hospital de la Santa Creu i Sant Pau, Barcelona, Spain,* [2] *Clínica Creu Blanca, Barcelona, Spain.*

Aim: To assess the presence and extent of myocardial necrosis and left ventricular function by CMR in a series of patients with chronic total occlusion of a coronary artery.

Methods: Forty-one patients (5 women; age 61 ± 10; 43 y.o.) who were found to have an occlusion of at least one coronary artery at a conventional angiography were submitted to a CMR exam including global and regional ventricular function, and late gadolinum enhancement studies. Regional contractility was analysed using the 17-segmental model and classified at each one as: 1= normal; 2 = hypokinesia; 3 = akinesia; 4 = diskinesia. The resultant mean value was considered as a segmental motility index (SMI). The presence of myocardial late contrast enhancement was assessed and classified as none, transmural, or non-transmural. The total mass of myocardial necrosis was also calculated on the late gadolinium enhancement images. Also, left ventricular ejection fraction (LVEF) was obtained.

Results: Coronary artery occlusion distribution was as follows: Left Main n = 1; LAD n = 10; LCX n = 2; RCA n = 20; LAD and RCA n = 6; LCX and RCA n = 2. Thirty-three patients (80%) showed late hyperenhancement and only in 12 (36%) of them gadolinium hyperenhancement had a transmural distribution. When comparing the group with and without late hyperenhancement there were no significant differences in terms of segmental contractility (SMI 1.27 ± 0.35 vs. 1.12 ± 0.09, p = 0.82, respectively) nor in LVEF (58.57 ± 12.62 vs. 65.00 ± 10.25, p = 0.19, respectively). Collateral circulation was judged as present by angiography in 29 patients. When comparing these patients with the ones with no collateral circulation there were no significant differences in total necrotic mass (6.48 ± 8.48 vs. 5.15 ± 5.13, p = 0.7, respectively), nor in SMI (1.26 ± 0.36 vs. 1.18 ± 0.20, p = 0.98, respectively), nor in LVEF (59.1 ± 13.89 vs. 61.00 ± 7.85%, p = 0.70, respectively). One patient with no collateral circulation (1/12) did not show late hyperenhancement.

Conclusions:

1. Twenty percent of patients with proven chronic total occlusion of a coronary artery do not present with myocardial necrosis in late hyperenhancement CMR studies.
2. The degree of impairment of segmental wall motion and LVEF does not differ between patients with and without myocardial necrosis, which indicates the presence of hibernating myocardium in the group of patients not showing late hyperenhancement.
3. In these patients, the presence of collateral circulation does not seems to imply significant differences in terms of necrotic mass or left ventricular systolic function.

411. COMPENSATION FOR LONGITUDINAL CARDIAC MOTION INFLUENCES LEFT VENTRICULAR VOLUMES AND MASS MEASUREMENTS

Bernard P. Paelinck, MD, PhD, Patrick Berkovic, MD, Maarten Hemmink, MD, Paul Parizel, MD, PhD, Christiaan J. Vrints, MD, PhD. ***University Hospital Antwerp, Edegem, Belgium.***

Introduction: Accurate assessment of left ventricular (LV) volumes, ejection fraction and mass has important diagnostic and prognostic implications. Software for automatic quantitative analysis of cine MR images uses automated segmentation of endocardial and epicardial borders of short-axis cardiac images. Border detection is however hampered by through-plane motion and partial volume averaging in the basal and curved apical segments.

Purpose: To evaluate the impact and reproducibility of software that compensates for longitudinal cardiac motion, compared with standard software for the analysis of left ventricular volumes and mass.

Methods: Twenty-three consecutive patients underwent 1.5-Tesla cine MR imaging of the entire heart in the long-axis and short-axis orientation with breath-hold SSFP imaging. Offline analysis based on short-axis images was performed using standard software (Medis MASS) and using software based on short-axis and both two-chamber and four-chamber images to

determine apex and base and to compensate for longitudinal left ventricular expansion and shortening (CAAS-MRV). Intraobserver and interobserver reproducibility was assessed by using Bland-Altman analysis.

Results: Compared with MASS software, CAAS-MRV resulted in significantly smaller end-diastolic (156 ± 48 mL versus 167 ± 52 mL, $p = 0.001$) and end-systolic LV volumes (79 ± 48 mL versus 94 ± 52 mL, $p < 0.001$). In addition, CAAS-MRV resulted in higher LV ejection fraction (52 ± 14% versus 46 ± 13%, $p < 0.001$) and calculated LV mass (154 ± 52 g versus 142 ± 52 g, $p = 0.004$). Intraobserver and interobserver limits of agreement were similar for both methods.

Conclusions: Compensation for partial volume effects and through-plane LV motion resulted in smaller LV volumes, higher ejection fraction and higher calculated LV mass as compared to standard analysis software. Reproducibility of software using compensation for long-axis LV motion to analyze LV volumes and mass is high.

412. COMPARISON OF A FAST PHASE-SENSITIVE INVERSION RECOVERY SEQUENCE (PSIR) AND A CONVENTIONAL SEGMENTED 2D GRADIENT ECHO—RECALL SEQUENCE IN ASSESSING DELAYED CONTRAST ENHANCEMENT IN NONISCHEMIC CARDIOMYOPATHY

Thomas Elgeti, MD, Moritz Wagner, Hassan Abdel-Aty, MD, Bernd Hamm, MD, PhD, Rainer Dietz, MD, PhD, Jeanette Schulz-Menger, MD. ***CharitÃ© University Medicine, Berlin, Germany.***

Background: Reliable detection of myocardial scarring in nonischemic cardiomyopathy is time-consuming using techniques requiring determining optimal inversion time. Therefore, we evaluated an inversion-time-free approach using a fast phase-sensitive inversion recovery sequence (PSIR) to detect and quantify late enhancement (LE).

Patients and Methods: Sixteen patients (mean 40 y, 7 female) with nonischemic cardiomyopathy and evidence of LE were evaluated. Cine-SSFP in three long axes and in the left ventricular short axis was performed after 0.2 mmol/kg gadolinium DTPA using a segmented 2D IR turbo fast low-angle shot (GRE) sequence (TE 4.3 ms, TR 750 ms, α 30°, slice thickness 8 or 10 mm, voxel size 1.7 × 1.3 × 8/10 mm) with meticulously adjusted inversion time to null normal myocardium as the standard of reference. Secondly, a fast 2D PSIR- sequence (TE 1.1 ms, TR 700 ms, α 40°, slice thickness 8-10 mm, voxel size 2.5 × 1.7 × 8/10 mm) with TI values of 300 ms was acquired, producing 2 image types—$PSIR_{IR}$ and $PSIR_{Mag}$—in each slice position. $PSIR_{Mag}$ images were excluded from final analysis as image quality was inadequate in some cases. Altogether 40 short-axis slices with LE were evaluated. CNR ($SI_{delayed\ enhancement} - SI_{remote\ myocardium}/ SD_{noise}$) and area (in cm^2) of LE were calculated and compared by two experienced readers. Image quality and confidence level for LE were rated on a five-point scale. Ten patients served as controls for evaluating interobserver variability.

Results: All images were interpretable. CNR was 5.89 for $PSIR_{IR}$ and 12.07 for the conventional GRE images. The mean area of LE was 1.01 ± 0.62 cm^2 for the GRE sequence and 1.10 ± 0.62 cm^2 for $PSIR_{IR}$ (not significant, $p = 0.086$). Two patients with a septal "central line sign" in GRE images showed no delayed enhancement in the PSIR images. The Bland-Altman plot showed a random distribution and no systematic or mean difference. The overall interobserver variability of $PSIR_{IR}$ and GRE was good, resulting in an interclass correlation coefficient of $ICC_{GRE} = 0.93$ and a slightly lower $ICC_{IR} = 0.89$. Imaging time was reduced from 132 s to 19 s. The confidence level and image quality of $PSIR_{IR}$ were comparable to conventional GRE (confidence:1.33 ± 0.84 vs 1.29 ± 0.5, p = ns ; image quality 1.0 ± 0.52 vs.1.44 ± 1,0; p = ns).

Conclusion: Detection and quantification of late enhancement in nonischemic cardiomyopathies are feasible at a significantly shorter scan time using a fast phase-sensitive inversion recovery sequence although the central lign sign was not seen in 2 cases.

413. CMR CORRELATES OF ARRHYTHMIC RISK IN THE MADIT II POPULATION

Chizor Iwuchukwu, MD,[1] Saadi Siddiqi, MD,[1] Sunil Mathew,[1] Thomas O'Donnell, PhD,[2] Jeannette McLaughlin, RN,[3] William Schapiro, RT,[1] Jing Han, PhD,[1] Yi Wang, PhD,[1] Kathy McGrath, RN,[3] Steven M. Greenberg, MD,[3] Stuart Schecter, MD,[3] David Hoch, MD,[3] Vinny Jayam, MD,[3] Joseph Levine, MD,[3] Nathaniel Reichek, MD, FACC, FAHA.[1] ***[1]St. Francis Hospital, Stony Brook University, SUNY, Roslyn, New York, USA, [2]Siemens Corporate Research, Princeton, New Jersey, USA, [3]St. Francis Hospital, Roslyn, New York, USA.***

Background: MADIT II eligible patients (prior myocardial infarction(MI), LV ejection fraction (EF) ≤ 30%) are at increased risk of lethal ventricular arrhythmias. Infarct size and heterogeneity are proposed markers of inducibility of ventricular tachycardia (VT) and outcome risk. We examined LV structure and function including infarct size (Scar) and heterogeneous periphery (gray zone, GZ), (Fig.), in such patients using cardiovascular MRI (CMR).

Methods: Sixty-one patients meeting MADIT II criteria had CMR and were followed for 22 ± 8 months; 43 underwent EPS at intake. CMR delayed enhancement (DE) and volumetric LV cine imaging were performed. Using semiautomated software (Siemens Corporate Research), Scar was defined as signal 2 s.d. above mean remote signal intensity (SI). GZ size was assessed

TABLE 1
Combined Clinical End points and Inducibility

	Combined Clinical End Points				Inducibility at intake		
	No event (n = 27)	Event (n = 34)			Non inducible (n = 14)	Inducible (n = 29)	P
Age	Mean (*s.d.*)	Mean (*s.d.*)	p	p* (age adjusted)	Mean (*s.d.*)	Mean (*s.d.*)	
Age	63.5 (11.5)	69.4 (10.6)	0.04	—	69.1 (9.2)	69.9 (9.1)	0.78
Clinical EF (%)	26.0 (4.4)	22.9 (4.5)	0.01	**0.02**	24.9 (4.3)	23.4 (4.6)	0.38
CMR EF (%)	29.3 (10.3)	25.3 (7.8)	0.09	**0.02**	28.0 (12.6)	26.1 (8.0)	0.62
%Scar	22.0 (12.1)	25.4 (11.0)	0.34	0.30	23.2 (17.0)	24.7 (10.2)	0.78
Scar Mass (gm)	39.3 (16.9)	58.1 (31.9)	0.02	**0.04**	36.7 (18.8)	62.8 (32.3)	**0.04**
Gray Zone 75% (gm)	13.6 (6.8)	18.4 (17.0)	0.21	0.31	10.1 (5.5)	20.5 (17.7)	**0.02**
Grey Zone 50% (gm)	31.3 (13.9)	42.3 (24.0)	0.07	0.10	27.9 (14.2)	46.0 (24.2)	0.07

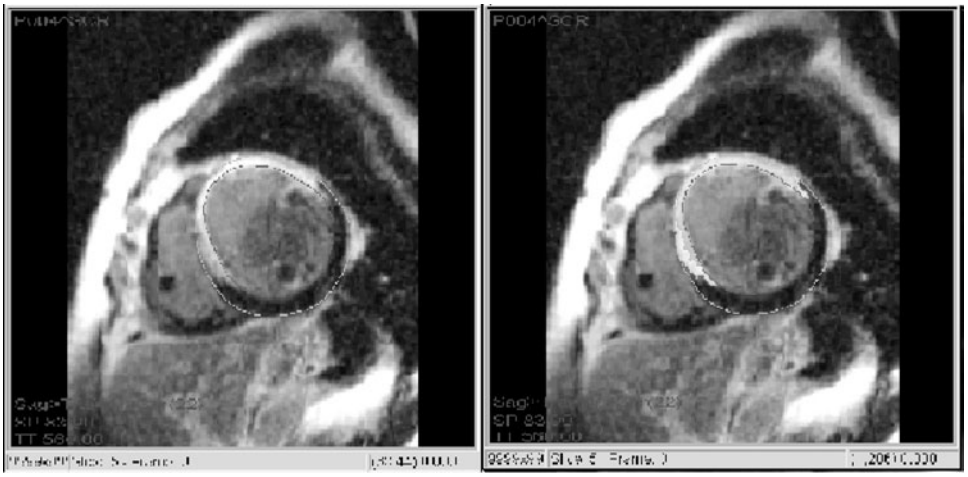

FIG. 1. Myocordial Sear with delayed enhancement (left). Infaret core (red), Gray Zone (yellow) with signal intensity thresholding (right).

at thresholds of 50% and 75% of maximal Scar. Scar, GZ mass, clinical and CMR EF were compared to inducibility of sustained monomorphic VT at EPS and to a combined clinical endpoint including EPS inducibility and follow-up arrhythmic events (sudden death, late EPS inducibility, documented VT, valid ICD firings).

Results: (Table)Absolute Scar size and GZ size at 75% SI were associated with inducibility (p = 0.04, p = 0.02), while clinical and CMR EF and absolute Scar size were associated with a combined clinical event(p = 0.02, p = 0.02, p = 0.04).

Conclusions: Clinical EF, CMR EF, infarct size and grey zone size are all potential markers of increased risk in patients meeting MADIT II criteria.

414. QUANTIFICATION OF MYOCARDIAL INFARCTION SIZE WITH SINGLE-SHOT DELAYED ENHANCEMENT IMAGING. HISTOPATHOLOGIC CORRELATION

Susanna Prat Gonzalez, MD,[1] Borja Ibanez, MD,[1] Antonio Pinero, MD,[1] Gemma Vilahur, PhD,[1] Thomas O'Donnell, PhD,[2] Walter Speidl, MD,[1] Valentin Fuster, MD, PhD,[1] Juan Jose Badimon, PhD,[1] Javier Sanz, MD.[1] [1]*Mount Sinai Medical Center, New York, New York, USA,* [2]*Siemens Corporate Research, Princeton, New Jersey, USA.*

Introduction: Delayed enhancement (DE) imaging of myocardial infarction (MI) with magnetic resonance imaging (MRI) is usually performed with segmented, inversion-recovery fast gradient echo sequences. Single-shot inversion-recovery steady state free precession (SSFP) may be used as an alternative technique because of its shorter imaging time. Single-shot SSFP has been compared with segmented, fast gradient echo, but validation against histopathology, the *gold standard*, has not been performed.

Purpose: Our aim was to validate the extent of MI as assessed by DE-MRI using single-shot SSFP with the more classical histological staining of infarcted area in a porcine model of experimental MI.

Methods: Male Yorkshire albino pigs (n = 6, weight 35 ± 5 kg) underwent the experimental induction of an anterior MI. The MI was induced by 90-minute balloon occlusion of the left anterior descending artery distal to the first diagonal branch. MRI was performed 3 weeks after the infarct, using a 1.5 Tesla clinical magnet, electrocardiographic gating and a ded-

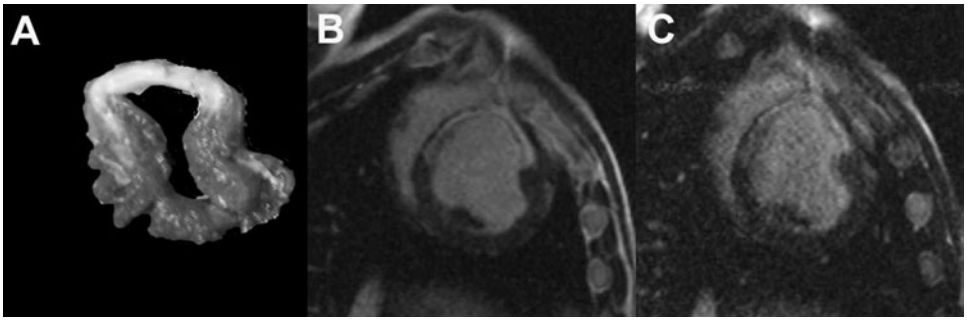

icated phased-array surface coil. DE imaging was performed 10-15 minutes after the administration of 0.2 mmol/kg of Gd-DTPA. The entire ventricle was imaged with contiguous short-axis views. Multislice, single-shot, inversion-recovery SSFP (TrueFISP®) was performed first, during one single breath-hold. Imaging parameters were: TR 3 ms, TE 1.3 ms, TI optimized to null normal myocardium, slice thickness 8 mm, no gap, gating factor 3-4, flip angle 50^o, bandwidth 1150 Hz/px, temporal resolution 432 ms. Subsequently, images were acquired with a segmented, inversion-recovery fast gradient echo sequence (TurboFLASH®) during consecutive breath-holds. Imaging parameters were: TR 8 ms, TE 4 ms, TI optimized to null normal myocardium, slice thickness 8 mm, no gap, gating factor 2-3, flip angle 25^o, bandwidth 160 Hz/px, temporal resolution 184 ms. The field-of-view and matrix size were kept constant for both sequences: 300 $\times$ 225 mm, and 256 $\times$ 144, respectively, leading to an in-plane spatial resolution of 1.6 $\times$ 1.2 mm. After the MRI, the pigs were sacrificed, and staining of the necrotic area was performed with triphenyltetrazolium chloride (TTC). The extent of DE on MRI images was quantified as percentage of the left ventricle using prototype software. Regions of DE were defined as those areas with signal intensity $>$3 standard deviations of the mean signal of remote normal myocardium. In addition, standardized measurement of signal-to-noise ratio (SNR) and contrast-to-noise ratio (CNR) of normal and infarcted myocardium were determined for both sequences. MI sizes by the different techniques were compared using 1-way ANOVA, Pearson's correlation and Bland-Altman analysis. SNR and CNR were compared with paired t-test.

Results: Both MRI sequences were successfully performed in all animals. There were no significant differences in MI size between the imaging modalities (single-shot TrueFISP 16.9 $\pm$ 6.5%, TurboFLASH 17.8 $\pm$ 6.7%), and histopathology 18.8 $\pm$ 7.4%; p = 0.88). Panels A-C (A-histology, B-TurboFLASH, C-single-shot TrueFISP). In comparison with histopathology, the MI size as determined by single-shot TrueFISP showed excellent correlation (r = 0.91, p = 0.01) and agreement (mean bias $-$2%, limits of agreement 4.1%/-8%). SNR and CNR were lower for single-shot TrueFISP than for conventional TurboFLASH imaging, although these differences were not statistically significant (Table).

	Single-shot TrueFISP	TurboFLASH	p
SNR normal myocardium	11.5 $\pm$ 4.2	18.2 $\pm$ 12.1	0.67
SNR infarcted myocardium	35.4 $\pm$ 13.6	64.6 $\pm$ 49	0.64
CNR	23.8 $\pm$ 11.2	46.3 $\pm$ 39.2	0.43

Conclusions: Our data provides a validation of MI size quantification with single-shot TrueFISP as determined by histopathology. Although at the expense of lower temporal resolution in comparison with conventional TurboFLASH, single-shot TrueFISP allows for accurate quantification of true MI size in one single breath-hold with good SNR and CNR. Single-shot TrueFISP may become a useful tool for fast imaging of MI extent, particularly in those patients that require short examination times.

415. ANATOMICALLY ORIENTED MEASUREMENT OF RIGHT VENTRICULAR VOLUMES AND FUNCTION BY 4D SEMI-AUTOMATED RV RECONSTRUCTION OF CARDIAC MR IMAGES

Petra S. Niemann, MD, PhD,[1] Thomas Balbach, PhD,[2] Christian Galuschky, PhD,[2] Michael Blankenhagen, PhD,[2] Michael Silberbach, MD,[1] Craig Broberg, MD,[1] Michael Jerosch-Herold, PhD,[1] David J. Sahn, MD.[1] ***[1]Oregon Health & Science University, Portland, Oregon, USA, [2]TomTec Imaging Systems, Unterschleissheim, Germany.***

Introduction: Impaired right ventricular (RV) function is a common occurrence in patients with congenital (CHD) and sometimes coronary artery disease (CAD). In patients with CHD and CAD we have used a multiplanar gradient-echo cine protocol covering the entire body, inflow, outflow and apical regions of the RV.

Purpose: The aim of our study was to characterize right ventricular function and anatomy in patients utilizing a new semi-automated 4D RV reconstruction analysis method.

Methods: In our study 30 subjects, 9 with grossly normal cardiac anatomy and mild CAD and 21 with major CHD (ToF, ASD, VSD, PDA, and transposition post Mustard), mean age 40.9 $\pm$ 12.11 y, were evaluated for RV volume and function.

All images were acquired with a 1.5 Tesla MR magnet with ECG gated segmented gradient echo-sequencing. MRI cine-loops were recorded in short axis, long axis and rotated long axis views to cover the entire RV including tricuspid valve, apex and RV outflow tract. Post acquisition processing was performed with a semi-automated analysis program developed to compute RV volumes (TomTec). Sagittal, 4-chamber and coronal views were used for semi-automated contour detection with manual correction of boundaries. End-diastolic and end-systolic volumes (EDV, ESV), stroke volumes (SV) and RV ejection fraction (EF) were delineated. All data was also measured with the GE MRI analysis software for RV EDV, ESV, SV and EF as comparison.

Results: Acquisition of cine DICOM loop cardiac images was part of the routine clinical cardiac MRI; no additional imaging time was required. There was good myocardial contour detection in all subjects. The dedicated RV analysis software was capable of giving results within 3–5 min for each patient. The RV free wall, tricuspid valve, RVOT and apex could well be visualized and reconstructed regardless of RV size or shape into a dynamic RV model. For the dedicated 4D RV software, mean RVEF was 48% ± 12%, mean EDV was 137.6 mL ± 84.8 mL, mean ESV was 77.17 mL ± 57.27 mL, and mean SV was 69.6 mL ± 28.3 mL. Measurements obtained with the GE MR standard analysis software showed comparable results: mean RVEF was 46% ± 16%; mean RV EDV was 148.8 mL ± 94.1 mL, mean RV ESV was 87.1 mL ± 89.5 mL, and mean RV SV was 79.62 ± 32.4 mL (correlation coefficient = 0.91). Intraobserver variability for the GE MR analysis was a mean of 5.2% for RVEF, 3.7% for RV EDV, 6.6% for RV ESV, and 6.7% for RV SV, but was lower for the dedicated RV 4D reconstruction analysis method (RVEF, 2.8%; RV EDV, 3.8%; RV ESD 4.2%; RV SV 3.8%).

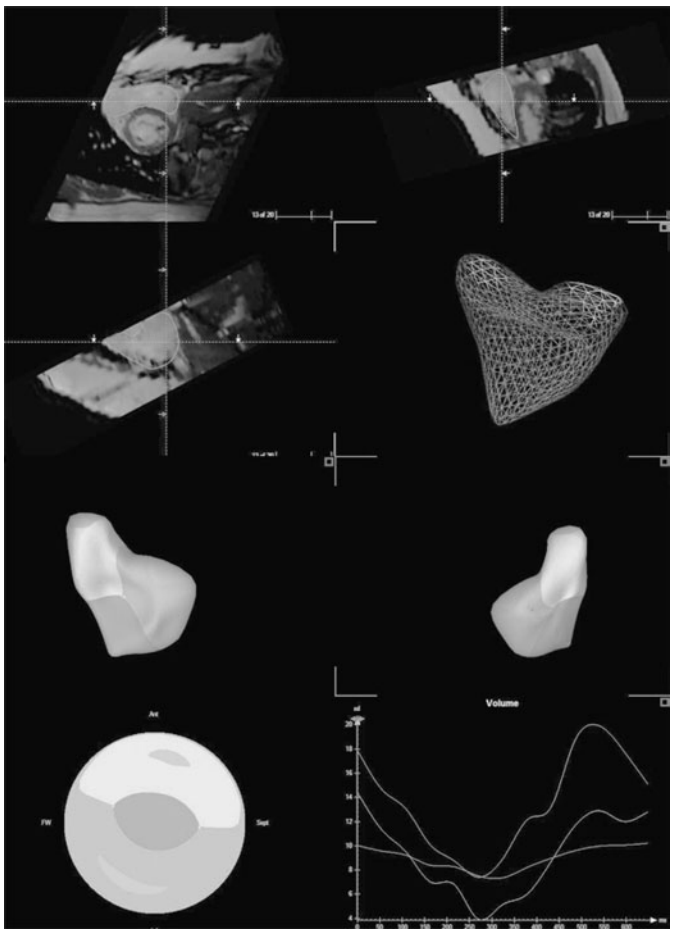

Conclusions: Highly reproducible and precise measurements of right ventricular volume and function could be obtained with multiplanar cine MR imaging using this new 4D semi-automated RV reconstruction method. This novel, anatomically oriented RV analysis method should be useful for MRI studies of the RV in both CHD and CAD patients.

416. AN OFFLINE ANALYSIS METHOD FOR DETERMINING LEFT VENTRICULAR MYOCARDIAL VELOCITY, STRAIN, AND TWIST FROM GRADIENT-ECHO CINE MRI IMAGES

Petra S. Niemann, MD, PhD,[1] Helene Houle, PhD,[2] Luiz Pinho, MD,[1] Craig Broberg, MD,[1] Michael Jerosch-Herold, PhD,[1] David J. Sahn, MD.[1] [1] *Oregon Health & Science University, Portland, Oregon, USA,* [2] *Siemens Imaging Systems, Mountain View, California, USA.*

Introduction: Myocardial velocities are widely used for evaluating segmental myocardial performance. Quantitative analysis of the myocardium by tissue phase mapping (TPM) with cine phase-contrast velocity MR imaging has been used to detect changes in tissue stress and strain related to ischemic or pre-ischemic changes.

Purpose: We describe a novel MR speckle tracking/border detection method for MR gradient-echo loops capable of analyzing circumferential, longitudinal and radial velocities and evaluating regional myocardial tissue strain and twist.

Methods: We enrolled 29 subjects into our study age 14 to 71 years. All patients underwent cardiac MRI for evaluation of either congenital or ischemic heart disease. All MRI images were acquired with an ECG gated 1.5 or 3.0 Tesla Magnet with segmented gradient-echo cine-loop sequences for short and long axis views to cover the entire left ventricle, followed by specific cine-phase contrast MR imaging in one third of the subjects. Gradient-echo cine-loop images were converted from DICOM to AVI format and could be analyzed by the Vector Velocity Imaging (VVI Siemens) myocardial velocity method. Post-processing of 1-2 heartbeats provided full quantification of myocardial Langrangian circumferential, radial and longitudinal velocities, strain and twisting in short and long axis views of the left ventricle. Results were compared to circumferential and radial velocities obtained by TPM with cine phase-contrast velocity imaging.

Results: The VVI method showed reproducible ventricular myocardial wall tracking for the left ventricle in all gray scale MR cine loop short and long axis views. VVI myocardial velocity analysis software was capable of giving results within 3–5 minutes for each patient. Mean peak systolic radial velocity for angle independent thickening was 4.2 ± 1.8 cm/s; mean peak circumferential velocity for shortening in transverse views was 6.8 ± 2.3 cm/sec; and mean peak longitudinal shortening velocity in long axis views was 8.9 ± 3.1 cm/s. Mean circumferential strain was measured at −21.6% ± 8% with higher strain measurements in the septal area (-26% ± 5%), while mean twist was -7° ± 5° with counterclockwise rotation near the apex. These results were close to measurements obtained by TPM, where the mean radial velocity was 4 cm/s ± 2 cm/s and the mean circumferential velocity was 7 cm/s ± 3 cm/s ($p \leq 0.01$).

Conclusions: This new analysis method for myocardial velocity, strain and twist analysis is applicable to gradient-echo sequenced MR cine loops, and was easy to use and reproducible. Myocardial tissue velocity measures obtained with VVI were compatible to values obtained with TPM in cine phase-contrast velocity MR imaging.

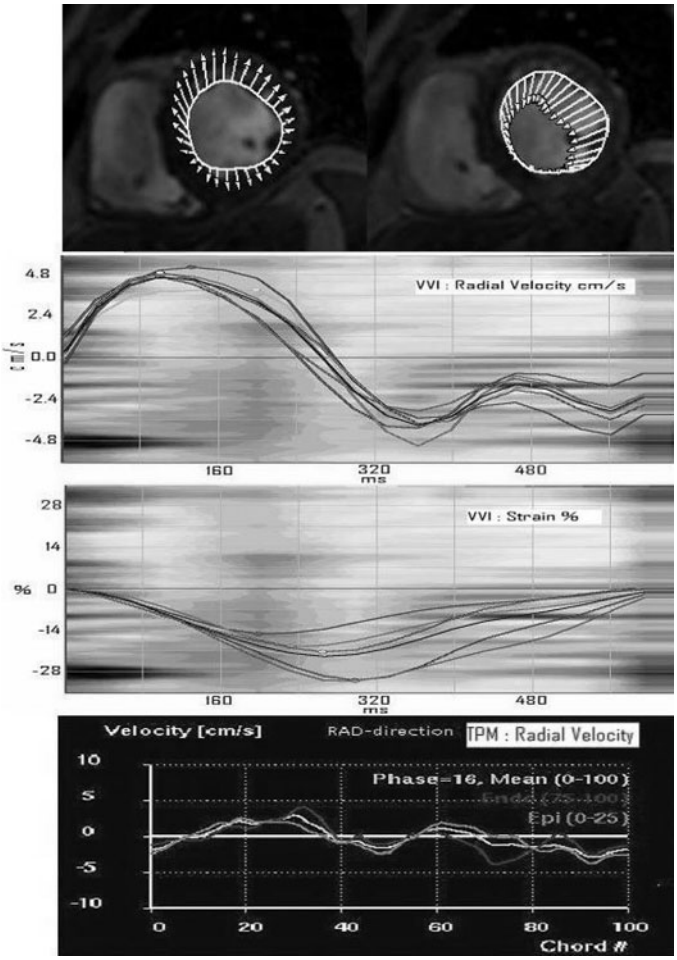

417. ASSESSMENT OF REGIONAL STRAIN IN ADULT CONGENITAL HEART DISEASE USING 2D-SPAMM

Daniel Virnich, MD, Howard Dinh, MD, Greg Fishbein, MD, John Child, MD, Richard Finn, MD. ***University of California, Los Angeles, Los Angeles, CA, USA.***

Body: Regional circumferential strain is a measure of mechanical contractile properties of the myocardium. The clinical significance of circumferential strain (Sc), Sc heterogeneity, and its relationship to patients with abnormal ventricular motion secondary to functional single ventricles (FSV) has not been studied.

Hypothesis: Regional Sc heterogeneity is greater in FSV compared to healthy subjects.

Methods: A population of patients with FSV (n = 6, age 39.8 ± 13.06) and volunteers (n = 19, age 43 ± 14) were scanned with a 1.5T MRI using 2D-FLASH spatial modulation of magnetism sequence with grid tags (1 mm diameter, 7 mm space) and temporal resolution of 46 ms. The basal, mid, and apical short axes were imaged with Sc assessed off-line by strain analysis software (Cardiac Imaging Modeler v5). Sc was calculated for all 16 segments of the LV. The strain index of heterogeneity (Ish) is defined as the segmental strain standard deviation at the time of peak global strain/average Sc × 100%.

Results: FSV patients demonstrated reduced LVEF and peak Sc. Ish values were significantly higher for FSV compared to controls (Table 1). Representative mid-LV Sc graphs for a control and FSV patient are shown (Fig. 1).

Conclusion: FSV patients have depressed Sc and increased regional Sc heterogeneity. Studies are on-going in larger cohorts of patients with congenital heart disease.

TABLE 1
Sc (%) and Ish in study groups

	CHD (n = 6)	Control (n = 19)	P
Sc Apex	−12.4 ± 4	−23.5 ± 3.6	<0.001
Sc Mid	−13.6 ± 2.8	−22.2 ± 3	<0.001
Sc Base	−12.8 ± 1.5	−16.4 ± 4.7	0.08
Ish Apex	−47 ± 28.8	−13.9 ± 7.6	<0.001
Ish Mid	−45.6 ± 34.3	−13.7 ± 8.7	<0.001
Ish Base	−37.6 ± 15.3	−26.7 ± 25.2	0.33
Sc Rate Neg Apex	−73.4 ± 22.8	−123.6 ± 22.1	<0.001
Sc Rate Neg Mid	−81.8 ± 12.4	−118 ± 20.8	<0.001
Sc Rate Neg Base	−73.6 ± 10.8	−92.1 ± 23	=0.07
Ish Neg Apex	−491.5 ± 630.5	−17.2 ± 6.3	0.01
Ish Neg Mid	−161.1 ± 47.3	−17.7 ± 9.7	<0.001
Ish Neg Base	−247.9 ± 150	−26.1 ± 14.6	0.07
Sc Rate Pos Apex	39.2 ± 14.7	93.8 ± 32.9	<0.001
Sc Rate Pos Mid	43 ± 16.2	77.2 ± 23.1	<0.01
Sc Rate Pos Base	40.3 ± 14.9	48.9 ± 21	0.36
Ish Pos Apex	253.6 ± 330.4	31.6 ± 18.7	<0.01
Ish Pos Mid	243.9 ± 216.5	25 ± 14.4	<0.001
Ish Pos Base	204.8 ± 131.5	50.4 ± 33.9	<0.001

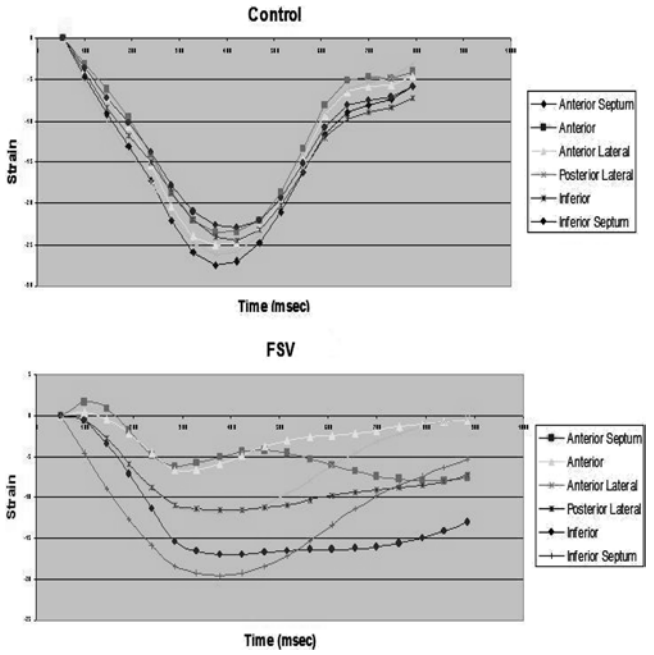

FIG. 1. Representative Mils-LV Sc Graph Control vs. FSV Control.

418. DETECTION OF NEOVESSELS IN ADVANCED ATHEROSCLEROTIC PLAQUES OF HYPERCHOLESTEROLEMIC RABBITS USING PARAMAGNETIC MICELLES TARGETED TO ALPHAVBETA3-INTEGRINS AND CMRI

Fabien Hyafil, MD,[1] Willem J. M. Mulder, PhD,[1] Esad Vucic, MD,[1] Jean-Christophe Cornily, MD,[1] Karen Briley-Saebo, PhD,[1] James R. Tunstead, PhD,[1] Laurent J. Feldman,[2] Gustav J. Strijkers, PhD,[3] Zahi A. Fayad, PhD.[1]
[1]Mount Sinai School of Medicine, New York, New York, USA, [2]Bichat Hospital, Paris, France, [3]Eindhiven University of Technology, Eindhoven, Netherlands Antilles.

Introduction: Neovessels are involved in atherosclerotic plaque growth and rupture. Cyclic RGD peptides bind with a high affinity to alphaVbeta3-integrins expressed on activated endothelial cells. We synthesized a novel contrast agent formed of micelles containing both paramagnetic and fluorochrome molecules targeting the alphaVbeta3-integrins.

Purpose: The aims of this study were to test whether micelles targeted to alphaVbeta3-integrins allowed for the detection of neovessels in advanced atherosclerotic plaques of rabbits using MRI and to confirm the specific binding of micelles to endothelial cells of neovessels using fluorescence microscopy.

Methods: RGD-micelles were synthesized by covalently binding cyclic RGD peptides to pegyleated micelles containing an amphiphilic gadolinium chelate and a fluorescent rhodamine (average size: 30 nm; R1 = 11.2 $s^{-1}mM^{-1}$ at 1.5 Tesla). Atherosclerotic plaques were induced in the aorta of 6 New-Zealand White rabbits by a repeated balloon injury (4 weeks apart) and 4 months of hypercholesterolemic diet. Two non-injured rabbits fed a chow diet were used as controls. A T1-weighted MRI of the aorta was acquired before and 2 hours after intravenous injection of 3 μM Gd/kg of RGD-micelles. Two weeks later, a competition study was performed in 2 rabbits. The same imaging protocol was repeated 15 minutes after the pre-injection of RGD-micelles without gadolinium. Contrast to noise ratio (CNR) was calculated by dividing in the signal to

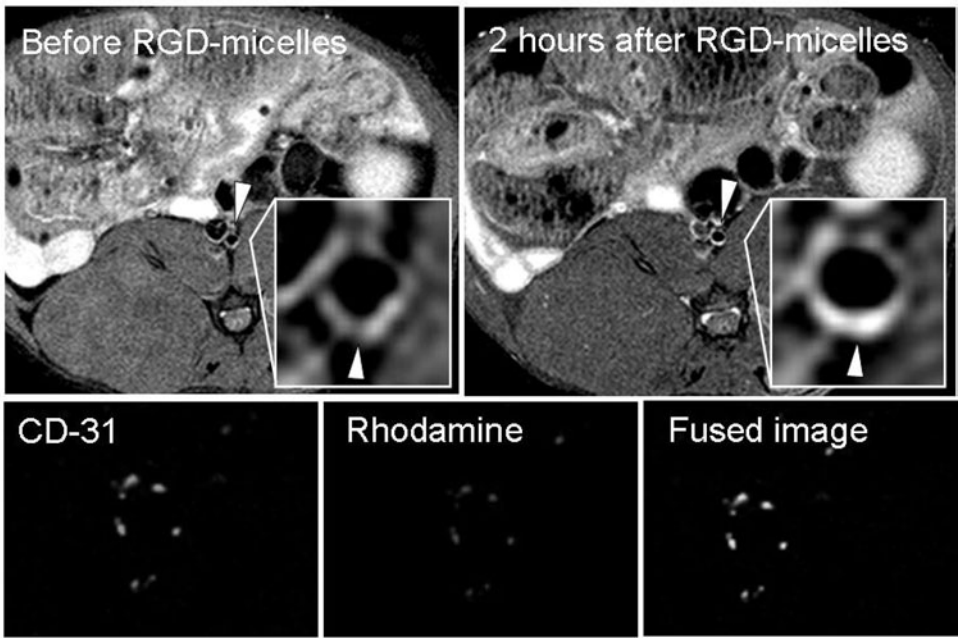

FIG. 1.

noise ratio of atherosclerotic plaques by the signal intensity of muscle. Enhancement of atherosclerotic plaques was measured as follows: Enhancement = [(CNR after contrast agent / CNR before contrast agent) x100] − 100. Immediately after the imaging, the rabbits were sacrificed. The presence of RGD-micelles containing rhodamine was compared to the location of neovessels studied by immunohistochemistry (anti-CD31 antibody) on fluorescence microscopy of aortic cross-sections corresponding to MRI.

Results: Increased signal intensities (Fig.) were detected 2 hours after RGD-micelles injection on axial MRI views in the aortic wall of all (6/6) atherosclerotic rabbits (mean increase of 15.7 ± 5%), but not in control rabbits (2/2). Pre-injection of RGD-micelles without gadolinium lead to a 37% decrease of the enhancement in atherosclerotic plaques. The highest MR signal intensities after injection of RGD-micelles were found predominantly in atherosclerotic plaques rich in neovessels on corresponding aortic cross-sections. On fluorescence microscopy, we confirmed that RGD-micelles colocalized with neovessels in the intima of atherosclerotic plaques (Fig. 1), whereas no fluorescence was detected in the aortic wall of control rabbits.

Conclusions: Neovessels were detected with MRI in advanced atherosclerotic plaques of rabbits using paramagnetic micelles targeted to alphaVbeta3-integrins. Addition of fluorescent rhodamine in the micelles confirmed the specific binding of RGD-micelles to the endothelium of neovessels on histology.

419. CONTRAST ENHANCED CMR PRIOR TO PROPHYLACTIC IMPLANTATION OF A CARDIOVERTER/DEFIBRILLATOR IDENTIFIES PATIENTS WITH INCREASED RISK FOR VENTRICULAR ARRHYTHMIAS

Philipp Boyé, Udo Zacharzowsky, Hassan Abdel-Aty, Alexander Schirdewan, Rainer Dietz, Jeanette Schulz-Menger. ***Franz-Volhard Klinik Charite Campus Buch, Berlin, Germany.***

Introduction: Patients with severely reduced left ventricular ejection fraction (LVEF) due to chronic myocardial infarction are at increased risk for life threatening ventricular arrhythmias. In these patients the prophylactic implantation of an implantable cardioverter/defibrillator (ICD) has shown to reduce mortality. Despite the increasing number of devices, their use is still limited by high costs and possible adverse events including inappropriate discharge and progression of heart failure. Ventricular tachycardia is related to infarct size and seems to be related to infarct morphology. Contrast enhanced cardiovascular magnetic resonance imaging (ceCMR) is a valuable tool to detect and quantify myocardial fibrosis in the setting of chronic myocardial infarction and might therefore be a valuable tool for a better risk stratification in this group of patients.

Hypothesis: The purpose of this study was to identify in patients with prophylactic ICD-implantation following MADIT-critieria the subgroup developing ventricular arrhythmias by assessing the impact of size and transmural extent of myocardial fibrosis applying ceCMR.

Methods: We prospectively enrolled 25 patients (23 males, age 68 ± 10 years) with chronic myocardial infarction and clinical indication for ICD therapy following MADIT I or II criteria. Prior to implantation (9 ± 16 days) patients were investigated on a 1.5 Siemens Sonata clinical scanner using 3 long axis orientations plus a 3D stack of short axes to assess left ventricular function (GRE SSFP, slice thickness 10 mm, full coverage, no gap), and delayed contrast enhancement 10–20 minutes after administration of 0.2 mmol/kg gadolinium DTPA (IR-GRE, slice thickness 6 mm, full coverage, no gap) to assess left ventricular infarct morphology. After implantation, patients were routinely followed up including ICD readout after 3 and than every 6 months after implantation for a mean of 534 ± 212 days.

ICD data were evaluated by an experienced electrophysiologist blinded to the CMR data. CMR data were assessed quantitatively with MASS software (MEDIS, Netherlands) for LVEF and morphology of myocardial infarction by manually contouring the infracted area. Primary endpoint of the study was the occurrence of an appropriate discharge (DC) or antitachycard pacing (ATP) of the device due to either ventricular fibrillation (VF) or sustained ventricular tachycardia (sVT).

Results: LVEF was 32 ± 10% as assessed by CMR. Endpoint was reached in 5 cases (3 DC, 2 ATP). There was no significant association between the endpoint and LVEF, total infarct mass (mean 51 ± 31 g) or infarct size related to left total ventricular mass (30 ± 15%). The degree of transmurality as defined by transmural to non-transmural extent in each scar, was significantly associated with the occurrence of the endpoint, meaning that scars with mainly transmural (>75%) or non-transmural extent (<25%) were less likely to induce ventricular arrhythmia than scars with a transmural extent of 25–75% (Chi-Square, $p = 0.012$).

Discussion: The results of this study show that patients with transmural and therefore non-viable areas of myocardial infarction are less likely to suffer from ventricular arrhythmias than patients with mainly non-transmural extension of infarction. These findings are consistent with previous results that the surface-area between viable and infarcted myocardium rather than total infarct size or transmural extent could predict ventricular arrhythmias. Further follow-up and larger trials are needed to clarify this issue.

Conclusion: In patients with chronic myocardial infarction fulfilling the MADIT-criteria (MADIT I or II) a subgroup at higher risk could be identified. Although these are preliminary results in a small group of patients, this study supports the hypothesis that patients with large infarcts with mainly non-transmural extent of the scar are at increased risk for ventricular arrhythmia.

420. COMPREHENSIVE VISUALIZATION OF MULTI-STRESS LEVEL FUNCTIONAL ANALYSIS RESULTS

Marcel Breeuwer, PhD,[1] Gilion L. T. F. Hautvast,[1] Tarinee Tangcharoen, PhD,[2] Eike Nagel, PhD.[2] ***[1]Philips Medical Systems, Best, The Netherlands, [2]German Heart Center, Berlin, Germany.***

Introduction: Patients with ischemic heart disease usually suffer from a reduction of left-ventricular pump function with increasing stress level. To evaluate the reaction of the heart to stress, dobutamine stress cine cardiac MRI has become a well-established method (1). A stress examination usually consists of 4–5 cine image acquisition at increasing stress levels. Presently, left-ventricular wall motion at various stress levels is primarily visually assessed, by comparing movies of the beating heart on a single computer display. Quantitative analysis tools are commercially available, but none of these offers the possibility to comprehensively visualize and compare analysis results over stress levels.

Purpose: We propose new methods for the comprehensive visualization of left-ventricular quantitative functional analysis results over multiple stress levels, especially for local parameters such as wall thickness, wall motion and wall thickening and more global systolic and diastolic parameters such as (time of) peak ejection rate, (time of) early and late peak filling rates.

Methods: Left-ventricular functional parameters are calculated after semi-automatic detection of the left-ventricular epi- and endocontours (2) and after the calculation of the volume over time curves v(t) based on the endocontours (using the well-known Simpson's Rule) and the various wall parameters on the basis of endo- and epicontours. From the volume curves a variety of systolic and diastolic functional parameters and their associated moment of occurring in the cardiac cycle are calculated (end diastole, end systole, peak ejection rate, early and later peak filling rates, etc. [3]).

The first new method visualizes local functional parameters such as wall thickness and wall thickening as curves in a radial graph, where the angle α represents the position on the myocardium and the radius ρ represents the value of the parameter. All stress levels are represented as different curves in the same graph, different graphs are used for different slices or segments of the heart. For example, the division proposed by the American Heart Association (4) could be adopted, resulting in 3 graphs for the apical, mid and basal segments, respectively (Fig. 1). A user-adjustable ruler has been added to the radial graphs, to indicate where to measure the displayed parameter as function of the stress level (Fig. 1).

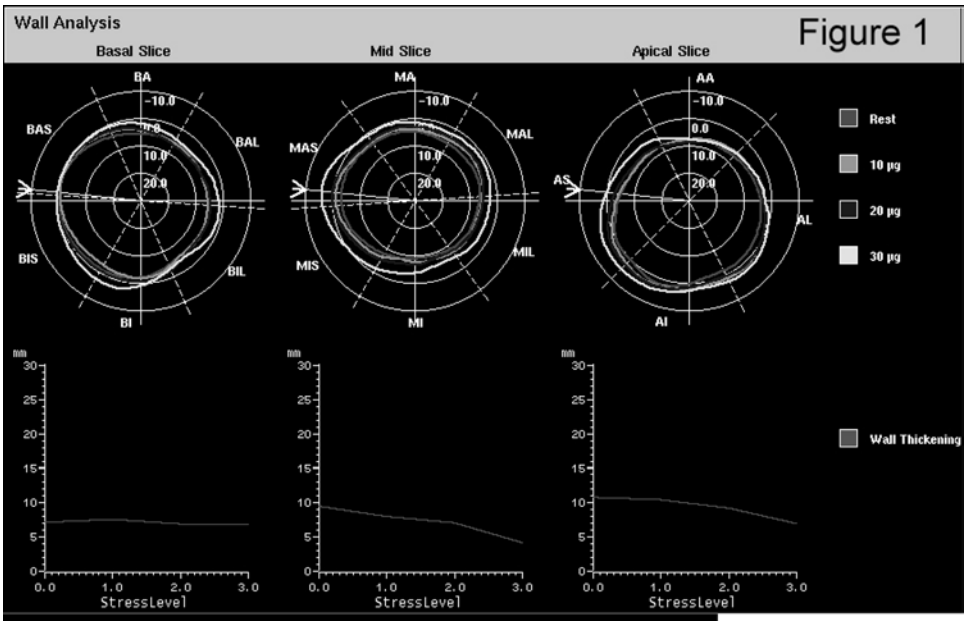

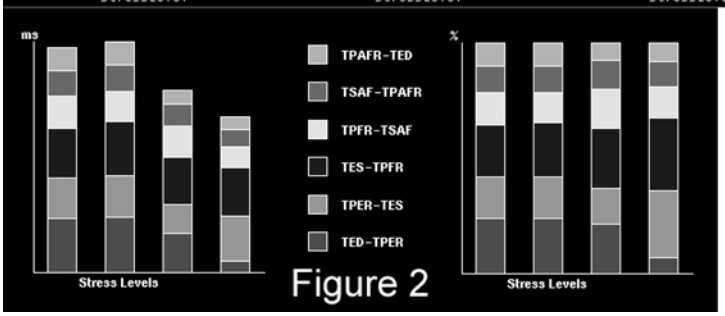

In the second new method, the various time moments that are derived from the volume curve v(t) are represented as a collection of stacked bar graphs, using one stacked bar per stress level (Fig. 2). The height of a bar segment can be chosen equal to the absolute length of a time interval (Fig. 2, left), but it can also be made equal to the relative time duration w.r.t. the complete cardiac cycle (Fig. 2, right). In Fig. 2, the abbreviations have the following meaning: T = time, ED = end diastole, ES = end systole, PER = peak ejection rate, PFR = (early) peak filling rate, SAF = start atrial filling, PAFR = late (atrial) peak filling rate.

Results: Examples of the new visualizations methods are shown in Figs. 1 and 2. Evaluation in a clinical setting is ongoing, first results are encouraging. The methods show very clearly the behavior of the various heart segments as function of their position and stress level.

Conclusions: We have presented two new visualization concepts that substantially simplify the interpretation of multi-stress level quantitative functional analysis results by comprehensively visualizing these results.

REFERENCES

1. Wahl A, et al. European Heart Journal 2004;25:1230–1236.
2. Hautvast GLTF, et al. CARS 2005, Int. Congress Series 2005;1281:351–356.
3. Breeuwer M, et al. submitted to SCMR 2007.
4. Cerqueira MD, et al. Circulation 2002;105:539–542.

421. 3D MYOCARDIAL STRAIN IN PATIENTS WITH TRANSFUSION INDUCED IRON OVERLOAD

Gregory C. Brown, Ass Dip RT SMRT,[1] Alistair Young, BE PhD,[2] Brett Cowan, BE MbChB,[3] Beau Pontre, PhD,[3] Karen Teo, MBBS,[1] Tim St. Pierre, PhD,[4] Stephen G. Worthley, MBBS PhD FRACP FACC.[1] [1]***Cardiovascular Research Centre. Royal Adelaide Hospital, Adelaide, Australia,*** [2]***Department of Radiology with Anatomy, University of Auckland, Auckland, New Zealand,*** [3]***Centre for Advanced MRI, University of Auckland, Auckland, New Zealand,*** [4]***School of Physics. University of Western Australia, Perth, Australia.***

Introduction: Myocardial T2* is an established investigation to determine the myocardial iron status in patients with transfusion induced iron overload (1). A T2* of less than 10 ms suggests severe myocardial iron loading (2) and increased risk of myocardial impairment including lowered ejection fraction, heart failure and sudden cardiac death.

Purpose: This study investigated peak 3D systolic strain and diastolic relaxation rates in iron overload patients using SPAMM tagging

Methods: Twenty-four patients (10 male, average age 32, range 23–51 years) with congenital hemoglobinopathy (22 thalassaemia major, 1 thalassaemia intermedia and 1 Diamond-Blackfan anaemia) managed by transfusion and s.c. Desferal (Novartis AG) chelation had myocardial T2* measurements (3), R2-CMRI liver iron quantification(4), and short and long axis 7 mm grid tagged SPAMM Cine imaging acquired on a Siemens Sonata 1.5T scanner. The average of serum ferritin readings for the preceding 12 month average was recorded. Subjects were divided into 2 groups on the basis of their myocardial T2*, using a 10 ms cut-off to indicate significant iron overload.

	T2* > 10 ms	T2* < 10 ms	p value
General parameters			
Number (n)	9	15	
Male: Female	2:7	8:7	
Age	33.3 years	30.0 years	NS
Myocardial T2*	23.6 ms	6.1 ms	<0.001
Liver Iron concentration	9.57 mg/g d.w.	11.02 mg/g d.w.	NS
Serum Ferritin	1830 μg/L	3429 μg/L	NS
LV Ejection Fraction (LVEF)	56.6%	47.4%	0.002
Peak systolic strain			
Circumferential	18.6%	16.3%	0.03
Longitudinal	15.4%	13.5%	0.03
Shear	6.00%	4.14%	0.02
Peak diastolic strain relaxation			
Circumferential	−105%/s	−104%/s	NS
Longitudinal	−93%/s	−95%/s	NS
Shear	−35%/s	−24%/s	0.02

Tags were tracked on all phases of the short and long axis cines using a semi-automated algorithm, and peak 3D circumferential, longitudinal and shear strains were calculated and averaged over all regions as a measure of systolic myocardial function. Peak strain relaxation rate was similarly calculated as a measure of diastolic myocardial function. A t-test between groups with $p < 0.05$ was considered to be statistically significant.

Results: In all cases, peak systolic strain was significantly reduced in the T2* < 10 ms group indicating reduced systolic function. Peak diastolic relaxation was significantly reduced only for shear strain. Neither liver iron concentration or serum ferritin was significantly different between the two groups.

Of note, one patient with a T2* of 5 ms and LVEF of 33% died of pre-existing heart failure one month after the MRI.

Conclusions: Reduced LVEF in patients with T2* < 10 ms is consistent with the literature. The tagging results show that peak 3D myocardial strain is also reduced consistent with systolic impairment, but that only shear strain relaxation was reduced, suggesting a lower degree of diastolic dysfunction in this population. Neither liver iron, nor serum ferritin were significantly different between the high and low T2* groups.

REFERENCES

1. Anderson, et al. EHJ 2001;22:2171–2179.
2. Tanner, et al. Blood ASH 2005;106:3838a.
3. Westwood, et al. JMRI 2003;18:616–620.
4. St.Pierre, et al. BLOOD 2005;105:855–861.

422. LOW DOSE CONTRAST AGENT INJECTION IMPROVES MYOCARDIAL TAG DEFINITION AT 3 TESLA

Daniel K. Thomas, MD,[1] Michael Jerosch-Herold, PhD,[2] Bastian Cheng, MS,[1] Hans H. Schild, MD,[1] Torsten Sommer, MD.[1] [1]***University of Bonn, Bonn, Germany,*** [2]***University of Oregon, Portland, Oregon, USA.***

Introduction: At 1.5 Tesla (T) injection of contrast media (CM) before acquisition of cardiac tagged images is not recommended, because of unfavourable effects on image quality and tag definition. The deleterious effects of CM on tag-definition and tag-fading (T1 relaxation) might be less pronounced at higher field strengths.

Purpose: We investigated, whether the injection of low-dose CM (as needed for perfusion imaging) affects tag-definition and tag-fading at 3 T.

*Methods:*Ten patients were scanned with two tagging sequences (FOV 260-280, TR/TE 5-6/2.5-3, thickness 8 mm, tag spacing 8 mm, 16 cardiac phases) with a flip-angle of 8 and 14 degrees before (pre-contrast) and after low dose CM injection (post-contrast) for perfusion imaging (0.04 mmol Gd-DTPA/kg/bw). All scans were acquired in the same mid-ventricular short axis location during resting conditions. Images were assessed qualitatively with respect to tag definition, blurring and artefacts by consensus reading (2 observers) using a 5 point rating scale (1 = excellent, 5 = nonreadable). Contrast-noise-ratio (myocardium/tag) and signal-noise-ratio (myocardium) were determined for quantitative comparison.

Results: Post-contrast tagged images (fig.d-f, flip-angle 8) received a better score compared to pre-contrast (fig. a-c, flip-angle 8) images (2.6 vs. 3), indicating a superior image quality. CNR and SNR were superior in post-contrast images compared to pre-contrast images at diastole (fig. a+d,first phase image, 43.41 vs. 28.41 for CNR and 46.01 vs. 29.87 for SNR) and end-systole (fig. b+e, 21.21 vs. 17.92 for CNR and 35.92 vs. 26.79 for SNR). No significant difference was observed between pre-contrast and post-contrast images at end-diastole (fig. c+f, last phase image).

Conclusions: Myocardial tagging at 3 Tesla can be performed after injection of low-dose contrast agent (i.e., 0.04 mmol Gd-DTPA/kg/bw) resulting in an increase in image quality. This effect will be even more pronounced during stress exams where tag-fading due to T1 relaxation will be less due to fast heart rates, and good CNR and SNR are of high importance for image reading and quantitative analysis.

423. AFFINE REGISTRATION OF SHORT AXIS CINE CARDIAC MAGNETIC RESONANCE IMAGES FROM DOBUTAMINE STRESS EXAMS

Gilion Hautvast, MSc,[1] Marcel Breeuwer, PhD,[1] Tarinee Tangcharoen, MD,[2] Eike Nagel, PhD.[2] [1]***Philips Medical Systems, Best, The Netherlands,*** [2]***Deutsches Herzzentrum Berlin, Berlin, Germany.***

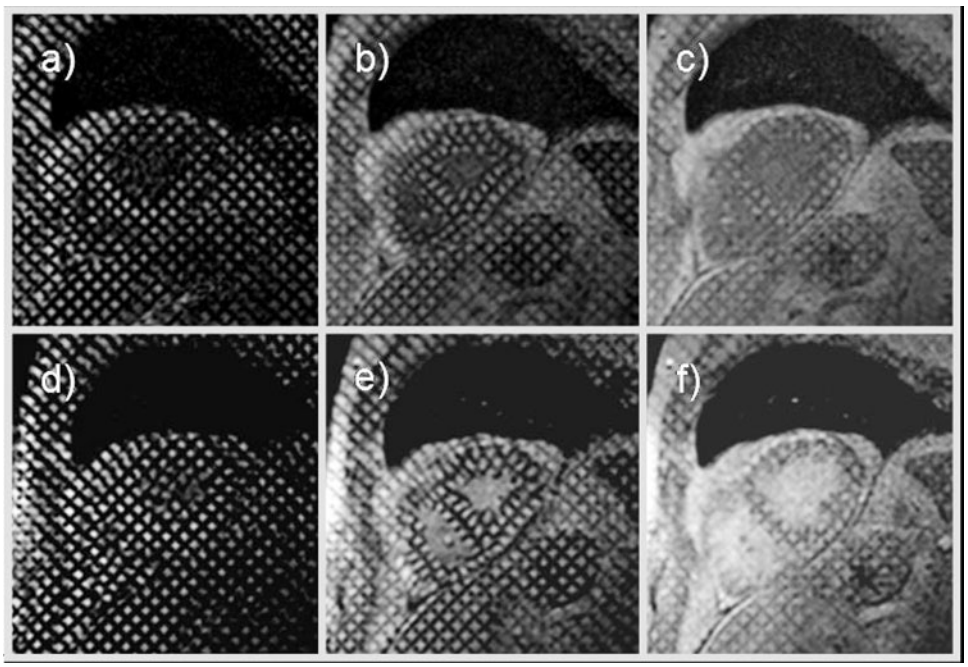

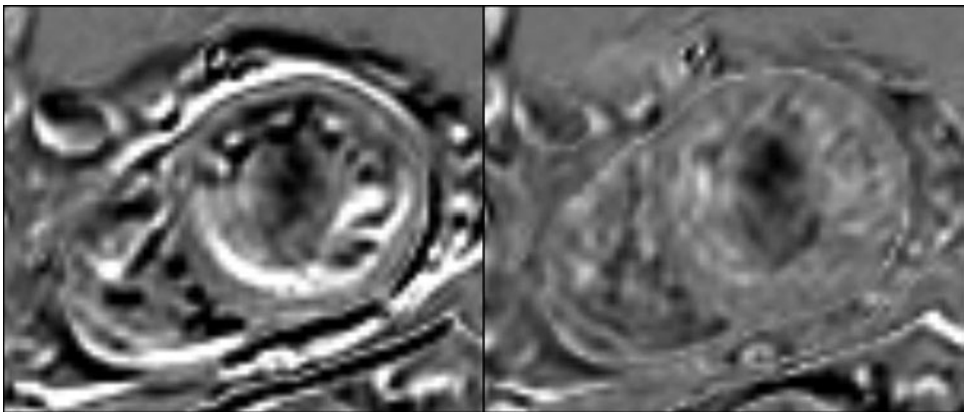

FIG. 1. Difference between images from two stress levels before and after registration.

Introduction: In dobutamine stress magnetic resonance (DSMR), short-axis (SA) cine Cardiac MR (CMR) scans are made at different levels of pharmocologically induced stress. Comprehensive analysis of these scans is currently done visually, but would preferably consist of quantification of ventricular function and wall motion at all stress levels, which requires delineation of all acquired images. In currently available clinical analysis applications, scans can only be analyzed separately, ignoring the close relation between the images from different scans. To allow for faster analysis, a more comprehensive, dedicated analysis application is desirable. For such an application, image registration is necessary to be able to deal with misalignments caused by image acquisition during different breath holds.

Purpose: To develop and optimize an affine registration algorithm for automatic registration of SA cine CMR images. Cardiac contours obtained by applying the resulting transformation should be positioned accurately for use in a dedicated analysis application of DSMR exams.

Methods: We have implemented a multi-resolution registration framework, capable of registration using various optimization methods (simple gradient, uphill and gradient descent) and similarity measures (Mutual Information [MI], Normalized MI, joint entropy and joint correlation). Furthermore, there are a number of parameters controlling the scale and step size in the coarse-to-fine registration approach.

With increasing heart rates, the relative length of ventricular diastole decreases, causing temporal misalignment of the images from different stress levels. To avoid this problem, image registration is performed only at end diastole (ED), which is detected at acquisition by ECG triggering, guaranteeing optimal temporal alignment. Consequently, only ED contours can be transformed accurately. In the future these ED contours may be propagated using an automatic contour propagation method (1).

The affine registration algorithm was optimized and technically validated using images from DSMR exams from 10 patients. Cine CMR imaging with retrospective ECG triggering was used to acquire 25 phases for 3 SA slices at 3-6 levels of cardiac stress. All images were 256×256 in size and covered a field of view of 380×380–400×400 mm. Golden standard delineations for all images were obtained by averaging four delineations from two experts (root-mean-square (RMS) inter-observer variance 1.11 ± 0.66 mm). The accuracy of the affine registration was evaluated by validating the transformed contours, by computing RMS positioning errors with respect to the golden standard. To determine the most robust and accurate setting for registration of SA cine CMR images from DSMR exams, we performed full factorial experiments in which registration is performed and evaluated at all possible settings in the parameter space. The results of these experiments were analyzed using Student-T tests and analysis of variances (ANOVA).

Results: In the full factorial experiment, 23040 settings were tested. Registration was most accurate using gradient descent optimization and joint correlation. Student T-tests confirmed that the observed differences were significant ($\alpha = 0.05$, p value $\leq$ 0.0014). Significant interactions between the other parameters have been identified using ANOVA and an optimal setting is concluded. Transformed contours were positioned with 1.39 ± 1.40 mm RMS positioning errors of the transformed contours with respect to the golden standard, which were 4.02 ± 3.22 mm before registration. Difference images from before and after registration (Fig. 1) provide an impression of the registration accuracy.

Conclusions: Affine registration has been used to register SA cine images acquired during DSMR exams. Registration is most accurate using gradient descent optimization in combination with the joint correlation similarity measure. The obtained transformation can be used to accurately position cardiac contours.

REFERENCE

1. Hautvast GLTF, et al. Automatic cardiac contour propagation in short axis cardiac MR images. In proc. of CARS 2005, Elsevier ICS 2005;1281:351–356.

424. ROBUST MR SEGMENTATION OF THE LEFT VENTRICLE USING AN OUTLIER HANDLING BASED ACTIVE SHAPE MODELS

Karim Lekadir, Robert Merrifield, Guang-Zhong Yang. ***Imperial College London, London, United Kingdom.***

Introduction: With the increasing capabilities of CMR, the extraction of global properties such as ejection fraction, cardiac output and LV mass from the delineated endo- and epi-cardial borders is becoming a routine task in clinical studies. This often calls for extensive segmentation from large datasets. In these cases, automatic techniques based on statistical shape modelling, such as the Active Shape Models (ASM) (1), would allow the use of prior knowledge about the variability across individuals to provide accurate results. In practice, however, the ASM search is hampered by inconsistencies in image quality and the presence of image artefacts, thus introducing outliers for the ASM control points. The aim of this work is to propose an outlier-immune ASM framework that can be used for accurate extraction of the LV boundaries.

Methods: The proposed technique is based on an invariant shape metric, the Ratio of Inter-landmark Distances (RID), which allow outlier analysis to be carried out before the pose and shape parameter estimation of the ASM. The idea behind the method is that the outliers are associated with RIDs that are invalid. To detect these extreme RIDs, statistical tolerance intervals are calculated for each RID from the training set and at the segmentation stage, each RID found outside the corresponding interval is considered to be invalid. By considering all RIDS for each point, the likelihood of a point to be an inlier can be calculated. An iterative procedure is then used for outlier detection where the point with the lowest measure is rejected at each iteration. The likelihood measures of the remaining points are updated and the procedure is repeated until the lowest likelihood measure is close to 1, suggesting that all remaining points are valid. After outlier identification, replacement points are suggested such that the new RIDs lie within or are close to the tolerance intervals. A final local adjustment is carried out using gray-level appearance information to allow the points to fit well to the underlying image features. After outlier correction, a plausible shape can be safely generated by the model fitting procedure of the ASM search.

Validation and Results: For validation, the LV datasets were collected from 32 subjects using a 1.5T MR scanner (Sonata, Siemens, Erlangen Germany) and a TrueFISP sequence (TE = 1.5 ms, TR = 3 ms, slice thickness = 10 mm, pixel size of 1.5 to 2 mm) within a single breath-hold. The acquisition scheme provided a comprehensive anatomical coverage of the LV as well as its inflow and outflow tracts. The endo- and epi-cardial boundaries of the left ventricle were first delineated manually by an expert observer as the ground truth. The ASM based technique was then applied to these 32 datasets, with initial position and orientation prescribed by the intersection of the vertical and horizontal long axis images. The average segmentation error for the endo- and epi-cardial borders was 0.88 mm $\pm$ 0.26 mm and 1.27 mm + 0.50 mm, respectively. The volume of the myocardium was calculated from both the manual and automatic delineations and the average volumetric error was found to be 2.7% $\pm$ 2.6%. The average computation time needed for complete LV segmentation was 0.6 $\pm$ 0.2 seconds.

Conclusions: The use of traditional statistical shape modelling for automatic segmentation of LV is complicated by the presence of outliers due to noise and artifacts. The proposed technique provides robust segmentation of the endo- and epicardial borders of the LV by the effective use of RIDs for ASM. The results show the high accuracy achieved, demonstrating the potential clinical value of the technique.

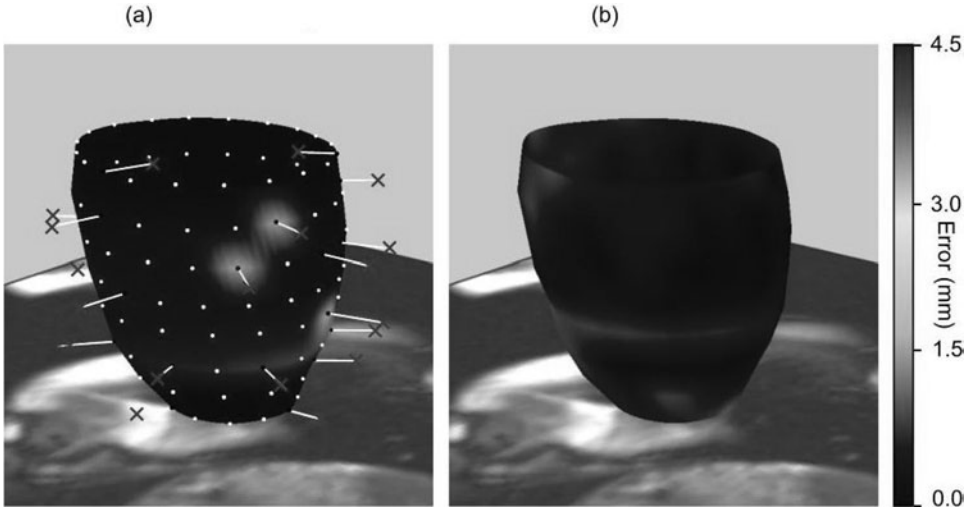

FIG. 1. Illustration of the proposed segmentation technique (outliers are represented in crosses).

425. GADOLINIUM ENHANCED CARDIOVASCULAR MAGNETIC RESONANCE IN PATIENTS WITH QUIESCENT VASCULITIS AND EARLY CHRONIC KIDNEY DISEASE

Nicola C. Edwards, B Med Sci, BM BS MRCP,[1] Jonathan N. Townend, MB ChB, MD, FRCP, FESC,[2] Charles J. Ferro, MB ChB, MD, MRCP,[2] Richard P. Steeds, MB ChB, MA, MD, MRCP.[2] [1] ***University of Birmingham, Birmingham, United Kingdom,*** [2] ***Queen Elizabeth Hospital, Birmingham, United Kingdom.***

Introduction & Purpose: Premature cardiovascular disease (CHD) is a major cause of morbidity and mortality in patients with systemic vasculitides such as systemic lupus erythematosus (SLE). The causes may be multi-factorial. Rates of myocardial infarction and heart failure exceed those in age-matched controls by 5–6 fold and are postulated to relate to the high prevalence of subclinical atherosclerosis observed on imaging modalities including SPECT and carotid ultrasound. However, with underlying systemic immunological, thrombotic and vascular inflammatory mechanisms, it is not clear whether increased cardiovascular risk is due to atherosclerotic disease or to complications arising from the vasculitis itself. Baseline CMR scans have been obtained in patients with early, non-diabetic chronic kidney disease (estimated GFR 40–80 mL/min) and no known history of cardiovascular disease as part of a randomised controlled trial of spironolactone in the prevention of cardiovascular complications associated with CKD. We present the results of baseline CMR imaging in 10 patients with known quiescent systemic vasculitis and mild CKD as a comparison with 70 patients with CKD due to nonvasculitic aetiologies.

Methods: Ten patients (70% SLE and 30% Wegeners Granulomatosis-WG) with no prior history of cardiovascular disease underwent CMR on a 1.5 T scanner (Siemens Sonata Symphony). Serial contiguous short axis (SA) cines were piloted from VLA/HLA of the RV and LV (ECG-gated, True-FISP; TR 45ms, TE 1.7 ms, -FA60°, slice thickness 7 mm). These slices were repeated 10–15 minutes after intravenous injection of 0.2 mmol/kg gadolinium-DTPA (Magnevist) with serial contiguous SA segmented inversion recovery T1 weighted cines (TR 1.4 ms, TI 200–240 ms, slice thickness 7 mm, fat saturation band across the spine) to detect late gadolinium enhancement (LGE) indicative of myocardial fibrosis or infarction. Results were compared with a 'non vasculitis' mild CKD control group (n = 70).

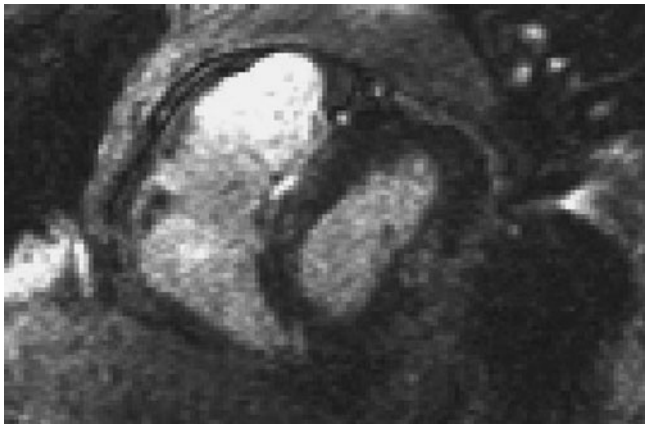

FIG. 1.

Results: All patients had quiescent vasculitis (CRP < 3) with stable renal disease (mean eGFR 56 mL/min) and well controlled blood pressure (mean ambulatory BP 124 ± 4/80 ±2 mmHg). No patients had evidence of pericardial effusion or pericardial thickening. Four patients (40%) (two WG, two SLE) displayed LGE in a diffuse mid wall pattern indicative of fibrosis (Fig. 1 shows an example of LGE in the infero-lateral wall). In all patients, mean LV mass index (LVMI g/m^2), ejection fraction and ventricular dimensions were within limits previously reported for the general population and did not differ by aetiology (Table 1). In the patients with non-vasculitic renal disease investigated in this study, two patients (3%) had LGE but in a typical subendocardial distribution indicative of previous infarction.

Conclusion: Myocardial scarring indicative of fibrosis was present in 40% of patients with quiescent vasculitis. There was no evidence of subendocardial LGE to suggest myocardial infarction as was seen in the control group. To our knowledge, this is the first report of mid-wall LGE in quiescent vasculitis but supports previous post-mortem studies demonstrating patchy myocardial fibrosis in SLE. This data raises the possibility that myocardial damage in vasculitic disease such as SLE and Wegeners Granulomatosis is due to sub-clinical inflammatory and immunological processes other than "conventional" coronary artery disease and may thus have important implications for treatment in this patient group.

TABLE 1
Ventricular dimensions & function

	SLE n = 7	Wegeners n = 3	Non-vasculitis n = 70
LVMI (g/m^2)	67	62	67
Ejection fraction (%)	66%	73%	69%
LVEDV/BSA (mL/m^2)	47	69	60
LGE (%)	2 (10%)	20 (10%)	2 (3%)

426. INFARCT TRANSMURALITY AND INFARCT SIZE ASSESSED BY DELAYED ENHANCEMENT MAGNETIC RESONANCE IMAGING: ASSOCIATION WITH TIME-TO-TREATMENT, ST-SEGMENT RESOLUTION, AND TIMI-FLOW GRADES

Holger Thiele, MD, PhD, Axel Linke, Enno Boudriot, Dietmar Kivelitz, Gerhard Schuler. ***University of Leipzig—Heart Center, Leipzig, Germany.***

Introduction: The TIMI flow, ST-segment resolution (STR) and time-to-reperfusion are associated with mortality in ST-elevation myocardial infarction (STEMI) after either fibrinolysis or percutaneous coronary intervention (PCI). As a result of excellent spatial resolution delayed enhancement magnetic resonance imaging (DE-MRI) allows assessment of infarct transmurality (IT), which might allow to assess the so-called wavefront phenomenon in humans.

Purpose: To assess infarct size and transmurality depending on time-to-treatment.

Methods: This study analyzed 134 STEMI patients randomized to prehospital fibrinolysis or prehospital initiated facilitated PCI. Reperfusion times, 90 minutes STR and TIMI-flow grades pre and post PCI (for facilitated PCI patients) were assessed. IS was determined as percentage of left ventricular mass (%LV) by DE-MRI and IT was analysed by a score ranging from 0-64.

Results: According to tertiles of time-to-reperfusion, IS was significantly smaller in the lowest with 5.1% LV (interquartile range [IQR] 2.0; 11.5) versus 11.3%LV (IQR 5.0; 15.6) in the middle and 14.4%LV (IQR 5.8; 15.6) in the upper tertile ($p < 0.001$). Similarly, IT was significantly smaller in the lower (5.5; IQR 2.0; 10.0) in comparison to the middle (11.0; IQR 4.0; 18.0) and upper tertile (13.0; IQR 6.5; 17.5; $p = 0.001$). STR also correlated significantly with IS and IT ($p < 0.001$). In the groups with complete (>70%), intermediate (70—30%), and no (< 30%) STR IS was 4.2% LV (IQR 1.6; 10.5), 13.6% LV (IQR 8.0; 16.4), and 12.4% LV (IQR 7.7; 17.9; $p < 0.001$). In facilitated PCI patients the preinterventional TIMI flow correlated with IS (TIMI flow 0-I 10.8%LV [IQR 7.6; 17.3] vs. TIMI II-III 3.9%LV [IQR 0.9; 9.6]; $p = 0.002$) and IT (TIMI flow 0-I 11.5 [IQR 8.0; 16.5] vs. 5.0 [IQR 2.0; 9.5]; $p = 0.003$). In a multivariate model time-to-reperfusion was the strongest predictor of IS and IT ($p = 0.001$) followed by type of reperfusion and STR ($p = 0.002$).

Conclusions: Early STR, time-to-reperfusion and TIMI flow before PCI correlate with IS and more importantly with IT, underlining the assumed pathophysiological link between early flow restoration and perfusion in the infarct related artery, which is well-known as the wave-front phenomenon. This may explain why these clinical, angiographic and electrocardiographic measures are associated with long-term survival.

427. IMPACT OF PAPILLARY MUSCLES ON LEFT VENTRICULAR FUNCTIONAL PARAMETERS

Gilion Hautvast, MSc, Marcel Breeuwer, PhD. ***Philips Medical Systems, Best, The Netherlands.***

Introduction: Short-axis (SA) cine cardiac magnetic resonance (CMR) is commonly used to obtain measurements for the end diastolic volume (EDV), the end systolic volume (ESV), the stroke volume (SV) and the ejection fraction (EF) of the left ventricle (LV). The influence of the papillary muscles on the outcome of these measurements has been a matter of debate and investigated in many studies. Recent advances in analysis techniques (1-3) allow for obtaining more functional parameters of the LV.

Purpose: Our purpose is to determine the influence of papillary muscles on the estimation of all LV functional parameters.

Methods: To obtain LV functional parameters, we have used a prototype LV analysis application that includes algorithms for semi-automatic delineation (1), automatic exclusion of papillary muscles and trabeculae (2) and automatic detection of LV functional parameters (3). The combination of these algorithms allows for delineation within 3-5 minutes per data set, after which quantification is instant.

The automatic detection algorithm for LV functional parameters is capable of detecting six events from volume-time curves: time of end diastole (TED), time of peak ejection rate (TPER), time of end systole (TES), time of early peak filling rate (TEPFR), time of start atrial filling (TSAF) and time of late (atrial) peak filling rate (TAPFR). From these events, the algorithm computes five volumes: EDV, ESV, SV, early diastolic filling volume (EDF) and late (atrial) filling volume (ADF). Based on the derivative of the volume-time curve, three rates are determined: peak ejection rate (PER), early peak filling rate (EPFR) and late (atrial) peak filling rate (APFR). Additionally, the EF and the cardiac output (CO) are computed.

SA cine CMR images were acquired from 77 patients. The acquired images consist of 9–14 contiguous slices and 15–50 phases. All images are 256–256 in size, covering a field of view ranging from 350 × 350 mm up to 480–480 mm. Unfortunately, 56 images were acquired using prospective ECG triggering, such that the atrial filling period was not imaged and TSAF, TAPFR, APFR, EDF and ADF can not be determined. We acknowledge E. Voncken of the UMC Utrecht, the Netherlands, and S. Flamm of St. Luke's Episcopal Hospital, Houston, USA, for providing us with clinical image data.

Results: LV functional parameters have been determined from all images with and without exclusion of the papillary muscles. Mean differences were calculated and the significance of differences was determined using two sided student-t tests ($\alpha = 0.05$). Differences in the detected times for all events (TED, TPER, TES, TEPFR, TSAF, TPAFR) are small (mean < 22 ms) and not significant (p values > 0.16). Furthermore, EDF did not differ significantly (p value 0.51, mean difference 1.5 mL). For remaining parameters, we found significant differences (p values < 0.018) of on average -34.4 mL for EDV, -24.2 mL for ESV, -10.2 mL for SV, 7.45 mL for ADF, 0.08 mL/ms for PER, -0.09 mL/ms for EPFR, 0.07 mL/ms for APFR, 6.4% for EF and -0.55 L/min for CO.

Conclusions: Papillary muscles significantly influence the outcome of nearly all rates and volumes determined by the automatic LV functional parameter detection algorithm. Despite this influence, the detection algorithm detects the important events in the cardiac cycle at the same times, regardless whether papillary muscles are excluded or not.

REFERENCE

1. Hautvast GLTF, et al. Automatic cardiac contour propagation in short axis cardiac MR images. CARS 2005, Elsevier ICS 2005;1281:351–356.
2. Hautvast GLTF, et al. Automatic exclusion of Papillary Muscles and Trabeculae from Blood Volume Measurements in Cine Cardiac Magnetic Resonance Images. CINC 2007, In Press.
3. Breeuwer M, et al. Efficient, accurate and robust left-ventricular diastolic functional analysis based on short-axis cine cardiac MRI. SCMR 2007, Submitted.

428. FLOW SENSITIVE 4D MRI IN THE THORACIC AORTA AT 3T: FINDINGS IN NORMAL VOLUNTEERS AND PATIENTS WITH AORTIC PATHOLOGIES AND SURGICAL REPAIR

Michael Markl, Max Russe, Alexander Berger, Aurelien F. Stalder, Andreas Harloff, Jürgen Hennig, Alex Frydrychowicz. ***University Hospital Freiburg, Freiburg, Germany.***

Purpose and Introduction: Respiration controlled flow sensitive 4D MR imaging in combination with advanced color-coded data processing was evaluated for the assessment of normal and pathological aortic 3D blood flow at 3T (1-3) Application in a volunteer and patient study revealed considerable changes in local blood flow characteristics associated with pathologies of the thoracic aorta.

Methods: In a study with 11 patients with aortic pathologies and 19 volunteers, all examinations were performed on a 3T system (TRIO, Siemens, Germany). Data acquisition included the entire thoracic aorta (spatial resolution $= 2.4 - 3.8 \times 1.6 - 2.1 \times 3.0 - 4.5$ mm^3) using an ECG gated rf-spoiled gradient echo sequence with interleaved 3-directional velocity encoding ($\alpha = 5^\circ$, venc = 150 cm/s, TE = 3.7ms, TR = 6.1 ms, temporal resolution 48.8 ms). Measurements were performed during free breathing using improved navigator gating, with real-time adaptive k-space ordering and dynamic adjustment of the navigator acceptance criteria for high efficiency respiration control with a wide data acceptance window (12-14 mm) (4-7). Additionally, advanced data visualization tools were utilized to evaluate local hemodynamic changes associated with aortic pathologies (8).

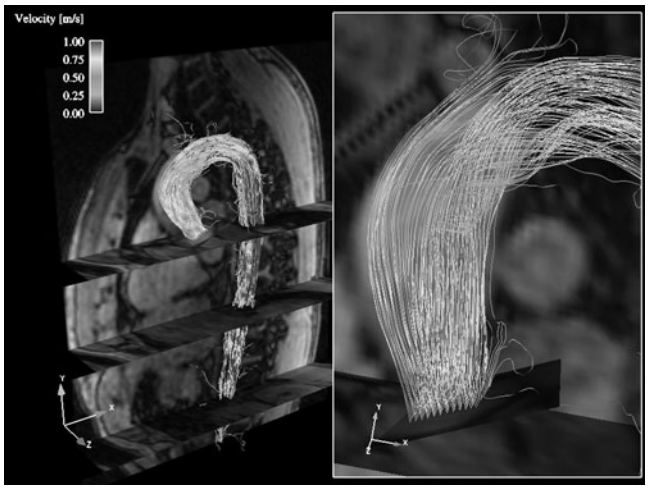

FIG. 1. Overview over the measured systolic three-directional blood flow velocities in the entire thoracic aorta illustrated by 3D stream-lines originating from an emitter plane close to the aortic valve in a normal volunteer. High and mildly right handed helical systolic ventricular out-flow is clearly visible in the magnified view of the ascending aorta and aortic arch. Color coding corresponds to the locale blood flow velocity magnitude.

Results: Four dimensional blood flow visualization was successfully performed for all subjects. In contrast to normal thoracic aortic hemodynamics as exemplary illustrated in figure1, flow sensitive 4D MRI revealed substantial blood flow alterations as a consequence of congenital malformations (n = 1), aneurysms (n = 3), aortic stenosis (n = 3), and surgical repair (n = 4). Individually observed hemodynamic consequences of pathologies are summarized in Table 1 and illustrated in Fig. 2 for a patient with a severe stenosis in the descending aorta.

Conclusions: Results from the volunteer and patient study indicate that flow sensitive 4D MRI is a powerful tool for the assessment of global and local blood flow characteristics in the aorta both for the exclusion and detailed description of vascular alterations. The complete spatial and temporal coverage of the

TABLE 1
Summary of findings in patients with pathologically altered vascular hemodynamics

Patient	Aortic Pathology	MR-Finding
1	Thrombosis, luminal narrowing in arch	Helical flow, vortex formation distal to thrombosis (Fig. 2)
2	Dacron prosthesis in DAo	Complex flow acceleration in DAo, roll-like vortex formation
3	Severe stenosis in DAo	Retrograde flow distal to stenosis, secondary: vortex flow in AAo
4	Mild aneurysm in AAo	Dynamically moving flow vortex, accelerated flow at anterior wall
5	Valve graft in AAo, Typ-A-dissection	Flow accel. distal to graft, diastolic backflow in false lumen
6	Patent ductus arteriosus	Atypical RV & LV outflow, proof of Eisenmenger's physiology
7	Mild stenosis in left subclavian artery	Accelerated flow through and distal to stenosis
8	Aortic coarctation and bypass repair	High flow through bypass, helical flow in DAo, aortic steal effect
9	Ectatic AAo, Aortic valve stenosis	Local flow acceleration, Consideable helical flow in AAo & arch
10		pre- intervention: 'Umbrella' type flow along aneurysm walls
11	Large Aneurysm in distal DAo	post-intervention: improved but vertical flow at site of repair

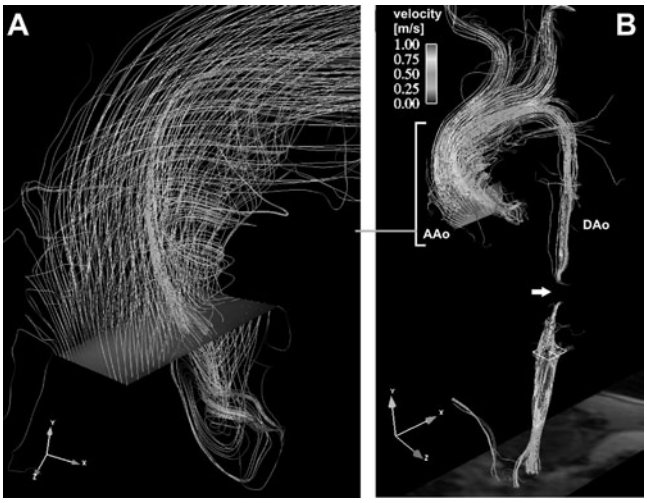

FIG. 2. Flow sensitive 4D MRI at 3T and subsequent visualization using 3D stream-lines of the aorta (b) revealed vortical and retrograde flow in the ascending aorta (a, open white arrows) and accelerated flow distal to the stenosis in combination with retrograde flow in the posterior part of the vessel. Note that 3D flow visualization was hampered by velocity aliasing and the small diameter of the stenosis (b, solid white arrow).

entire thoracic aorta provide a comprehensive overview over 3D blood flow patterns and permit retrospective data evaluation which may help to overcome limitations of flow imaging in predefined 2D planes.

REFERENCES

1. Wigstrom L, et al. MRM 1999;41:793–799.
2. Bogren HG, et al. JMRI 2004;19:417–427.
3. Markl M, et al. JCAT 2004;28:459–468.
4. Ehman RL, et al. Radiology 1989;173:255–263.
5. Frydrychowicz, et Al. JCAT 2006, in press
6. Bailes DR, et al. JCAT 1985;9:835–838.
7. Weiger M, et al. MRM 1997;38:322–333.
8. Buonocore MH. MRM 1998;40:210–226.

429. THE MIMICKING OF SOUND TO ENHANCE SCANNING (MOSES): A TECHNIQUE FOR STABILISATION OF RESPIRATION FOR IMPROVED SCAN EFFICIENCY AND IMAGE QUALITY IN CORONARY MRA

Permi Jhooti, PhD, Oliver Weber, Klaus Scheffler. ***University of Basel, Basel, Switzerland.***

Introduction: Navigator-gated free-breathing coronary MRA was shown to reliably exclude severe coronary artery disease (1) and thus to be a valuable tool in certain clinical questions. However, the relatively low positive predictive value reflects a reduced reliability. Potential problems of current implementations include limited signal to noise ratio and residual respiratory artefacts. Improved respiratory patterns bear the potential to reduce artefacts and to result in higher image quality with improved clinical predictive value. In this study, we investigated the possibility of guiding patient respiration by the use of a respiratory-similar tune played at a patient specific tempo.

Method: Music Software was used to develop a musical loop which was felt a subject would be able to breathe along with to guide the rate of respiration. Prior to entering the scanner this loop was played back to the subject so they could find a tempo which they felt comfortable breathing along with. Two 3D T2-prepared, fat-suppressed, steady-state free-precession coronary scans with 32 slices were performed, the first without any auditory feedback. For the first scan the subject was given no instructions and simply breathed normally. For the second scan the loop was started prior to the scan so the subject could regulate their breathing to be in time with the musical loop. The diaphragm position during both scans was recorded for later analysis.

Results and Discussion: Figure 1 displays the respiratory patterns for the diaphragm positions recorded with no sound played (Fig. 1a) and with sound (Fig. 1b). The end expiratory positions are marked and it can be seen that with the scan performed with sound the end expiratory position is more stable. As navigator MRCA methods commonly require an acceptance window to be defined around the end expiratory position a stable position is desirable.

The tempo used in this particular example was a rate designed to encourage slow and steady breathing. As can be seen the rate of respiration in the scan performed with sound is much slower with a larger range of motion (24 v 18 mm) and fewer end expiratory positions (73 v 104) over the course of the scan. We would therefore predict less motion during data acquisition. Initial results on the effect of tempo change have shown a reduction in respiratory range (28 to 21 mm) and an increase in end expiratory positions (116 to 202) when the tempo of the sound

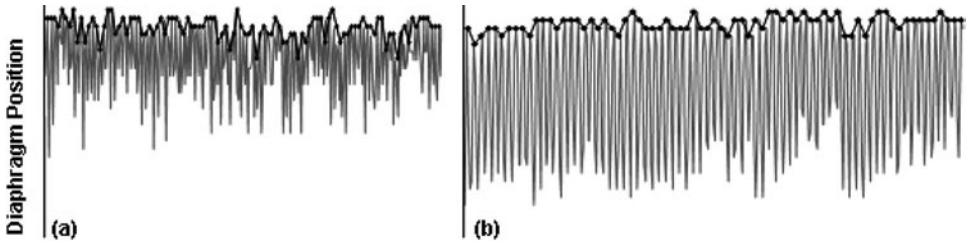

FIG. 1.

was increased from 50 to 100 beats per minute. Altering the tempo could therefore be used to alter the rate of breathing to reduce the range of motion and increase scan efficiency. However, increased rate of breathing may affect motion during data acquisition and therefore image quality.

Conclusions: Initial results have proved promising allowing regulation of the breathing pattern to reduce the shifts in the end expiratory diaphragm position. Altering the tempo of the sounds has been shown to influence the range of respiratory motion and therefore the number of end expiratory positions and scan efficiency during the scan. More detailed analysis and experiments are now underway to determine the effects o image quality and scan efficiency in coronary MRA as well as the robustness of such a technique.

REFERENCE

1. Kim WY, et al. N Engl J Med 2001;345:1863–1869.

430. CARDIAC MRI FOR DIFFERENTIAL DIAGNOSIS OF THE APICAL BALLOONING SYNDROME

Florian Behrendt, Dietmar Kivelitz, Kathrin Schindler, Gerhard Schuler, Holger Thiele. ***University of Leipzig–Heart Center, Leipzig, Germany.***

Introduction: The apical ballooning syndrome has first been described in Japan and has recently been recognized in western countries. The underlying mechanisms of this clinical entity mimicking acute coronary syndromes are still controversially discussed. Coronary spasm, coronary emboli with spontaneous fibrinolysis, regional myocarditis, and stunning as a result of excessive catecholamines are some of the potential mechanisms. Cardiac MRI might be an imaging tool to further elucidate the underlying mechanisms.

Purpose: Assessment of cardiovascular MRI parameters for the identification of apical ballooning syndrome.

Methods: Between January 2005 and July 2006 22 consecutive patients, showing a left ventricular dysfunction with apical ballooning not explainable by the coronary artery status and initially admitted with an acute coronary syndrome, underwent cardiac MRI. Cardiac MRI using a 1.5 T MRI scanner (Philips Intera CV) included a steady-state free precession technique for the assessment of left ventricular function and a T2-weighted spin echo sequence for the assessment of oedema. For the assessment of delayed enhancement a 3D inversion recovery gradient echo sequence was applied after administration of. 0.15 mmol/kg of body weight Gadoteridol (Gadovist, Schering, Germany).

Results: Between January 2005 and July 2006 2089 patients were admitted presenting with an acute coronary syndrome with ST-elevation or non-ST-elevation myocardial infarction. Of these, 22 (1.0%) patients (21 female, age 68±12 years) were identified with apical ballooning syndrome without significant coronary artery disease. Cardiac MRI revealed extensive delayed enhancement in the territory of the left anterior descending coronary in 4 patients and a delayed enhancement pattern suggestive of acute myocarditis in 1.

In all other patients neither delayed enhancement nor oedema was detected. In these latter patients cardiac MRI showed impaired left ventricular ejection fraction which normalized at 3 months follow-up (EF baseline: 49.6 ± 11.0%; EF 3 months: 67.9 ± 4.5%; $p < 0.001$ versus baseline). Similarly, the end-diastolic volume (EDV) and endsystolic volume (ESV) improved at follow-up (EDV baseline: 131.5 ± 27.2 mL; EDV 3 months: 115.1 ± 22.3 mL; $p < 0.001$ versus baseline; ESV baseline 65.7 ± 21.7 mL; ESV 3 months: 37.3 ± 10.2 mL; $p < 0.001$ versus baseline). One patient showed initial involvement of the right ventricular function which completely resolved at follow-up. There were no differences in patient characteristics between the patients with presumed coronary emboli with spontaneous lysis and myocarditis in comparison to those with classical apical ballooning syndrome with the exception that in patients with apical ballooning syndrome emotional stress as a trigger could be identified in 11 (65%) versus 0 ($p = 0.03$).

Conclusions: The apical ballooning syndrome is a phenomenon mimicking acute coronary syndromes which has a prevalence of approximately 0.7% in our series of patients. Cardiac MRI allows to differentiate apical ballooning syndrome from other rare causes such as myocarditis and coronary emboli with spontaneous lysis. Therefore, cardiac MRI should be performed in all patients with suspected apical ballooning syndrome for further differential diagnosis.

431. CLINICAL USE OF DSMR LEADS TO A REDUCTION OF INVASIVE ANGIOGRAPHIES IN PATIENTS WITH SUSPECTED CAD IN COMBINATION WITH A LOW EVENT RATE

Sebastian Kelle, MD, Christina Egnell, MD, Thomas Kokocinski, MD, Thomas Thouet, MD, Juliane Vierecke, MD, Susanne Vogel, MD, Amedeo Chiribiri, MD, Eckart Fleck, MD, Eike Nagel, MD. ***German Heart Institute Berlin, Berlin, Germany***

Introduction: Assessment of regional left ventricular wall motion during dobutamine-stress MR (DSMR) is well established for the identification of myocardial ischemia. However, it is little known on its prognostic value and its potential to reduce the number of invasive catheterizations.

Purpose: To determine whether the integration of DSMR into clinical decision making reduces the number of invasive angiographies in patients with suspected CAD in combination with a low event rate.

Methods: Medical records of 130 consecutive patients with intermediate posttest likelihood for CAD after exercise ECG

and dobutamine stress echo who underwent DSMR for the detection of coronary artery disease were reviewed. One hundred twetny-seven patients were followed for a median of 23 months. The occurrence of cardiac death, myocardial infarction, percutaneous coronary intervention (PCI), and coronary artery bypass surgery (CABG) was evaluated. A positive DSMR was defined as new or worsening wall-motion abnormality (WMA) during dobutamine stress.

Results: The following events were observed: cardiac death: 0; myocardial infarctions: 2; revascularizations (PCI and CABG): 18 (14.2%) patients. DSMR was positive in 34 (26.8%) patients. Patients with inducible ischemia at DSMR were more likely to undergo revascularization during follow-up as compared with patients without ischemia (31/34 [91.2%] vs. 25/93 [26.9%]). Four (4.3%) of the 25 patients with a negative DSMR who underwent invasive angiography were found to have significant CAD. In patients with positive DSMR a significantly higher number of events was found in comparison to patients with negative DSMR ($p < 0.0001$).

Conclusions: When DSMR is used for clinical decision making in patients with intermediate posttest likelihood of CAD after exercise ECG and dobutamine stress echo, 55.9% of patients did not require cardiac catheterization. No hard events are observed in this patient group. Patients who were catheterized despite a negative DSMR had a 4.3% likelihood of CAD.

432. HIGH-DOSE DSMR AT 3 TESLA IN PATIENTS WITH SUSPECTED OR KNOWN CAD—A FEASIBILITY STUDY

Sebastian Kelle, MD, Ashraf Hamdan, MD, Bernhard Schnackenburg, PhD, Uwe Köhler, PhD, Eckart Fleck, MD, Eike Nagel, MD. ***German Heart Institute Berlin, Berlin, Germany.***

Introduction: The assessment of inducible wall motion abnormalities during high dose dobutamine-stress MR (DSMR) is well established for the identification of myocardial ischemia at 1.5 Tesla in patients. Its feasibility at higher field strengths has not been reported.

Purpose: To evaluate image quality for DSMR at 3 Tesla.

Methods: Nine consecutive patients (2 women) (60 ± 12 years) underwent DSMR for the detection of coronary artery disease. All patients were examined with a Philips Achieva 3.0 Tesla system, using a spoiled gradient echo-cine-sequence. Technical parameters were: spatial resolution $2 \times 2 \times 8$ mm, 30 heart phases, spoiled gradient echo TR/TE = 4.5/2.6 ms, flip angle 15°. Dobutamine was administered using a standard protocol (10 μg increments every 3 minutes up to 40 μg dobutamine/kg body weight/minute plus atropine if required to reach target heart rate). The examination was terminated, if new or worsening wall-motion abnormalities or chest pain occurred or target heart rate was achieved.

Results: In one patient the exam had to be terminated due to ECG failure due to a broken lead. Target heart rate was reached in 5 patients. Five patients had a positive stress test (4 before target heart rate), in 2 patients the exam was stopped due to chest pain. Five of 5 patients with a positive DSMR were examined with invasive angiography, significant CAD was found in all of these patients.

Conclusions: Initial results of high-dose DSMR at 3.0 Tesla show diagnostic image quality in all patients.

433. ANALYSIS OF MYOCARDIAL MOTION IN PATIENTS WITH HEART FAILURE AND CORONARY ARTERY DISEASE USING HIGH-TEMPORAL-RESOLUTION MR TISSUE PHASE MAPPING.

Tammy J. Pegg, MB ChB MRCP,[1] Oliver J. Rider, BM ChB MRCP,[1] Steffen E. Petersen, DPhil,[1] Theodoros D. Karamitsos, MD,[1] Jane M. Francis, DCCR, DNM,[1] Matthew D. Robson, PhD,[1] Clare E. Jackson, PhD,[1] Bernd A. Jung, PhD,[2] David P. Taggart, MD, DPhil FRCS,[1] Stefan Neubauer, MD, FRCP,[1] Joseph B. Selvanayagam, DPhil FRACP.[1] [1] ***University of Oxford, Oxford, United Kingdom,*** [2] ***Department of Radiology, University of Freiburg, Freiburg, Germany.***

Introduction: Phase Contrast Magnetic Resonance Imaging or Tissue Phase Mapping (TPM) is an established technique for examining 3-dimensional myocardial velocities. Unlike tissue Doppler, TPM is not limited by transducer angulation and hence potentially affords superior reproducibility and complete 3-dimensional myocardial coverage. However, as earlier data acquisition with TPM was typically based on multiple breath-hold 2D measurements, the spatial and temporal resolution were limited by the length of the breath-hold period—a particular problem for heart failure patients. Recently, a navigator gated high temporal resolution TPM has become available and successfully trialled in volunteers.

Purpose: In this study, we aimed to apply Navigator TPM in patients with heart failure secondary to coronary artery disease (CAD), and in combination with delayed hyperenhancement, to separately examine motion in severely dysfunctional non hyperenhancing myocardium and transmural scar.

Methods: Seven patients with 3 vessel CAD and impaired left ventricular function and five healthy volunteers underwent navigator gated high temporal resolution TPM, (temporal resolution 13.8 ms, spatial resolution 1–3 mm) using black blood k-space segmented gradient echo sequence for the analysis. In addition patients underwent delayed hyperenhancement imaging (DE-CMR) for the quantification of myocardial scar using a T1-weighted turboFLASH sequence, with 0.1 mmol/Kg Gd-DTPA bolus injection. DE-CMR and TPM data analysis was performed utilizing customized software (Matlab version 6.5; Mathworks, Natick, Massachusetts, USA). Myocardial

TABLE 1
Mean peak myocardial velocities ± standard deviation.

	Normal segments n = 80	Affected segments n = 60	Transmural scar segments n = 17
Radial velocity (cm/s)			
Systole	3.38 ± 0.96	3.30 ± 1.39*	3.12 ± 1.30*
Diastole	−5.46 1.71	−4.33 ± 2.11*	−4.53 ± 1.55*
Longitudinal velocity (cm/s)			
Systole	−6.00 ± 3.99	−4.79 ± 2.98*	−4.50 ± 3.94[a]
Diastole	10.40 ± 4.00	8.40 ± 3.80*	7.83 ± 3.99*

*$p < 0.05$; [a]$p = 0.09$

segments were divided according to the AHA criteria ensuring concordance between DE-CMR and TPM analysis. Visual assessment of resting regional wall motion score was performed by two cardiologists and graded (1= normal, 2 = mild hypokinesia, 3 = severe hypokinesia, 4 = akinesia, 5 = dyskinesia). Each segment was categorized as normal (healthy controls), affected (a non scarred myocardial segment with resting regional wall abnormality) or scarred (>50% transmural scar). All other segments were excluded from the analysis.

Results: Seven patients (6 men; mean age 68 ± 10 years) had a mean ejection fraction of 37% ± 15 and the 5 healthy controls (3 men; age 56 ± 4 years) an ejection fraction of 69% ± 5. In total 192 segments were analysed, 77 (69%) patient segments are included in final analysis (22 segments were excluded because of subendocardial scar, 7 segments because of normal resting regional wall motion, 6 segments because of motion artefact affecting a single mid-ventricular slice). Sixty segments were termed affected, the mean resting regional wall motion score of these affected segments was 3.03 ± 0.68. Seventeen had transmural scar, with a mean resting regional wall motion score 3.89 ± 0.96 ($p < 0.05$). All 80 segments in healthy volunteers were included in the analysis.

In the longitudinal direction, peak systolic velocity was significantly lower in affected myocardium −4.79 cm/s ($p < 0.05$), and showed a trend towards significance in transmural scar −4.50 cm/s ($p = 0.09$) compared to normal volunteers −6.00 cm/s (Table 1). Systolic peak radial velocities were similar in affected myocardium and transmural scar compared to normal 3.30 and 3.12 vs 3.38 cm/s (p = NS). Diastolic radial velocities were significantly lower in affected myocardium −4.33 cm/s ($p < 0.05$) and transmural scar −4.53 cm/s ($p < 0.05$) compared to normal volunteers −5.46 cm/s. Longitudinal diastolic relaxation was also slower in affected segments 8.40 cm/s, and transmural scar 7.83 cm/s ($p < 0.05$) compared to 10.40 cm/s in normal volunteers ($p < 0.05$).

Conclusions: TPM using a high temporal resolution navigator sequence is feasible in CAD patients with heart failure. In combination with DE-CMR, we demonstrate that severely dysfunctional non-scarred myocardium and transmural scar both exhibit a similar impairment of systolic and diastolic velocity in radial and longitudinal directions. This technique has potential to be a powerful tool in the investigation of dysfunctional myocardium and in assessing the effectiveness of medical and interventional therapies in CAD and cardiomyopathy.

434. COMBINED ADENOSINE STRESS PERFUSION AND STRESS TAGGING PROTOCOL FOR DETECTION OF CAD AT 3 TESLA

Daniel K. Thomas, MD, Carsten Meyer, MD, Katharina Strach, MD, Mathias Hackenbroch, MD, Hans H. Schild, MD, Torsten Sommer, MD. ***University of Bonn, Bonn, Germany.***

Introduction: While adenosine-stress perfusion imaging is a very sensitive technique for the detection of coronary artery disease (CAD), its specificity is rather low. In contrary the use of standard adenosine-stress cine imaging lacks high sensitivity, but is very specific for detection of CAD. Detection of wall motion abnormalities (WMAs) can be improved by the use of myocardial tagging techniques. Both, myocardial perfusion imaging and myocardial tagging benefit from high field strength due to increased CNR, SNR as well as improved tag persistence and tag definition, allowing for high image resolution and combination with parallel imaging techniques.

Purpose:

1. To integrate myocardial tagging into a comprehensive adenosine-stress-protocol for detection of coronary artery disease (CAD) at 3 Tesla.
2. To investigate the additive value of myocardial tagging in a combined adenosine-stress perfusion-tagging protocol for detection of significant CAD in a mixed patient population (known or suspected CAD).

Methods: Patients with known or suspected CAD, admitted for non-invasive adenosine stress cardiac magnetic resonance (CMR) imaging, were included. The study protocol was approved by the local ethics committee. Adenosine-stress perfusion and adenosine-stress tagging images were acquired in 3 identical short axis locations. Sequence parameters were as follows: Slice thickness 8mm, FOV 320-380 mm, reconstructed matrix 256x256, sense factor 2-2.5 for both sequences. TE 3.0

ms, TR 1.4 ms, flip 15°, 3 slices/RR-interval, shared sat-prepulse for the perfusion scan as well as TE 3.7 ms, TR 2.2 ms, flip 10°, 16 cardiac phases, 8 mm tag separation, grid-tag pattern, for the tagging scan. A patient to patient and a vessel to vessel analysis were performed. A positive catheter—finding at invasive coronary angiography (CA, refererence standard) and thus significant CAD was defined as a luminal stenosis or flow limiting restenosis >70% in native and graft vessels. A true positive CMR—finding was defined as one or more perfusion deficits or new WMA during adenosine-stress in angiographically corresponding regions.

Results: To date we evaluated 22 patients (male: 16, female: 6; median age: 63; 5 patients with suspected, 17 patients with known CAD), where both CMR exams and invasive CA were completed. The tagging sequence extended imaging time by 1.5–3 minutes and was well tolerated by all patients. In the figure a stress-induced perfusion deficit is shown in the lateral wall (arrow, b). A dark rim artefact (asterisk, b) can already be observed under resting conditions (a). The catheter shows an interruption of the posterolateral branch (full arrow, c) with retrograde inflow (dotted arrow, c). The tagging sequence (d) did not demonstrate any WMAs. Sensitivity and specificity for detection of significant CAD by adenosine stress perfusion were 0.92 and 0.70 respectively. The sensitivity of adenosine stress tagging was less (sens. 0.67), while the specificity was very high (spec. 1.0). The vessel-to-vessel analysis yielded lower values for sensitivities, but higher values for specificities for both perfusion (LAD: sens. 0.57, spec. 0.87; RCA: sens. 0.83, spec. 0.94; CX: sens. 0.86, spec. 0.93) and tagging imaging (LAD: sens. 0.57, spec. 1.0; RCA: sens. 0.67, spec. 1.0; CX: sens. 0.43, spec. 1.0). The combination of both techniques did not increase sensitivity.

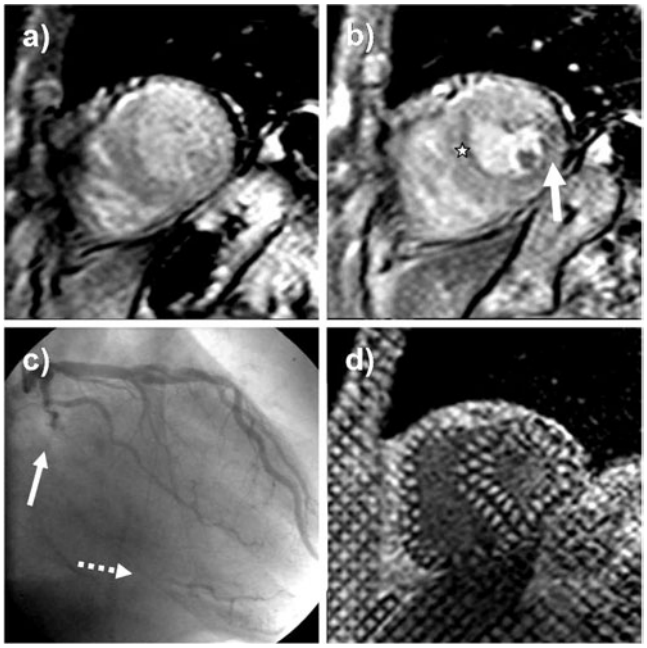

Conclusions: The implementation of a combined adenosine stress perfusion and tagging protocol at 3 Tesla is feasible and well tolerated by patients. The application of the protocol to a mixed patient population (known or suspected CAD) for detection of significant CAD delivers good values for sensitivity and specificity. While the sensitivity of adenosine stress tagging is rather poor compared to perfusion imaging, its specificity is very high. This technique should thus prove very useful in cases of inconclusive perfusion studies (eg. in the presence of artefacts), to help avoid false positive results.

435. ADDITION OF THE LONG AXIS INFORMATION TO SHORT AXIS CONTOURS REDUCES INTERSTUDY VARIABILITY OF THE LEFT VENTRICLE IN CARDIAC MAGNETIC RESONANCE STUDIES

Sharon W. M. Kirschbaum, MD,[1] Timo Baks, MD,[1] Ed Gronenschild, PhD,[2] Jean-Paul Aben, BsC,[3] Annick C. Weustink, MD,[1] Piotr A. Wielopolski, PhD,[1] Gabriel P. Krestin, MD, PhD,[1] Pim J. de Feyter, MD, PhD,[1] Robert-Jan M. van Geuns, MD, PhD.[1] [1]***Erasmus MC, Rotterdam, The Netherlands,*** [2]***Department of Medical Informatics, Maastricht University, Maastricht, The Netherlands,*** [3]***Pie Medical Imaging, Maastricht, The Netherlands.***

Introduction: Left ventricular function and mass are used in clinical practice as parameters of cardiac function and currently more used as end-points in clinical trials, therefore, it is important to keep variability low. Variability is introduced during acquisition when the short axis (SA) series are planned on the 4-chamber localisation images. Furthermore, during post procedure analysis variability is introduced by the observer making decisions on inclusion or exclusion of the basal and apical slice, which can be difficult on short axis images and therefore subjective. Identification of the location of the mitral valve plain and apex can better be performed on the long axis images. Including this information may, therefore, improve reproducibility and allow inconsistent planning procedure.

Purpose: Investigate the influence of mitral valve plain and apex selection on interstudy variability of left ventricular analysis by cardiac magnetic resonance (CMR)

Methods: A total of twenty patients with documented heart failure and twenty volunteers underwent CMR examination twice for measuring endocardial end diastolic volume (EDV), endocardial end-systolic volume (ESV), mass and ejection fraction (EF). The boundary of the left ventricle, the mitral valve plain and apex were marked manually on the 2 and 4 chamber long axis images. Automatic epicardial and endocardial contour detection was performed on the short axis (SA) images using the intersection of the outlines from the long axis as starting condition. These results were compared to analysis by the same observer based on the short axis only.

Results: The percentage interstudy variability decreased significantly for all subjects when the information of the long axis was included; for ESV, 9.6% vs. 4.7%, ($p = 0.0004$); for EDV, 4.9% vs. 2.5% ($p = 0.004$); for mass, 7.4% vs. 5.0% ($p = 0.01$); and for EF 12.2% vs. 5.6% ($p = 0.00005$), respectively.

Conclusions: Identification of mitral valve plain and apex on long axis images reduces interstudy variability for all parameters.

436. MYOCARDIAL EDEMA IS A FEATURE OF TAKO-TSUBO CARDIOMYOPATHY AND IS RELATED TO THE SEVERITY OF REGIONAL SYSTOLIC DYSFUNCTION

Hassan Abdel-Aty, Myra Cocker, Matthias G. Friedrich. ***Stephenson CMR Centre at the Libin Cardiovascular Institute of Alberta, Departments of Cardiac Sciences and Radiology, University of Calgary, Calgary, Alberta, Canada.***

Background: Acute reversible cardiomyopathy (Tako-Tsubo) is a unique form of cardiomyopathy related to emotional stress and mostly affects women. Tissue characterization of Tako-Tsubo using CMR is not well defined. T2-weighted CMR sensitively identifies myocardial edema, the presence of which as a marker of acute myocardial injury although conceivable has not been previously described in Tako-Tsubo. Furthermore, whether T2-weighted signal abnormality relates to the regional systolic dysfunction is unknown.

Methods: We studied 7 Tako-Tsubo patients (all females, 75 $\pm$ 8y) and 5 healthy subjects (2 females, 36 $\pm$ 9y) using 1.5T scanner. Three sequences were applied: SSFP (global and regional function), T2-STIR (myocardial edema) and inversion recovery gradient echo 10 minutes after IV Gadolinium-DTPA (irreversible injury). All sequences were acquired in short and long axis slices (2, 3 and 4-chamber). Image analysis: 1) Visual: T2 and LE images were evaluated for the presence of focal high signal, 2) Quantitative: systolic wall thickening and myocardial T2 SI were measured per segment (16-segment model) and per slice (base, mid-ventricular and apex).

Results: A well-defined transmural area of high T2 signal was readily visible involving the mid-anterior wall and all apical segments in all patients but none of the controls. Patients showed a significant gradient in percent systolic thickening from base to apex (base: 150 $\pm$ 78, mid: 62 $\pm$ 30, apex: 31 $\pm$ 40; $p = 0.002$). This was not observed in controls (base: 94 $\pm$ 23, mid: 99 $\pm$ 30, apex: 116 $\pm$ 21; p = ns). In patients, T2 SI increased progressively from base to apex (base 94 $\pm$ 16, mid: 119 $\pm$ 16, apex: 127 $\pm$ 15; $p = 0.005$) in contrast to controls with an opposite pattern (base: 70 $\pm$ 16, mid: 70 $\pm$ 14, apex 64 $\pm$ 17; $p = 0.02$). The same relations were observed when the relative (to skeletal muscle) T2 SI was considered. A significant inverse relation between segmental thickening and segmental T2 SI ($r = -0.63$, $p < 0.0001$) was observed in patients but not in controls. In 3 patients, minute apical foci of late enhancement were also noted.

Conclusion: We provide first evidence that edema as defined by increased T2 signal intensity is a feature of Tako-Tsubo cardiomyopathy. This was co-localized with regional systolic dysfunction. T2-weighted CMR may be very helpful for diagnosing and staging this entity.

437. RAPID PHASE-MODULATED WATER EXCITATION SSFP FOR FAT-SUPPRESSED CINE MRI

Hung-Yu Lin, MS, Subha Raman, MD, Orlando Simonetti, PhD. ***The Ohio State University, Columbus, Ohio, USA.***

Introduction: Suppression of bright fat signal is essential in many cardiovascular magnetic resonance (CMR) applications to improve lesion conspicuity, suppress motion and chemical shift artifacts, and minimize blurring in long readout acquisitions. Several techniques have been proposed to suppress fat while maintaining the magnetization steady-state in SSFP, including fat-saturation pre-pulses (1) and the "iterative decomposition of water and fat with echo asymmetry and least squares estimation" (IDEAL) method (2). These techniques have limited success in cardiac SSFP imaging due to increasing sensitivity to off-resonance artifacts and/or prolonged repetition time (TR) and acquisition time.

Purpose: The phase-modulated water excitation (WE) method has been described for spectrally and spatially-selective rapid gradient-echo imaging (3). The purpose of this study was to investigate the performance of phase-modulated binomial WE pulses with cine SSFP to achieve and maintain a fat suppressed steady-state. Our hypothesis was that sufficient fat signal suppression could be achieved with minimal impact on TR, total scan time, and cine SSFP image quality using rapid binomial WE pulses. Numerical simulation, phantom and healthy volunteer imaging trials were performed to provide validation of the fundamental concepts underlying rapid water excitation.

Methods: Spectral-spatial selective excitation can be achieved using a binomial pulse train. The simplest binomial pulse (1-1) consists of two α° pulses with interpulse delay (τ) chosen to allow 180° of phase evolution between water and fat spins ($\tau = 2.2$ ms at 1.5 Tesla). In SSFP applications, it is critical to keep the pulse duration as short as possible to avoid lengthening the TR. Rather than 180° of phase evolution between pulses, phase-modulated WE employs a partial off-resonance phase evolution to shorten the combined binomial pulse duration. This strategy was used in designing a minimum time spectral- spatial selective binomial pulse for cine SSFP. We propose an SSFP sequence utilizing a simple 1-1 binomial slice-selective RF pulse with 1.1 msec interpulse spacing to allow 90° of fat-water phase evolution. The frequency response of three different binomial WE pulses were investigated by numerical simulation, imaging of water and fat phantoms, and normal volunteer imaging. Six

Signal-to-noise and contrast-to-noise measures

Sequences	Interpulse Phase Evolution (°)	Interpulse Delay (ms)	SA in Myocardium	SA in Fat	Noise	CNR
Standard SSFP	N/A	N/A	267.4 ± 20.6	694.7 ± 48.2	4.4	−97.1
1-1 WE SSFP	90°	1.1	305.2 ± 25.1	217.8 ± 37.3	4.4	19.86

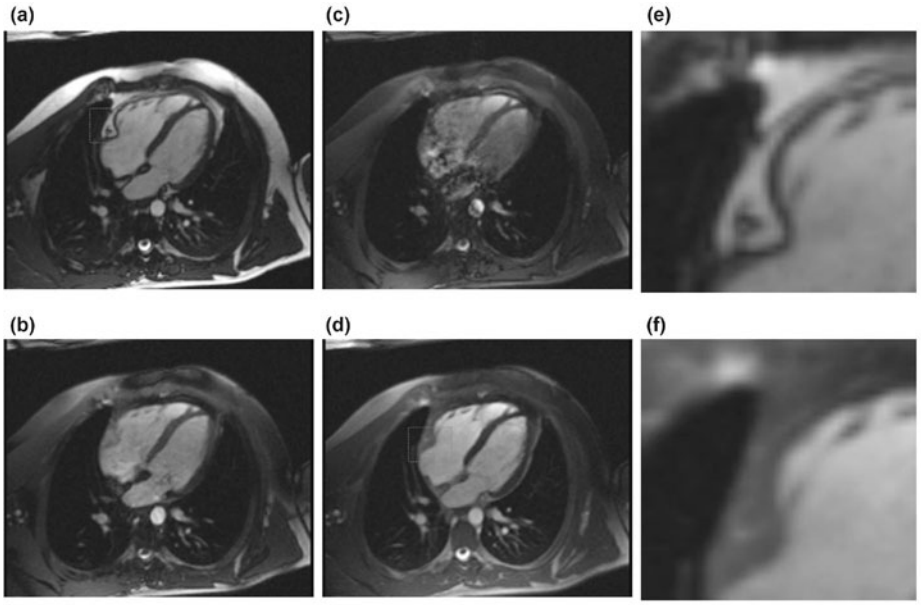

FIG. 1. Healthy volunteer cardiac images in four-chamber view using (a,e) Conventional slice-selective RF pulse, (b) spectral-spatial binomial 1-1 water excitation pulse with 180° phase evolution (interpulse delay = 2.2 msec), (c) spectral-spatial binomial 1-2-1 water excitation pulse with 180° phase evolution (interpulse delay = 2.2 msec). (d,f) spectral-spatial binomial 1-1 phase-modulated ater excitation pulse with 90° phase evolution (TR/TE/FA $_{effective}$/Slice Thickness/Matrix = 8.8 ms/2.2 ms/70°/5 mm/256 × 192). Note that the Fig. (e) and (f) are the magnified images corresponding to rectangular region in Fig. (a) and (d), respectively.

healthy volunteers (1 woman; aged 46 years, and 5 men; aged 22–57 years, with a mean age of 43.25 ± 13.72) underwent MRI of the heart at 1.5 Tesla (MAGNETOM Avanto, Siemens Medical Solutions) to compare retrospectively-gated SSFP cine with and without WE.

Results: In-vivo results using four different excitation pulses are demonstrated in Fig. 1. Binomial WE pulses (Fig. 1b-d) show marked fat signal reduction compared to conventional cine SSFP (Fig. 1a) in cardiac four-chamber view. Fat suppression is excellent for 1-2-1 WE (Fig. 1c), and the heart is clearly delineated. However, severe field inhomogeneity artifacts and flow artifacts appear because of the long duration of the 1-2-1 WE pulse, leading to unacceptable TR. The 1-1 pulse with 90° phase evolution (Fig. 1d and 1f) demonstrates effective fat suppression and minimal scan time increase without any noticeable artifact compared to standard cine SSFP (Fig. 1a and 1e). *In vivo* measurements demonstrated that the WE-SSFP increased the myocardium-fat contrast-to-noise ratio from -97.1 to 19.9 without inducing any perceptible artifacts (Table 1).

Conclusions: Fat suppression can be achieved in SSFP cine while maintaining steady state equilibrium using rapid, phase modulated, binomial water excitation. This technique is similar to the alternating TR SSFP approach described by Leupold et al (4), but without the constraints of specific TR ratio or flip angle.

REFERENCE

1. Scheffler K, et al. MRM 2001;45:1075–80.
2. Reeder SB, et al. JMRI 2005;22:44–52.
3. Thomasson D, et al. MRM 1996;35:563–8.
4. Leupold J, et al. MRM 2006;55:557–65.

438. DUAL OR SINGLE BOLUS APPROACH IN QUANTITATIVE CMR PERFUSION IMAGING: IS THERE ANY DIFFERENCE?

Wolfgang Utz,[1] Andreas Greiser,[2] Jeanette Schulz-Menger,[1] Rainer Dietz.[1] ***[1]AG MRT, Franz Volhard Klinik, Charité, Helios Klinikum Berlin, Berlin, Germany, [2]Siemens AG Medical Solutions, Erlangen, Germany, Erlangen, Germany.***

Background: In myocardial MR perfusion imaging a dual-bolus approach has been proposed to overcome the limitations of T1

saturation effects on the arterial input function and to improve accuracy of perfusion quantification. While feasibility and good reproducibility of this technique has been demonstrated for human perfusion imaging, its impact on myocardial perfusion reserve (MPR) in comparison to a single bolus approach has not been investigated before. We report on regional and global MPRs as assessed by fully quantitative model constrained deconvolution using either the pre-bolus or main-bolus as arterial input function.

Methods: Eleven patients (5 female, range 44–83 years) were examined on a 1.5 T clinical MR scanner (Siemens Sonata) in a stress-rest perfusion protocol within 7 days after invasive exclusion of stenotic coronary artery disease. Gd-DTPA dosages of 0.005 and 0.05 mmol/kg bw were used as pre-bolus and main-bolus and administered with equal bolus volumes during maximum vasodilation (Adenosine, 140 mug/kg b.w.) and during rest after 20 min. Three short axes were acquired every heart beat using an accelerated TurboFLASH pulse sequences (TR 172 ms; TE 1.25 ms; flip angle 12°; inversion time 100 ms; parallel imaging (GRAPPA1) acceleration rate 2; FOV 320-370 mm; matrix size 94 × 192; in plane resolution 1.7–2.0 × 2.6–3.0 mm; slice thickness 10 mm; bandwidth 500 Hz/Px).

According to the 16-segment-model subendocardial and transmural MPRs of 176 myocardial segments were determined by Fermi model based deconvolution of segmental time-signal intensity curves using commercially available software (CMR-Tools, London). For comparison, the time-signal intensity curve of either pre-bolus or main-bolus served as arterial input function. Linear regression analysis and paired student's t-test was used to check for statistical differences between both techniques.

Results: Linear regression analysis revealed a moderate to strong positive correlation of regional transmural (subendocardial) MPRs of r = 0.70 (0.59) between by both techniques. Furthermore the slope of linear relation was 1.02 for the transmural and 1.03 for subendocardial MPRs. On a segmental basis there were no statistically significant differences of transmural MPRs (p = 0.1) and only weak differences of subendocardial MPRs (p = 0.04) between both techniques.

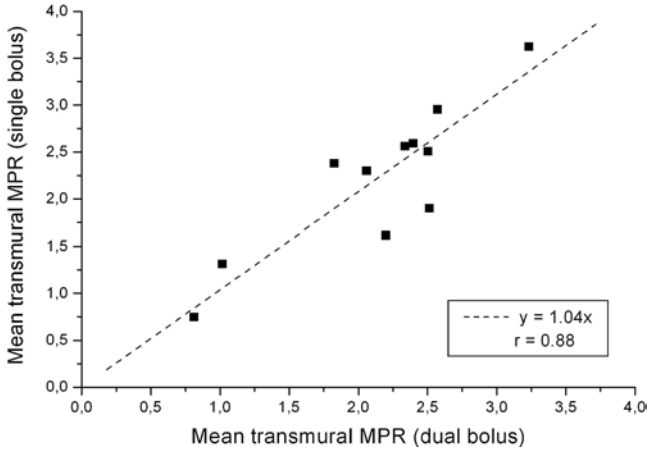

On a per patient basis (Fig. 1) however, the coefficient of variation of regional MPRs was markedly reduced using the dual bolus method in comparison to a single bolus evaluation (20% vs. 32%, p < 0.001). Also a strong positive correlation was detectable for global transmural (r = 0.88) and subendocardial (r = 0.75) MPRs between both techniques with slopes of 1.04 and 1.05.

Conclusion: Mean MPR values remain virtually unchanged between a dual- and a single bolus approach in quantitative MR perfusion imaging, indicating that T1 saturation effects on arterial input function cancel out each other in a stress-rest protocol. A reduced regional variance of MPRs however may allow for a better discrimination of segments supplied by a stenotic vessel.

REFERENCE

1. Griswold MA, et al. Magn Reson Med 2002;47:1202-10.

439. CAN T2-WEIGHTED MAGNETIC RESONANCE IMAGING DETECT MICROVASCULAR OBSTRUCTION IN ACUTE MYOCARDIAL INFARCTION?

Dietmar E. Kivelitz,[1] Kathrin Schindler,[1] Christian Lücke,[1] Josef Friedenberger,[2] Gerhard Schuler,[2] Holger Thiele.[2]
[1]Department of Radiology, University of Leipzig–Heart Center, Leipzig, Germany, [2]Department of Cardiology, University of Leipzig–Heart Center, Leipzig, Germany.

Introduction: The presence of hypo-enhanced regions at the core of hyper-enhanced acute myocardial infarctions is a marker of microvascular obstruction (MO) seen in magnetic resonance imaging (MRI) in the first few minutes after contrast infusion or as persistent MO (PMO) on delayed contrast enhanced imaging (1). In acute ST-segment-elevation myocardial infarction (STEMI) myocardial edema can be recognized as an increased signal intensity using T2-weighted sequences. However, increased signal intensity in STEMI on T2-weighted images can be inhomogeneous which may reflect areas of microvascular obstruction. Until now there are no reports that have compared the inhomogeneity of changes in T2 relaxation time with the presence of MO and PMO.

Purpose: To investigate the potential of T2-weighted sequences to detect MO in acute STEMI.

Methods: Sixty-seven patients, 51 male and 16 female, underwent cardiac MRI 2–4 days after an acute STEMI (symptoms < 12 h) treated by primary coronary intervention (PCI). MRI was performed using a 1.5 T scanner (Philips Intera CV). ECG-gated T2-weighted STIR (short tau inversion recovery) sequence in three short axis views (basal, mid and apical) were acquired to visualize myocardial edema. After administration of. 0.15 mmol/kg of body weight Gadobutrol (Gadovist, Schering, Germany) a 3D inversion recovery gradient echo sequence in the same orientation was applied to assess the size of the myocardial infarction and to determine the presence of MO after 2 minutes

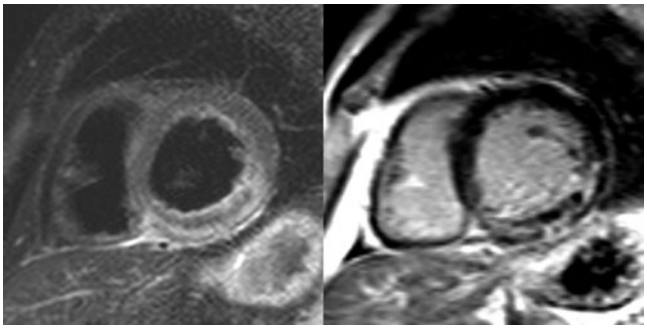

FIG. 1. T2-weighted STIR (a) and contrast enhanced late enhancement sequence (b) in a short axis view in a patient with STEMI of the inferior wall. Excellent morphologic correlation of the area of MO. MO can be recognaized as a low signal intensity zone surrounded by bright signal in both sequences.

and PMO after 15 minutes. Segments of myocardial infarction were compared regarding the presence of low signal intensity surrounded by bright signal intensity in the T2-weighted image with areas of low or absent signal surrounded by late enhanced tissue in the contrast enhanced study.

Results: In 67 patients, we compared 201 short axis slices with STIR, early and late contrast enhanced sequences. In 161 (80%) of these slices myocardial infarction was present as defined by late contrast enhancement. Overall, in 72 (45%) of the infarcts both MO and PMO were present, additionally in 7 (4%) only MO and in 4 (2.5%) cases only PMO was present. The T2-weighted STIR sequence showed areas of decreased signal intensity (SI) surrounded by increased SI in 67 (42%) infarct areas. There was agreement regarding decreased SI center between STIR und MO in 82% and between STIR and PMO in 85.5% (Fig. 1). However, STIR images showed a decreased SI in the infarct center in 4 regions without evidence of MO or PMO.

Conclusions: Areas of microvascular obstruction appear as areas of decreased signal intensity surrounded by increased SI in T2-weighted images. There is a good correlation of the T2-weighted images with MO and PMO; therefore, T2-weighted sequences are suitable to detect areas of microvascular obstruction. The decreased signal intensity in the T2-weighted images in the area of MO may be due to hemorrhage or hemostasis in the obstructed microvasculature.

REFERENCE

1. Hombach et al. Eur Heart J 2005.

440. INFLUENCE OF THE PAPILLARY MUSCLES AND CARDIAC PHASE ON ACCURATE LEFT VENTRICULAR MASS MEASUREMENTS BY CMR

Sharon W. M. Kirschbaum, Timo Baks, MD, Amber Moelker, Gabriel P. Krestin, MD, PhD, Pim J. de Feyter, Robert-Jan M. van Geuns, MD, PhD. ***Erasmus MC, Rotterdam, The Netherlands.***

Introduction: Left ventricular mass is an important variable in the prognosis of cardiac patients because it is associated with an increase in the incidence of heart failure, ventricular arrhythmias, reduced left ventricular ejection fraction and sudden cardiac death. Although end-diastolic measurements are most frequently used, little information on the influence of the cardiac phase on this measurement is available. Additionally inclusion or exclusion of the papillary muscle and trabeculations is of influence on accuracy.

Purpose: To evaluate different analysis strategies on left ventricular mass in 28 Yorkshire landrace swine.

Methods: Twenty-eight pigs underwent a cardiovascular magnetic resonance (CMR) scan to measure left ventricular mass. One day after the CMR was made, the animals were sacrificed. Estimated mass and true mass at autopsy were compared by calculating the correlation coefficient and the difference between both measurements. In addition variability was calculated.

Results: Excellent agreement was reached using the fastest strategy when the papillary muscle was ignored; end diastolic (ED) phase ($r = 0.82$) end-systolic (ES) phase ($r = 0.85$) but with a significant underestimation for the ED phase (-13.1 ± 9.1 g) and the ES phase (-16.1 ± 9.4 g). When the papillary muscle was added to the myocardial mass the correlation improved for the ED phase ($r = 0.87$) and ES phase ($r = 0.90$) and the underestimation was reduced for both phases (ED phase; -9.1 ± 7.8 g, ES phase; -11.9 ± 7.0 g).

The lowest percentage variability was found for the ED phase including the papillary muscles to the myocardium ($8.0 \pm 5.3\%$).

Conclusions: LV mass was determined most accurately by using the ED phase and including the papillary muscle.

441. IMPROVED ENDOTHELIAL FUNCTION WITH COMBINED CHELATION THERAPY IN β-THALASSAEMIA MAJOR

Mark A. Tanner, MRCP,[1] Renzo Galanello, MD,[2] Carlo Dessi, MD,[3] Annalisa Agus, MD,[2] Gill Smith, MSc,[1] Mark A. Westwood, MD,[1] Ravi Assomull, MRCP,[1] Sunil V. Nair, MRCP,[4] J. Malcolm Walker, MD,[4] Dudley J. Pennell, MD.[1] ***[1]Royal Brompton Hospital, London, United Kingdom, [2]Ospedale Microcitemico, Cagliari, Italy, [3]Osedale Microcitemico, Cagliari, Italy, [4]University College Hospital, London, United Kingdom.***

Introduction: Myocardial iron toxicity is the dominant cause of ventricular dysfunction in In β-thalassemia major (TM). Endothelial dysfunction can also occur and might further contribute to cardiovascular complications. Endothelial function can be determined by measurement of flow mediated dilatation of the brachial artery (FMD), which can be assessed reproducibly by cardiovascular magnetic resonance (CMR).

Purpose: To report the changes in endothelial function, LV ejection fraction and B-type natriuretic peptide (BNP) from a

randomized placebo controlled trial comparing combined chelation therapy (deferiprone and deferoxamine) with deferoxamine monotherapy.

Methods: Sixty-five patients (male 27, female 38, age 28.7 ± 4.8 years) with mild-moderate myocardial iron loading (heart T2* 8–20 ms) were randomized to receive either deferoxamine with placebo (placebo group), or deferoxamine with deferiprone (combined group). CMR assessments were made at baseline and after 12 months.

Results: Endothelial function improved significantly in the combined treatment group as compared to the placebo group (+8.8% vs 3.1% $p = 0.013$). There were also greater improvements in LV ejection fraction (+2.4% vs +0.6%, $p = 0.02$), and serum ferritin (−870 vs −194 μg/L; $p < 0.001$). These findings were in accord with improved myocardial T2* in the combined group (+43% vs +23%, $p = 0.017$). There was no significant change in BNP in either combined or placebo groups (+1.8 pmol/L vs +3.3 pmol/L, $p = 0.76$).

Conclusions: In patients with mild-moderate cardiac iron loading, endothelial function is markedly depressed. The combined therapy of deferiprone and deferoxamine is superior to deferoxamine alone in improving endothelial function in this setting.

442. COMBINED CHELATION THERAPY WITH DEFERIPRONE AND DEFEROXAMINE IN SIDEROTIC CARDIOMYOPATHY

Mark A. Tanner, MRCP,[1] Renzo Galanello, MD,[2] Carlo Dessi, MD,[2] Gill C. Smith, Jr, MSc,[1] Mark A. Westwood, MD,[1] Annalisa Agus, MD,[2] Dudley J. Pennell, MD.[1] [1]*Royal Brompton Hospital, London, United Kingdom,* [2]*Ospedale Microcitemico, Cagliari, Italy.*

Introduction: In thalassaemia major (TM), myocardial iron toxicity can result in a cardiomyopathy, with heart failure responsible for the vast majority of deaths. Severe cardiac siderosis can be treated by continuous intravenous deferoxamine, but not all deaths can be prevented and patient compliance can be poor. Combined chelation therapy with deferiprone and intermittent subcutaneous deferoxamine has proven effective in the treatment of mild-moderate myocardial siderosis, but the use of this treatment in the setting of severe myocardial iron loading has not been prospectively examined.

Purpose: To report the changes in myocardial iron (T2*) and ventricular function in patients with severe myocardial iron loading following treatment with the combination of oral deferiprone and subcutaneous deferoxamine.

Methods: Myocardial iron loading was assessed using T2* cardiovascular magnetic resonance (CMR) in 167 patients with TM receiving standard chelation monotherapy with subcutaneous deferoxamine. Of these patients, 22 were identified as having severe myocardial siderosis (T2* < 8 ms). 15 of these patients were allocated unblinded combination therapy and underwent CMR assessments at baseline 6 and 12 months to determine myocardial iron loading, left ventricular volumes and function.

Results: Myocardial T2* improved significantly from a baseline of 5.7 ± 0.98 ms to 7.9 ± 2.47 ms at 12 months (+39%, $p = 0.010$). Left ventricular ejection fraction improved from a baseline of 52.1 ± 11.8% to 65.6 ± 6.7% at 12 months (+13.5%, $p < 0.001$). Serum ferritin fell from a baseline of 2057 μg/L to 666 μg/L at 12 months ($p < 0.001$).

Conclusions: In severe myocardial siderosis, combined chelation therapy provides an effective means of reducing myocardial iron in concert with an improvement in cardiac function. This treatment should be considered as an alternative to continuous intravenous deferoxamine.

443. PHASE VELOCITY MAGNETIC RESONANCE IMAGING IS FUNDAMENTALLY FLAWED WHEN COMPARED WITH DOPPLER ECHOCARDIOGRAPHY

Vikas K. Rathi, MD, Robert W. W. Biederman, MD, Diane Vido, MS, Srinivas Vengala, MD, Mark Doyle, PhD. *Allegheny General Hospital, Pittsburgh, Pennsylvania, USA.*

Introduction: Blood flow and velocity can be measured using phase contrast magnetic resonance (PC-MR) imaging. The ability to measure velocity in a spatially and temporally resolved manner allows PC-MR data to be used in a manner different from Doppler echocardiography (D-Echo). However, it has not been clinically established that PC-MR provides equivalent information to D-Echo when confining measurement to similar variables.

Methods: We imaged two patient (Pt) groups ($n = 57$) to examine two distinct flow-fields 1) Mitral inflow in 31 subjects (21 diastolic dysfunction pts and 10 normal) to assess relatively low velocity and moderate temporal acceleration and 2) Aortic flow in 26 subjects (19 severe aortic stenosis and 7 normal) to assess high velocities and high temporal acceleration. All Pts received flow-field examination following ASE guidelines by Echo (Philips, Andover, New Jersey, USA) and with a PC-MR scan (GE signa CVi, Milwaukee, Wisconsin, USA) performed to assess three velocity components in a through-plane manner. The PC-MR images were acquired using retrospective ECG gating under free breathing conditions, with parameters: slice thickness 7 mm, FOV 38 cm^2, matrix 256 × 192, TR 7.0 ms, TE 3.2 ms, flip angle 20^0 and 2 excitations. Complete coverage of the cardiac cycle was accomplished using view-sharing to acquire 40 cardiac phases per cycle, resulting in a high temporal resolution (19 ± 3 ms). The velocity encoding was set at 150 cm/s for mitral flow and 500 cm/s for aortic flow. The slope of the linear regression curve fitted to compare local Doppler maximal velocities with the corresponding PC-MR velocities were calculated.

Results: Compared to D-Echo, PC-MR systematically underestimated maximal velocity for the mitral E and A flow-field (slope = 0.77, r = 0.81, $p < 0.001$), and systematically overestimated maximal velocity for aortic stenosis flow (slope = 1.24, r = 0.88, $p < 0.0001$). The D-Echo mitral E and A velocities and aortic stenosis velocity were characterized by maximal velocity and acceleration values (mean ± SD) of 0.68 ± 0.24 m/s, 8.4 ± 3.3 m/s^2; and 4.4 ± 0.6 m/s and 35 ± 7.2 m/s^2, respectively. Morphologic waveform analysis and diastolic function classification of the mitral flow-field showed 100% agreement between PC-MR and Doppler echocardiography.

Conclusions: Currently, PC-MR can result in systematic error when imaging clinically encountered flow-fields. The form of error is dependant on the exact mode of interaction between the flow-field and PC-MR acquisition variables. PC-MR measurement of maximal velocity is influenced by the acceleration and velocity components of the flow-field. Theoretical considerations indicate that the temporal distribution of PC-MR data can result in overestimation of maximal velocity, while low temporal resolution (<16 Hz) is likely responsible for underestimation of maximal velocity in a pulsatile flow-field. For the first time, a direct comparison with Doppler echocardiography has shown that these error terms are manifest in commonly encountered clinically relevant flow-fields. Although the application is robust and clinically feasible especially for flow quantification in shunts, for instance. PC-MR requires further development if it is to be used to accurately measure flow-fields in routine clinical scenarios where absolute velocities are necessary. Likely machine remedies under investigation include: interleaved acquisition, careful registration of the data, and accounting for acceleration components. Our data is based on a single vendor at our site, therefore a vendor specific investigation should be undertaken interrrogating PC-MR at variable clinical acceleration factors.

444. INTERVENTRICULAR MECHANICAL ASYNCHRONY IN PULMONARY ARTERIAL HYPERTENSION: RIGHT-TO-LEFT DELAY IN PEAK SHORTENING IS DUE TO RIGHT VENTRICULAR OVERLOAD AND IMPAIRS LEFT VENTRICULAR FILLING

J. T. Marcus, C.T. Gan, Jaco J.M. Zwanenburg, Anco Boonstra, Cornelis P. Allaart, Marco J.W. Gotte, Anton Vonk-Noordegraaf. ***VU University Medical Center, Amsterdam, The Netherlands.***

Introduction: In pulmonary arterial hypertension (PAH), leftward ventricular septal bowing (LVSB) is probably caused by a right-to-left (R-L) delay in myocardial shortening. The origin of either delayed or prolonged right ventricular (RV) shortening is unknown, and knowledge of this origin could have implications for treatment. A first potential mechanism is an electrical conduction delay: RV overload and concomitant remodeling may well lead to a (partial) right bundle branch block, right-to-left electrical dyssynchrony and subsequent mechanical dyssynchrony. This would become manifest as a delayed RV time to onset of shortening in comparison to the left ventricle (LV). An alternative mechanism could be initiated directly by the mechanical pressure and volume overload, inducing increased RV wall tension and prolonged RV myocardial shortening. In this case, the time to onset of shortening would be similar for both ventricles, whereas the time to peak shortening of the RV wall would be delayed compared to the LV.

Purpose: To explore in PAH whether the origin of interventricular asynchrony lies in the onset of shortening or in the duration of shortening.

Methods: In 11 PAH patients (mean pulmonary arterial pressure 54 ± 11 mmHg and ECG-QRS width 109 ± 17 ms), CMRI myocardial tagging (14 ms temporal resolution) was applied. For the LV free wall, septum and RV free wall, the onset time (Tonset) and peak time (Tpeak) of circumferential shortening were calculated. RV wall tension was estimated by the Laplace law.

Results: Tonset was 54 ± 11, 65 ± 4 and 65 ± 14 ms for LV, septum and RV respectively. Tpeak was 284 ± 55, 262 ± 18 and 383 ± 37 ms for LV, septum and RV. Maximum LVSB was at 384 ± 46 ms, coinciding with septal overstretch and RV Tpeak. The R-L delay in Tonset was 10 ± 11 ms ($p = 0.13$), and the R-L delay in Tpeak 99 ± 25 ms ($p < 0.0001$). The R-L delay in Tpeak was not correlated with the R-L delay in Tonset, nor with the QRS width, but did correlate with RV wall tension ($p < 0.01$) as shown in the Fig. 1. The R-L delay in Tpeak predicted leftward septal curvature ($p < 0.05$), and had a negative effect on LV end-diastolic volume ($p < 0.01$) and SV ($p < 0.05$).

Conclusions: In PAH, the origin of asynchrony lies in the duration of shortening. The R-L delay in myocardial peak shortening is caused by increased RV wall tension instead of electrical conduction delay. This R-L delay causes LVSB, which makes the last part of RV shortening ineffective and impairs LV filling.

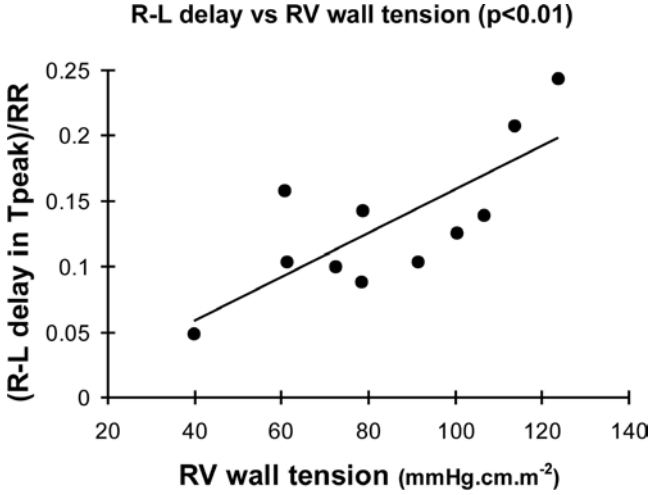

FIG. 1.

445. CONTRAST-ENHANCED CMR AND FDG MICROPET PROVIDE COMPLEMENTARY INFORMATION ON THE PROGRESSION OF SCAR FORMATION AFTER MYOCARDIAL INFARCTION IN MICE

Brent A. French, PhD, FAHA, Yaqin Xu, MD/PhD, Bijoy Kundu, PhD, R. Jack Roy, RT, Mark B. Williams, PhD, Stuart S. Berr, PhD. ***University of Virginia, Charlottesville, Virginia, USA.***

Introduction: ^{18}F-FDG PET has long been used for the assessment of myocardial viability, but Gd-enhanced cardiac MRI is gaining acceptance as the new gold standard due to its superior resolution and sensitivity in detecting non-viable myocardium.

Purpose: The purpose of the current study was to determine whether the two modalities yield complementary information regarding the progression of left ventricular (LV) remodeling after experimental myocardial infarction (MI) in mice.

Methods: Ten C57Bl/6 mice were subjected to a 1h coronary occlusion followed by 30d of reperfusion. Four of these were serially scanned by both MRI and PET on days 1, 7-9 and 28-30 after reperfusion. A 4.7T Varian Inova scanner was used for Gd-enhanced MRI. Cardiac triggering pulses were generated using SA Instruments monitoring devices model 1025 for MRI and 1025L for PET imaging (Stony Brook, New York, USA). A gradient echo MR pulse sequence was used to acquire data with TE = 3.7 ms, 14 cardiac phases (8–9 ms between phases), matrix 128 × 128 zero-filled to 256 × 256, field of view 2.56 × 2.56 cm^2, slice thickness 1 mm, flip angle 60^o for T1 weighting, and four signal averages. Six to seven short-axis slices were needed to cover the entire LV. For PET imaging, mice were fasted overnight prior to scanning. Mice were anesthetized with 1% isoflurane in oxygen and then injected via tail vein with 150 μl of solution containing 500 μCi ^{18}F-FDG. To approximate short-axis imaging, mice were positioned at a 45° angle on the imaging bed of a Focus 120 microPET scanner (Siemens, TN). List mode data from the 20 min scans were sorted into 14 bins per cardiac cycle. Data was corrected for random coincidences and normalized to compensate for the differences in detection efficiency. Images were reconstructed from the 3D sinograms using an iterative MAP algorithm with a zoom factor of 3 and 18 maximum iterations with no attenuation or scatter correction. The final images consisted of 95 slices covering the entire mouse. Each slice had 128 × 128 voxels that were 0.28 mm × 0.28 mm × 0.79 mm in size. Mid-ventricular, short-axis images of the heart were compared over time between MRI and PET. Hearts from parallel mice were immunostained for the study of neutrophil and macrophage infiltration.

Results: Gd-enhanced MRI revealed infarct expansion with thinning of the infarcted anterior LV wall between Day 1 (A) and Day 7 post-MI (B). ^{18}F-FDG PET revealed signal voids in the infarcted anterior LV when imaged Day 1 post-MI (C). Interestingly, these signal voids became hyperintense relative to normal myocardium when imaged at Days 7 or 9 post-MI (D). By 30 days post-MI, the signal voids in the infarcted anterior LV had largely returned on the PET images (E). Immunostains using an anti-Mac2 antibody revealed few monocytes/macrophages in the infarcted LV on Days 1 or 28 post-MI, but abundant macrophages in the infarct zone on Day 7 post-MI (F).

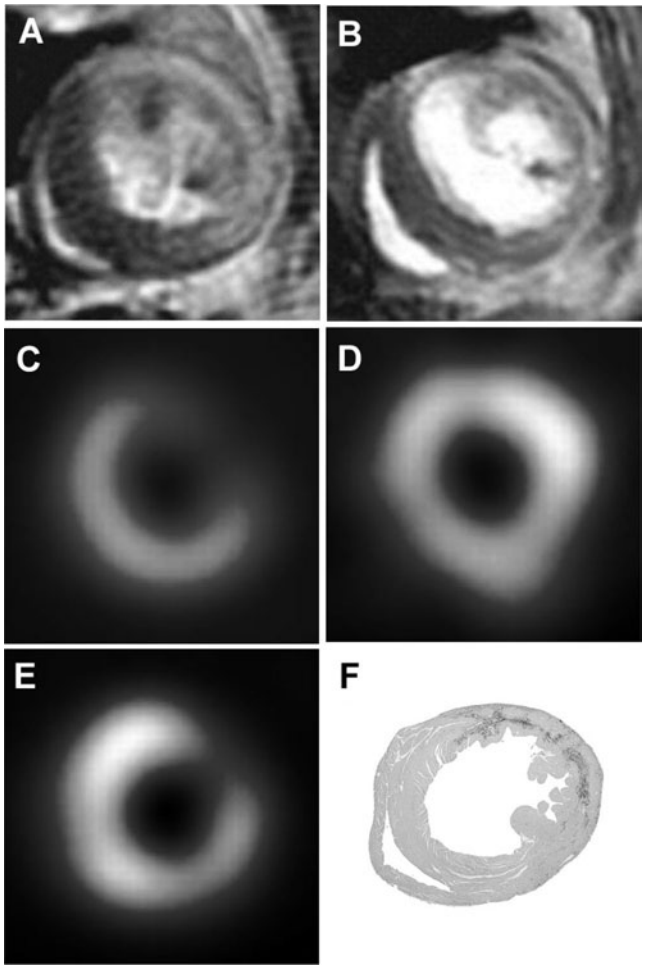

Conclusions: This study shows that the anticipated signal voids corresponding to sites of infarction on ^{18}F-FDG PET images are only apparent very early (≤1 day) or very late (approximately 28 days) after reperfused MI in mice. We also found that macrophage uptake of ^{18}F-FDG outstrips that of either cardiomyocytes or neutrophils in mice after MI. While the macrophage uptake of ^{18}F-FDG has the potential to confound the interpretation of isolated PET images, it could also be used to assess the progression of scar formation after MI in serial PET studies, or in PET studies undertaken in combination with Gd-enhanced cardiac MRI.

446. THREE DIMENSIONAL MRA AND 2D PHASE CONTRAST METHODS FOR IMAGING THE AORTIC ARCH IN MICE

Robert L. Janiczek, MS, Brett R. Blackmann, PhD, Scott T. Acton, PhD, Bradley D. Gelfand, BS, R. Jack Roy, BS, Frederick H. Epstein, PhD. ***University of Virginia, Charlotesville, Virginia, USA.***

Introduction: The focal development of atherosclerosis across many species correlates to the complex hemodynamic environment at branch points and regions of highly curved vessels. It is now well accepted that the differential shear stress forces imposed on the endothelium in regions prone to or protected from atherosclerosis have a profound impact on cellular phenotype and the development and progression of the disease. Since the early 1990's, mouse models of atherosclerosis (e.g., $APOE^{-/-}$ mice) have become the most prevalent in studying this disease and provide enormous insights into the biological mechanisms of vascular disease. The development of noninvasive vascular microimaging would enable serial studies of disease development and progression in transgenic and knockout mice *in vivo*.

Purpose: The purposes of this study were to develop 3D MR angiography (MRA) and 2D phase contrast (PC) methods for evaluating anatomy, flow, and wall shear stress in the aortic arch in mice.

Methods: All imaging was performed on a 4.7T MR system (Varian, Inc., Palo Alto, California, USA) using a 25 mm diameter cylindrical Litz radiofrequency (RF) coil (Doty Scientific, Columbia, South Carolina) and an MR-compatible physiological monitoring and gating system for mice (SA Instruments, Inc., Stony Brook, New York, USA). For 3D MRA, a gated slab-selective segmented RF-spoiled gradient echo sequence was developed. Imaging was performed after injection of the intravascular contrast agent Vasovist (Epix Pharmaceuticals, Lexington, Massachusetts). A 6 mm transverse slab was selected superior to the left ventricle using a 40° Shinnar-LeRoux RF pulse (1). Other parameters included a 5.2 ms TE, 8.6 ms TR, and flow compensation in all three directions. The sequence was both respiratory and ECG gated. Four k-space lines were acquired every heartbeat during diastole after application of three dummy RF pulses for background signal suppression and to reduce non-steady-state signal oscillations. 3D datasets were acquired with 100 micron isotropic resolution after zero-padding using a 25.6 $\times$ 25.6 $\times$ 12.8 mm^3 FOV and a 128 $\times$ 128 $\times$ 64 matrix.

A spoiled gradient echo ECG-gated cine PC sequence was developed using bipolar through-plane velocity-encoding gradients and flow compensation in the readout and phase-encode directions (2). Other parameters included a 2.9 ms TE, 8-10 ms TR, 25.6 $\times$ 25.6 mm^2 FOV, 1 mm slice thickness, 20° flip angle, 10 averages, 100 cm/s velocity encoding, and respiratory gating. Regional wall shear stress (WSS) was calculated according to the method outlined by Gelfand et al (3).

Results: An example maximum intensity projection from a 3D MRA is shown in Fig. 1A, excluding the pulmonary and venous systems for ease of visualization. The aortic arch, carotid arteries, and subclavian arteries are clearly visible, illustrating the anatomical definition that can be achieved using this technique.

Phase contrast data were obtained from five C57BL/6 mice inferior to the left subclavian artery in the aortic arch. Fig. 1B shows the average WSS for the inner and outer aortic radius as a function of time. As expected in a vessel of high curvature, WSS is lower on the inner radius, where atherosclerotic plaques predominately form. Average wall shear stress for the entire cardiac cycle along the inner radius was 1.86 dyne/cm^2, significantly smaller than for the outer radius (20.0 dyne/cm^2; $p < 0.001$). Total scan times were approximately 10 minutes for 3D MRA and 30 minutes for PC, depending on heart and respiratory rate.

Conclusions: Microimaging methods for the anatomy and flow of the aortic arch have been developed and will be used in the

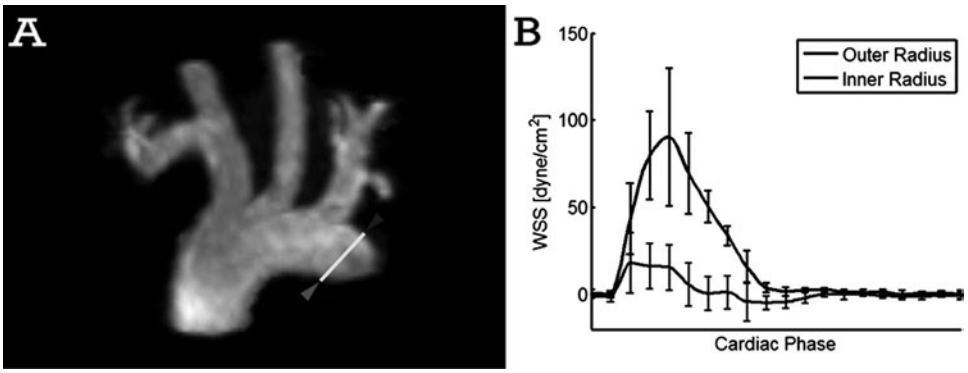

FIG. 1. (A) Example 3D MRA maximum intensity projection of the aortic arch. The yellow line represents the measurement plane for PC imaging, the red arrow the inner radius, and the blue arrow the outer radius of the aortic arch (B) Mean wall shear stress with standard deviation as a function of cardiac phase for the inner and outer radius of the aortic arch for five mice.

future to study the relationship between hemodynamics and the development and progression of vascular disease in transgenic and knockout mouse models of atherosclerosis.

REFERENCES

1. Pauly, et al. IEEE Trans Medical Imaging 1991;10:53–65.
2. Bernstein et al. JMRI 1992;2:583–8.
3. Gelfand, et al. JMRI. Accepted.

447. ASSESSMENT OF PATIENTS WITH ATRIAL FIBRILLATION AT HIGH RISK FOR THROMBOEMBOLISM BY CARDIAC MAGNETIC RESONANCE IMAGING—COMPARISON TO TRANSESOPHAGEAL ECHOCARDIOGRAPHY

Peter Bernhardt,[1] Günter Pilz,[2] Markus Klos,[2] Berthold Höfling.[2] [1]***University of Ulm, Ulm, Germany,*** [2]***Hospital Agatharied, Hausham, Germany.***

Background: Left atrial appendage (LAA) emptying velocities (LAAv), spontaneous echo contrast (SEC) and left atrial thrombi as determined by transesophageal echocardiography (TEE) are important predictors for cerebral embolism in patients with atrial fibrillation (AF). Aims of our study were to assess LAA volume, ejection fraction and flow velocity as well as presence of left atrial thrombi with cardiac magnetic resonance imaging (CMR), to correlate with TEE findings and to evaluate CMR's ability in detecting these AF patients at high risk for thromboembolism.

Methods: Consecutive patients with AF scheduled for TEE prior to cardioversion were included to the study. Patients with sinus rhythm and TEE indication served as controls. All patients were scanned in a 1.5-T whole body CMR scanner. Contiguous functional and T1-weighted images covering the entire LAA in long axes orientation and phase contrast sequences ortogonal to the LAA orifice were performed.

Results: Forty-nine patients (32 with AF and 17 with sinus rhythm) were included to the study. TEE determined LAAv highly correlated with LAA ejection fraction ($\kappa = 0.95$), LAAv ($\kappa = 0.78$) and with LAA dimension ($\kappa = -0.74$) evaluated by CMR as well as with degree of SEC ($\kappa = -0.84$). Patents with reduced LAAv (≤ 0.2 m/s) had significantly higher degree of SEC ($p < 0.001$). Sensitivity for detecting a thrombogenic milieu by CMR was 0.92, specificity was 0.97.

Conclusion: CMR is able to determine LAA size, ejection fraction, flow velocities and left atrial thrombi with a high correlation to TEE. Thus, patients suspected to have an increased embolic risk may be evaluated by CMR examination.

448. CMR AND HISTOLOGIC ASSESSMENT OF ADENOSINE A_{2A} RECEPTOR AGONIST MEDIATED REDUCTION OF REPERFUSED MYOCARDIAL INFARCT SIZE

Rajan A. G. Patel, MD, George A. Beller, MD, Alexis Broisat, PhD, Hasan K. Kabul, MD, Mirta Ruiz, MD, N. Craig Goodman, MS, Joseph M. DiMaria, BA, David K. Glover, PhD, Joel M. Linden, PhD, Christopher M. Kramer, MD. ***University of Virginia, Charlottesville, Virginia, USA.***

Background. Reperfusion injury after myocardial infarction (MI) is characterized by intense inflammation causing additional myocyte injury, alterations in contractility, and microvascular dysfunction. The acute inflammatory response after MI lasts 24–48 hours. Adenosine infusion during reperfusion after MI reduces infarct size (IS). ATL146e is a highly selective adenosine A_{2A} receptor agonist that decreases inflammation and IS as a percent of risk area (RA) at 2 hours post-MI in dogs without the side affects of adenosine (e.g., hypotension). Potent anti-inflammatory medications such as high dose NSAIDS and glucocorticoids have been shown to result in adverse remodeling or ventricular rupture after MI.

Hypotheses. At 48 hours post-reperfusion after MI in anesthetized dogs, the selective anti-inflammatory effects of a brief 2.5 hour infusion of ATL146e: **1)** will result in a sustained reduction in IS; **2)** will not result in adverse left ventricular remodeling as assessed by CMR; and **3)** will not cause ventricular rupture.

Methods. Twenty-five mongrel dogs underwent baseline CMR followed by thoracotomy and LAD ligation for 90 minutes. Thirty minutes prior to reperfusion, a 2.5 hour infusion of ATL146e (0.01 μg/kg/min) ($n = 13$) or vehicle ($n = 12$) was started. At 48 hours post-MI, dogs underwent CMR. Animals were anesthetized with 1% isoflurane during imaging and with pentobarbital during surgery. CMR was performed on a Siemens 1.5T Avanto scanner. Prospectively-gated SSFP imaging was utilized to acquire long axis views of the left ventricle (LV) in addition to a stack of contiguous short axis images. Parameters were FOV = 260 mm; in-plane resolution = 1.7 × 1.0 mm; slice thickness = 7 mm; Flip angle = 65°; TR = 2.8ms; TE = 1.35 ms; segments = 20. A phase-sensitive inversion recovery gradient echo sequence was utilized to assess late gadolinium enhancement (LGE) as a marker of IS in the same long axis (Fig. 1) and contiguous short axis images 15 minutes after Gd-DPTA infusion (0.15 mM/kg). Parameters were FOV = 250 mm; in-plane resolution = 1.3 × 1.0 mm; slice thickness = 7 mm; Flip angle = 25°; TR = 9.2 ms; TE = 4.18 ms; TI = 300 ms. Argus software (Siemens Medical Solutions) was utilized by a blinded operator to calculate the left ventricular end-diastolic volume index (EDVI), end-systolic volume index (ESVI), and ejection fraction (EF) from SSFP images and to quantify IS from LGE images. After the 48 hour scan, ex-vivo RA and IS measurements were performed with histochemical staining. Two-way analysis of variance was used to determine differences in volumetric parameters over time between groups. Student's t-test was used to determine differences in IS.

Results: IS by triphenyltetrazolium (TTC) stain as a percentage of RA was smaller in the ATL146-treated vs. control dogs

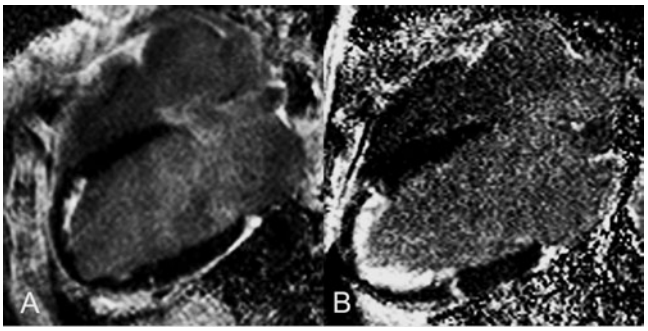

FIG. 1. LHE 48 hours post MI from A) an ATL 146e treated dog and B) a control dog.

(16.7 ± 3.7% vs. 33.3 ± 6.2%, p = 0.027). There was a trend toward smaller absolute IS as assessed by LGE in the ATL146e treated dogs (ATL146e: 14.2 ± 2.9 g vs. 21.6 ± 4.6 g, p = 0.186). At baseline no difference was seen in volumetric parameters between groups (EDVI: ATL146e 3.04 ± 0.07 mL/kg vs CTL 2.90 ± 0.14 mL/kg, p = ns; ESVI: ATL146e 1.46 ± 0.07 mL/kg vs. CTL 1.42 ± 0.08 mL/kg, p = ns). At 48 hours, there was no difference in EDVI (ATL146e 3.07 ± 0.19 mL/kg vs. CTL 2.67 ± 0.12 mL/kg, p = ns), but ESVI was larger in the ATL146e treated group (ATL146e 2.24 ± 0.12 mL/kg vs. CTL 1.84 ± 0.10 mL/kg, p = 0.024). No difference was observed in EF at baseline or 48 hours post-MI (baseline: ATL146e 52 ± 1% vs. CTL 51 ± 1%, p = ns; 48 hrs post-MI: ATL146e 26 ± 3% vs. CTL 31 ± 3%, p = ns). No dogs suffered ventricular rupture.

Conclusions: ATL146e infusion with reperfusion results in a persistent reduction in IS as a percent of RA in dogs at 48 hours. Absolute IS tended to be lower in the ATL 146e group. CMR data at 48 hours post-MI demonstrates an increase in ESVI in ATL146e treated dogs. Further imaging studies between 48 hours and 8 weeks post-MI are necessary to assess whether ATL146e results in adverse ventricular remodeling when administered as an adjunct to reperfusion after MI, despite the reduction in infarct size.

449. PROTEIN CAGE NANOPARTICLES AS CELLULAR MRI CONTRAST AGENTS

Masahiro Terashima, MD, PhD,[1] Masaki Uchida, PhD,[2] Charles H. Cunningham, PhD,[3] Yoriyasu Suzuki, MD,[1] Philip C. Yang, MD,[1] Philip S. Tsao, PhD,[1] Mark J. Young, PhD,[2] Steven M. Conolly, PhD,[4] Trevor Douglas, PhD,[2] Michael V. McConnell, MD, MSEE.[1] ***[1]Stanford University, Stanford, California, USA, [2]Montana State University, Bozeman, Montana, USA, [3]University of Toronto, Toronto, Ontario, Canada, [4]University of California, Berkeley, Berkeley, California, USA.***

Introduction: Macrophages and stem cells have been important targets for cellular MRI of cardiovascular disease and therapy. Protein cage architectures are nanoscale platforms amenable to both genetic and chemical modification, making them promising for cellular and molecular imaging. Human Ferritin (HFn) is a protein cage that can be synthesized to contain iron oxide (Fe) within its interior cavity (Fig. 1A).

Purpose: To evaluate the uptake of HFn-based iron-oxide nanoparticles (HFn-Fe) in macrophages and stem cells and their detection by MRI.

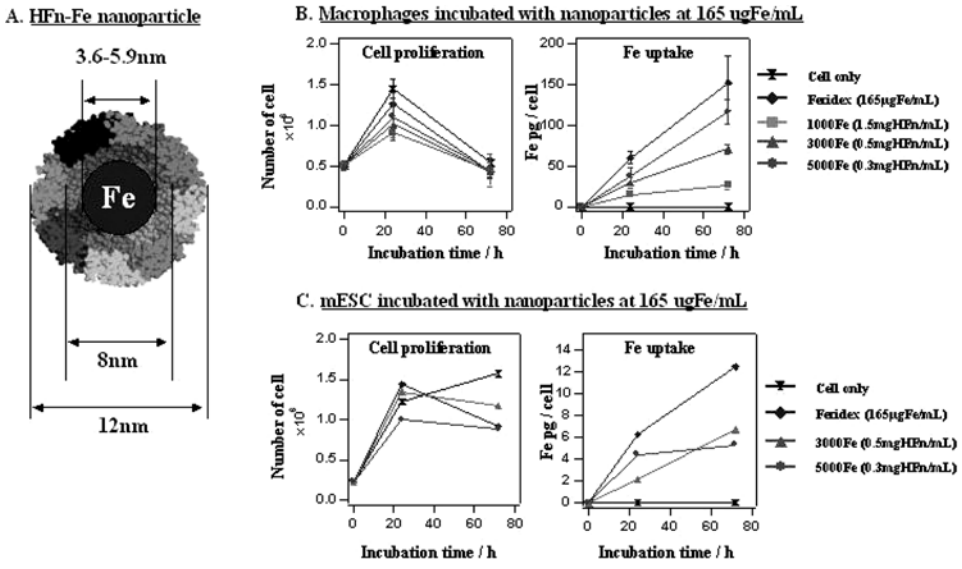

FIG. 1. HFn-Fe nanoparticles.

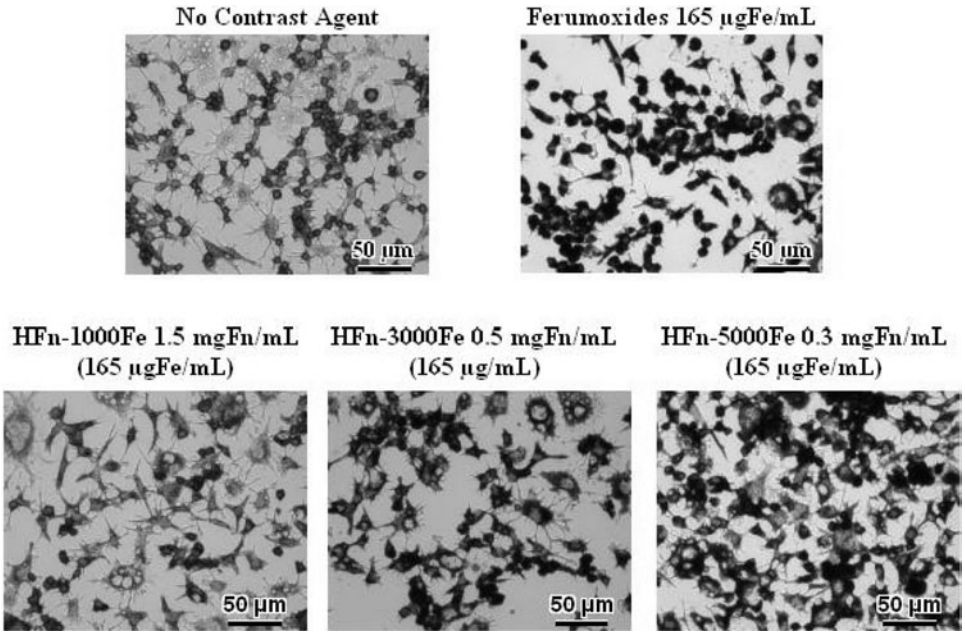

FIG. 2. Prussian Blue Iron Staining of Macrophages Incubated with HFn-Fe for 24 Hours.

Methods: Mouse macrophages (RAW cells: 1×10^6) and mouse embryonic stem cells (mESCs: 5×10^5) were incubated up to 72 hours with 165 ugFe/mL of HFn-Fe using 3 different densities of iron oxides (HFn-1000Fe, HFn-3000Fe, and HFn-5000Fe/cage). mESCs were co-incubated with 30 ug/mL of protamine sulfate. For comparison, cells were also incubated with ferumoxides (i.e., Feridex) under the same conditions. Cellular uptake was observed histologically by Prussian Blue iron staining as well as ex vivo MRI on a whole-body GE 1.5T scanner using a 2D GRE sequence (TR/TE = 100/10, FA = 30, matrix = 256 × 256, slice thickness = 1.0 mm, NEX = 1, FOV = 12 cm). Quantitative measurement of the iron content in the cells was performed by inductively coupled plasma-mass spectrometry analysis.

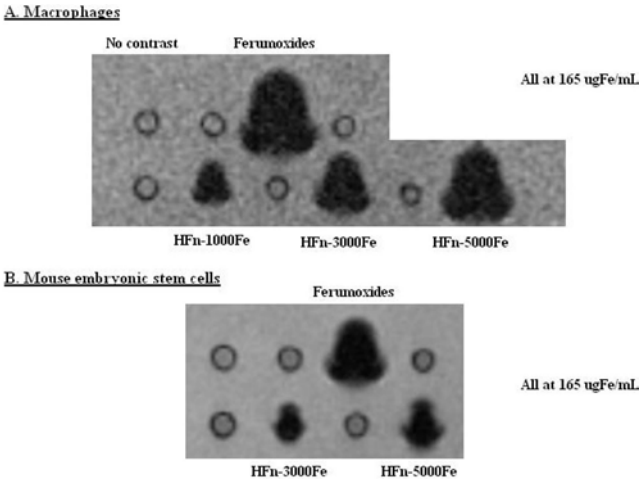

FIG. 3. MRI in vitro.

Results: HFn-Fe was taken up by macrophages and mESCs without significant impairment of cell proliferation (Fig. 1B). The iron content per macrophage was increased in association with the amount of iron nanoparticles within the HFn protein cage at 24 hours (HFn-1000Fe: 14.9 ± 0.9pg, HFn-3000Fe: 29.8 ± 6.2, HFn-5000Fe: 37.8 ± 10.6 pg/cell) and at 72 hours (Fig. 1B). HFn-Fe was also successfully taken up by mESCs (Fig. 1C). By histology, iron particles were clearly detected within cells incubated with HFn-Fe, as with ferumoxides (Fig. 2). The macrophages incubated with HFn-5000Fe demonstrated similar T2* effects to ferumoxides (Fig. 3), but HFn-5000Fe had less T2* effect in mESCs.

Conclusions: Human ferritin protein cage iron oxide nanoparticles show effective uptake by macrophages and mouse embryonic stem cells with promising MRI properties. These results encourage further investigation into the use of protein cage architectures as a new platform for cellular MRI contrast agents.

450. GD(DTPA)-BOLUS-ENHANCED PERCENT-INFARCT-MAPPING COMBINED WITH EARLY PERFUSION IMAGING TO DETECT MICROVASCULAR OBSTRUCTION

Pal Suranyi, MD,[1,2] Balazs Ruzsics, MD,[1,2] Kiss Pal, MD,[1,2] Brigitta C. Brott, MD,[3] Tamas Simor, MD,[1,2] Ada Elgavish, PhD,[1,2,4] Gabriel A. Elgavish, PhD.[1,2] [1]***Department of Biochemistry and Molecular Genetics , University of Alabama at Birmingham, Birmingham, Alabama, USA,*** [2]***Elgavish Paramagnetics Inc., Birmingham, Alabama, USA,***

[3] Department of Medicine, Division of Cardiovascular Disease, University of Alabama at Birmingham, Birmingham, Alabama, USA, [4] Department of Genetics, University of Alabama at Birmingham, Birmingham, Alabama, USA.

Introduction: Delayed contrast enhanced (DE) MRI is widely used to quantify myocardial infarct size. Following Gd(DTPA) administration, hypo-enhanced spots may be detected in the center of enhanced infarcts due to microvascular obstruction (MO). These may be mistaken for viable tissue. Percent-Infarct-Map (PIM) is our recently published method for the per-voxel quantification of infarcted tissue based on longitudinal relaxation-rate-enhancement (ΔR1).

Purpose: To eliminate observer bias in identifying these zones, we have used early perfusion images in conjunction with PIM to objectively differentiate these infarcted regions from viable tissue and to accurately quantify infarct size.

Methods: Four days after reperfused infarction, dogs (n = 5) were imaged using a 1.5T GE MRI system. Following Gd(DTPA) bolus (0.2 mmol/kg), serial, high-resolution T1-weighted perfusion images were generated for 12 minutes (Fig. 1). Percent signal-intensity-enhancement (SIE%) in all postcontrast images was then calculated pixel-by-pixel, utilizing the precontrast image. Between 2–3 minutes after Gd(DTPA), all regions (viable, patchy-infarct, reperfused infarct) appeared enhanced except those that were non-viable and hypoperfused due to MO (< Remote SI-2SD). These voxels automatically counted as 100% non-viable and a virtual MO-map was generated. Conventional DE images were acquired 15 minutes after Gd(DTPA) by nulling signal from viable myocardium. Next, in the same image orientations between 20–25 minutes after Gd(DTPA) R1-mapping was done to in an equatorial short-axis slice to generate PIMs (Fig. 1). Inversion-recovery-prepared, segmented, fast-gradient-echo images were generated with six inversion times (TI). In an automated procedure, non-linear curve fitting was applied to calculate R1-maps with voxel-by-voxel resolution. Based on relaxation-rate-enhancement(ΔR1) a computer algorithm calculated percent-infarct per-voxel, and generated the PIM.

In PIMs, percent-infarct-values were calculated per-voxel. In thresholded DE-images, enhanced voxels (i.e., SI > Remote SI + 2SD) were counted 100% infarcted, and nonenhanced voxels as 100% viable. MO-maps were then virtually merged with thresholded DE-images, and with PIMs (Fig. 1). Note that infarct size quantification was automated and the only manual input was tracing of endo- and epicardial contours and the selection of a remote, viable region. Triphenyltetrazolium-chloride-(TTC)-staining and microscopic histology (hematoxyllin-eosin stained 5 μm sections) was used to validate results. Percent-Infarct-per-Slice (PIS) was calculated for PIM, DE and TTC staining to compare the three methods.

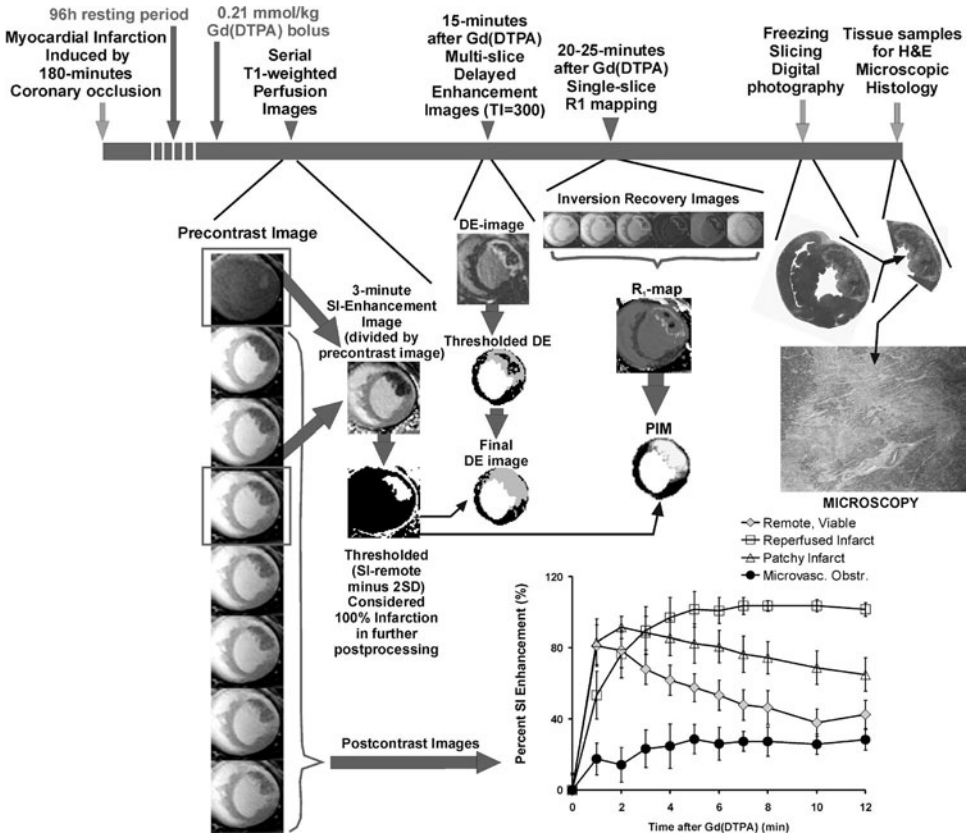

FIG. 1. Experimental timeline and the various imaging and post-processing techniques (see text) are shown.

Results: SIE curves from the four basic tissue types are shown in Fig. 1: a) MO (infarcted,yet not enhanced); b) Reperfused infarct (infarcted and maximally enhanced); c) Patchy infarct (partially infarcted thus partially enhanced); d) Remote, viable (100% viable, non-enhanced). PIS_{PIM} showed excellent correlation vs. PIS_{TTC} ($R^2 = 0.99$, $p < 0.05$). PIM slightly overestimated IF_{TTC} with a median [25th and 75th percentile] error of 2.6% [-0.86; 3.37]. Conventional DE overestimated PIS_{TTC} by a median of 18.8% [14.1; 25.9] ($R^2 = 0.86$, $p < 0.05$). MO regions corresponded to hemorrhage and nonresorbed coagulation necrosis on microscopy, while there was confluent granulation tissue in well perfused infarct regions and patchy infarct at the infarct borders.

Conclusions: T1-weighted perfusion images early after bolus Gd(DTPA) are useful for objective detection of MO. MO-maps, combined with the R1-based PIM yield more accurate infarct quantification than conventional DE-imaging.

451. EMPLOYING ULTRAFAST KT- BLAST AND KT-SENSE MEASUREMENTS FOR SINGLE BREATH-HOLD SHORT AXES VOLUME AND CINE PHASE CONTRAST AORTIC FLOW ACQUISITION

Henning Steen, MD,[1] Bernhard Schnackenburg, Dr. Ing,[2] Sebastian Kozerke, Dr,[3] Constanze Merten, MD,[1] Hugo A. Katus, MD,[1] Evangelos Giannitsis.[1] [1]***University Heidelberg, Heidelberg, Germany,*** [2]***Philips Medical Systems, Berlin, Germany,*** [3]***ETH Zürich, Zürich, Switzerland.***

Introduction: Multi-slice breath-hold cine short axes (SA) magnetic resonance imaging (MRI) is reference standard for end-diastolic and -systolic volume- (EDV, ESV), stroke volume- (SV) and ejection fraction- (EF) quantification of the left ventricle (LV) providing accurate and highly reproducible measurements. Free-breathing MRI phase velocity mapping (MRI-PC) is a powerful tool for vessel flow quantification offering results on SV and blood flow velocity. The draw-back of aforementioned techniques is its long scan duration. Recently, k-t BLAST/k-t SENSE imaging has been proposed to significantly accelerate dynamic CMRI studies generating functional information with a single breath-hold technique.

Purpose: We hypothesized that k-t BLAST/k-t SENSE offers fully covered LV cine MRI SA imaging in a single breath-hold technique. Furthermore, single breath-hold k-t BLAST/k-t SENSE MRI-PC is feasible providing accurate measurements when compared to non-breath-hold MRI-PC and multi-slice cine SA imaging.

Methods: In 8 volunteers, vector-ECG gated cine twelve-slice SA (bFFE; matrix = 256 ∗ 256; slice-thickness = 8; 35 phases) were planned on true 2-and 4-chamber views on a 1.5 T MRI system (ACHIEVA, Philips Medical Systems, Best, Netherlands) using a conventional cardiac phased-array coil. Subsequently, k-t BLAST/k-t SENSE single breath-hold cine twelve-slice images (3D-bFFE; matrix = 256 ∗ 256; 24 phases) were comparably planned using two different acceleration factors: kt-factor = 5 and 8 (kt-5; kt-8) leading to effective accelerations of 3.7/5.2 respectively. Likewise, a double breath-hold method with distinction of undersampling and training stages was additionally planned using the kt-factor 5 (kt-5-2BH,k-t net acceleration = 3.7).

Afterwards, three MRI-PC flow measurements were planned one centimeter behind the aortic valve on true 3-chamber views: a) conventional free breathing MRI-PC (Matrix 256 ∗ 256; voxel size = 1.1 ∗ 1.1 ∗ 9 mm; 35 phases), b) kt-5 MRI-PC (Matrix 256 ∗ 256; voxel size = 1.3 ∗ 1.3 ∗ 9 mm; net-acceleration = 3.3; 32 phases), c) kt-8 MRI-PC (Matrix 256 ∗ 256; voxel size = 1.3 ∗ 1.3 ∗ 9 mm; net-acceleration = 4.5; 32 phases). SV measurements for all three MRI-PC techniques were compared to the SV cine SA kt-5-2BH officiating as reference measurement for SV. Correlation measures were done using Pearson correlation coefficient, $p < 0.05$ was considered statistically significant.

*Results:*Good image quality could be achieved for all SA cine as well as MRI-PC measurements. For cine SA imaging, mean scan-time could be significantly reduced from 89 ± 24 s excluding breath-hold maneuvers for conventional cine imaging to 24 ± 3 s (kt-5), 17 ± 5 (kt-8) and 28 ± 3 (kt-5-2BH) (all $p < 0.05$). Heart rate was not significantly different between all SA and MRI-PC measurements (70 ± 4/minute, p = n.s.). The results (Fig. 1) and the correlation coefficients (Table 1A)

TABLE 1A

Correlation coefficiens	Short axes kt-5	Short axes kt-8	Short axes kt-5-2BH
DV	0.97	0.97	0.96
ESV	0.91	0.90	0.95
SV	0.93	0.93	0.95
EF	0.80	0.79	0.97

TABLE 1B

(Reference scan: Short axes kt-5-2BH)	
PC SV free breathing	0.89
SV kt-6 MRI-PC	0.92
SV kt-8 MRI-PC	0.92

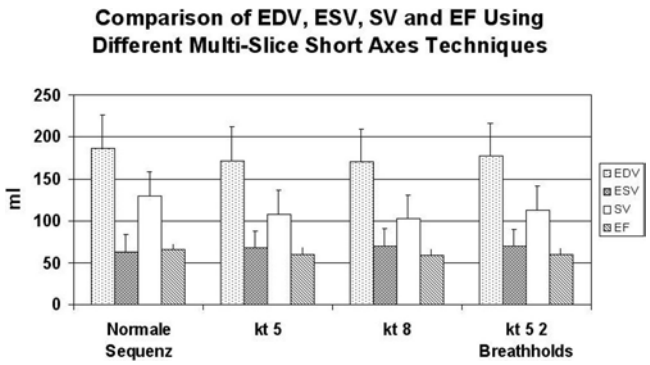

for EDV, ESV, SV and EF between conventional cine multi-slice SA and all kt-scans were excellent, whereas kt-5-2BH was considered best.

Also, SV correlation coefficients between conventional multi-slice cine SA kt-5-2BH and the different kt-MRI-PC approaches (Table 1B) were high and comparable for all three methods. Scan-time could be dramatically reduced from 169 ± 25 s for the free-breathing MRI-PC to 12 ± 1s (kt-5-MRI-PC) and 9 ± 1s (kt-8-MRI-PC).

Conclusions: In conclusion, the k-t BLAST/SENSE approach is a promising new imaging technique that permits significant scan-time reduction in cine multi-slice SA imaging as well as MRI-PC velocity measurement. In a short scan-time, a correct volume and flow quantification could be achieved leading to increased clinical applicability of MRI even in patients with decreased breath-hold capabilities.

452. ACCURACY OF LEFT VENTRICULAR THROMBUS DETECTION BY MRI WITH SURGICAL AND PATHOLOGICAL CORRELATION

Andrew M. Crean, MRCP FRCR,[1] Narinder Paul, MD,[2] FRCR, Yves Provost, MD,[2] Naeem Merchant, MD.[2] [1]***Leeds General Infirmary, Leeds, United Kingdom,*** [2]***Toronto General Hospital, Toronto, Ontario, Canada.***

Purpose: To investigate the diagnostic accuracy of MRI in identification of left ventricular thrombus with surgical and pathological identification of thrombus as the gold standard. To establish the relative accuracy of steady state free precession (SSFP) and delayed enhancement imaging in this context.

Method: Retrospective review of all patients referred to the cardiac MRI department of Toronto General Hospital for viability assessment from July 1998 to July 2006. All MRI examinations were double read by 2 experienced radiologists and the presence or absence of left ventricular thrombus was recorded. Note was made of the types of imaging sequence on which thrombus was seen. If delayed enhancement images were part of the study they were examined last in order not to bias appraisal of the cine sequences. All studies were graded subjectively for image quality as "good," "fair," or "poor." After a number of weeks (to minimize recall bias) cine and delayed enhancement images were reviewed in a random order and the volume of thrombus was calculated using an Advantage Windows workstation version 4.0 (GE Healthcare, Wisconsin, USA) with dedicated software (Medis, The Netherlands). Left ventricular end diastolic volume and ejection fraction were also calculated for each patient from a short axis cine stack (Mass Analysis Plus, Medis, The Netherlands).

Patients charts were scrutinised for subsequent left ventricular aneurysm resection and details of presence or absence of thrombus were noted form intra-operative and histopathological reports. Chart scrutiny did not occur until all MRI examinations had been rated for presence or absence of thrombus.

Results: One hundred and forty MRI examinations were identified over the study period, and 41 patients underwent subsequent left ventricular aneurysm resection. A radiological diagnosis of LV thrombus was made in 29 out of 140 patients. Sixteen of these patients underwent subsequent surgery with surgical and pathological examination confirming the presence of thrombus. One patient with a positive MRI was not confirmed to have thrombus at pathology. Of the remaining 25 patients undergoing surgery, 24 had no thrombus either on MRI or at pathology and 1 patient had thrombus identified at pathology but missed on MRI.

Fourteen MRI and pathology positive patients had both SSFP and delayed enhancement imaging. Thrombus was identified on both delayed enhancement and cine imaging in 5 out of 14 cases, by cine imaging alone in 1 case, and by delayed enhancement alone in 8 cases. Significantly less thrombus was detected by SSFP imaging than by delayed enhancement when volumes measured were compared on a case by case basis ($p < 0.001$ Wilcoxon signed ranks test) (Table below). All results presented as mean (standard deviation).

Volume SSFP	1.78 mL (SD 4.13 mL)
Volume delayed enhancement	8.3 mL (SD 9.17 mL)

Diagnostic accuracy for thrombus detection varied depending on whether cine imaging or delayed enhancement was used to make the diagnosis of thrombus (Table below):

	SSFP cine imaging	Delayed enhancement imaging	SSFP and DE imaging combined
Sensitivity	31%	93%	94%
Specificity	96%	96%	96%
Positive predictive value	83%	93%	94%
Negative predictive value	69%	96%	96%

Conclusion: Magnetic resonance imaging had a very high diagnostic accuracy for the detection of LV thrombus in this group of patients with pathological examination as the reference standard. However, this accuracy was largely attributable to the use of delayed enhancement imaging and sensitivity was unacceptably low with use of SSFP imaging alone. Furthermore, the observed volume of thrombus was significantly smaller when measurements were made based on SSFP images alone. The results of this study suggest that delayed enhancement imaging should be performed routinely when the clinical question of left ventricular thrombus is raised.

453. RF FIELD EFFECTS ON MULTI-POINT T_1 RELAXOMETRY

Warren D. Foltz,[1] Venkat Ramanan,[2] Duncan Stewart,[1] Graham A. Wright,[2] Alexander J. Dick.[2] [1] *St. Michael's Hospital, Toronto, Ontario, Canada,* [2] *Sunnybrook Health Sciences Centre, Toronto, Ontario, Canada.*

Introduction: In vivo, T_1 is often measured using multi-point or Look-Locker strategies, in which an inversion pulse is followed by a train of small-tip pulses (angle θ) and imaging intervals (duration ΔT). Ideally, the measured relaxation displays a time constant T1*, whereby $1/T_1 = 1/T_1^* + \log(\cos[\theta])/\Delta T$ (Eq. 1). One may thus infer a significant bias in multi-point T_1 relaxometry from imperfections of the RF field (B_1) because θ must be known accurately. One may also derive an analytical expression for T_1-based quantification of B_1, by equalizing Eq. 1 at variable ΔT. This abstract provides a basis for accurate multi-point T_1 relaxometry, based on optimization of the readout strategy and from T_1-based quantification of B_1.

Purpose: The overall purpose is the optimization of multi-point T_1 relaxometry, to facilitate quantification of partition coefficients of intravascular and extracellular contrast agents.

Methods: Our multi-point strategy, termed T_1prep, consists of a train of small-tip spectral-spatial pulses and spiral imaging gradients. Every even-numbered sequence iteration is acquired without a preceding adiabatic inversion, so that signal subtraction chops out the additive T_1 recovery term and T_1 is quantified from the monoexponential decay.

A numerical solution to the Bloch equations guided sequence optimization. First, SNR requirements to minimize noise contributions to T_1 precision (σ_{T1}) were predicted by Monte Carlo simulation. Second, RF field effects were simulated by varying ΔT at constant θ for RF field offsets between $\pm$ 30% (9 pulses of 120 ms; 7 pulses with ΔT of 160 ms; 5 pulses with ΔT of 240 ms; 4 pulses with ΔT of 320 ms; 3 pulses with ΔT of 480 ms; and 2 pulses with ΔT of 960 ms). Simulations were repeated with θ of 5°, 10°, 15°, 20°, or 25°. Model validation used water doped with MnCl2 (0.089 mmol, T1 $\sim$ 1012 ms) and the body or head coil of a 1.5T GE Signa. SNR predictions were validated by scaling of the ROI in subsequent analyses of a single base scan, because the per ROI SNR is linear with the per voxel SNR and the number of independent voxels. RF tuning predictions were evaluated by deliberate and incremental mis-tuning of the RF amplifier at SNR greater than 1000.

T_1-based quantification of B_1 was guided by the following expression: $\log(\cos[\theta]) = (1/T_{1B}^* - 1/T_{1A}^*)/(1/\Delta T_A - 1/\Delta T_B)$ (Eq. 2), whereby 'A' and 'B' denote measurements at two ΔT. Experimentally, ΔT of 35 and 50 ms were utilized with θ between 5° and 25° and a 27 cm diameter ball phantom (T1$\sim$110 ms, GE Medical Systems). The double-angle method provided gold standard validation of B1 ($\theta_1 = 60°$, $\theta_2 = 120°$, TR = 5000 ms).

Results: Reducing ΔT improved σ_{T1} at a given SNR, however all ΔT ensured $\sigma_{T1} < 5\%$ for SNR > 65, and $\sigma_{T1} < 1\%$ for SNR > 300. At high SNR with negligible ΔB_1, T_1 increased with θ but not with ΔT ($\Delta T_1 < 1\%$ for $\theta = 5°$, 1% for $\theta = 10°$, 4% for $\theta = 15°$, 8% for $\theta = 20°$, and 17% for $\theta = 25°$). At high SNR with significant ΔB_1, T_1 increased with θ and reduced with ΔT. T_1-based maps of B_1 tracked gold standard double-angle measurements, but were positively biased by an extent which decreased with nominal θ.

Conclusions: RF tuning may dominate bias in multi-point T_1 relaxometry, unless alleviated by increasing ΔT without cost to σ_{T1} at high SNR, or by reducing θ with significant cost to SNR. A shift in baseline T_1 with θ in well-tuned systems suggests an inherent sensitivity to the slice profile of 'soft' RF pulses. Possibly, slice profile effects dominate experimental mis-matches with theory at large θ and ΔB_1, and with double-angle estimation of θ.

454. EVALUATION OF RIGHT VENTRICULAR FUNCTIONAL RECOVERY AFTER THROMBOENDARTERECTOMY IN PATIENTS WITH CHRONIC PULMONARY THROMBOEMBOLISM: NON-INVASIVE MONITORING WITH MAGNETIC RESONANCE IMAGING

Misako Iino,[1] Steven Dymarkowski,[2] Lertlak Chaothawee,[2] Marion Delcroix,[2] Yutaka Imai,[1] Jan Bogaert.[2] [1] *Tokai University Hospital, Isehara, Japan,* [2] *Gasthuisberg University Hospital, Leuven, Belgium.*

Purpose: To evaluate the time course of ventricular functional recovery after thromboendarterectomy(PTE) in patients with

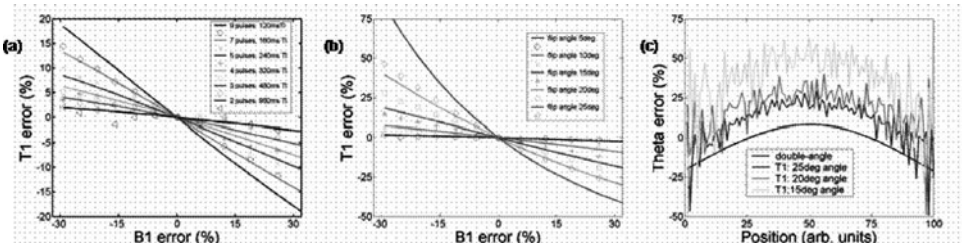

FIG. 1. (a) SNR and σ_{T1}; (b) ΔT_1 and ΔB_1 at constant θ and variable ΔT; (b) ΔT_1 and ΔB_1 at variable θ and constant ΔT; (c) overestimation of double-angle measurements of θ using multi-point T_1.

chronic thromboembolic pulmonary hypertension (CTEPH) using MRI.

Methods: Twenty-two CTEPH patients (14 M, 60 ± 13 yr, range 31–78) were enrolled since Jan 2003–Mar 2006. Cardiovascular magnetic resonance imaging (CMR) was performed before surgery, 1, 3 and 6 month after PTE. All patients were examined with 1.5-T unit (Intera CV; Philips Medical Systems, Best, the Netherlands) with Powertrak 6000 gradients, a dedicated cardiac software, a five-element synergy cardiac coil and a VCG triggering. For evaluation of ventricular function, breathhold SSFP-cine MRI was performed in cardiac short-axis and/r transverse direction. In post-processing analysis, RV function was calculated from transverse cine images, and left ventricular (LV) function from cardiac short-axis images. Velocity-encoded cine MRI was performed to assess pulmonary and aortic flow. Pulmonary flow were measured at pulmonary trunk and right and left main pulmonary artery. Septal inversion was assessed by non-ECG triggered real-time SSFP cine MRI in cardiac short axis during operator guided deep respiration. The degree of septal inversion was obtained by the ratio of RV diameter to biventricular diameter in cardiac early diastolic phase.

Results: For the RV, the ejection fraction (EF), end-diastolic and end-systolic volume improved from 31 ± 9%, 197 ± 71 mL and 139 ± 66 mL to 49 ± 12% ($p < .0001$), 129 ± 46 mL ($p < .005$) and 68 ± 40 mL ($p < .001$) after PTE respectively. After PTE, the mean RVEF increased significantly from 31 ± 9% ($n = 22$) before surgery to 47 ± 11% ($n = 21$, $p < .0001$), 49 ± 11% ($n = 15$, ns), and 55 ± 7% ($n = 14$, ns) at 1, 3, and 6 month follow up respectively. The LV EDV, ESV and EF did not change after PTE. The pulmonary arterial peak and mean velocity and flow volume changed from 69 ± 17 cm/s, 29 ± 9 cm/s and 284 ± 70 mL/s to 78 ± 23 cm/s ($n = 18$, $p <$ ns), 36 ± 8 cm/s ($n = 18$, $p < .05$) and 377 ± 74 mL/s ($n = 18$, $p < .001$) after surgery respectively. Leftwarded septal inversion decreased from ratio 0.67 ± 0.05 before surgery to 0.52 ± 0.1 ($p < .001$) at post operative follow-up period, showing a good correlation with the improvement in RVEF($r = 0.7$). There is a moderately correlation between the septal Inversion ratio and mean pulmonary arterial pressure measured by transesophageal echocardiography($r = 0.6$).

Conclusions: Significant improvement in RV function, increased pulmonary flow, and decreased RV overload are found early (i.e., 1 month) after PTE for CTEPH. MRI is an excellent technique to non-invasively monitor this functional recovery over time.

455. ECG-GATED MAGNETIC RESONANCE ANGIOGRAPHY IN CHILDREN WITH CONGENITAL AND ACQUIRED HEART DISEASE

Ashwin Prakash, MD, Beth F. Printz, MD, PhD, Martin R. Prince, MD, PhD. ***Columbia University College of Physicians and Surgeons, New York, New York, USA.***

Background: Contrast-enhanced Magnetic Resonance Angiography (MRA) is accurate for evaluating congenital heart disease. However, ghosting and blurring related to cardiac motion may interfere with image interpretation. This study evaluated a new ECG-gated MRA technique in children and young adults with congenital heart disease.

Methods: MRA of the chest was performed using an ECG gated 3D spoiled gradient echo sequence at1.5 T in 22 subjects with congenital or acquired heart disease (mean age 18 ± 9 years). The data acquisition loop order was reversed such that acquisition of all in-plane phase encoding steps for each slice was triggered by the QRS. The number of phase encoding steps was adjusted such that data for each slice were acquired in one R-to-R interval. In this way the scan time corresponded to the the number of slices time the R-to-R interval. Sequential k-space ordering was used. A control group of 20 subjects (mean age 18 ± 9 years) with congenital or acquired heart disease that underwent MRA imaging using a conventional non-ECG gated sequence was also evaluated. An 8-element cardiac coil with sensitivity encoding (acceleration factor = 2) was used for both techniques. The two groups were compared with respect to image quality for visualization of the proximal and higher order branches of the pulmonary arteries and veins (using a 3 point semi-quantitative scale), presence of ghosting related to cardiac motion, ability to visualize the origins of the coronary arteries and signal-to-noise ratio (SNR) in the left pulmonary artery.

Results: ECG-gated MRA was successful in all subjects. Use of the ECG-gated MRA sequence eliminated cardiac ghosting artifact in all subjects (vs. artifact in 14/20 controls, $p < 0.0001$) and allowed visualization of the origin of at least one coronary artery in 16/22 subjects (vs. 5/20 controls, $p = 0.06$). The average image quality grade for the pulmonary arteries and veins was similar in both groups (2.6 ± 0.4 vs. 2.5 ± 0.4, $p = 0.4$). Mean SNR in the left pulmonary artery was lower using the ECG-gated technique (46 ± 24 vs. 75 ± 46, $p = 0.02$). Mean imaging time per dynamic was 24 ± 7 seconds for the ECG-gated technique and 16 ± 8 seconds for the conventional technique ($p = 0.002$).

Conclusions: ECG-gated MRA of the chest is feasible in children and young adults with congenital heart disease and allows imaging free of ghosting and with improved visualization of the coronary arteries but without improvement in visualization of the pulmonary arteries or veins.

456. OPERATOR INDUCED VARIABILITY IN LEFT VENTRICULAR MEASUREMENTS WITH CARDIOVASCULAR MR IS IMPROVED AFTER TRAINING

Theodoros D. Karamitsos, MD, Lucy E. Hudsmith, MRCP, MA, BM BCh, Stefan Neubauer, MD, FRCP, Jane M. Francis, DCCR, DNM. ***University of Oxford, Oxford, United Kingdom.***

TABLE 1
Junior operators' coefficient of variability results before and after training

	Operator 1		Operator 2		Operator 3		Operator 4		Operator 5		Operator 6	
	PRE (%)	POST (%)	PRE (%)	POST (%)	PRE (%)	POST (%)	PRE (%)	POST (%)	PRE (%)	POST (%)	PRE (%)	POST (%)
EF	4.4	2.04	10.1	4.1	8.0	3.0	6.9	5.1	6.3	3.4	7.4	4.5
EDV	4.6	2.1	8.6	5.5	3.9	4.7	3.6	2.9	3.6	5.4	7.8	6.8
ESV	13.5	5.6	19.7	6.0	18.8	6.4	17.9	14.2	15.1	4.4	16.7	7.8
SV	4.4	3.4	12.9	9.6	11.1	7.2	7.5	3.1	6.8	8.6	12.3	11.1
MASS	10.9	3.9	7.1	8.3	8.2	6.0	6.0	7.8	5.6	7.4	8.4	6.7

Background: Cardiovascular Magnetic Resonance (CMR) has proven to be precise and reproducible for measuring left ventricular (LV) functional parameters. Reproducibility and accuracy of these measurements is usually reported between experienced operators. However, a growing number of cardiologists are seeking to gain experience in CMR, necessitating early involvement in post processing analysis.

Purpose: The aim of the study was to assess the interobserver variability of the manual planimetry of LV contours and phase selection between two experienced (gold standard) and six inexperienced operators before and after a two months training period.

Methods: Ten healthy normal volunteers (5 men, mean age 34 ± 14 years) comprised the study population. For each subject, left ventricular volumes, mass, and ejection fraction were manually evaluated using Argus software (version 25A; Siemens Medical Solutions, Erlangen, Germany) once by the experienced and twice by the six inexperienced operators. Epicardial and endocardial borders were traced on the end-diastolic frame, with only an endocardial border on the end-systolic frame. Following a period of software familiarisation, instructions were given to the inexperienced operators to select the basal slice for the left ventricle when at least 50% of the blood volume was surrounded by myocardium in both end-diastole and end-systole. Operators were free to select the end-systolic and end-diastolic frame. From these data, LV mass, ejection fraction, and end-systolic and end-diastolic volumes could be calculated. LV mass was determined by multiplication of the tissue volume by 1.05 g/cm^3 (specific density of myocardium). Selection of end systolic time, basal end-diastolic and end-systolic slices, and apical end-diastolic and end-systolic slices were also reported. Training involved hands-on standardised data acquisition, simulated off-line analysis (at least 25 scans analysed by each trainee), didactic lectures on CMR imaging, supervised analysis practice and mentoring. The agreement between operators was evaluated by means of Bland-Altman analysis. Spearman's rank correlation coefficient (Rs) was used to assess the correlation between the basal slice selection and the LV measurement differences.

Results: Training led to quality improvement in the measurement of the majority of the LV parameters (mean ejection fraction coefficient of variability pre-training $7.2 \pm 0.2\%$, post-training $3.7 \pm 0.5\%$, $p = 0.003$) (Table 1). Ejection fraction (EF–Fig. 1), end-diastolic volume (EDV) and stroke volume (SV) measurements were the parameters where the trainees showed the highest improvement. The end-systolic volume (ESV) and. LV mass measurements presented the highest variability even after training. The major source of error was the selection of the basal slice in end-diastole and end-systole (Fig. 2).

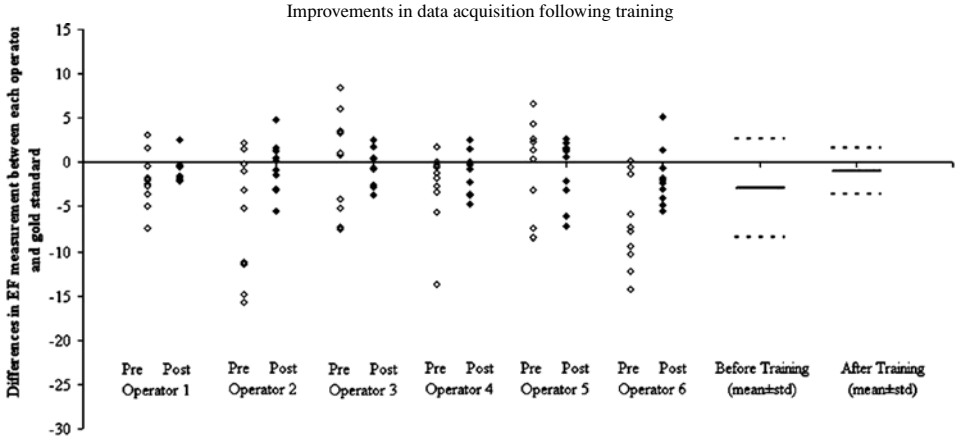

FIG. 1. A scatterplot of the differences in ejection fraction (EF) measurements between junior operators and gold standard before (open diamonds) and after training (closed diamonds). Mean values for differences in EF measurements made by junior operators before and after training together with the standard deviations are also plotted.

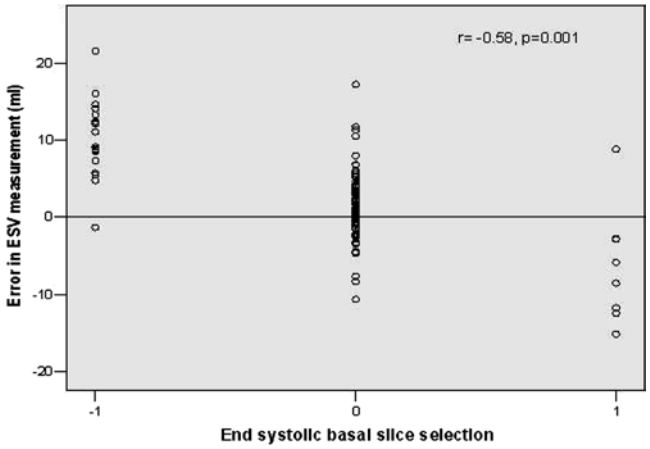

FIG. 2. Scatterplot of the errors in ESV measurements before and after training related to the selection of the basal slice in end systole.

Conclusions: An intensive two month training period significantly improved the accuracy of the majority LV measurements. Adequate training of new CMR operators involved in post processing analysis is of primary importance in order to maintain the accuracy and high reproducibility that benefits CMR in left ventricular function analysis.

457. SAMPLE SIZE CALCULATION FOR THE APPLICATION OF NON-CONTRAST AND CONTRAST-ENHANCED HIGH-RESOLUTION CAROTID MAGNETIC RESONANCE IMAGING IN CLINICAL TRIALS

Hunter R. Underhill,[1] Chun Yuan,[1] Tobias Saam,[1] Nayak L. Polissar,[2] Blazej Neradilek,[2] Baocheng Chu,[1] Norihide Takaya,[1] Wei Yu,[1] Minako Oikawa,[1] Jianming Cai,[1] Thomas S. Hatsukami.[1] ***[1]University of Washington, Seattle, Washington, USA, [2]The Mountain-Whisper-Light Statistical Consulting, Seattle, Washington, USA.***

Introduction: High-resolution MRI has been proven to reproducibly quantify the composition and morphology of the carotid arterial wall (1–3). As such, the incorporation of carotid MRI during clinical trials has been increasingly considered to identify plaque changes in response to therapy (4).

We have previously reported data to serve as the basis of sample size calculations for carotid MRI trials (5). Follow-up in the earlier study was 13 weeks. For calculation of sample size in longer trials, data from a more extended period are needed to account for the biologic variability introduced by normal disease progression. Moreover, potential benefits of contrast-enhanced MRI (CE-MRI) for improvement in image interpretation (6) were not directly compared to MRI without contrast enhancement in the previous study.

Purpose: We sought to: 1) determine the variation in carotid atherosclerotic disease in a population with extended follow-up using quantitative MRI; 2) identify the impact of contrast administration on measurement variation in wall measurements; and 3) provide a sample size calculation for the planning of future prospective clinical trials based on the variation in disease as assessed by both non-contrast and contrast-enhanced carotid MRI.

Methods: As part of an ongoing prospective observational investigation, participants with 50–79% carotid stenosis by duplex ultrasound received a high-resolution carotid MRI at 1.5 T with bilateral phased-array surface coils. Sixty-eight subjects were imaged using a standardized protocol of TOF, T1-/PD- and T2-weighted sequences at baseline and 18 months later. Fifty-six subjects were imaged with an identical protocol, but with the addition of a contrast-enhanced T1W sequence after infusion of 0.1 mmol/kg Gadolinium-DTPA-BMA (Omniscan). A subset ($N = 17$) of the latter group was imaged 36 months after the baseline evaluation. Two reviewers blinded to time point reached a consensus interpretation for each matched location and quantitative measurements were recorded using a custom-designed image analysis tool (CASCADE, University of Washington). Wall area (WA), lumen area (LA), normalized wall index (NWI $=$ WA/[LA $+$ WA]) and mean wall thickness were recorded for all images. For CE-MRI, mean percent LRNC, calcification and hemorrhage were measured as a proportion of the vessel wall in those subjects that exhibited a LRNC, calcification or hemorrhage. Combined biologic and measurement variation was assessed by comparing quantitative data between the baseline and follow-up scan.

Results: The standard deviation of change and its associated 95% upper confidence bound (UCB) is presented in Table 1. Power analysis (2-sided unpaired t-test, power $= 80\%$, $p < 0.05$) based on the conservative UCB values was used to determine the amount of change likely to be detected from a treatment arm of variable size **N** (Table 1) compared to a control arm of identical size **N** during a clinical trial. The calculated variation incorporated both true biological change and measurement error between time points.

Conclusions: A comparison of non-contrast and contrast enhanced results after 18 months of follow-up suggests that CE-MRI reduced the measurement variability of wall morphology. Consequently, a smaller population can be used with CE-MRI to achieve the same observable effect as non-CE-MRI. As expected, a comparison of the 18 month to 36 month data demonstrated an increase in the biologic variability for the group with a longer period of follow-up. As such, longer trial duration may increase the observable effect of the pharmacologic agent by allowing greater natural biologic change to occur. This study provides the basis for sample size calculations during future MRI trials in subjects with 50–79% carotid stenosis.

REFERENCES

1. Kang X, et al. MRM 2000;44:968–72.
2. Toussaint JF, et al. Circulation 1996;94:932–8.
3. Fayad ZA, et al. Ann N Y Acad Sci 2000;902:173–86.
4. Chu B, et al. Stroke 2004;35:2444–8.

TABLE 1
Power calculation of each morphologic or compositional measurement for treatment-arm samples of different size during a clinical trial. N = size of each arm.

	SD	SD UCB*	N = 10	N = 20	N = 50	N = 100
Mean Lumen Area (mm^2)						
18 Month Non-CE	3.3	3.7	5.0	3.4	2.1	1.5
18 Month CE	2.2	2.5	3.4	23	1.4	1.0
36 Month CE	3.1	4.0	53	3.7	2.3	1.6
Mean Wall Area (mm^2)						
18 Month Non-CE	4.2	4.8	6.4	4.4	2.7	1.9
18 Month CE	2.9	3.4	4.5	3.1	1.9	1.3
36 Month CE	4.6	6.0	7.9	5.4	3.4	2.4
Mean NWI						
18 Month Non-CE	0.031	0.035	0.046	0.032	0.020	0.014
18 Month CE	0.025	0.029	0.039	0.026	0.016	0.012
16 Month CE	0.046	0.059	0.078	0.053	0.033	0.023
Mean Wall Thickness (mm)						
18 Month Non-CE	0.17	0.19	0.25	0.17	0.1 1	0.08
18 Month CE	0.13	0.15	0.19	0.13	0.08	0.06
36 Month CE	0.20	0.25	0.33	0.23	0.14	0.10
Mean % LRNC						
18 Month CE	1.9	2.2	2.3	2.0	1.2	0.9
36 Month CE	5.5	7.1	9.4	6.4	4.0	2.8
Mean % Calcification						
18 Month CE	1.1	1.3	1.7	1.1	0.7	0.5
36 Month CE	1.1	1.5	1.9	1.3	0.8	0.6
Mean % Hemorrhage						
18 Month CE	1.9	2.2	2.9	2.0	1.2	0.9
36 Month CE	3.9	5.0	6.6	4.6	2.8	2.0

*95% upper confidence bound of standard deviation (SD).

5. Saam T, et al. JCMR 2005;7:799–808.
6. Takaya N, et al. JMRI 2006;24:203–10.

458. MYOCARDIAL SCARRING IN SURVIVORS OF CONGENITAL HEART SURGERY IN THE PRESENT ERA: ASSESSMENT USING DELAYED ENHANCEMENT MAGNETIC RESONANCE IMAGING

D. J. Patton, MD,[1] M. Harris, MD,[2] J. W. Gaynor, MD,[2] L. Montenegro, MD,[2] P. Gruber, MD,[2] T. L. Spray, MD,[2] M. A. Fogel, MD.[2] [1]***Alberta Children's Hospital, Calgary, Alberta, Canada,*** [2]***Children's Hospital of Philadelphia, Philadelphia, Pennsylvania, USA.***

We hypothesized that there is little myocardial scarring in survivors of surgery for congenital heart disease (CHD) in the

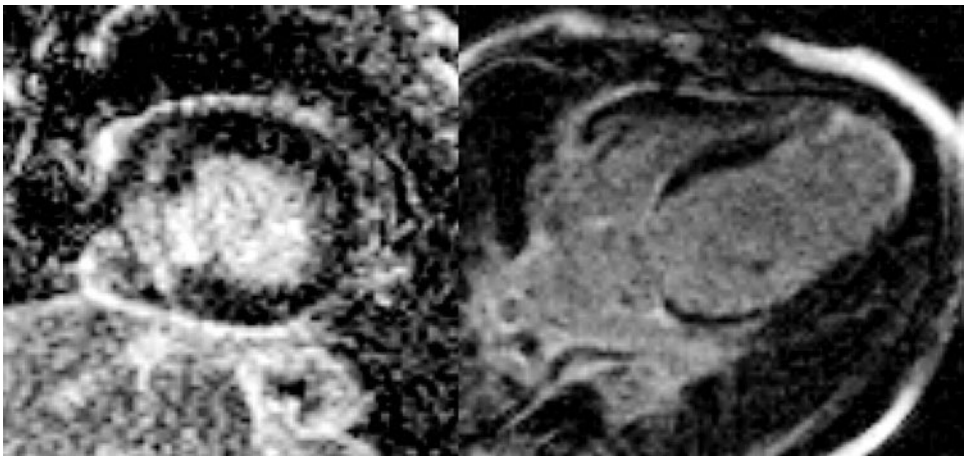

current era. Contrast enhanced cardiovascular magnetic resonance (CE-CMR) can label fibrosis and can test this hypothesis.

Methods: All CE-CMR studies from 10/04 to 4/06 after surgical repair of CHD were reviewed. After evaluation of anatomy and ventricular shortening, gadolinium was administered followed by delayed myocardial imaging. Enhancement of outflow tracts, conduits or patches was excluded.

Results: One hundred twleve patients (range 12 days–61 years), 76 of whom had surgical data available, underwent CE-CMR after surgical repair. Time from last surgery to CE-CMR was 9.6 ± 6.7 years. Five studies (4%) showed delayed enhancement, 4 of which had reasons other than surgery for myocardial scarring: 1) pulmonary atresia/intact ventricular septum with right ventricular dependent coronary circulation (Fig. 1); 2) the left ventricle in hypoplastic left heart syndrome; 3) Williams syndrome after repair of supravalvar aortic stenosis; and 4) residual coarctation. A patient with double outlet right ventricle had left ventricular apical scarring (Fig. 2). Age at repair, hospital stay, perfusion, cross clamp, and deep hypothermic circulatory arrest times were similar in patients with and without myocardial scarring. Ventricular shortening correlated with scar tissue visualization.

Conclusions: Myocardial scarring is present in a low proportion of survivors undergoing congenital heart surgery in the current era and ventricular shortening correlated with scar visualization.; nearly all fibrosis found in this study can be attributed to the underlying defect/physiology.

459. TRACKING THE DEVELOPMENT OF CARDIOMYOPATHY IN DUCHENNE MUSCULAR DYSTROPHY

Michael D. Puchalski,[1] William Gottliebson, MD,[2] Richard V. Williams, MD,[1] Jason Su, MD,[1] Nathan Pack, BS,[1] Edward DiBella, PhD.[1] [1]***University of Utah, Salt Lake City, Utah, USA,*** [2]***Cincinnati Children's, Cincinnati, Ohio, USA.***

Background: The development of a cardiomyopathy is a common cause of morbidity and mortality in Duchenne muscular dystrophy (DMD). The predisposition to the posterobasal and left lateral free wall of the left ventricle (LV) as the initial site of myocardial involvement is well known from pathology specimens. The purposes of this study were to assess whether cardiac magnetic resonance imaging (CMRI), utilizing delayed myocardial enhancement (DME), could identify fibrosis in areas of myocardium known to be at risk and to assess the relationship of the presence and extent of fibrosis to LV function.

Methods: The cardiology databases at Primary Children's in Utah and Cincinnati Children's were reviewed to identify patients with DMD who had undergone a CMRI in the last 2 years. Age, LV ejection fraction, LV mass, presence and location of DME were documented. Volumes were measured from contiguous slices in the short axis plane from base to apex using MASS (Medis, Inc.) to calculate ejection fraction and mass. DME images were acquired using a segmented inversion-recovery sequence in the short axis plane 10–15 minutes after the injection of 0.1 mmol/kg of gadolinium-DTPA. In patients with DME, manual and customized computer assisted sizing of the areas of hyperenhancement were performed on all slices. Summing the areas yielded a total volume which was converted to mass and expressed as a percent of the total mass of the LV. Pearson product-moment correlation was used to assess function vs age and the Fisher Exact test was used for analysis of function and DME with $p < 0.05$ being statistically significant. Normal function was defined as $>54\%$.

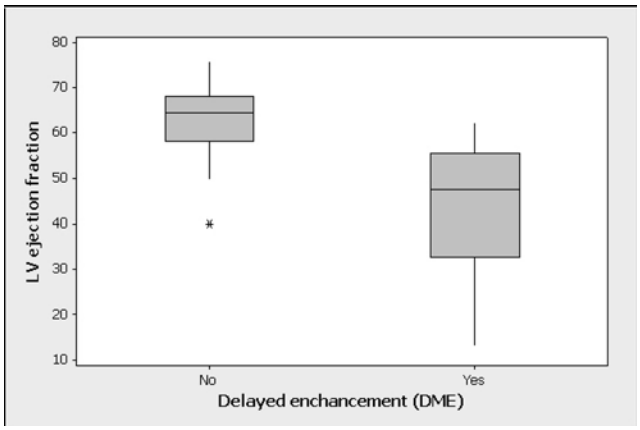

FIG. 1.

Results: A total of 69 DMD patients (mean age 14.3 ± 3.9 years) underwent CMRI with 33 given gadolinium-DTPA. Twelve patients had DME involving the posterobasal region of the LV (Fig. 1). Those patients with more involvement had spread to the inferior and left lateral free wall with progressive transmural fibrous replacement. There was relative sparing of the interventricular septum and right ventricle. A negative correlation was found between LV ejection fraction and age across the entire group ($r = -0.5$ and $p < 0.0001$). Patients with DME had a lower ejection fraction than those without (Fig. 2, $p < 0.001$).

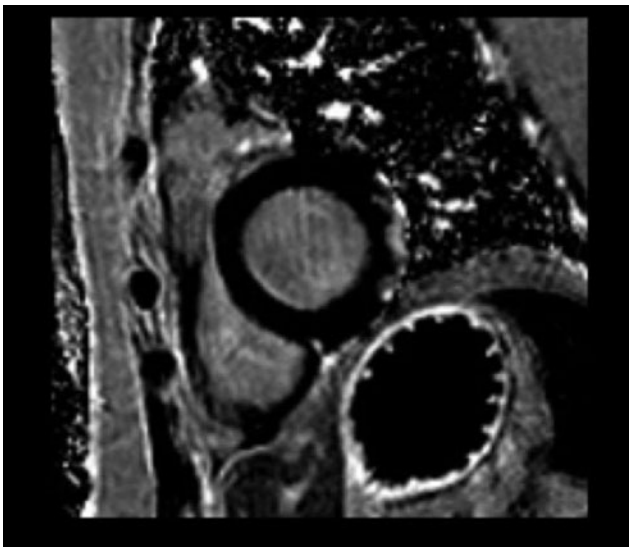

FIG. 2.

All patients with >20% of the LV mass having DME had poor LV function with a trend toward significance ($p = 0.09$).

Conclusions: DME performed by CMRI is able to detect fibrosis in regions of myocardium known to be at risk in a population of patients with DMD. LV ejection fraction decreases with age and in the presence of DME. Serial studies are warranted to determine if DME precedes a decrease in function and whether medical management is useful once DME is documented.

460. T2-WEIGHTED 3D DARK BLOOD TSE FOR CAROTID LUMEN MEASUREMENT—INITIAL EXPERIENCE

Yiu-Cho Chung, PhD,[1] Jason Hughson, BS,[2] Subha V. Raman, MD, MSEE,[2] Orlando P. Simonetti, PhD,[2] Renate Jerecic, PhD.[1] [1] ***Siemens Medical Solutions USA, Inc., Chicago, Illinois, USA,*** [2] ***The Ohio State University, Columbus, Ohio, USA.***

Introduction: Atherosclerotic plaque's vulnerability to rupture is related to plaque composition and morphology (1, 2). The excellent soft tissue contrast of MRI can be used to characterize carotid plaque composition, but comprehensive coverage of carotid plaque for morphology using 2D methods (3) is time-consuming. Recent 3D TrueFISP techniques (4, 5) are fast but contrast properties are not well understood. T2 weighted 3D dark blood TSE, aka SPACE (Sampling Perfection with Application optimized Contrast using different angle Evolutions), has been proposed for carotid plaque imaging (6). SPACE provides extended anatomical coverage and good T2-weighted contrast relevant to plaque visualization.

Purpose: To compare vessel lumen measurements using SPACE versus contrast enhanced MR angiography (ceMRA), and to assess SPACE's potential to quantify luminal stenosis in patients with carotid artery atherosclerosis.

Methods: Sequence: SPACE (6) was improved to use (a) selective 90° excitation pulse, (b) phase alternation and averaging to eliminate stimulated echoes. The voxel dimension was 0.8 mm × 0.8 mm inplane, 0.8–1.6 mm throughplane, interpolated to 0.4 mm × 0.4 mm × 0.4 to 0.8 mm. Total scan time was about 4.5–5.5 min (52 to 64 partitions). In ceMRA, voxel dimension was 1 mm × 0.8 mm inplane, 0.7 mm throughplane. Interpolation was done in k-space by partial Fourier (phase: 7/8, partition: 6/8), asymmetric echo (25%), reduced phase (80%) and partition (60%) resolution. Parallel imaging (rate 2) was used in both techniques. The voxel volume was 0.5 mm^3 to 1 mm^3 in SPACE, and 1 mm^3 in ceMRA.

Imaging: Imaging was performed in 7 patients with known carotid disease as part of an IRB-approved protocol. The studies were done on a 1.5T MRI system (Avanto, Siemens Medical Solutions, Erlangen, Germany) using carotid phased array coils (Machnet, The Netherlands). SPACE images were acquired before ceMRA. In 5 patients, T2-weighted dark blood 2D TSE (T2W-2DTSE) images were acquired before ceMRA for contrast comparison with SPACE.

Evaluation: Standard 3D MPR and MIP software was used to locate and measure the stenosis in SPACE and ceMRA images. In each diseased carotid artery, the site of greatest stenosis was identified. A stack of thin slices perpendicular to the vessel long axis and extending to a stenosis-free region of the common carotid artery was then reconstructed for lumen measurement. The correlation coefficients of lumen diameters measured from SPACE and ceMRA were calculated.

Results: Image acquisition was successful in all patients except one (suboptomal ceMRA images, excluded from measurement comparison). The correlation between measurements from two imaging methods was 0.91 for stenotic lumen diameters (11 stenoses total), improved to 0.97 when including common carotid artery measurements (Fig. 1a). For all diseased arteries, plaque morphologies depicted by SPACE and ceMRA were comparable. SPACE's image contrast was similar to T2W-2DTSE in all five cases, albeit at a lower resolution. Fig. 1b-1e show images obtained from one study. Note the correspondence between SPACE image and the MIP image from ceMRA in depicting plaque morphology, and the contrast similarity between SPACE and T2W-2DTSE.

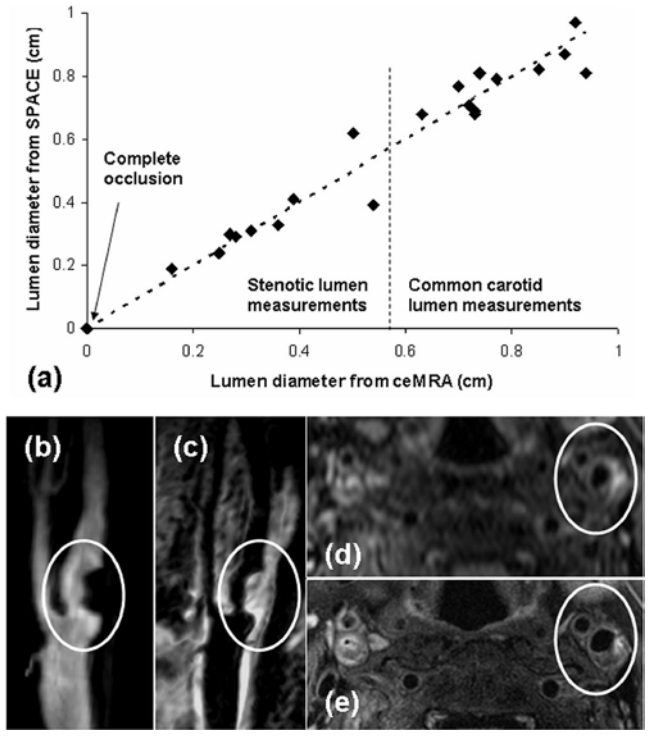

FIG. 1. (a) Correlation between lumen diameter measurements based on SPACE and ceMRA images (22 meaurements). The dotted line shows the ideal relationship (i.e., correlation = 1). (b)–(e) Carotid stenosis in one patient. (b) ceMRA depicts the sterosis (MIP image) at the left carotid artery. (c) SPACE shows the plaque morphology and soft tissues around it (minimum intensity projected image). The T2 contrast in SPACE (d) is comparable to the T2 contrast in conventional 2D TSE (e) at a lower resolution.

Conclusions: Lumen diameters measured from SPACE were comparable to those from ceMRA in this small patient population, suggesting that spatial resolution from SPACE may be sufficient for clinical assessment of carotid stenosis and plaque morphology. The T2 contrast from SPACE, comparable to T2W-2DTSE, may provide additional diagnostic information regarding plaque composition. SPACE may be a valuable clinical tool for plaque characterization and measurement in carotid artery disease patients.

REFERENCES

1. Fayad, Fuster. Neuroimaging Clin N Am 2002;12.
2. Rothwell, et al., Stroke 2000:31:615–21.
3. Fayad, et al. Cardiovascular MR. ed. Lardo et al. Mosby, Inc. 2003;333–46.
4. Koktzoglou, et al. Proc. 13th ISMRM 2005;1743.
5. Koktzoglou, et al. Proc 14th ISMRM 2006;652.
6. Chung, et al. Proc 14th ISMRM 2006;653.

461. CONTRAST-ENHANCED MAGNETIC RESONANCE IMAGING REVEALS EARLY DECREASE OF THE TRANSMURAL EXTENT OF REPERFUSED ACUTE MYOCARDIAL INFARCTION

Constanze Merten, MD, Henning Steen, MD, Christian Kulke, MD, Hugo A. Katus, Evangelos Giannitsis, MD. ***University Heidelberg, Heidelberg, Germany.***

Introduction: In patients (pts.) with acute myocardial infarction (AMI), infarct size and mural infarct extent (MIE) are of high prognostic value for clinical outcome and possible recovery of contractile function of affected myocardium. Contrast-enhanced magnetic resonance imaging (CEMRI) is a non-invasive imaging technique that has proven to be highly accurate for determination of myocardial infarct size and degree of MIE. In animal and human studies it has been shown that within several weeks infarct sizes markedly decrease. Interestingly, only scarse data is available about the so-called infarct shrinkage early post AMI.

Purpose: We hypothesized that MIE would measurably decrease already within several days after successful reperfusion due to decreased myocardial edema and secondly that this process could be detected non-invasively by CEMRI.

Methods: We studied 19 patients with ST-segment elevation myocardial infarction (STEMI) within 24 hours after sympton onset. All patients obtained TIMI 3 flow after primary percutaneous coronary intervention with stent implantation of the infarct related artery (IRA). A first MRI scan on a clinical whole body 1.5 Tesla scanner (Siemens Symphony, Erlangen, Germany) was performed within 24 hours (day-1). To assess infarct size, CEMRI images were acquired in 4 short-axes slices using gadolinium DTPA (0.2 mmol kg/bw). An identical follow up MRI scan (day-7) was performed before discharge. For regional evaluation, 4 CEMRI short-axes slices were divided into 22 segments: six basal, six baso- midventricular, six apico-midventricular and four apical segments.

TABLE 1
Patient characteristics

Age (years)	62,6±10.6
Gender (% male)	17/19 (89)
Diabetes (%)	3/19 (16)
Hypertension (%)	13/19 (68)
Hyperlipidemia (%)	9/19 (47)
Smoking (%)	7/19 (37)
Family history (%)	5/19 (26)
Obesity (%)	17/19 (89)
BMI (kg/m^2)	28.3±3,2
LAD (%)	5/19 (26)
RCA (%)	14/19 (74)

Data as mean ± SD or percent. BMI = body mass index; LAD = left anterior descending; RCA = right coronary artery.

In each segment the MIE was visually assessed by two blinded observers and classified I-IV (I =< 25%; II = 26–50%; III = 51–75%; IV > 75%) of left ventricular wall thickness. Data were expressed as mean number of affected segments per pt. ± SEM. For comparison of day-1 to day-7 MIE a paired t-test was used. Patient characteristics are shown in Table 1.

Results: The mean total number of CMRI segments did not change between day-1/day-7 CEMRI scan (7.1 ± 0.5 vs. 7.2 ± 0.7 segments, p = 0.7).

There were no significant changes in the mean number of I/II segments (0.3 ± 0.1 vs. 0.5 ± 0.3 segments, p = 0.5 and 1.3 ± 0.3 vs. 1.6 ± 0.2 segments, p = 0.4). The mean number of IV segments decreased significantly (3.9 ± 0.6 vs. 2.4 ± 0.4 segments, p = 0.027) whereas the mean number of III segments increased significantly (1.6 ± 0.4 vs. 2.7 ± 0.5 segments, p = 0.011, Fig. 1).

*Conclusion:*Our results demonstrate a detectable early decrease of MIE in reperfused AMI. employing CEMRI. The process of myocardial infarct shrinkage early after reperfused AMI could be detected even qualitatively by CMRI without measuring infarct volumes.

The fact that infarct shrinkage can already be visualised by CEMRI within the first week after AMI should be taken into

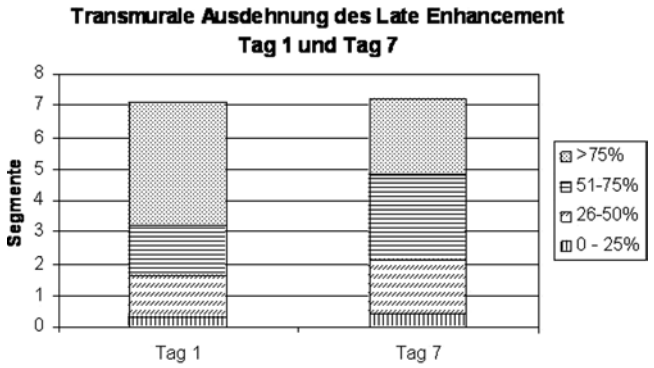

FIG. 1. Transmural extent of late enhancement.

account when determining infarct size and MIE in the clinical setting as well as in research or pharmaceutical trials using these parameters as a clinical endpoints.

462. DETECTION OF LEFT VENTRICULAR THROMBUS WITH CARDIAC MAGNETIC RESONANCE IMAGING IN PATIENTS WITH ACUTE ST-SEGMENT ELEVATION MYOCARDIAL INFARCTION (STEMI)

Kathrin Schindler, Christian Luecke, Josef Friedenberger, Gerhard Schuler, Holger Thiele, Dietmar Kivelitz. ***Herzzentrum Leipzig, Leipzig, Germany.***

Introduction: Previously published studies show differences regarding the prevalence of intraventricular thrombi in patients with acute myocardial infarction (MI) (4–56% [1]) Until now there are no exact results about the occurrence of left ventricular thrombi in acute STEMI.

Methods: To investigate the extent of myocardial infarction we examined 103 consecutive patients undergoing primary percutaneous coronar intervention (PCI) in acute STEMI within 12 h after symptom onset by cardiac magnetic resonance imaging within 2–4 days.

Routinely all patients were examined with transthoracic echocardiography (TTE) or transesophageal echocardiography (TEE).

MRI was performed using a 1.5 T scanner (Philips Intera). ECG-gated cine steady-state free precession (SSFP) sequences were performed in the 2-chamber and 4-chamber view as well as in the short cardiac axis from base to apex. After administration of 0.15 mmol/kg body weight Gadobutrol (Gadovist, Schering, Germany) a 3D inversion recovery gradient echo sequence in the same orientations was applied to assess the size of the myocardial infarction.

All images were analyzed regarding the presence of intraventricular thrombi.

Results: Forty-five and six tenths percent of the patients had an anterior MI, 37.9% an inferior MI. In 6.8% of the cases the infarction was localized in the septum and in 4.9% in the lateral wall.

In 2.9% of the cases, MRI did not show an infarct-typical area in late enhancement sequences.

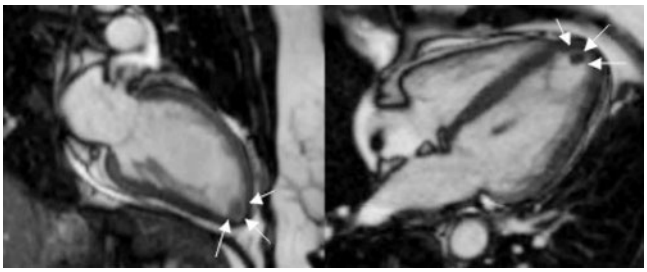

FIG. 1. Cine SSFP 2-chamber und 4-chamber view of a 55-year-old woman with acute anterior STEMI and left ventricular thrombus (arrows).

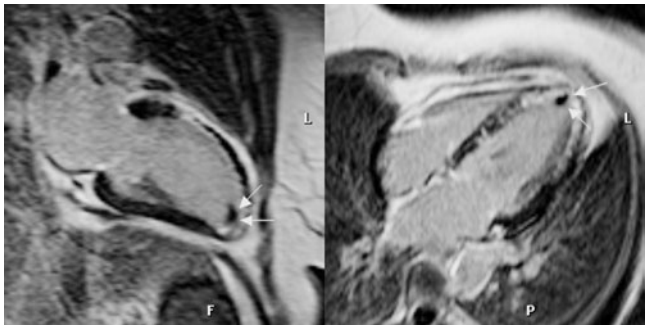

FIG. 2. Picture 2: Same patient as in picture 1, late enhancement sequences in 2-chamber and 4-chamber view.

In 9 patients (8.7%), we detected left ventricular thrombi, but none of these were seen in TTE or TEE.

In one case an intraventricular thrombus was detected by TEE, but in the subsequently performed MRI no thrombus was found.

In all cases the left ventricular thrombi could be detected in the late enhancement sequence, 4 (44.4%) of them were missed in the cine SSFP sequences.

Comparing the cine SSFP with the late enhancement sequences we noticed that especially in late enhancement sequences the intraventricular thrombi can be detected better due to the superior contrast between the hypointense thrombus in comparison to the hyperintense infarction area (2).

Remarkable was also that 7 (77.8%) of the 9 patients with left ventricular thrombus in MRI had an anterior MI, whereas only 2 (22.2%) had an inferior MI.

Conclusion: In our study TEE and TTE missed left ventricular thrombi in all 9 patients as compared to MRI. There was one false-positive result in TEE as compared to MRI. Patients with acute anterior MI have a higher risk of developing left ventricular thrombi than in other infarct-locations.

Therefore, it could be potentially important to screen in particular high-risk patients (with anterior MI) with cardiac magnetic resonance imaging to exclude left ventricular thrombi and to lower the risk of embolic events.

Especially late enhancement sequences are suitable to detect intraventricular thrombi.

REFERENCES

1. Weir, et al., Eur Heart J 2006;27:353.
2. Barkhausen J, et al., AJR 2002;179:1539–44.

463. PREVALENCE OF LIPOMATOUS METAPLASIA IN SCAR FOLLOWING MYOCARDIAL INFARCTION

Christian Luecke, Kathrin Schindler, Gerhard Schuler, Holger Thiele, Dietmar Kivelitz. ***Herzzentrum Leipzig, Leipzig, Germany.***

Introduction: Myocardium may undergo lipomatous metaplasia in scar formation after myocardial infarction (MI) (1). While

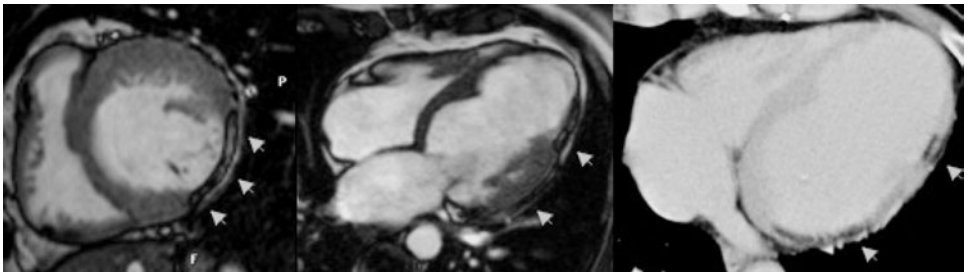

FIG. 1. Left (sa) and mid panels (4cv) show typical high signal intensity with surrounding low signal intensity in the mid anterolateral and inferolateral wall of left ventricle within CINE-SSFP sequences. Cardiac CT (right panel) reveals an area of fat density (-42 ± 12 HU) in the mid lateral wall.

fat-cells can been found in histological specimens, in previously published case reports it has been shown that cardiac magnetic resonance imaging (MRI) is capable to detect lipomatous metaplasia (1).

Cine steady state free precession (SSFP) sequences can have a repetition time which is close to the opposed phase echo time and therefore a dark line encompasses the border zone between fat and water containing tissues which can be used to detect fat in myocardial tissue (2).

Purpose: The purpose of our study was to assess the prevalence of lipomatous metaplasia in patients with previous myocardial infarction or chronic ischemic heart disease.

Methods: We examined 342 patients (270 m, 73 f) at an average age of 63 years with a history of chronic ischemic heart disease by cardiac MRI using a Philips Intera 1.5 T system. For Cine MRI a steady state free precession sequence (SSFP) was applied in the 2-chamber view (2cv), 4-chamber view (4cv) and in the short cardiac axis (sa) with the following parameters: FOV: 350–390 mm, matrix = 256 ∗ 205, TR = 3.6 ms, TE = 1.8 ms, flip angle: 60°). Criterion of proof of fat was higher signal intensity surrounded by lower signal intensity in SSFP-sequences in at least two imaging planes.

Results were correlated with cardiac catheterization findings and imaging findings were compared to cardiac computed tomography (CT) if available.

*Results:*Thirty-seven patients (11%) showed fat in the myocardium, which was confirmed by cardiac CT in 13 patients. Twenty-five of these 37 patients underwent cardiac catheterization. In 23 (92%) patients fat was present in coronary artery territories which were supplied by stenosed vessels (>50% stenosis). In 2 (8%) patients no corresponding coronary artery stenosis was seen. Fig. 1 shows an example of positive findings in cardiac MRI and cardiac CT.

Conclusions: CINE SSFP is able to detect fat within the myocardium and we could show that the myocardial scars of 37 patients (11%) with a history of chronic ischemic heart disease contain fat, indicating fatty degeneration or lipomatous metaplasia after myocardial infarction. This fat is more likely to be found in territories with coronary artery stenosis (92%), than in regions that did not show stenosis in cardiac catheterization (8%).

REFERENCES

1. Estornell J, et al. Eu Heart J 2006.
2. Dixon WT. Radiology 1984;153:189–94.

464. ASSESSEMENT OF CORRELATION BETWEEN PATTERNS OF MYOCARDIAL FIBROSIS VISUALIZED ON CONTRAST ENHANCED MRI AND ECHOCARDIOGRAPHIC STRAIN IMAGING IN PATIENTS WITH HYPERTROPHIC CARDIOMYOPATHY

Dirk Lossnitzer, MD, Andreas Haars, MD, Katharina Kolbe, Medical Student, Henning Steen, MD, Stephanie Lehrke, MD, Hugo A. Katus, MD, Evangelos Giannitsis, MD. ***University Heidelberg, Heidelberg, Germany.***

Background: Echocardiography and MRI are supplementary methods for the evaluation of LV-hypertrophy (LVH) and function in hypertrophic obstructive/non-obstructive cardiomyopathy (HN-/OCM) patients (pts.). MRI is the accepted reference standard for the evaluation of cardiac morphology, quantification of systolic left ventricular (LV) function, assessment of tissue characteristics and myocardial fibrosis by employing gadolinium-based (Gd) delayed contrast enhancement MRI (DCE). Echocardiography is essential for the evaluation of hemodynamic profiles and diastolic dysfunction. Regional myocardial echocardiographic STRAIN/strain rate (S/SR) can be aquired with a high temporal resolution and enable functional tissue characterization of HN-/OCM-pts.

Purpose: The aim of this study was to determine the correlation between DCE-patterns visualized on MRI and myocardial contractility measured with echocardiography on a segmental basis in 30 pts. with HN-/OCM. We hypothesized that a decrease in S/SR would be directly attributable to local myocardial scarring.

Methods: Using a vector-ECG gated short axis (SA) multislice cine SSFP sequence (balanced FFE; TR/TE = 2.9/1.45 ms; reconstr. voxel-size = 1.5 ∗ 1.5 ∗ 8 mm; SENSE-factor = 2; flip angle = 60°) planned on true cine SSFP two- and four-chamber views, we assessed LV mass (g). Regional distribution of DCE was assessed employing a 3D FFE multi-slice inversion recovery sequence (TR/TE = 2.9/1.0; reconstr. voxel

size = 2.0 ∗ 2.0 ∗ 5 mm;SENSE = 2; TI = 200–280 ms) 15 minutes post-Gd (0.2 mmol/kg) in 30 pts. with HN-/OCM on a 1.5 T MRI Whole body scanner (ACHIEVA, Philips Medical Systems, Netherlands) using a cardio-dedicated five-element phased array coil. S/SR-imaging was acquired on a Vivid 7 GE-System (GE Medical Systems, Milwaukee, Wisconsin, USA) in conventionally planned apical two-, three- and four-chamber views. We compared DCE and wall-thickness with MRI radial thickening measured on cine SA images and mid-ventricular echocardiographic S/SR.

Results: MRI and S/SR imaging could be successfully performed in all pts. Ninety percent of HN-/OCM patients showed DCE (5–54% of LV-mass). A typical DCE pattern could be either found in 66% with predominant DCE in the areas of right ventricular insertion or in areas of maximal LVH. There was a good correlation between radial thickening and DCE distribution (r = -0.584, p = 0.0001) revealing a compromised contractility in predominantly affected scar regions. Comparing S/SR with DCE on the same mid-ventricular level, a significant and close correlation could be demonstrated (r = 0.792, p = 0.0001), showing a decreased S/SR in fibrotic septal regions. In profound septal hypertrophy without relevant scarring a good contractility could be demonstrated.

The decreased S/SR was independent of regional wall thickness (p = n.s.) as well as of similarly measured normal values in non- affected areas of the lateral wall. At RV-insertion areas, compromised contractility could not be assessed properly by S/SR in pts. with typically predominant scarring due to predefined apical standard views. Twenty percent of the midventricular segments showing echocardiographic reverberations could not be analyzed.

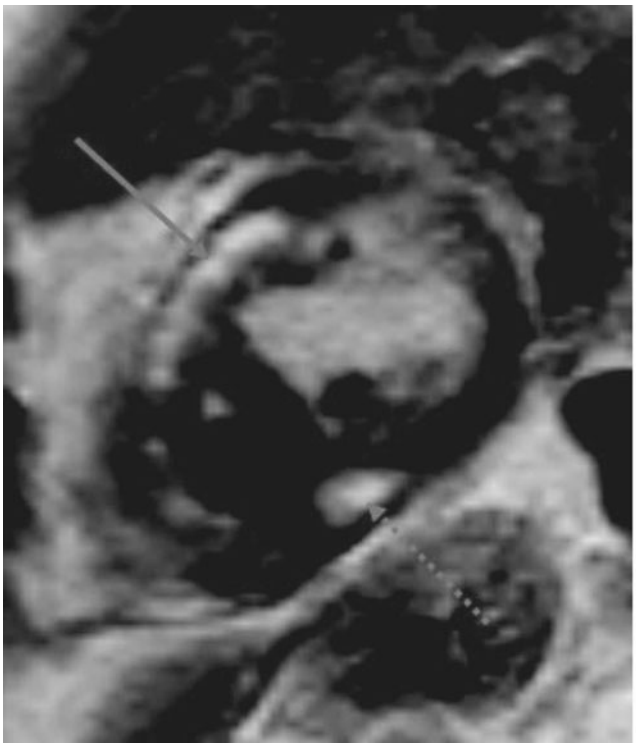

FIG. 1. SA scar image off a pt. with HOCM revealing anteroseptal (arrow) and inferoseptal (dashed arrow) pronounced DCE with concomitantly reduced S/SR.

Conclusion: S/SR imaging can adequately demonstrate decreased contractility in HN-/OCM pts. in areas of DCE. Compromised regional S/SR seemed to be a correlate for excessive myocardial scar development rather than for myocardial hypertrophy alone. In profound septal hypertrophy without relevant scarring a good contractility could be demonstrated.

465. THE ROLE OF DELAYED ENHANCEMENT FOR LEFT VENTRICULAR REDUCTION OF FUNCTION, CLINICAL STATE AND LEFT VENTRICULAR OUTFLOW TRACT OBSTRUCTION IN HYPERTROPHIC CARDIOMYOPATHY

Andreas Haars, MD, Katharina Kolbe, Medical Student, Stephanie Lehrke, MD, Dirk Lossnitzer, MD, Hugo A. Katus, MD, Evangelos Giannitsis, MD, Henning Steen, MD.
University Heidelberg, Heidelberg, Germany.

Backgound: Cardiac MRI (CMRI) has become reference standard for proper assessment of left ventricular hypertrophy (LVH) and function in patients (pts.) with hypertrophic non-/obstructive cardiomypathy (HN-/OCM). Gadolinium (Gd) contrast delayed MRI (CEMRI) patterns reveal septal myocardial fibrosis and are found in ∼80% of pts.

Purpose: We hypothesized that myocardial fibrosis is of major importance for the development of left ventricular decrease of function (LV-Dec = EF < 50%) and could potentially lead to signs of congestive heart failure (CHF).

Methods: A vector-ECG gated short axis (SA) multi-slice cine SSFP sequence (balanced FFE; TR/TE = 2.9/1.45 ms; reconstr. voxel-size = 1.5 ∗ 1.5 ∗ 8 mm; SENSE-factor = 2) was acquired for the assessment of LV mass (g) as well as a 3D FFE SA multi-slice inversion recovery sequence (TR/TE = 2.9/1.0; reconstr. voxel size = 2.0 ∗ 2.0 ∗ 5 mm; SENSE = 2; TI = 200–280 ms) 15 minutes post-Gd (0.2 mmol/kg) for measurement of CEMRI in 42 HN-/OCM pts. (HNCM = 26/HOCM = 14) using a five-element phased array coil on a conventional 1.5T MRI whole body scanner (ACHIEVA, Philips Medical Systems, Netherlands).

Total CEMRI-mass/per body surface area (BSA) was related to LV-ejection fraction (LV-EF), LV-mass/BSA, NYHA-stage (New York Heart Association), NT-pro-BNP levels (ng/L) and Mc Kenna risk score (a = sustained ventricular tachycardia (VT); b = hypotension under physical exertion; c = non-sustained VT; d = inducible VT/VF; e = sudden cardiac death in family history; f = LVH > 30 mm; f = unclear syncope).

Results: MRI could be successfully performed in all 42 pts. Ninety percent of HN-/OCM pts. showed CEMRI

(5–54% of LV-mass) with significantly less CEMRI in HOCM (6.1 g/m^2± 4.3) compared to HNCM (23.8 g/m^2± 15.8 p = 0.0001). There was a moderate relation between regional basal septal contractility and CEMRI distribution (r = -0.53, p = 0.0001) revealing significantly higher mobility in HOCM pts. (0.21% vs. 0.13%, p = 0.008). CEMRI-mass/BSA significantly correlated with compromised LV-EF (r = -0.77, p < 0.0001), NT-pro-BNP levels (r = 0.67, p = 0.0001) and NYHA I-vs. II/III (p = 0.004), weak albeit still significant with the McKenna risk score (r = 0.385, p = 0.035). Systolic LV-Dec was found only in patients with more than 28% CEMRI -mass/BSA (mean = 40.0% ± 7.9).

Conclusion: MRI is a powerful tool in the morphological and functional assessment of pts. with HN-/OCM. CEMRI mass showed a significant relation to compromised systolic left ventricular function, elevated NT-pro-BNP levels and NYHA-stage independent from LVH. In basal septal hypertrophy, regional scar distribution and contractility seems to play an essential role for the development of left ventricular outflow tract obstruction. Further studies should be performed to evaluate the prognostic value of CEMRI for LV-decrease of function and risk of sudden death.

466. DEVELOPMENT OF A CATHETER AND PROTOCOL FOR MR-GUIDED INTRAMYOCARDIAL INJECTIONS

Gabriele A. Krombach, PD Dr. med.,[1] Arno Bücker, Prof. Dr. med. MSc,[2] Sylvia Kinzel, PD Dr. med. vet.,[3] Jochen Pfeffer,[1] Michael Friebe, Dr.,[4] Christian Hohl, Dr. med.,[5] Rolf W. Guenther, Prof. Dr. med.[5]
[1] University Hospital, RWTH Aachen, Aachen, Germany, [2] Diagnostic Radiology, University Hospital Homburg, Germany, [3] Department of Experimental Medicine, University Hospital, RWTH Aachen, Germany, [4] Tomovation, Reutlingen, Germany, [5] Diagnostic Radiology, University Hospital, RWTH Aachen, Germany.

Introduction: Molecular interventions, targeted at the myocardium in order to initialize angioneogenesis or to increase the amount of contractile myocytes are already used in patients. The substances are injected directly into the myocardium in order to reach high concentrations and to minimize systemic side-effects. Injections have been performed during bypass-surgery. However, a catheter-based approach can render this new therapy available for a broader range of patients. For this purpose, MRI guidance is advantageous over fluoroscopy, since MRI provides for delineation of the myocardium and ischemically injured regions. Accordingly, the aim of this study was to develop a catheter and protocol for MRI-guided intramyocardial injection substances.

Methods: In 14 pigs reperfused myocardial infarction was induced by occluding the left anterior coronary artery for 45 minutes. Two hours after reperfusion MRI was started at a 1.5 T closed bore system (Intera, Philips, Best, The Netherlands). In order to delineate the infarcted myocardium in 7 animals, SHU555A (Schering, Berlin, Germany) -a small particle of iron oxide (SPIO)—was injected intravenously, at a dose of 1.4 mL. In the remaining 7 animals, MS325, a gadolinium-containing blood pool contrast medium, was intravenously injected to delineate the infarct. For real-time image guidance, a radial steady-state free-precession sequence with a frame rate of 15/s was applied (TR 2.5 ms, TE 1.2 ms, 45° flip angle, 80 radials, 8 mm slice thickness, matrix 128 × 128, FOV 320 × 320 mm^2, sliding window reconstruction). As soon as sufficient contrast between both regions was achieved on real time imaging, a MRI-compatible self-made needle-catheter was repeatedly guided from a carotid artery sheath into the left ventricle and inserted into the myocardium. Two mL of Gd-DTPA-BMA (Omniscan, Amersham Bucheler, Braunschweig, Germany) were injected at concentrations of 0.1 or 0.4 mmol/mL.

After the interventions were finished, the hearts were excised and stained with 2,3,5-triphenyltetrazolium chloride (TTC), to delineate the infarct.

Results: Intravenous injection of SHU 555A caused a significant decrease of the T1 value of the infarct (778 ± 63 ms before, and 641 ± 67 ms 2 h after injection of SHU 555A). The infarct was hyperintense compared to remote myocardium on T1-weighted gradient echo images. The contrast between the infarct and remote myocardium was sufficient for delineating the infarct on real-time images (T1 remote myocardium 2 h after injection: 702 ± 19 ms).

After the intravenous injection of MS 325 the T1-value of the ischemically injured myocardium rapidly decreased (992 ± 31 ms before, and 366 ± 32 ms 2 h after injection of MS325).

In all animals, the catheter could be directed into the border region of the infarct. Two intramyocardial injections were performed at different locations in all animals. Injection sites, infarct region, and remote myocardium, could clearly be differentiated over the course of the observation period.

The T1 values of the injection sites slowly increased over the observation period of 30 min (240 ± 25 ms 3 min after intramyocardial injection of 0.1 mmol/mL Gd-DTPA BMA (370 ± 33 ms 15 min after intramyocardial injection and 468 ± 37 ms 30 min after intramyocardial injection [p < 0.05]).

Discussion: The technique described here may be used for the minimally invasive delivery of substances, such as gene-constructs, to the myocardium. If a high molecular contrast medium is intravenously injected, the infarct can stably be delineated over the course of the intervention. By using extracellular contrast medium as tracer, intramyocardial injection sites remain visible for a sufficient long period of time, so that repeated injections into the same region with consecutive local overdosing during an intervention with multiple injections can be avoided.

467. COMPARISON OF THE DETECTION OF CHRONIC MYOCARDIAL INFARCTION USING ELECTROCARDIOGRAPHIC/ECHOCARDIOGRAPHIC

EVALUATION AND DELAYED ENHANCEMENT MAGNETIC RESONANCE FINDINGS

Marcin Basiak, Jr, MD,[1] Jolanta H. Misko, Sr, MD, PhD,[1] Anna Wycisk, Sr, MD, PhD,[2] Barbara Paraniak, Jr, MD,[1] Jacek Brzezinski, Sr, MD, PhD,[1] Marek Konopka, Sr, MD, PhD.[1] [1]***HELIMED, Silesian Centre for Diagnostic Imaging, Katowice, Poland,*** [2]***Medical University of Silesia, Katowice, Poland.***

Introduction: Accurate assessment of myocardial infarction (MI) is critical for proper management of patients with chronic coronary disease. Commonly the presence of acute MI is assessed by measurement of cardiac markers and electrocardiographic (ECG) changes. In routine clinical practice location and transmurality of chronic MI are measured by ECG findings and wall motion abnormalities detected by echocardiography (ECHO). Recently, delayed enhanced cardiovascular MR (DE-CMR) offer precise definition and quantification of the necrotic myocardial tissue.

Purpose: The aim of this study was to evaluate the differences between standard ECG and ECHO assessment of presence, location and transmural extension of chronic MI with that performed by means of DE-CMR.

Methods: The study group consisted of 29 patients (pts) with chronic coronary disease after acute coronary events (ACS); 17 pts with known previous MI and 12 pts without defined MI based on conventional methods. Presence of MI was defined as biomarkers (CK MB, troponin I) elevation during the acute phase of ACS and/or relevant ECG changes. Location and transmurality of MI was defined by ECG (Q or non-Q wave) and wall motion abnormalities was detected by the ECHO. Wall motion abnormalities were divided into seven potential regions: septal, anteroseptal, anterior, anterolateral, inferior, lateral, inferolateral and two types of extension: transmural and subendocardial. To correlate DE-CMR and conventional evaluation of MI we divided the left ventricle into three regions according to usual coronary artery supply: 1—LAD (septal, anteroseptal, anterior, anterolateral region) 2- LCx (lateral, inferolateral) and 3- RCA (inferior). Extension of MI was defined as subendocardial with $<$ 50% of myocardial wall thickness, or transmural—with $>$50% of wall thickness.

Results: In 3/12 pts without known MI we have found subendocardial necrosis on DE-CMR. In pts with known MI a mismatch in location between ECG/ECHO and DE-CMR was present in 14/17 pts: within the same coronary artery supply area in 10/17 pts, and in 4/17 pts with regard to segments supplied by different coronary arteries. Transmural extension of MI differed in 7/17 pts.

Conclusions: In pts with a history of ACS, the use of DE-CMR enables more accurate assessment of presence, location and transmural extension of MI than conventionaly used ECG/ECHO, which could be useful for revascularization procedure planning.

468. ASD SIZE, SHAPE, ANGULATION, AND LOCATION DEFINED BY CARDIAC MAGNETIC RESONANCE EN FACE IMAGING: VARIABILITY OF ASD MORPHOLOGY IN PATIENTS UNDERGOING PERCUTANEOUS ASD CLOSURE

Freddie M. Williams, MD,[1] Anna Lisa Crowley, MD,[2] Ray J. Kim, MD,[2] John Kevin Harrison, MD.[2] [1]***University of Virginia Health System, Charlottesville, Virginia, USA,*** [2]***Duke University Medical Center, Durham, North Carolina, USA.***

Objective: Previous reports have shown the effectiveness of velocity encoded magnetic resonance (veMR) to assess atrial septal defects (ASDs). While current ASD closure device shape is circular, we hypothesized that there is great variability in ASD morphology and veMR can describe ASD location and morphology.

Methods: We performed veMR (1.5T Siemens) in secundum ASD patients undergoing Amplatzer device closure. Optimal imaging plane (en face) was determined from 2 orthogonal in plane views and positioned when ASD flow was maximal. ASD area and eccentricity (long axis/short axis dimension) were measured. Reference lines were defined along posterior aortic wall abutting right atrium (Fig. 1 dashed line) and bisecting long axis of ASD (Fig. solid line). Angle between these 2 reference lines was measured in counterclockwise fashion (Fig. 1α). Distance from aortic valve (AV) to nearest point of ASD (Fig. 1 dotted line) was measured. During subsequent cardiac cath, the pulmonary to systemic blood flow ratio (Qp/Qs) was measured, and ASD was closed with Amplatzer device.

Results: In 2 of 33 patients (6.1%), the ASD was parallel to the ASD ($\alpha = 0^\circ$); in 14 patients (42.4%) α was 1-45°; in 12 patients (36.4%) α was 46–90°; in 5 patients (15.2%) α was $>90^\circ$. In 5 patients (15.2%), the distance from the ASD to AV was $\leq$ 0.5 cm; in 12 patients (36.4%) distance was >0.5 and $\leq$ 1; in 5 patients (15.2%) distance was >1 and $\leq$ 1.5; in 11 patients (33.3%) distance was >1.5. In 1 patient (3.0%), the eccentricity of the ASD (long/short length) was 1; in 14 patients (42.4%) eccentricity was >1.0 and $\leq$ 1.5; in 12 patients (36.4%) eccentricity was >1.5 and $\leq$ 2.0; in 6 patients (18.2%) eccentricity was >2.0. The mean ASD area was 2.0 cm^2 $\pm$ 1.3 cm^2. The mean Amplatzer device size was 20.2 mm $\pm$ 6.6 mm. The mean Qp/Qs was 1.6 $\pm$ 0.5.

Conclusion: Great variability exists in the size, shape, angulation, and location of secundum ASDs, as defined in vivo

á	Patients	Distance from AV to ASD, cm	Patients	Eccentricity	Patients
0°	2	$\leq$ 0.5	5	1	1
1–45°	14	$>0.5 \leq 1.0$	12	$>1 \leq 1.5$	14
46–90°	12	>1 .0 ≤ 1.5	5	$>1.5 \leq 2.0$	12
$>90^\circ$	5	>1.5	11	>2.0	6

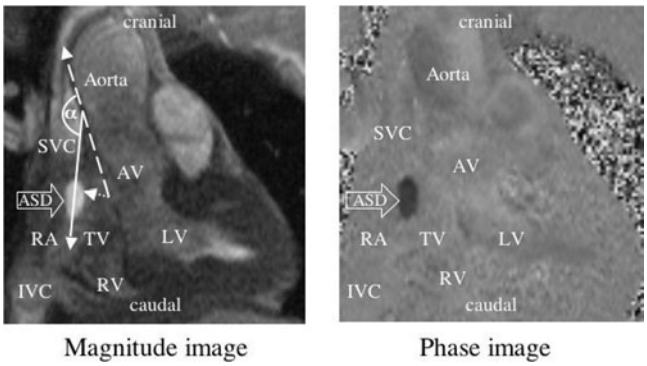

FIG. 1.

by veMR imaging. Such data may be useful in pre-procedural planning and in future device development.

469. TISSUE CHARACTERIZATION IN HYPERTROPHIC NON-OBSTRUCTIVE AND OBSTRUCTIVE CARDIOMYOPATHY: TYPICAL FOCAL HYPERINTENSITIES IN T2 WEIGHTED IMAGES SUGGESTING INTRAMYOCARDIAL FIBROSIS

Katharina Kolbe, Medical Student, Andreas Haars, MD, Stephanie Lehrke, MD, Dirk Lossnitzer, MD, Hugo A. Katus, MD, Evangelos Giannitsis, MD, Henning Steen, MD.
University Heidelberg, Heidelberg, Germany.

Backgound: Cardiac MRI (CMRI) has recently become the method of choice for accurate and observer-independent assessment of myocardial hypertrophy and left ventricular (LV) function in patients (pts.) with hyper-trophic non-obstructive or obstructive cardiomyopathy HN-/OCM. A typical contrast enhanced delayed gadolinium (Gd) MRI pattern (CEMRI) has been found in about 80% of the pts. with severe HN-/OCM.

Likewise, T2-W spin-echo hyper-intensities offer information on myocardial fibrosis, edema or necrosis without the disadvantage of contrast agent administration.

Interestingly, there is only scarce information about characteristic signal-properties in T2-weighted (T2-W) images in HN-/OCM.

Purpose: We hypothesized that T2-W MRI could detect septal hyper-intensities similar to T1-W CEMRI images and that these hyper-intensities would be preferably detectable in pts. with HN-OCM but not in pts. with pronounced LVH. This is due to the fact, that essentially only HN-/OCM pts. reveal significant myocardial tissue degradation into intra-myocardial fibrosis or increased levels of interstitial fluids in fibrotic areas.

Methods: We scanned 24 pts. with HNCM, 12 pts. with HOCM and 12 pts. with hypertensive heart disease (septal wall thickness $\geq$ 15 mm) by employing a vector-ECG gated multi-slice short axes (SA) fat-saturation black-blood T2-W Turbo-Spin imaging sequence (TR/TE = 2.9/1.0 ms; reconstr. voxel-size = $2.0 * 2.0 * 5.0$ mm) planned on true two- and four-chamber SSFP image planes (balanced-FFE; TR/TE = 2.9/1.45 ms; reconstr. voxel-size = $1.5 * 1.5 * 8$ mm) employing a cardiac five-element phased array coil on a 1.5T whole body MRI scanner (ACHIEVA, Philips Medical Systems, Netherlands). T2-W SA images were obtained on a mid-ventricular level by drawing six equally-defined areas for segmental hyper-intensity assessment on the LV myocardium to measure regional signal intensities (SI). Two additional focal segments were drawn at the anterior and posterior insertion of the right ventricle (antero-septal/infero-septal). SI was measured as mean SI plus standard deviation (SD) of mean SI for intra-individual analysis. Hyper-intensity was defined as SI more than two SD above the acquired mean SI level. Hypo-intensity was conversely defined as being two SD below the acquired SI level. Acute myocardial necrosis was excluded by measurement of cardio-specific Troponin T.

Results: T2-W MRI could be successfully accomplished in all pts. with excellent image quality. Typical hyper-intensities larger than 2 SD could be found segmentally in 66% of all HN-/OCM pts. in regions of pronounced hypertrophy including the focal antero-septal and infero-septal areas. In LVH pts., no segmental hyper-intensities larger than 2 SD could be measured.

A focal hyperintensity (antero-septal and infero-septal) could be shown in 34% of the segments of HN-/OCM pts. These focal signal changes were less accentuated in hypertensive heart disease pts. (17%). There was a good and significant correlation between the presence of T2-W hyper-intensity and CEMRI areas ($p < 0.0001$; $r = 0.528$). All pts. revealed a negative Troponin T test suggesting no acute cardiac necrosis as reason for the T2-W hyper-intensity.

Conclusion: We could demonstrate the existence of typical signal patterns in T2-W in HN-/OCM. Hyper-intensity in T2-W imaging suggests chronic myocardial fibrosis with elevated levels of interstitial fluid due to myocyte disarray instead of acute myocardial necrosis due to negative Troponin-T levels. T2-W assessment may provide additional diagnostic information for HN-/OCM as there are severely hypertrophied HN-/OCM pts. without typical CEMRI patterns but detectable hyper-intensities

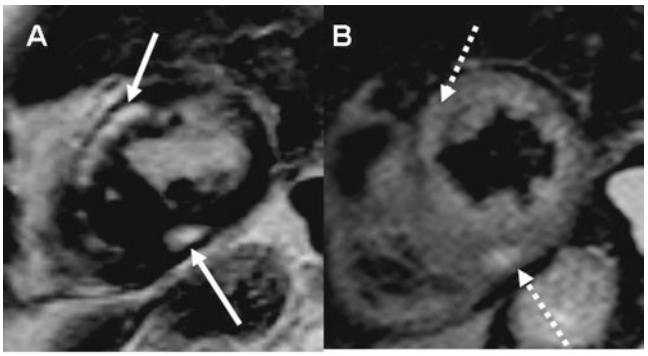

FIG. 1. CEMRI mid-ventricular short axis view with delayed hyper-enhancement antero- and inferoseptal (arrows) with corresponding T2-W slice (dashed arrows).

in T2-W scans. There is a need for further investigations correlating MRI with histology results.

470. THE ROLE OF CARDIAC MRI (CMR) AND CORONARY CT ANGIOGRAPHY (CCTA) IN THE DIAGNOSIS OF ACUTE MYOCARDITIS

Orly Goitein, MD, Oren Agranat, MD, Shlomi Matetzky, MD, Yael Eshet, MD, Guy Rozen, MD, Ariel Bentancur, MD, Eli Konen, MD. ***Sheba Medical Center, Tel Hashomer, Israel.***

Introduction: The hallmark of acute myocarditis is inflammatory myocardial changes and myocyte necrosis. Most cases are related to viral etiology and spontaneous recovery is the rule. However sudden death and progression to chronic dilated cardiomyopathy can occur (5–10% of the cases). The presenting clinical picture may mimic acute myocardial infarction. The distinction between these diagnoses is difficult, as even endomyocardial biopsy, albeit considered the standard of reference, has limited diagnostic accuracy.

Purpose: To describe the role of cardiac MRI (CMR) and cardiac CT angiography (CCTA) in the diagnosis of acute myocarditis.

Methods: Twenty-two consecutive patients (all males) with clinically suspected myocarditis, were enrolled in the study (average age 33 years, range 21–53). The combination of fever, signs and symptoms of upper respiratory infection with one or more of the following: chest pain, elevated Troponin-I and CPK levels, decreased left ventricular (LV) function and LV hypokinesis, lead to the clinical suspicion of myocarditis. All patients underwent CMR, and 13/22 pts underwent CCTA, within 36 hours of presentation. CMR was performed using a 1.5 Tesla scanner (Excite General Electric). Cine sequences were acquired in the short axis and the axial planes using steady state free precession. Contrast enhanced CMR was performed in the short axis 6–10 minutes following the administration of Gadolinium DTPA (0.02 mmole/Kg; Soreq Radiopharmaceuticals, Israel) using segmented inversion recovery gradient echo (IR-GRE) sequence to null the normal myocardium. CCTA was performed using a 64 slice scanner (Brilliance, Philips) following the uneventful administration of 100 mL, non iodinated contrast (Iomerone 400; Bracco, Italy) at a rate of 4–5 mL/sec. Curved multiplanar reformats were used for interpretation.

Results: Abnormal patchy epicardial areas of delayed enhancement were seen in 15/22 (68%) patients. The inferolateral segments were involved in all these cases. Average LV ejection fraction was 55% (range: 38-67%). All CCTA scans performed (13/13) were within normal limits.

Conclusions: Combined evaluation using CMR and CCTA offers comprehensive evaluation of patients with suspected myocarditis. CCTA can exclude ischemic etiology, while CMR may have a confirmatory role for the diagnosis of myocarditis by demonstrating a typical pattern of epicardial delayed enhancement in the inferolateral segments.

471. DELAYED ENHANCEMENT IS ASSOCIATED WITH MORE ADVANCED DIASTOLIC DYSFUNCTION IN PRIMARY SYSTEMIC AMYLOIDOSIS

Raymond Q. Migrino, MD, Vi Nguyen-Liu, BA, Jingli Wang, MD PhD, Phillip Pratt, PhD, Kirkwood Pritchard, PhD, Parameswaran Hari, MD. ***Medical College of Wisconsin, Milwaukee, Wisconsin, USA.***

Introduction: Primary systemic amyloidosis (PSA) is a rare but often fatal disease involving abnormal production of immunoglobulin light chains by plasma cells and subsequent tissue deposition leading to multi-organ dysfunction. Treatment with chemotherapy and autologous stem cell transplantation improves survival. However, cardiac involvement is associated with poor outcomes and in advanced cases, precludes candidacy for chemotherapy. Oxidative injury leading to diastolic dysfunction has been shown in animal models following exposure of cardiac tissue to light chains from patients with PSA. Subendocardial post-gadolinium delayed enhancement in the myocardium (DE) has been reported in patients with PSA and was associated with amyloid deposition, but the structural and functional significance of such finding is still not well established.

Purpose: We compared the systolic and diastolic function as well as survival of primary systemic amyloidosis patients with and without delayed enhancement using MRI and 2D echocardiography.

Methods: Fifteen patients (7 females) with biopsy proven PSA (kidney, bone marrow or other tissue [fat pad, axillary node, hip]) underwent cardiac MRI and standard 2D B mode and Doppler echocardiogram. Patients were divided into two groups: DE+ (presence of subendocardial DE 10–15 minutes following gadolinium gadodiamide injection using cardiac gated inversion recovery prepared segmented gradient echo sequence, $n = 11$ or 73%) and DE- (absent DE, $n = 4$ or 27%). Left ventricular (LV) ejection fraction (EF) and mass were obtained from MRI. Ratio of early diastolic mitral inflow velocity to early diastolic velocity of lateral mitral annulus (E/E', a sensitive marker of diastolic dysfunction), stage of diastolic dysfunction (normal, mild or delayed relaxation pattern, moderate or pseudonormal pattern, and severe or restrictive pattern) and left atrial size were obtained from echo.

	DE+	DE−	p value
LVEF (%)	68 ± 14	64 ± 6	NS
LV mass (g)	157 ± 40	110 ± 17	0.05
E/E′	13.7 ± 7	6.1 ± 0.8	0.007
Left atrial size (cm^2)	20.4 ± 5	13 ± 3.6	0.04
Age (years)	61 ± 10	54 ± 8	NS

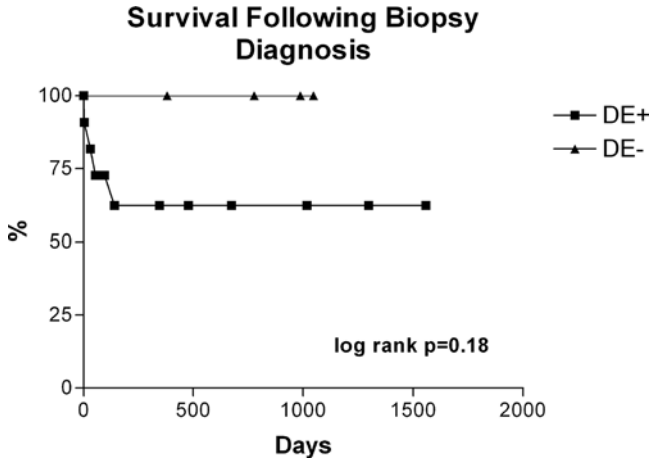

Results: (Table and Fig.) During follow up, 4 DE+ patients and 0 DE- patient expired. Seven of 11 (64%) DE+ patients had moderate or severe diastolic dysfunction (1 had normal diastolic function and 3 had mild diastolic dysfunction) whereas no DE- patient had moderate or severe diastolic dysfunction (2 had normal diastolic function, 1 had mild diastolic dysfunction).

Conclusions: 1. Subendocaridal delayed enhancement is common in patients with primary systemic amyloidosis. 2. Presence of delayed enhancement, although not associated with difference in systolic function, is associated with more advanced diastolic dysfunction, greater left ventricular mass and left atrial size in patients with PSA. 3. There is a trend towards higher mortality in patients with DE, but this did not reach statistical significance. 3. Delayed enhancement MRI may be useful in prognostication of patients with primary systemic amyloidosis, and its usefulness in targeting patients for early or more aggressive therapy needs to be tested prospectively.

472. ABNORMAL MYOCARDIUM CHARACTERIZED BY LATE GADOLINIUM ENHANCEMENT IMAGING IS ASSOCIATED WITH ADVERSE CARDIAC PROGNOSIS IN PATIENTS CLINICALLY SUSPECTED TO HAVE NON-ISCHEMIC OR INfiLTRATIVE CARDIOMYOPATHY

Alireza Maghsoudi, MD, Vignendra Ariyarajah, MD, Mouaz Al-Mallah, MD, Frank Rybicki, MD, PhD, Sharmila Dorbala, MBBS, Marcelo F. Di Carli, MD, Sui Tsang, BSc, Raymond Y. Kwong, MD, MPH. ***Brigham and Women's Hospital, Boston, Massachusetts, USA.***

Introduction: Late gadolinium enhancement (LGE) by CMR has been reported in non-ischemic dilated cardiomyopathy and various types of infiltrative cardiomyopathy. However, the prognostic significance of LGE in the assessment of patients suspected to have these conditions is unknown.

Purpose: We aimed to test the hypothesis that LGE is associated with major adverse cardiac events (MACE) in patients with a clinical suspicion of non-ischemic or infiltrative cardiomyopathy.

Methods: We performed gadolinium-enhanced CMR in 122 patients (73 M, mean age 49 ± 14 years) with a clinical suspicion of non-ischemic (n = 13) or infiltrative cardiomyopathy (n = 109). Exclusion criteria included any clinical history or evidence of any prior coronary artery disease including myocardial infarction. LGE imaging was performed using a 1.5 Tesla scanner (GE Signa CVi) with a T1-weighted inversion recovery FGRE pulse sequence 10–15 minutes after a cumulative dose of 0.15 mmol/kg of intravenous gadolinium. In all CMR studies, we assessed the global and regional left ventricular function, and reported the presence or absence of LGE blinded to the clinical outcome. In all patients, we obtained their vital status and non-fatal MACE including heart failure admissions and significant ventricular arrhythmias requiring treatment.

Results: After a median follow-up period of 13 months (range 6 months to 3.9 years), 17 (14%) patients experienced adverse events including 6 deaths, 7 heart failure admissions, and 4 cases of significant ventricular arrhythmias. Mean left ventricular ejection fraction of the study cohort was 53 ± 13%. LGE was detected in 32 patients (26%). Presence of LGE in this study cohort was associated with an elevated left ventricular end-systolic volume (184 ± 58 versus 173 ± 52 mL, p = 0.005). While regional left ventricular dysfunction was not significantly associated with MACE, abnormal LGE portends to a 2.6-fold elevated hazard to MACE during the follow-up period (95% cI: 1.00–6.99, p = 0.05).

Conclusions: Abnormal LGE by CMR is associated with adverse cardiac outcomes in patients suspected to have non-ischemic or infiltrative cardiomyopathy.

Kaplan Meier Event-free Survial of Study Cohort with Suspected Non-ischemic or Infiltrative Cardiomyopathy

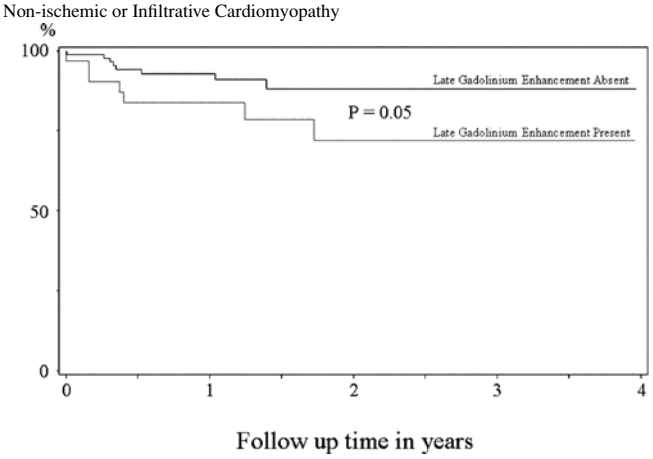

473. STRATEGIC TARGETING OF ATHEROSCLEROSIS: EX VIVO AND IN VIVO IMAGING USING OXIDATION-SPECIFIC GADOLINIUM MICELLES IN APOE−/− MICE

Karen C. Briley-Saebo, PhD,[1] Juan Gilberto Aquinaldo, PhD,[1] Esad Vucic, PhD,[1] Sotirios Tsmikas, PhD,[2] Zahi A. Fayad, PhD.[1] [1]***Mount Sinai School of Medicine, New York,***

TABLE 1
Summary of physical and chemical properties

	Hydrated diameter (nm)	r1, 60 MHz, water ($s^{-1}mM^{-1}$)	r1, 60 MHz, blood ($s^{-1}mM^{-1}$)	Blood half-life (hrs)	Liver uptake 24 hrs p.i. (w/w%)	Liver uptake 48 hrs p.i. (w/w%)
Untargeted	15 ± 3	11.6 ± 0.4	10.6 ± 0.6	1.15	6.8	Not detected
MDA2-micelle	23 ± 3	9.3 ± 0.4	8.7 ± 0.7	15.3	6.7	1.6

TABLE 2
Ex vivo and In vivo Efficacy in ApoE−/− mice

	Untargeted 24 hrs p.i. (% NENH)	MDA2 micelle 24 hrs p.i. (% NENH)	Untarargeted 48 hrs p.i. (% NENH)	MDA2 micelle 48 hrs p.i. (% NENH)	Untargeted 72 hrs p.i. (% NENH)	MDA2 micelle 72 hrs p.i. (% NENH)	Untargeted 94 hrs p.i. (% NENH)	MDA2 micelle 94 hrs p.i. (% NENH)
Vessel wall	20 ± 19	41 ± 19	3 ± 20	64 ± 2	-1 ± 5	75 ± 22	-3 ± 9	70 ± 12
Lymph	-6 ± 5	234 ± 78	1 ± 12	256 ± 58	-3 ± 10	17 ± 24	-2 ± 10	25 ± 18
Bone	7 ± 10	56 ± 6	-12 ± 13	59 ± 5	6 ± 9	59 ± 5	1 ± 6	29 ± 8
Kidney	37 ± 20	33 ± 21	3 ± 7	31 ± 3	8 ± 10	30 ± 2	7 ± 10	5 ± 21
Liver	35 ± 19	34 ± 18	10 ± 6	34 ± 7	4 ± 6	33 ± 4	9 ± 10	9 ± 18

New York, USA, [2]University of California, San Diego, La Jolla, California, USA.

Introduction: Peroxidation of low-density lipoproteins (LDL) has been identified as one of the key factors associated with the progression of atherosclerotic disease and plaque vulnerability. Previous studies have shown that the radio-labeled monoclonal antibody MDA2 is specifically taken up by atherosclerotic lesions containing abundant oxidation-specific epitopes.

Purpose: The aim of the current study was to synthesize, characterize, and evaluate the *ex vivo* and *in vivo* MR efficacy of MDA2 labeled gadolinium micelles in ApoE−/− mouse models of atherosclerosis.

Methods: Untargeted and MDA2-micelles were synthesized by dissolving PEG-DSPE, malamide-PEG-DSPE, Rhodamine-DSPE, and GdDTPA-bis(stearyl-amid)) in chloroform:methanol. Micelles were formed using established methods. The MD2A antibody was SATA modified prior to convent attachment to the micelle surface. The resultant micelles were characterized with respect to size (light scattering), longitudinal relaxivity (r_1), pharmacokinetics, and liver uptake in ApoE−/− mice. The *ex vivo* efficacy was evaluated by incubating the abdominal aortas of wild type (WT, $n = 8$) and APO−/− ($n = 8$) mice for 24 hours in DMEM containing untargeted or MDA2-micelles (at 5 mM Gd). *Ex vivo* aortas were imaged at 9.4T MR using T_1-weighted sequences (resolution $= 78 \times 39 \times 78\ \mu m^3$). The *in vivo* efficacy was evaluated following the administration of a 0.075 mmol Gd/kg dose of either untargeted or MDA2-micelles in ApoE−/− mice ($n = 6$). The normalized signal enhancement (%NENH), relative to muscle, for the vessel wall, lymphatic drain, liver, kidney, and bone was determined at 9.4T using T_1-weighted sequences over a four-day period post injection (p.i.). *Ex vivo* and *in vivo* abdominal aortas (at 48 hours post injection) were fixed for histology and confocal microscopy.

Results: Table 1 summarizes the properties associated with the micelles. Addition of the antibody caused significant increases in the hydrated particle size, blood half-life, and liver retention. The r_1 values indicate that the micelles do not interact with endogenous components of blood. However, shielding of the water exchange sites by the antibody resulted in a reduction of the MDA2-micelle r_1 values. The *ex vivo* study showed significant enhancement of the vessel wall of ApoE−/− mice following incubation with MDA2-micelles (SNR $= 101 \pm 10$), relative to untargeted micelles (SNR $= 36 \pm 13$). Table 2 shows the *in vivo* MR efficacy of untargeted and MDA2-micelles in ApoE−/− *mice* as a function of time p.i. These results strongly suggest that MDA2-micelles were present in the vessel wall, lymphatic drain, and bone (marrow). The excretion is presumable via the kidney and liver, as reflected in the %NENH values. Maximum vessel wall enhancement occurred 72-94 hours p.i., as shown in Fig. 1**.** No significant enhancement was observed following administration of the untargeted micelles at any of the time points studied. Histology and confocal microscopy confirmed the presence of MDA2-micelles in the extracellular matrix of atherosclerotic plaque.

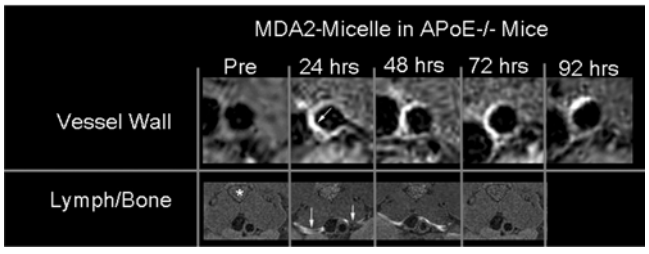

FIG. 1. Enhancement of the vessel all (arrow), lymphatic drain (arrows), and bone (*) as a function of time following the administration of 0.075 mmol Gd/kg MDA2-micelles.

Conclusions: The results of this study suggest that it is possible to non-invasively image intraplaque lipid peroxidase using MDA2-labeled gadolinium micelles. Additionally, significant and sustained MR enhancement was observed in other tissues, such as lymphatic drain and bone marrow, which also exhibit oxidative epitopes.

474. EFFICACY OF GADOLINIUM LABELED DISCOIDAL HIGH-DENSITY LIPOPROTEIN IN THE VESSEL WALL OF APOE−/− MICE

Karen C. Briley-Saebo, PhD,[1] Yanqing Ma, PhD,[2] Juan Gilberto Aquinaldo, PhD,[1] Kevin J Williams, PhD,[3] Edward A. Fisher, PhD,[2] Zahi A. Fayad, PhD.[1] [1]*Mount Sinai School of Medicine, New York, New York, USA,* [2]*New York University School of Medicine, New York, New York, USA,* [3]*Thomas Jefferson University, Philadelphia, Pennsylvania, USA.*

Introduction: High-density lipoprotein (HDL) nanoparticles naturally target atherosclerotic plaque. The mediation of HDL through the vessel wall is dependent upon the shape or loading of HDL. Previously, spherical gadolinium labeled HDL (Gd-*s*HDL) particles have been used to target atherosclerotic plaque within the vessel wall of ApoE−/− mice. However, it has been hypothesized that discoidal gadolinium labeled HDL (Gd-*d*HDL) may be more effective due to increased receptor mediated uptake of rHDL through the vessel wall.

Purpose: The aim of this study was to synthesize, characterize, and evaluate the *in vivo* efficacy of gadolinium labeled discoidal HDL (Gd-dHDL) in ApoE−/− mouse models of atherosclerosis.

Methods: Gd-sHDL was prepared by incubating human HDL with an excess of GdDTPA-bis(steryl-amide). Gd- *d*HDL was prepared by isolating the ApoA-1 protein from human plasma. The lipids (Soy PC, GdDTPA-BSA, and a fluorescent label) were hydrated in buffer and mixed ApoA-1 (ratio of 3:150) using the sodium cholate dialysis methods. The HDL formulations were dialyzed against FPLC and purified by FPLC. The HDL formulations were characterized with respect to size (FPLC, non-denaturing gel electrophoresis, and light scattering) and longitudinal relaxivity (60 MHz, water, 40° C).

TABLE 1
Summary of physical and chemical properties and CMR efficacy in ApoE−/− mice.

	Spherical gd-sHDL	Discodial Gd-dHDL
Size	10.4 nm (FPLC) 30 kDa (electro) 14.0 ± 1.8 nm (light scattering)	8.1 nm (FPLC) 30 kDa (electro) 9.3 ±1.9 nm (light scattering)
r1 ($s^{-1}mM^{-1}$)	10.4 ± 0.3	9.7 ± 0.3
MR Efficacy %NENH in Vessel Wall	35 ± 5	50 ± 6

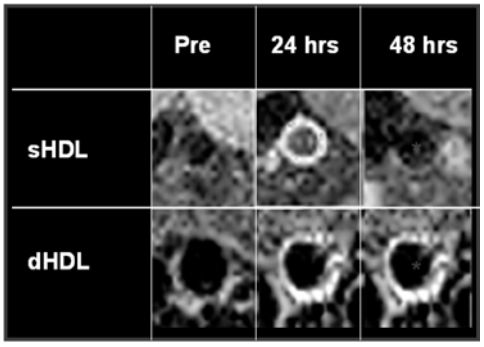

FIG. 1. MR signal enhancement of the vessel wall of the abdominal aorta of ApoE−/− mice as a function of time post injection for spherical (sHDL) and discoidal (dHDL)gadolinium labeled high density lipoprotein. *Indicates the vessel lumen.

The *in vivo* MR efficacy was evaluated in ApoE−/− mice following the administration of a 5 mmol Gd/Kg dose of Gd-sHDL (n = 2) or Gd-*d*HDL (n = 3) via tail vein injection. The normalized signal enhancement (% NENH), relative to muscle, was determined at 9.4T using T_1-weighted sequences over a seven-day time period post injection.

Results: Table 1 summarizes the results obtained for each formulation. dHDL was significantly smaller than that of sHDL, when measured by both electrophoresis and light scattering. No significant difference in the longitudinal relaxivities were observed between the two formulations. Enhancement of the vessel wall of ApoE−/− mice was clearly observed for each formulation, with maximum enhancement occurring 24-48 hours post injection, as shown in Fig. 1. For Gd-*d*HDL re-circulation into the plaque was observed over a seven day time period days post injection, as shown in Fig. 2.

Conclusions: Gd-*d*HDL nanoparticles may be more effective than Gd-*s*HDL particles for MR imaging of atherosclerotic plaque. The results suggest that it may be possible to visualize the re-circulation of Gd-*d*HDL in the vessel wall of ApoE−/− mice.

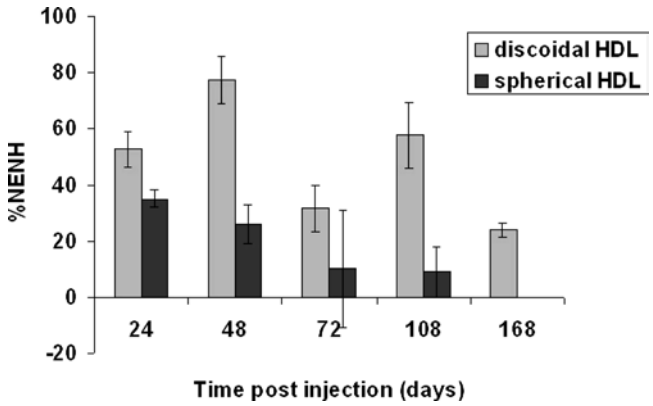

FIG. 2. Evolution of the normalized nhancement (%NENH) of the vessel wall of ApoE−/− relative to muscle as a function of time post injection.

475. THE MULTIDISCIPLINARY STUDY OF RIGHT VENTRICULAR DYSPLASIA: MRI FINDINGS IN FAMILY MEMBERS OF AFFECTED INDIVIDUALS

Robson Macedo, MD,[1] Harikrishna Tandri, MD,[1] Crystal Tichnell, RN,[1] Wojciech Zareba, MD, PhD,[2] Frank Marcus, MD,[3] Hugh Calkins, MD,[1] David A. Bluemke, MD.[1] [1]***Johns Hopkins Hospital, Baltimore, Maryland, USA,*** [2]***University of Rochester, Rochester, New York, USA,*** [3]***University of Arizona, Tucson, Arizona, USA.***

Introduction: Magnetic resonance imaging (MRI) is frequently used for screening family members of patients diagnosed with arrhythmogenic right ventricular dysplasia (ARVD). We report MRI findings in the first-degree relatives of probands from the multidisciplinary study of ARVD (US ARVD study).

Methods: The study included forty-five first-degree relatives of ARVD probands and 20 control subjects free of clinical cardiovascular disease. The MRI scan included ECG gated black blood images of the myocardium acquired in the transaxial and/or short axis plane using either double inversion recovery fast/turbo spin echo technique, spin echo T1 or proton density weighted images. Fat suppressed images were obtained using either chemical shift fat suppression or inversion recovery technique. ECG gated bright blood cine images were obtained using steady state free precession images, (e.g., TrueFISP, Fiesta, balanced fast field echo) in the transaxial and short axis planes. All MRI data was obtained on 1.5 T scanners. Left ventricle (LV) and right ventricle (RV) end diastolic diameters (EDD), end diastolic volumes (EDV) and function were quantified for both groups. The RV outflow tract (RVOT) area, RV free wall diameter and presence of fat in the RV wall was also assessed. The Student's t-test was used to compare the study group to the normal volunteers. Mean and standard deviation values for RV size/function were calculated.

Results: Of the 45 family members, 21 were females and 24 males with mean age 36 ± 16.9 years. Among these family members, 8/43 (19%) had RV fat infiltration (Fig. 1), 4/44 (9%) had RV free wall thinning, 1/44 (2%) had RV free wall hypertrophy and 10/43 (23.%) had RV regional dysfunction. Six (13%) family members had a final diagnosis of ARVD based on Task Force Criteria. For the family members, the mean RVOT area (7.55 ± 2.6 cm^2), LV EDD (46.4 ± 5.73 mm) and RV EDD (35.9 ± 5.2 mm). LV EDV (137.6 ± 42.3 mL) and RV EDV (138.8 ± 48.0 mL) were not statistically different from the normal volunteers.

Conclusions: MRI frequently detects qualitative abnormalities in the RV in first-degree relatives of patients with ARVD, although chamber sizes/ volumes of the family members are normal overall. There is a high prevalence of ARVD in the first-degree relatives consistent with the genetic basis of the disease and continued follow up of family members is likely important to determine if these mild RV abnormalities will progress in these family members.

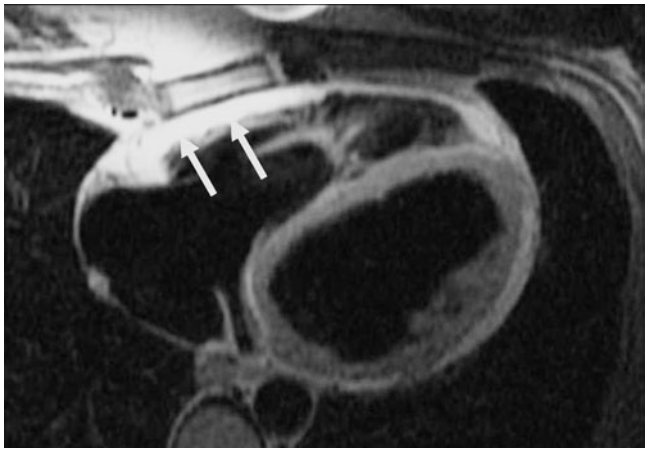

FIG. 1. Axial Black-Blood image of the heart showing RV fat infiltration (arrows).

476. DETECTION OF METASTATIC MELANOMA TO THE HEART: A NON CONTRAST APPROACH USING MELANIN INVERSION RECOVERY IMAGING (MIRI)

Andrew M. Crean, MRCP FRCR,[1] Christoph Juli, MD FRCR.[2] [1]***Leeds General Infirmary, Leeds, United Kingdom,*** [2]***Papworth Hospital, Cambridge, United Kingdom.***

Purpose: To describe the novel use for a standard inversion recovery (delayed enhancement) CMR sequence in detection of metastatic melanoma to the heart by exploiting the intrinsic paramagnetic effects of melanin.

Method: Four studies in 3 patients with a past history of excised primary cutaneous melanoma were examined by CMR for symptoms suggestive of cardiac dysfunction. In each case an inversion recovery sequence with an arbitrarily chosen inversion time of 200 ms was used to acquire axial or short axis images prior to the injection of gadolinium contrast. The acquisition was repeated following an injection of 0.2 mmol/kg gadolinium contrast agent (gadodiamide, Amersham UK) with identical parameters and following a delay of 8 minutes in the same imaging plane.

Number, location and volume of each separately identified lesion were compared between the non contrast and post-contrast inversion recovery sequences. Volume measurements were made offline using a dedicated software package (QMass v6.1.6, Medis, Netherlands).

Results: Multiple metastatic lesions were identified throughout the heart in patients 1 and 2. A single intraventricular lesion was identified in patient 3. There was no difference in the number or location of lesions identified between pre and post contrast studies. Mean tumour volume for the MIRI sequence was 10.5 mL (SD 7.6 mL); mean tumour volume for the post gadolinium delayed enhancement sequence was 10.6 mL (SD 6.2 mL); $p =$ ns (Wilcoxon signed ranks test).

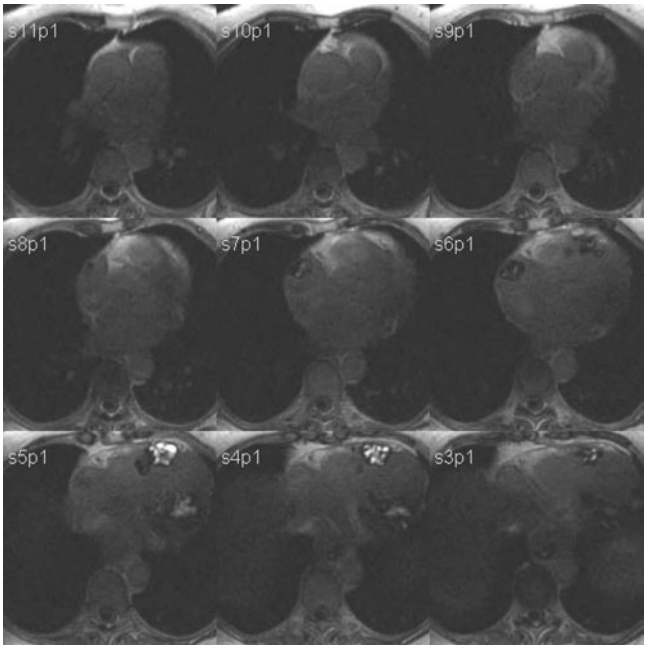

A representative MIRI image demonstrating cardiac metastases with *intrinsic contrast* due to the T1 shortening properties of melanin is shown below.

Conclusion: Non gadolinium melanin inversion recovery imaging (MIRI) appears to provide comparable results to conventional delayed enhancement imaging in the detection of cardiac melanoma.

477. AUTOMATED VOLUMETRIC QUANTIFICATION OF MYOCARDIAL INFARCTION FROM DELAYED ENHANCED MULTIDETECTOR COMPUTED TOMOGRAPHY: VALIDATION USING DELAYED ENHANCED MRI

Richard T. George, MD, Karl H. Schuleri, MD, Joshua M. Hare, Joao A. C. Lima, MD, Albert C. Lardo, PhD. ***Johns Hopkins University, Baltimore, Maryland, USA.***

Introduction: Delayed enhanced magnetic resonance imaging (DE-MRI) is well validated for the automated analysis of infarct size and the differentiation of viable and non-viable myocardium. However, attenuation density thresholds for the automated analysis of delayed enhanced multidetector computed tomography (DE-MDCT) have not yet been established.

Purpose: The purpose of this study is to validate a novel DE-MDCT volumetric infarct analysis approach versus DE-MRI by determining the appropriate attenuation density thresholds (DT) for the accurate automated assessment of myocardial enhancement patterns during DE-MDCT.

Methods: Seven porcine models of anterior myocardial infarction (MI) (2 hour occlusion/reperfusion) underwent sequential imaging with DE-MDCT and DE-MRI ten to eleven days following MI. DE-MDCT was initiated 10 minutes following contrast infusion (iopamidol 370 mgI/mL, 150 mL) according to the following parameters: collimation = 0.5 mm × 64, tube voltage/current = 120 kV/ 400 mA, rotation time = 0.4–0.5 seconds (heart rate dependent). DE-MRI was performed 10 minutes following Gd-DTPA (0.2 mmol/kg) injection according to the following protocol: pulse sequence = fast gradient-recalled echo, field of view 30 × 23 cm, slice thickness = 8 mm, 4.2 msec echo time, matrix = 256 × 160, bandwidth = 19 kHz, flip angle = 20°. MDCT images were reconstructed at 80% of the R-R interval with a 3 mm slice thickness and analyzed using a custom perfusion software package that uses a step-based algorithm to: a) detect voxels within the defined DT range with continuity in the X, Y, and Z directions; b) generate clusters that meet the DT definition; and c) define the infarct as the largest cluster detected. Density thresholds were defined for hyperenhanced infarcts as 1.0, 1.5, and 2.0 standard deviations above the remote myocardial density and expressed as a percentage of total myocardial volume for DE-MDCT. DE-MRI images were analyzed using a previously described method that defines the infarct by a signal intensity two standard deviations above the remote myocardial signal intensity.

Results: Infarct size with DE-MDCT using a DT of 1.0 standard deviation showed the best agreement with DE-MRI. Infarct size by DE-MDCT and DE-MRI was 26.9% ± 8.0% and 24.2% ± 6.4%, respectively. Using this threshold, there was no statistically significant over/underestimation of infarct size, mean difference -2.7% (p = 0.19).

Conclusions: The automated volumetric quantification of MI using DE-MDCT imaging compares best with DE-MRI using a threshold of 1.0 standard deviation above the remote myocardial density.